On the Structural Mechanics of Multi-layered Subsea Pipelines

by

Renato Marques Corrêa da Silva

Department of Mechanical Engineering
University College London
Torrington Place
London WC1E 7JE

Thesis submitted for the degree of Doctor of Philosophy in the Faculty of Engineering, University of London

October 1997

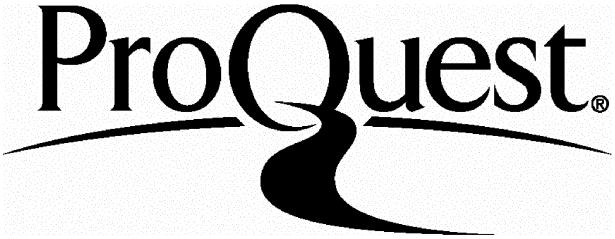

ABSTRACT

During the 1990s the world-wide offshore industry has been increasingly developing oil and gas fields in deep water – classified here as generally above 300 metres (984 feet) water depth – often combined with production from reservoirs at higher temperatures. Subsea pipelines form an essential element of these developments and one of the limitations on deep water development has been the inability to provide large diameter conventional steel pipelines and risers capable of withstanding large external hydrostatic pressures.

The work presented in this thesis investigates the performance of multi-layered pipe cross-sections for the required increase in hydrostatic pressure capacity and thermal insulation for such subsea pipelines. A fundamental investigation into the structural mechanics of such multi-layered pipes is presented with an emphasis on three principal issues – The mechanics of multi-layered pipe loading due to internal pressure, its collapse due to external pressure, and the behaviour of such pipe geometry when in a free submerged catenary configuration.

Initially, the stresses induced by internal pressure have been investigated based on the Lame's equations. The results were compared with a finite element analysis and demonstrated good agreement. The stress distribution due to internal pressure was then investigated for a wide range of multi-layered pipe geometries and Young's Moduli of the core material. Comparisons are also presented with the stresses within equivalent single walled pipes. The much more complex external pressure problem was then addressed. The stability of a cylindrical multi-layered shell is a complex problem and in response to this, the investigation presented in this thesis followed a staged approach. Based on the previous work of Raville (1955), an elastic classic model was developed. Following this, using the concept of an elastic foundation, a new formulation was developed to derive critical external pressure loads. This work has been compared to that of Montague (1975) for critical external pressure based on two dimensional elastic plastic deformations up to maximum shear stress or Tresca failure theory. In addition, another approach for the elastic plastic model has been developed based on three dimensional Mises failure theory. A finite element analysis was then

used to compare results from these different approaches for obtaining the critical external pressure. These four methods are used for a comparative investigation of collapse pressure predictions for a wide range of pipe geometries and Young's Moduli of the annular material. These comparisons give an indication of the applications of these methods and also give some insight into possible collapse mechanisms for multi-layered pipes.

This thesis also examines the performance of a multi-layered pipeline in an underwater catenary configuration and compares this to the performance of a single walled equivalent pipe. This was done by the development of an analytical catenary model aimed at optimising the catenary geometry around the two critical stress points of the catenary (the top connection at far position and touch down point at near position). The results demonstrated the significant improvement that multi-layered pipes could deliver for reductions in top tension and steel wall thickness when used in a catenary configuration.

In overall terms, this work demonstrated that multi-layered subsea pipelines can provide a wide range of structural performance benefits both locally and globally. Locally, appropriate design and material selection can yield combinations of reduced steel volume and greater internal and external pressure capacity. In global terms, the buoyancy contribution from the thicker walls of multi-layered pipe will yield significant reductions in top tension when in a catenary configuration.

This investigation has only examined a relatively narrow range of structural benefits of multi-layered pipes. Much further work needs to be done on local structural behaviour, internal layer bonds, on the internal damping of such pipes, and on the mechanics of the pipe segment connections.

ACKNOWLEDGEMENTS

I am very grateful to my supervisor Professor Minoo H. Patel, for his excellent guidance and continuous encouragement throughout this research. Without his advice, this thesis would not have been written.

My appreciation is extended to Dr. Joel Witz and Dr. Geoff J. Lyons for their valuable advice on special issues.

It has been a pleasure being with colleagues of the Santa Fe Laboratory for Offshore Engineering. In particular, I want to thanks Mr. Mark Dixon and Mr. Owen Pearson for their advice on using the FEM computer program ABAQUS.

The author expresses deep appreciation to Petróleo Brasileiro s/a – Petrobrás which supported this research and extends also his gratitude to Petrobrás colleagues for their encouragement.

Finally, I wish to give warm and special thanks to my family, Mrs. Selma, Ms. Renata and Ms. Carolina for their patience and support over the last three and half years living in a foreign country with a quite different weather and culture.

CONTENTS

LIST OF FIGURES

LIST OF TABLES

LIST OF PRINCIPAL SYMBOLS

a	Mean radius of the outer face or skin
b	Mean radius of the inner face or skin
$A, B, C \ldots$	Arbitrary constants
$A'_n, B'_n, C'_n \ldots$	Arbitrary constants
$A_n, B_n, C_n \ldots$	Arbitrary constants
$\overline{A}, \overline{B}, \overline{C} \ldots$	Arbitrary constants
co	Core thickness
D	Diameter
E, E_s, E_f, E_c	Modulus of elasticity or Young modulus
f	Faces or skin thickness
G, $G_{r\theta}$	Modulus of elasticity in shear, and the same in the core in r-θ plane
h	Wall thickness
I	Second moment of area
k	Numeric factor
K	Flexural rigidity
L, l	Length or span
ln	Natural logarithm
M, M_o	Bending moment
m, n	Numeric factors
M_x, M_y, M_{xy}	Bending and twisting moments per unit distance in shell
N	Shearing force, normal force, axial force, matrix
$\overline{N}_\theta, \overline{N}'_\theta$	Small direct stress, tangential direction in the plane of outer and inner faces
N_θ, N'_θ	Direct stress resultants, tangential direction in the plane of outer and inner faces
N_x, N_y, N_{xy}	Normal and shearing forces per unit distance in middle surface of shell
OD	Outside diameter
P	Axial force
p, q	Intensity of distributed load
P_{cr}	Critical buckling load
P_E	Beam-column critical Euler load
p_i, p_1, p_2, p_e	Uniform normal pressures
Q	Shearing force
q_1, q_2, q_3	Dimensionless numeric factor
Q_x, Q_y	Shearing forces per unit distance in shell
r	Radius of curvature
S	Shear stiffness

s Length, distance

t Wall thickness

T Shear force

u Displacement in radial direction

u, u', u_c Radial displacements of outer face, inner face, and core, respectively

$\bar{v}, \bar{v}', \bar{v}_c$ Small tangential displacements of outer face, inner face, and core, respectively

$\bar{u}, \bar{u}', \bar{u}_c$ Small radial displacements of outer face, inner face, and core, respectively

u, v, w Displacements in x, y, and z directions

v, w Displacements in tangential and radial directions

x, y, z Rectangular co-ordinates

α, β Numeric factors

χ Change of curvature in shell or core position parameter

δ Deflection, radial displacement

ε Unit normal strain

$\bar{\varepsilon}_\theta, \bar{\varepsilon}_\theta, \bar{\varepsilon}_{\theta c}$ Small tangential strains in outer face, inner face, and core, respectively

$\varepsilon_\theta, \varepsilon'_\theta$ Tangential strains in outer and inner face, respectively

ξ, κ Constant parameter

ϕ Angle, angular co-ordinate

γ Shearing unit strain

η Core to face thickness ratio

λ Numerical factor

μ Mises stress ratio

ν Poisson's ratio

θ Angle, angular co-ordinate

ρ Mass per unit of volume

σ_{cr} Compressive unit stress in critical load

$\bar{\sigma}_r, \bar{\sigma}'_r, \bar{\sigma}_{rc}$ Small normal stress in radial direction in outer face, inner face, and core

$\sigma_r, \sigma'_r, \sigma_{rc}$ Normal stress in radial direction in outer face, inner face, and core, respectively

σ_r, σ_h Unit normal stress in radial, and circumferential directions, respectively

$\sigma_x, \sigma_y, \sigma_z$ Unit normal stress in x, y, and z directions, respectively

σ_{yp} Yield-point stress

$\bar{\tau}_{r\theta}, \bar{\tau}'_{r\theta}$ Small shear stress in the plane of the middle surface of the outer and inner faces

$( )'$ Partial derivative with respect to x, $\partial( )/\partial x$

$( )^{\bullet}$ Partial derivative with respect to ϕ times radius, $a\partial( )/\partial\phi$

1. Introduction

1.1 Pipes – offshore and sub-sea applications

The use of cylindrical shell members has, for a long time, been associated with aerospace and submarine structures. In the last two decades, however, the exploitation of offshore oil reserves has led to the construction of structures in which unstiffened and stiffened cylindrical shells have been extensively used as primary structural members. Such cylindrical shells are also used as compliant dynamically sensitive structures such as pipelines, vertical risers and tethers.

Demand from the modern world for non-renewable oil and gas resources has motivated industries working in this field to explore and produce hydrocarbons in increasing quantities. Geological processes, over long time scales, lead to the accumulation of oil and gas in subsurface reservoirs. The main goal of the oil industry is to discover these reservoirs and to extract as much oil as possible from them as cheaply as possible. Over the last seventy years, the industry has identified almost all of the hydrocarbon reservoirs underneath on-shore sites – these being capable of production at low cost. Such reservoirs in the Arabian Gulf, and increasingly in the Russian Federation, provide a substantial proportion of the world's needs. However, the industrial importance of hydrocarbons has meant that most countries in the world require secure access to locally controlled supplies. This has prompted offshore exploration and production in many areas – the Gulf of Mexico, North Sea, offshore Mexico and Brazil and in the seas off China and Australia.

In such offshore developments, the oil industry now faces new technological challenges. The exploitation of a reservoir may be divided into three main phases – the first being a geological survey which determines the location of a potential offshore hydrocarbon reservoir below the seabed. The second phase is exploration drilling which requires a rig and facilities to drill a well down to the zone of interest. Production tests will then be carried out to discover if there is oil in sufficient quantities to make the third and last phase economically feasible. The drilling phase lasts for up to three months and carries the most risk since the whole investment of many millions of dollars in the well may have to be written off. The third and last

phase – that of oil production is the most expensive. A production unit has to be designed, fabricated and installed capable of producing well fluids, separating the oil from water and sand and pumping it through pipelines to ships or onshore sites to reach a refinery. In the refinery, the oil will be converted into petroleum and other derivatives. This phase can last from 3 to 25 years, requiring that the production facilities be designed for long term use.

Since Roman times, the main means of transporting and managing liquids has been the pipeline. A single hollow circular cylinder is the most basic concept of a pipe. However, the oil industry also needs special pipes such as risers. A riser is the slender pipe structure that carries petroleum from the well head at the seabed up to the surface platform. Another important type of pipeline is the export line from the production unit; designed to deliver produced oil to ships or onshore sites for delivery to refineries. Any riser structure has two parts, the dynamic segment and the static segment that is laid or buried on the seabed; see Figure 1.1.1 There are also other types of slender structures such as control umbilicals – carrying hydraulic or electric lines for control of subsurface equipment, and also for well annulus access – allowing intervention in the well or for gas lift purpose – for injection of water or gas injection into the reservoir, and so on.

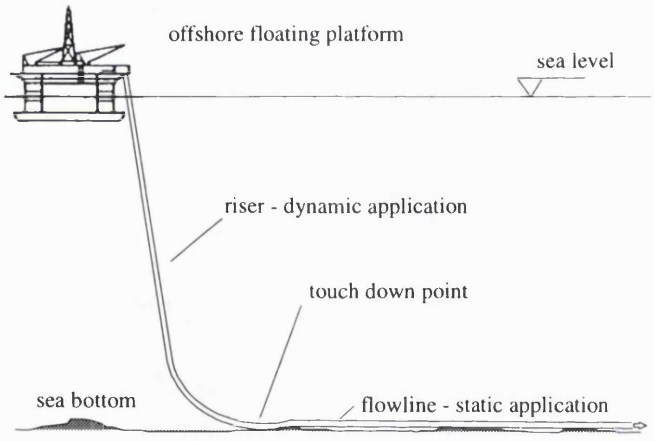

Fig. 1.1.1 Floating production system – riser sketch.

Any riser has to cope with high internal and external pressures, the latter being a function of water depth. It also has to resist the aggressive chemical environment of the open sea and loads due to currents and waves. The traditional solution for pipeline systems is the steel pipe, manufactured in big diameters by welding and protected against corrosion. The internal diameter of the pipe, nominal pressures, and weather information of the installation site are the main parameters used to

determine the required wall thickness. This wall thickness could be the parameter that would make the whole pipeline project feasible or not.

Consider an offshore pipeline where the steel strength and wall thickness is such that the design can be welded with good and reliable results. It means that the pressures involved, water depth, installation, and laying requirements have resulted in stresses' compatible with the design code and welding standards that are being used. On the other hand, there is an important limitation of welded steel pipes that arises from water depth. As water depth increases, hydrostatic pressure rises proportionally, so the steel strength or wall thickness of such a pipeline has to be increased to cope with external pressure loads. However, the maximum available steel strength is limited by the grade of steel being used. If the steel grade is improved for increased strength, the steel becomes more difficult to weld and hence less reliable. In addition, the wall thickness can only be increased up to a point due to manufacturing capabilities and also by the welding process employed. In conclusion, the maximum possible wall thickness of a steel pipe determines a clear limit to external hydrostatic pressure loads, in other words the maximum water depth in which it can be installed.

Steel pipe applications fall clearly into two areas. The first of this is the static application in which the pipe is not subjected to cyclic loads or varying tension and bending during its service life. The second of these is dynamic applications where the steel pipe has to withstand cyclic tension and bending throughout its life. Of course, any offshore static pipe system has to be installed before it starts operation and the loads induced during the installation phase are cyclic and typically worse than the loads faced during service. As a consequence, installation procedures have to be carefully considered for any offshore pipeline design. Such installation procedures can be divided into two phases – the first being manufacturing and handling procedures that ensure the integrity of the pipe during fabrication, storage, and transportation and the second being the installation or laying phase for deploying the pipeline on the sea bed.

Offshore pipeline installation operations can use several approaches. These are illustrated in Figures 1.1.2 to 1.1.5 by line drawings reproduced from the brochures of engineering contractors working in the field. The most common and cheapest

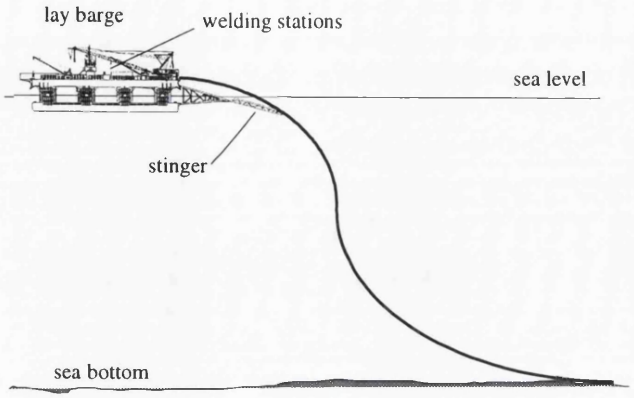

Fig. 1.1.2 Pipeline installation – S-lay method.

installation method is the S-lay method shown in Figure 1.1.2. Here the pipeline is horizontally welded in stretches on a lay barge. It is then gradually paid out and deployed on the seabed through a stinger assembled on the barge's stern. During the whole laying operation the pipeline is kept in tension and at a specific laying angle. Unfortunately, this method is restricted to sites of up to 500 m water depth. The main governing parameter during laying operation is the maximum stress obtained in the sag bend, this stress needs to be kept below a safe level recommended by internationally agreed codes.

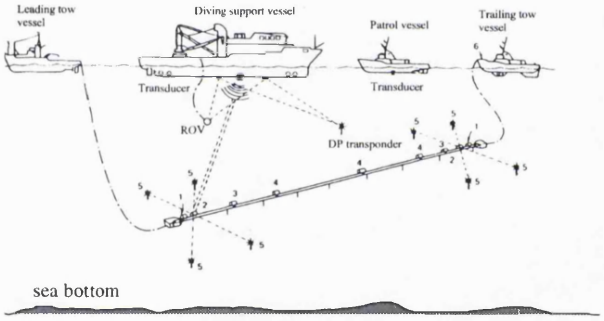

Fig. 1.1.3 Pipeline installation – bottom tow method.

Another installation method is the bottom tow; see Figure 1.1.3. In this method, the pipeline is welded and assembled onshore, filled with an inert gas and towed to the installation site by two installation ships holding the pipeline close to the seabed. The newest method for deep water laying is the J-lay, see Figure 1.1.4. In this method the ship or rig pays out the pipe into the water vertically and the pipe bends near to the sea bottom before it assumes the horizontal position on the seabed. The final option is the reel method that requires the whole pipe to be welded and

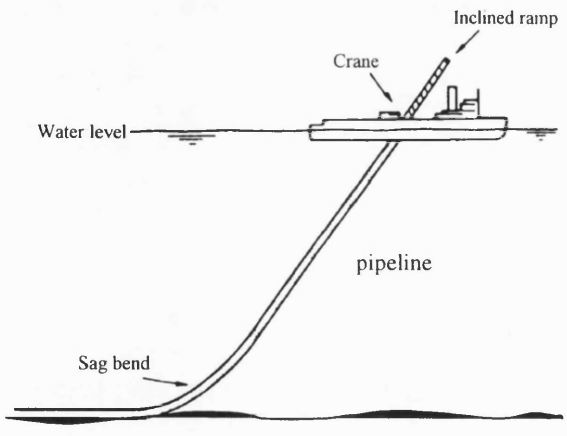

Fig. 1.1.4 Pipeline installation – J-lay method.

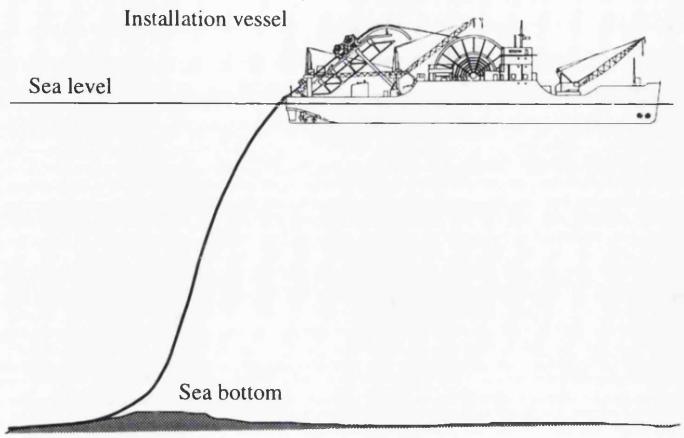

Fig. 1.1.5 Pipeline installation – reel method.

manufactured onshore and then reeled in a big radius reel on a special ship. During this reeling operation, the pipeline has to be bent through plastic deformation to match the ship reel radius, see Figure 1.1.5. It means that during the laying operation the pipe has to be plastically deformed again just before installation on the seabed. The pipe wall thickness and steel material properties need to be designed to be compatible with this hardening process to keep the induced residual stresses within a safe range.

1.2 Concept of multi-layered pipes

Dynamic pipes or risers are needed to assure continuity of flow between the well and floating rig and also between the rig and an onshore site or a refinery. The lengths of these risers are small compared to the complete pipeline length. However, they require a complex design to cope with cyclic and dynamic loads during long term service. A flexible pipe is one common solution for dynamic applications. These pipes are composed of concentric layers of helically wound inter-locked strips and wires together with polymer cylinder layers, see Figure 1.2.1. Each of these layers is designed to fulfil a specific function such as providing resistance to external pressure induced collapse and internal pressure containment, whilst maintaining the ability to bend to a small radius of curvature (say from 1m to 6m). Such flexible pipes are manufactured in both unbonded and bonded construction.

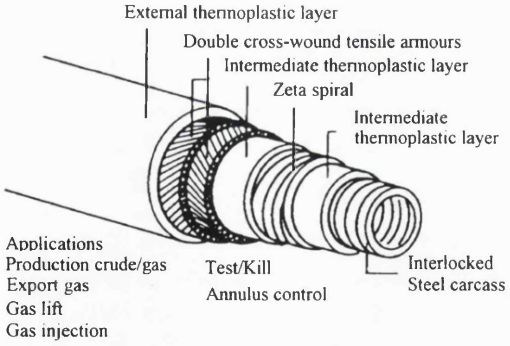

Fig. 1.2.1 Unbonded flexible riser.
(from Coflexip Stena Offshore)

The unbonded form allows adjacent layers to slip past each other whereas the bonded form uses vulcanising and adhesives to lock the layers together. Each form of construction has its merits and drawbacks although unbonded pipes cover internal pipe diameters ranging from 2 inches to about 12 inches. The flexible pipe solution has two main drawbacks for the oil industry. The first is the geometric increase of price with diameter and collapse pressure; the second is a manufacturing limitation in terms of diameter. At present, flexible pipes for deep water are only manufactured up to about 12 inches internal diameter.

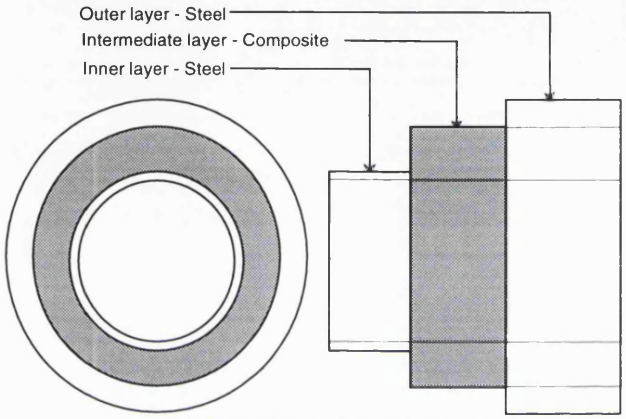

Fig. 1.2.2 Multi-layered pipe concept.

Steel pipes have been used for dynamic applications such as tensioned drilling and production risers for many decades now. However, their most appropriate application is in shallow to moderate water depths. These risers also impose tight horizontal offset limits on floating surface vessels and require large capacity tensioners on the surface vessel. As a consequence there are very few deep water vertical steel riser designs deployed at present.

Taking all of the above into account, the objective of this thesis is to investigate the structural mechanics of a new multi-layered pipeline concept that overcomes some of the limitations of present day pipe designs. The concept proposes a pipe cross-section where an inner and outer steel wall surrounds an annulus made up of a homogeneous non-metallic material. As shown in Figure 1.2.2, the separation of the steel wall into an inner and outer layer can potentially offer six advantages:

(1) The reduction of steel wall thickness in each steel wall makes it possible to circumvent thickness related welding problems and hence enables the pipe to achieve higher external pressure capacity;

(2) The separation of the structure in inner and outer steel walls substantially increases the bending stiffness of the pipe wall therefore contributing to its collapse resistance;

(3) The higher external diameter of the outer shell and the annulus filler material leads to a better distribution of internal stresses.

(4) The increased volume of the pipe wall can provide increased buoyancy force – although of course it also affects greater hydrodynamic inertia and drag forces.

(5) The annulus material can provide extra damping properties to the whole structure reducing the effects of vortex induced vibration for risers facing severe current profiles.

(6) The annulus material can also provide insulation for high temperature product applications combined with part protection of the inner layer material.

British steel has developed a product called Hydrotherm which uses the concept of multi-layered pipe. However, this pipe-in-pipe concept does not take into account the structural role of the core material. The product is designed to deliver additional insulation protection not strength. Other developments have used the pipe-in-pipe concept in offshore application, however, their aim was always insulation purposes.

1.3 General overview of the thesis

The overall objective of the work in this thesis is to investigate the structural mechanics of such multi-layered pipes from several viewpoints – these being:

(a) An analytical and finite element analysis based investigation of the behaviour of such pipes under internal pressure.

(b) Continuation of the above work, considering multi-layered pipe behaviour and collapse under external pressure;

(c) An evaluation of the effect of increased buoyancy of multi-layered pipe in typical offshore catenary riser configurations and comparison of this performance with that of an equivalent single walled pipe.

The thesis is divided into six parts starting with a comprehensive literature review. This describes several studies on the stability of shell structures. Most of them use numerical solutions calibrated with experimental data mainly to set parameters that take imperfections into account. However, these studies deal with specific single cylindrical pipelines that have only one layer. On the other hand, some limited

research has been reported on multi-layered structures, most of them, related to aeronautical applications of sandwich shell structures. Some of the most relevant derivations and developments of theory that are referred to and used in the main body of the thesis are presented in Appendices 1 to 4.

The main body of the work presented starts firstly with the analysis of internal pressure and presents a simple extension of Lame's stress and strain analysis of single walled pipe to a multi-layered cylindrical structure. A comparison using a finite element analysis package is carried out here to verify results. The analytical model is used to compare the structural mechanics of single walled and double walled pipes on a like-for-like basis. This is done by comparing the von Mises stresses in the two configurations using the same cross-sectional area of steel. These comparisons are presented for a wide range of pipe geometries and Young's Moduli of the annular layer.

The second part of the work is concerned with analysis of the buckling of a multi-layered pipeline structure due to external hydrostatic pressure and uses three analytical models to investigate the problem. Two of them, the elastic spring layers and the thin sandwich wall consider elastic collapse only. The third method is a theory based on a limited von Mises stress state, where the skin layers deform plastically before the core buckles. The results from all three analyses are compared with results from a finite element package. Again the collapse pressures obtained from the three analytical models and the finite element analysis are compared for a wide variation of pipe geometries and material properties of the annular material. The comparisons give an indication of the applicability of the four different methods used and also give some insight into the way in which collapse with external pressure is likely to occur for a multi-layered structure.

The third part of the work investigates the specific global problem of the effects of using a multi-layered pipeline in a deep water catenary configuration. The additional buoyancy due to the thick wall and to smaller core material density impart significant buoyancy to a multi-layered pipe which in turn will reduce catenary top tension requirement. On the other hand, the core material could be selected also to induce more weight for big diameter gas pipelines. This part of the work seeks to

quantify these system level improvements and compares these to the effect of using single walled pipe in this application.

The analytical work is applied to several case studies in section six to quantify the typical structural performance gains achieved. The thesis concludes with a discussion and conclusions section.

2. Literature review

2.1 General ideas on stability of shell structures

A fundamental performance requirement for subsea pipelines is their ability to withstand external hydrostatic pressure – proportional to the water depth and rising at a rate of 10.055 kPa per metre of water depth. This pressure collapse load is a critical design case for moderate to deep water pipelines and risers.

The collapse of a pipeline due to external pressure is caused by a structural elastic instability. This is strongly influenced by imperfections in or ovality of the cross-section which may be introduced during manufacture of the pipe. The basic concept of structural stability, using the principles of energy conservation in mechanical systems, can be explained as follows: Figure 2.1.1 illustrates a ball bearing on a smooth surface remaining stable after a small displacement in the case of (a), unstable after a small displacement in (b) and in locally neutral equilibrium in (c). For each case, the ball bearing is seeking its lowest energy state of equilibrium.

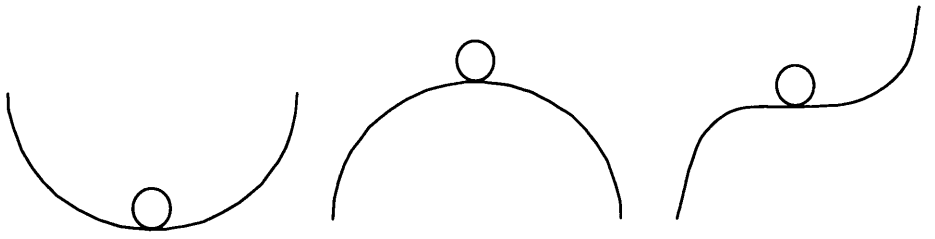

Fig. 2.1.1 Stability Conditions.

Similarly in the case of a strut column, elastic stability or buckling due to axial compression loads can be explained as shown in Figure 2.1.2. Under smaller loads, the strut column compresses axially without bending (see Figure 2.1.2(a)). At the critical axial load, a state of lower energy is reached with column bending, see Figure 2.1.2(b), leading to the strut column buckling phenomenon. At this critical load, therefore, the strut column has become elastically instable. The development of the instability is strongly influenced by a small perturbation in the strut column perpendicular to its axis.

The neutral equilibrium condition is defined as the situation where exists a transition

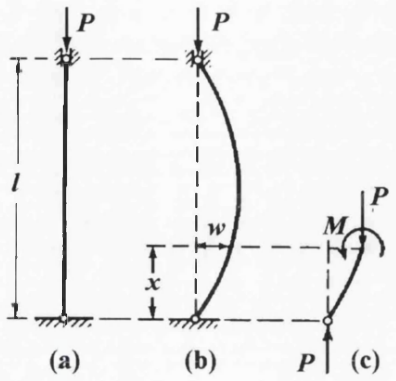

Fig. 2.1.2 Strut column axial collapse.

from stable to unstable equilibrium of the column, this load is usually referred to as the critical load. To determine the critical load for a column, the problem have to be solved and the load that will keep the structure in both equilibrium configuration in a straight line and in a slightly bent configuration. This method is called the method of neutral equilibrium.

The most used approach for the stability of shells are based on linear elasticity concepts. The linear theory predicts stresses and deformations for shells which have very small or deformations within the elastic limit. These deformations assumed that the equilibrium equations for deformed elements are the same as if they were not deformed and Hooke's law applies. The non-linear theory of elasticity is concerned with cases where large deflections take place. Such large deflections are often required when dealing with post buckling problems. The non-linear theory for shells leads to more complex equations and for this reason are more limited.

A typical collapse failure mode is that of ductile collapse. The term ductile collapse implies the study of structural behaviour in situations when a structural material is loaded beyond the regime of its linear response. The term material non-linearity is more commonly used to characterise this situation.

A paper by Donnell /15/ in 1956 on the effect of imperfections on buckling of cylinders founded the basis for the geometric non-linear analysis of shell structures. This paper used the concept of imperfections based on the mathematical modelling factor *U*, or unevenness factor, assumed to depend only on the material and manufacturing process. The buckling of thin cylinders under external pressure is studied by finite-deflection theory, assuming the same modelling of imperfections as had been assumed in Donnell's previous paper /16/ of 1959. Unlike the axial compression case, only a small elastic post buckling reduction in resistance is found, and this only for long cylinders. However, if reasonable imperfections are assumed, failure loads initiated by yielding are found to be of the same order as those indicated

by experiments.

In numerical, non-linear, large deflection analyses of marine structures, use is made of various general upper and lower bound theorems. The collapse theorems applicable to static and dynamic loads can be found in standard textbooks. For cyclic loads, Polizzoto /59/, 1993 presents several useful theorems.

The use of the finite element method (FEM) to determine the eigenvalue of a shell structure provides only the upper bound to the collapse load. This implies that the structure may collapse under a smaller load. In general safety can be ensured and over design can be avoided by either using the lowest upper bound or the maximum lower bound. Berak and Gerdeen /6/, 1990 presented the basic theory for applying collapse theorems in finite element analysis. Mackenzie et al. /44/ and /45/, 1993 used the collapse theorems in an elastic compensation method to obtain upper and lower bound solutions. Piche /57/, 1993 presented a useful method for estimating the lower bound buckling load using matrix norms.

A review of modern literature on structural analysis leads to the conclusion that computational techniques are obviously predominant among the different approaches and is used as a means for the practical solution of the problem. The reason behind this statement can be found in the rapid development of powerful computers and in the availability of efficient and reliable software. Advanced finite element techniques that have been developed over the last 25 years have accumulated long-term experience and insight into the mechanical behaviour of structures and structural elements by generations of engineers. Nevertheless, these numerical computations are based on mathematical models, and so they are dependent on the validity of assumptions and suppositions, such as:

- material properties and constitutive relations;
- idealisation and simplification of construction details;
- imperfections and the initial state of displacements and stresses;
- boundary conditions and the influence of adjacent structures;
- external loads and their simplified distribution in space and time;
- temperature and other environmental conditions.

Therefore, the importance of experiments remains for checking theoretical perceptions, for confirming the theory and in highlighting its weak points and uncertainties.

There are basically two fundamental approaches to classical mechanics that form the foundation of structural mechanics and the theory of structures. The first is the Newtonian or vectorial approach that is the basis of the equilibrium method. This approach goes back to Newton and uses the equilibrium condition as an axiom to establish the governing differential equations of the problem. The integration of this differential equation then yields the required solution. The second approach goes back to Leibniz and Lagrange and uses a scalar function termed the work function as the starting point. The equilibrium of the system is then associated with a stationary value of this function. Since this work function is usually given in the form of an integral, the problem of finding the equilibrium equation is to find the extreme values of this integral. The method of finding such a value is a subject treated in a branch of mathematics known as the calculus of variations. Since all work and energy methods are some special forms and variants of the Lagrangian method, this subject is mathematically and historically closely linked to the development of the calculus of variations founded by Euler and Newton.

The energy method leads to the same differential equations as does the equilibrium method. However, there are reasons for using energy methods rather than equilibrium method. The energy method is more analytical than the equilibrium method the source of error is, therefore, different. The equilibrium method depends more of the geometrical and mechanical visualisation of the system. In energy methods the differential equation and the boundary conditions are established provided the corresponding variational principle is found. Moreover, energy methods are limited in use because it is difficult to solve differential equations exactly except for simple shapes and structures. Another reason for using energy methods is to provide a short solution for otherwise very complicated problems, as can be seen for some highly statically indeterminate structures. Finally, there are philosophical reasons for studying energy methods that have been stressed by Helmholtz with relation to duality present in several problems. For this reason the

inverse problem of the calculus of variations becomes of great importance. In addition, there is another limitation employing energy method in comparison with equilibrium method only conservative systems possess a work function. Therefore, a limited number of engineering problems can be solved using the energy methods.

The mathematical problem is to solve a set of homogeneous differential equations with homogeneous boundary conditions. In general such problems only have a trivial solution. But the coefficients of the equations depend on the magnitude of the basic load, and the load for which a nontrivial solution is possible is known as the critical load. This is a typical formulation of an eigenvalue problem. This technique may be used to illustrate the Euler strut column, (see Figure 2.1.2). The basic load is P. It is possible to formulate equilibrium equations for the finite portion of length x along the axis of the column with a total length of l. The elastic law gives $M - Pw = 0$ where $M = -EI \cdot w''$ is the moment in the column as a function of x. This leads to an homogeneous differential equation for w:

$$w'' + \frac{P}{EI} w = 0 \tag{2.1.1}$$

The boundary conditions are $w=0$ for both ends of the column are also homogeneous. The problem may now be solved in the well-known way leading to the critical load solutions, P_{cr} in (2.1.2), where n is an integer number. The Euler load denoted by P_E is obtained for n=1.

$$P_{cr} = n^2 \frac{\pi^2 EI}{l^2} \tag{2.1.2}$$

2.2. Application methods for shell structures

The most important consideration for conventional offshore single walled pipelines is the resistance to collapse of the tube bearing the combined action of hydrostatic pressure and bending moment. Once the internal diameter to pass the flow rate has been determined for a particular design, there is a requirement to determine the wall thickness. To obtain the wall thickness maximum hydrostatic pressure loads in conjunction with axial loads and bending moment and the allowable stress in the pipe wall need to be considered. An interesting physical phenomenon for pipelines under external hydrostatic pressure is that under certain conditions, a local buckle

can propagate along the pipe length. Thus the propagation pressure under these conditions is an important parameter for the design of subsea pipelines.

The allowable stress in a pipeline wall is limited by the codes and regulations that include design criteria such as those prepared by Battelle, Shell and Det Norske Veritas (DnV). The Battelle criterion is the result of a research programme headed by the Deep Water Offshore Pipeline Group, from 1973 to 1979, and was validated for up to 900 m of water depth. The Shell rules are the result of a joint industry project co-ordinated by the Shell Development Company, from 1974 to 1977 – the goal being the laying of a 30 inch pipeline in 914 m water depth. The DnV criterion is a result of a study carried out by DnV. There are also other well known codes and standards issued by international organisations for pipeline stressing.

The state of the art of pipeline design as well as that of subsea structures in general has been developed as the offshore industry has needed to work in deeper water with larger diameter pipeline systems. Considering the uncertainty of the manufacturing process that induces imperfections in a pipeline's roundness, the design process still needs experimental data and empirical relations to reach a safe and reliable design. The cost of a pipeline system is of the order of hundreds of million of dollars. Any improvement in the design parameters with respect to wall thickness therefore implies a huge economy. On the other hand, the potential danger that a failed oil pipeline represents for the environment also needs to be considered with great care. Therefore, any improvement in this field needs to be backed by well-founded analytical work and good experimental results supporting it. Today there is a lot of work being conducted on collapse and propagation pressure on single walled pipelines.

The most important parameter to be defined during design is the wall thickness. This parameter will command the whole design, its installation, manufacturing and welding design. The structural integrity needs to be checked during initial pipe laying and trenching as well as during operation. Pipe stresses can arise due to external and internal hydrostatic pressures, pipe bending on an undulating seabed, and temperature induced stresses. Subsea pipelines laying on the sea bed without burial have to possess sufficient stability, that is, submerged weight to ensure that

lateral current and wave forces do not cause the pipe to move. The required submerged weight is achieved either with concrete coating or by an increase of the wall thickness. There are four primary load conditions that are considered during a pipeline design: the pipeline laying and burial, the pipeline installed but non-operational, the testing prior to operation and the normal operation.

The installation and testing conditions normally need to be such as to withstand specific environmental criteria such as current profile, wave height and period that are unlikely to be exceeded during these phases. In the remaining conditions, however the riser part of a pipeline is expected to survive to maximum likely environmental conditions such as the 100-year return period current profile and wave height with an acceptable margin of safety.

There are several international codes of practice that deal with requirements and design criteria for pressure vessels, pipelines and risers. These are:

- Det Norske Veritas has, for a long time, published rules for design of ships with detailed recommendations for structural analysis. At the start of offshore operations rules were also developed for offshore structures. The DnV code includes rules for the design of different types of shells elements.
- DnV Standard for Insurance Warranty Surveys in Marine Operations – Part 2:RP5–Lifting.
- DnV 1981 – Det Norske Veritas rules for the design construction and inspection of submarine pipelines and pipeline risers.
- DASt, 1980, Deutscher Ausschuss fur Stahlbau, Richtlinie 013. Treats a large number of shells elements and load cases.
- DIN 18800, Teil 4, Stahlbauten, Stabilititatsfalle, Beulen von Schalen.
- ASME Code Case N-284, 1980. The ASME code gives indications on how the results of computer programs for buckling analysis should be interpreted.
- ECCS, 1988, European Convention for Construction Steel work, develops recommendations for the design of shells with respect to buckling.
- API RP 2A, 1982, American Petroleum Institute, Washington D.C.
- API-SPEC, 1977, Specification for fabricated Structural Steel Pipe.

- API RP 17B – Recommended Practice for Flexible pipe.
- BUREAU VERITAS – NI 364 DTO ROO E – Non bonded Flexible Steel Pipes Used as Flow-Lines
- VERITEC – Guidance's for Flexible Pipes
- NACE RP-01-75 – Control of Internal Corrosion in Steel Pipelines and Piping Systems
- ANSI B 31.4 – American National Standards Institute – Liquid petroleum transportation piping system.
- ANSI B 31.8 – American National Standards Institute – Guide for gas transmission and distribution piping system.
- IP-6 – 1973 – Institute of Petroleum, Petroleum pipelines safety code.
- BS 5500, Specification for Unfired Fusion Welded pressure Vessels.
- BS 8010 Annex B and C – British Standard for pipeline system and subsea pipelines (1990).

This review concentrates on internal and external pressure issues with some other issues also covered on the performance improvement of multi-layered subsea pipelines.

During this literature review, a lot of prior work was found on cylindrical shells. This review is, however, confined to work that is relevant to underwater pipelines and cylindrical shells with medium to thick walls and exclude material on very thin shells. There is also considerable previous work on propagation pressure in thin walled metallic pipes, which is not described here. The relevant prior work on single walled pipes is presented in four sections below which are initially listed here for convenience.

- On buckling propagation pressure of single walled pipe;
- On buckling of single walled pipe due to pressure load only;
- On buckling of single walled pipe under axial load;
- On buckling of single walled pipe with combined loads.

On buckling propagation of single walled pipe:

Dyau and Kyriakides in 1993 /21/ presented work on the propagation pressure of

long cylindrical shells under external pressure. Local imperfections induced in long tubes subjected to high external pressures can lead to local collapse, from which a propagation buckle can be initiated. This results in catastrophic collapse of large sections of the structure. The propagation pressure is the lowest pressure at which such a buckle will propagate. For common steel tube structures the propagation pressure is typically half an order of magnitude lower than the collapse pressure of the intact tubes. This paper deals with experimental and analytical results for establishing propagation pressure. A three dimensional analysis, in combination with experimental results, is used to demonstrate a mechanism of initiation of propagating buckles in long tubes and to study the parametric dependence of the propagation pressure and the effect of axial tension.

Dyau and Kyriakides /19/ in 1993, also worked on the localisation of collapse in cylindrical shells under external pressure. It is well known that long cylindrical shells used in many practical applications involving external pressure loading collapse catastrophically due to limit load instability. The limit load is due to interaction between geometric non-linearities and material non-linearities due to plasticity. This paper addresses the mechanism of collapse triggered by the limit load instability. It is found that following the limit load the collapse quickly localises to a section of the shell a few diameters long. The deformations and stresses in the region of localisation grow with decreasing overall pressure whereas the rest of the structure remains intact and retains only a small residual effect from the limit load instability as it unloads. However, under favourable conditions the localised collapse triggers an instability that propagates along the length of the shell and has the potential of catastrophically collapsing the whole structure. The characteristics of the localisation are parametrically studied through experiment and analysis.

Kyriakides and Chang in 1992 /36/ worked on the effect of axial tension on the propagation pressure of long cylindrical shells. The paper describes the results of an experimental study in which the propagation pressure of long metal tubes was measured in the presence of a constant axial load. Tension was found to significantly reduce the propagation pressure.

Wierzbicki and Bhat /76/ in 1986, worked on the initiation and propagation of

buckles in pipelines. The paper derives a simple closed-form solution for the pressure necessary to initiate and propagate the buckle down the tube. The calculations are performed assuming that the dominant effect on plastic energy dissipation was from the circumferential bending mode. Using a rigid plastic material idealisation a simple moving hinge model which describes the deformation of a ring into a dumbbell shape is proposed. Strain hardening effects are taken into account in an approximate way. The propagation pressure is shown to be controlled by the thickness to diameter ratio of the shell and the ratio of the work hardening modulus to the flow stress of the material. The resulting analytical solution for propagation pressure is compared with the experimental results of Kyriakides et al, 1984 /40/ and the previous analytical solution due to Palmer and Martin 1975 /55/. The solution for the initiation pressure is derived on the basis of the same structural model in conjunction with a new conceptual model for buckle initiation. The solutions for both pressures are shown to correlate well with experimental results reported in the literature.

Kyriakides, Yeh and Roach /39/ in 1984 worked on the determination of the propagation pressure of long circular tubes. The paper attempts to model quasi-static steady-state propagation through a plane strain large deflection, inelastic analysis of the collapse of a circular ring. An energy balance type of argument is used to obtain a lower-bound estimate of the propagation pressure from the ring response. The result is compared with experimental results obtained from stainless steel and aluminium tubes having diameter to thickness ratios ranging between 100 and 10. Good agreement with experimental results was found for ratios D/t>20.

Kyriakides, Babcock and Elyada /40/ in 1984, worked on the initiation of propagation buckles from local pipeline damage. The paper deals with the initiation of a propagating buckle in offshore pipeline. If the external pressure is high enough, then a propagating buckle can be initiated by locally denting the pipe. Such a buckle will propagate at any pressure above the propagation pressure of the pipe. The pressure at which a local geometric imperfection transforms itself into a propagating buckle is known as the initiation pressure. This pressure depends on the geometric characteristics of the damage. The paper restricts itself to a parametric study of

damage produced by point, knife and plate indent. It is found that the geometry of these types of damage can be well represented by the ratio of minimum diameter to maximum diameter of the most damaged section.

On buckling of single walled pipe due to pressure load only:

Yeh and Kyriakides /74/ in 1986, worked on the collapse of inelastic long thick-walled tubes under external pressure both experimentally and analytically. A two-dimensional non-linear formulation of the problem is presented. It is general enough to include initial geometric imperfections of the tube cross section such as initial ovality and wall thickness variation. In addition, the effects of residual stresses and of initial inelastic anisotropy are considered. Experiments on tubes with *D/t* values between 10 and 40 were carried out with good agreement between experiments and theory provided all parameters are modelled correctly. A study of the effect of the various parameters of the problem on the collapse pressure is also presented.

Yeh and Kyriakides /75/ in 1988, worked on the collapse of deep water pipelines. The paper describes a series of full-scale collapse experiments using X-42 and X-65 grade steel tubes. The initial geometric imperfections of the tubes were measured using a specially designed scanning facility prior to collapsing them under external pressure. Geometric deviations from a circular shape were recorded at 90 points around the circumference. The wall thickness was also recorded at the same points. At least 31 circumferential scans were made over lengths of 9 diameters. The stress-strain characteristics in the axial and circumferential directions were measured for each tube. The measured parameters were used to calculate numerically the collapse pressures of the tubes.

Kyriakides and Yon in 1984 /37/ worked on the collapse of circular confined rings under external pressure. The paper presents a study of the large deflection collapse of circular rings confined in a rigid cavity under external pressure. The ring is assumed to be inextensible and to have an initial localised imperfection that causes a small section of its circumference to be detached from the confining wall. The cavity formed is pressurised and its growth examined. The formulation is general enough to allow for large deflections of the ring as well as material non-linearities.

Li and Kyriakides /42/ in 1991, worked on the response and stability of two concentric, contacting rings under external pressure. The problem considered involves two concentric, smoothly contacting rings under external pressure. The outer ring is initially circular but the inner ring has a localised initial imperfection that causes a small section of the ring to be detached from the outer one. Pressure is applied externally but also in the cavity formed by the imperfection. The formulation used is general enough to allow for large deflections with the material of both rings assumed to be linearly elastic. The non-linear response of the structure was found to be characterised by a limit load type of instability. The mode of collapse and the limit load are shown to depend on the geometric characteristics of the two rings and those of the initial imperfection.

On buckling of single walled pipe under axial load:

Bandyopadhyay, Shteyngart, and Eckert in 1994 /5/ worked on the plastic buckling of cylindrical shells. Cylindrical shells exhibit buckling under axial loads at stresses much less than the respective theoretical critical stresses. This is due primarily to the presence of geometrical imperfections even though such imperfections could be very small (for example, comparable to thickness). Under internal pressure, the shell regains some of its buckling strength. For a relatively large radius-to-thickness ratio and low internal pressure, the effect can be reasonably estimated by an elastic analysis. However, for low radius-to-thickness ratios and greater pressures, the elastic-plastic collapse controls the failure load. In order to quantify the elastic-plastic buckling capacity of cylindrical shells, an analysis program was carried out by use of the computer code BOSOR5 developed by Bushnell of Lockheed Missiles and Space Company. BOSOR was developed as a special purpose program for the analysis of buckling and vibration of axisymmetric shells under otherwise rather general conditions. BOSOR determines the buckling load by use of eigenvalue theory. The analysis was performed for various radius-to-thickness ratios and imperfection amplitudes.

Heinen, Hennenberg and Fischer /29/ in 1994 worked on the stability of elastic shell structures by setting up generally valid stability equations for shells. After transformation into integral equations, ordinary time dependent differential equations are derived through series expansion of the disturbance-induced

displacements. Any fundamental state can be substituted in these equations, and its kinetic stability can be investigated. This is demonstrated in this paper for cylindrical shells subjected to sudden axial loads.

Donnell and Wan /16/, in 1950, published a basic paper on the effects of imperfections on buckling of thin cylinders and columns under axial compression. The paper introduces the concept of imperfections in the mathematical model through the unevenness factor that depends only on the material and manufacturing process. The paper presents results using finite-deflection theory.

On buckling of single walled pipe with combined loads:

Bai, Igland, and Moan /3/, in 1995, worked on the collapse of thick tubes under combined tension and bending. This paper presents finite element analyses of the collapse behaviour of thick tubes ($10 < D/t < 40$) under pure bending and combined tension and bending loads. Parametric studies of collapse moment and critical curvature for thick tubes under pure bending have been carried out to study the effects of diameter to thickness ratio D/t, yield parameter to Young's modulus ratio σ_y/E, strain-hardening parameter n and material anisotropy parameter S . Formulae to predict collapse moment and curvature are derived based on these parametric studies. It has been confirmed that the modelling uncertainty of the derived equations is small. The responses of thick tubes under combined tension and bending have been studied. The effect of loading paths is presented. Criteria to determine ultimate collapse of tubes, for example, limit load, extreme fibre strain and mean axial strain, are discussed. Parametric studies have been carried out on the effect of the collapse envelopes on diameter to thickness ratio D/t, material grade, strain-hardening parameter n and material anisotropy parameter S. Formulae for moment-tension, curvature-tension and curvature-axial strain envelopes are proposed based on the sensitivity study.

Estefen /24/ in 1994, worked on the ultimate strength behaviour of submarine pipelines under external pressure and bending. Moan et al /46/ in 1994, worked on limit states for the ultimate strength of tubular subjected to pressure, bending and tension loads.

Kyriakides and Ju /38/ in 1992, worked on the bifurcation and localisation instabilities in cylindrical shells under bending. This two-part series of papers is concerned with the response and various instabilities that govern the behaviour of circular cylindrical shells under pure bending. Part I describes the experimental study and Part II presents the numerical simulation of the various phenomena observed experimentally. Experiments were conducted on long aluminium 6061– T6 shells with 11 different diameter-to-thickness ratios ranging from 60.5 to 19.5. For such geometry, the structural response and inherent instabilities are strongly influenced by the plastic characteristics of the material. Thinner shells were found to develop short wavelength periodic ripples on the compressed side of the shell. The shells buckled locally and collapsed soon after the appearance of the ripples. Thicker shells were found to exhibit limit load instability as a direct consequence of the ovality of the shell cross-section caused by bending. Following the limit load, the ovality was found to localise, leading to the eventual collapse of the shells. For shells with intermediate *D/t* values, short wavelength ripples developed at the same time as localisation of ovalness was recorded. The shells buckled locally and catastrophically following the development of a limit load.

Ju and Kyriakides /32/ in 1992, covered the bifurcation and localisation instabilities in cylindrical shells under bending. This second phase study is concerned with the prediction of the response and various instabilities found in Part 1 above to govern the elastic-plastic flexure of circular cylindrical shells. Sanders' shell kinematics and the principle of virtual work were used to formulate the problem. A Rayleigh-Ritz procedure was used to discretize the problem. The resultant non-linear equations were iteratively solved using Newton's method. The three types of behaviour involving bifurcation into short wavelength ripples, localisation following the attainment of a natural limit load and interaction of the two was studied. In each case the predicted response was found to be in very good agreement with experimental results.

Dyau and Kyriakides /22/ in 1992, presented work on the response of elastic-plastic tubes under combined bending and tension. This paper is concerned with the response of long, relatively thin-walled tubes bent into the plastic range in the presence of axial tension. The work is motivated by the design needs of pipelines

installed and operated in deep offshore waters. The problem is studied through a combination of experiment and analysis. In the experiments, long metal tubes were bent over a smooth, circular, rigid surface (mandrel). Bending of the tubes was achieved by shear and axial ends' loads. The experimental arrangement is such that a significant section of the test specimen is loaded and deformed in an axially uniform fashion. The ovality induced in the specimen was measured as a function of the axial load in the tube for two mandrel radii. A two-dimensional numerical simulation of the problem has been developed and validated against the experimental results. This analysis was used to conduct a parametric study of the effect of tension on the ovality induced in a long tube during bending.

Ju and Kyriakides /31/ in 1991, worked on the bifurcation buckling versus limit load instabilities of elastic-plastic tubes under bending and external pressure. Commonly used procedures for installing offshore pipelines can induce substantial bending to the line in the presence of external pressure. These combined loads can lead to catastrophic collapse of the structure. For typically used steels and higher diameter-to-thickness ratios (*D/t*), bending is limited by a bifurcation type of instability; for lower *D/t* values, the structures exhibit limit load types of instabilities. Similar distinctions can be made for bending in the presence of external pressure. Previous work (Corona and Kyriakides, 1988) addressed primarily the limit load types of instabilities. In this paper, this analysis is extended to include bifurcation instabilities. The predictions from the two types of analyses are critically compared to experimental results and recommendations about the regime of applicability of each are made.

Corona and Kyriakides /10/ in 1991, worked on experimental investigation of the degradation and buckling of circular tubes under cyclic bending and external pressure. Cyclic bending of tubes into the plastic range of the material leads to a progressive accumulation of ovality of the tube cross-section. Persistent cycling leads to local catastrophic buckling of the tube. This paper presents an experimental study of the problem. The main objective of the study was to establish the effect of the cyclic bending history and of the external pressure on the rate of accumulation of ovalness and on the onset of instability. The cyclic loading histories examined

include curvature symmetric bending, bending about a mean value of curvature and moment-controlled bending about a mean value of moment. The rate at which ovalness accumulates in curvature-controlled cyclic bending was found not to be significantly affected by a mean curvature in the cycles. Moment-controlled bending about a mean moment leads to ratchet in curvature as well as in ovalness. External pressure accelerates the accumulation of ovalness and leads to buckling in fewer cycles than in the corresponding pure bending cases. This was found to be true for all bending histories considered. Significant similarities were observed between the response and onset of instability in the monotonic bending case and all cyclic bending cases. For a group of aluminium tubes' instability was found to occur when the ovalness of the cross-section reached a critical value. This critical value was found to be relatively independent of the bending history followed.

Ellinas and Croll /23/ in 1986, worked on the elastic-plastic buckling design of cylindrical shells subjected to combined axial compression and pressure loading. The paper describes a procedure for predicting the elasto-plastic axisymmetric collapse of cylinders subjected to combinations of axial compression and pressure loading. This allows the modelling of radial pressure induced deformations, boundary effects and initial geometric imperfections in terms of an equivalent imperfection in a column type bifurcation analysis. Together with the incorporation of more rational means of specifying geometric tolerances, it is used to develop compact design-orientated procedures for predicting safe loads for this form of elasto-plastic collapse of cylinders.

Murphey and Langner in 1985 /52/ presented work on ultimate pipe strength under bending collapse and fatigue. The paper deals with pipeline installation in deep water. The suspended pipe spans were subjected to significant bending and external pressure loads, including cyclical bending and to a lesser extent tension and torsion loads. They present some relations for predicting ultimate buckling and collapse loading conditions as well as the deformation of pipe under loads less than ultimate and the fatigue life of pipeline girth welds under cyclic loads.

2.3 Composite shell structures under external pressure

The composite cylinder structure has not been studied as extensively as the single cylinder. Multi-layer and double walled shell structures appear more recently in the development of new materials. The target is the aeronautical industry where weight versus strength is often more important than the cost itself. Therefore, most of the work done on sandwich or double walled shells has been for aeronautical applications.

There are also two books on sandwich construction /58/ by Plantema, 1966 and /2/ by Allen, 1969. These books describe structural sandwich construction and include the whole theory for its analysis.

Montague has addressed the double-skin composite construction structural problem aimed at subsea applications for pressure vessels – see /49/ in 1979, /50/ in 1981 and /51/ 1969. He describes theoretical and experimental work on steel-concrete-steel composite cylindrical shells subjected to external pressure. The results present good correlation with failure predictions on a lower bound analysis. He reaches the conclusion that this form of construction can be relied upon to provide a totally stable structure up to the pressures causing yielding of the steel skins with a reserve of strength beyond this pressure. The conclusion is that the composite shell is insensitive to initial non-circular imperfections up to an external pressure that causes the steel skins to yield. Up to this pressure, the radial displacements are nearly axisymmetric. A vessel with concrete filler will sustain a higher pressure before the steel skins start to yield than will a similar vessel with a resin-glass filler because the concrete is stiffer.

The problem of the thick cylinder under external pressure including the sandwich structure has also been addressed by Baker /4/ in 1972 in the last chapter of his book. He presents a summary of sandwich type construction that is a composite construction consisting of three integrally attached layers. The middle layer of the sandwich is the core; the outer and inner layers are the facing sheets. He based his work in the papers by Zahn and Kuenzi /79/ in 1963 on buckling of cylinders for sandwich construction in axial compression-orthotropic cores; March et al /43/ in 1958, on buckling of sandwich cylinders in torsion; Kiciman et al /33/ in 1961, on

the stability of honeycomb sandwich cylinders and Kuenzi et al /34/ in 1965 on sandwich cylinders of finite length under uniform external pressure. Most of the work done in the stability of sandwich structures was based on the previous work of Raville in 1954 and 1955.

Raville has derived expressions for the buckling of sandwich cylinders under uniform external lateral pressure for long cylinders /63/ in 1954, including skins of moderate and unequal thickness /64/ in 1955, and including finite length /65/ in 1955. These works were issued on the ANC-23 panel on sandwich construction of the Department of the Air Force-Navy-Civil subcommittee in the Forest Products Laboratory of United States Department of Agriculture Forest Service. Following this work Norris and Zahn /54/ in 1963 issued numerical results and algebraic equations based on the Raville mathematical model that results in practical curves and a simplified equation which can be easily used for prediction of buckling loads on sandwich panels.

The work done by Choo et al /11/ in 1991, addressed the limit strength of composite sandwich cylinders subjected to external pressure. Zhou et al in 1985 /80/ also worked on the computation of non-linear instability for multi-layered cylindrical-shells.

Brown and Hyer in 1994 /8/ showed the influence of layer waviness on the stress state and failure pressure of thick cross-ply composite cylinders loaded by external hydrostatic pressure. Layer waviness is idealised as a single isolated region of waviness in an otherwise perfect cylinder. The waviness occurs in only the circumferential direction and is assumed to extend indefinitely in the axial direction. Waviness is assumed to occur because particular circumferential layers experience local radial displacement during consolidation, resin richness and resin depletion occurring on either side of the locally displaced layers. Stresses are computed by using a finite element analysis that models the isolated region of waviness in the cylinder on a layer-by-layer basis. Some details of the model are discussed; the model accounting for a range of amplitudes of waviness, a range of cylinder radius-to-wall thickness ratios, and whether the isolated waviness is located near the inner radius or near the outer radius of the cylinder wall. The paper illustrates the

behaviour of the three primary stresses, namely inter laminar shear, inter laminar tension, and fibre-direction compression, all of which are important to failure. Pressure capacity is determined by applying the maximum stress failure criterion. It is shown that inter laminar shear, while absent in the perfect cylinder, can be responsible for a 50% reduction in pressure capacity relative to the wave-free perfect cylinder. Also it is shown that fibre-direction compressive stresses are increased by the presence of waviness, and that inter laminar normal tensile stresses caused by the waviness are potentially responsible for failure.

Bonanni /7/ in 1994 presented a paper on the stability analysis of thick-section composite cylinders under hydrostatic pressure including three-dimensional (3-D) effects and non-linear material response. The work described in this paper integrates a 3-D micro-mechanics-based non-linear constitutive model for laminated composite materials into 3-D structural analyses performed with the ABAQUS general-purpose finite element code. The non-linear model and its incorporation into ABAQUS are described. The method is demonstrated through 3-D stability analyses of thick, unstiffened AS4/3501-6 carbon/epoxy circular cylinders under external hydrostatic pressure. The results of two-dimensional (2-D) shell finite element analyses of these cylinders are also presented for comparison. The cylinders analysed are geometrically identical and are subjected to the same loading and boundary conditions. Five different ply lay-ups are considered, including cross-ply, quasi-isotropic, and layers oriented at 45 degrees. Modelling the non-linear material response is found to reduce the predicted cylinder collapse load by up to 50% when layers oriented at 45 degrees to the cylinder axis are present in the laminate. The role of material non-linearity in the plane of the laminate versus through-thickness non-linearity is discussed for the cylinders analysed.

Dong and Etitum /14/ in 1995 presented work on three-dimensional stability analysis of laminated anisotropic circular cylinders. A linear bifurcation stability of laminated anisotropic circular cylinders is investigated on the basis of three-dimensional elasticity using Biot's incremental deformation theory. A finite element code employing radial discreteness is formulated for the calculations. By this approach, the laminate's thickness profile may be composed of an arbitrary number of bonded

elastic anisotropic layers, each of which may have its own mechanical properties, thickness and initial stress state. Using a solution that is periodic axially and circumferentially in the variational derived equilibrium equations yields an algebraic eigenvalue problem, where the critical (lowest) eigenvalue is sought. It represents the ratio of the buckling stress state to initial stress state and its associated eigenvector contains the radial distribution of the displacements. A parametric study on a series of regular symmetric and antisymmetric cross-ply and angle-ply laminated composite cylinders under axial compression and torsion was conducted, where the data can be used to assess the accuracy and range of validity of stability predictions based on shell theories. An example of the axial compression of a thick-walled laminated composite cylinder is presented to illustrate an instability phenomenon where internal and surface deformations are present.

Chryssostomidis and Papadakis /12/ in 1994 worked on the buckling analysis of sandwich shell structures subjected to hydrostatic load. This paper examines the buckling phenomenon of sandwich cylindrical shell structures subjected to hydrostatic pressure. Global bifurcation buckling is considered, and the effect of discrete ring stiffeners on the critical pressure is analysed. The local buckling problem is discussed, including the influence of the shape and the thickness of the core stiffeners on the critical load. Finally, the paper treats the sensitivity of local and global buckling on the thickness distribution between the inner and outer shells of the sandwich structure.

Hamidzadeh and Chandler /28/ in 1991 worked on the circumferential vibrations of three layered sandwich cylinders. The problem of forced vibrations of three layered cylinders of infinite extent subjected to boundary stresses that do not vary along the axis is considered. Linear viscoelastic theory is employed and the vibration of a thick single cylinder is accurately formulated. A solution for a cylinder with three constrained layers is developed by utilising the stresses and displacements at all interfaces, and by complying with the compatibility requirements at each interface. Computed results are compared with an available approximate solution and satisfactory agreement is established. The reported solution is exact and is not limited to thin cylinders.

DiSciuva and Carrera /13/, in 1990, worked on the static buckling of moderately thick, anisotropic, laminated and sandwich cylindrical shell panels. This paper deals with the development of linearized equations governing the buckling behaviour of moderately thick, anisotropic, laminated and sandwiched cylindrical shell panels faced with fibre-reinforced plastic under uniform shear and normal membrane forces. The formulation takes into account the transverse shear flexibility. Two approaches for the approximate solution of the elastic stability equations are developed. The first approach is an analytical approach of the Galerkin type and rests upon the principle of virtual work. The second is a finite-element displacement approach. Some numerical results are presented and compared with other results from the open literature.

Dorninger and Rammerstorfer /18/ in 1990, worked on layered composite shell elements for elastic and thermoelastic stress and stability analysis at large deformations. A finite shell element for layered fibre reinforced composite shells has been developed. The degeneration principle is used in combination with specific kinematics assumptions. The thermoelastic material is either described by the behaviour of the local components, that is fibre and matrix material laws and geometrical configuration in each layer, or by the overall orthotropic layer material laws. Thickness integration for obtaining the different contributions to the shell element's stiffness matrix is performed analytically and prior to the numerical in-plane integration. This leads to a considerable saving in computer time during the incremental-iterative analysis. Geometrical non-linearity in terms of large deformations and material non-linearity in terms of layer cracking are taken into account. Accompanying eigenvalue analyses allow the determination of the – sometimes rather complicated – buckling behaviour with non-linear pre-buckling deformations.

Palchevskii /56/ in 1988, worked on the stability of a multi-layer cylindrical shell with inter-layer pressure. The problem of the stability of a cylindrical shell or circular ring with one side connected to a surrounding elastic or absolutely rigid space has been studied in a number of investigations. In solving this problem for thin shells it is possible to neglect the variation of the shell geometry as a result of

subcritical behaviour, and also changes in the area of contact with the surrounding space during the loss of stability. Consequently, the solution can be obtained as a linear formulation, as in the present paper.

2.4 Discussion of the literature review

The literature review was divided in two main blocks, the first (section 2.2) being concerned with the single walled cylindrical shell. In spite of the fact that this work is not directly related to multi-layered pipes, the review identified concepts and issues that are relevant to the work of this thesis.

The propagation of buckles is a very important topic for offshore pipelines because its occurrence can lead to huge consequential losses of revenue. In fact, the design requirement to avoid propagation of buckles governs the wall thickness definition according to some standards (for example the Institute of Petroleum IP-6 code). In practice design includesbuckling arrestors which consist of local increases in the wall at some position along the pipeline. The device acts to increase locally the external pressure resistance and is thus able to block the buckling propagation and isolate the amount of pipe damaged. The review of the literature in this field presents most of the fundamental work that guides designers and regulatory authorities in this field. The review shows that the field has been thoroughly explored in theoretical terms and that theories are validated by experimental data.

The work on collapse pressure analysis of single walled pipes is discussed in greater detail in the following section 2.5 and is, therefore, not considered further here.

Section 2.3 of the review investigates previous work on composite shell structures under external pressure. There was much less directly relevant work that was found on the specific problem addressed here - that is underwater pipes with a homogeneous annular material surrounded by thin steel shells. The majority of the relevant prior work was concerned with aeronautical applications and honeycomb constructions. The most relevant work found was that of Raville in a series of papers /63/, /64/ and /65/ from 1954. He has developed an elastic stability analysis based on Timoshenko's theory to determine the collapse pressure of a multi-layered cylinder. Another later investigation by Montague /47/ in 1975 has extended the approach to

an elasto-plastic failure of the annular material.

Exhaustive attempts were made during the literature review to find appropriate experimental data to use in the present research. The only appropriate work that reported experimental data in sufficient details to enable it to be used was from Montague /47/. He provided all the appropriate geometric and material properties details to enable a comparison with theory. The limited amount of other experimental work found had insufficient supporting data to enable it to | property

2.5 Theoretical background to present work

This last section of the literature review brings together the specific elements of the previous work that form the starting point of the work presented in this thesis on the collapse of multi-layered pipes under external pressure.

This previous work is based ultimately on the analysis of a single wall cylinder subjected to external pressure which has been considered extensively in the literature. Timoshenko /73/, 1936, (art. 11.5, page 474), presents a good overview of the classic approach to the problem although Donnell /17/, 1976, (art. 7.3 page. 406), Brush /9/, 1975, (art. 5.5a, page. 161) and Flugge /27/, 1973, (art. 8.2.2.3, page 459) also deal with the subject in comparable depth.

The stability equations for cylindrical shells have been available in the literature since the late 1800s. For cylinders subjected to axial compression, Lorenz presented the earliest analytical solutions, in 1911. Solutions for buckling under uniform lateral pressure were given by Southwell in 1913 and by Von Mises in 1914. In 1932, Flugge presented a comprehensive treatment of cylindrical shell stability, including combined loading and cylinders subjected to bending. Results for cylinders subjected to torsional loading were given by Schwerin in 1925 and Donnell in 1933.

The Donnell equations form the basis for more stability analyses in the literature than any other set of cylindrical shell equations. The equations give accurate results for cylindrical panels that are relatively flat before deformation and for complete cylindrical shells whose displacement components in the deformed configuration are

rapidly varying functions of the circunferential co-ordinates. In recent years much more of the work in shell analysis has been oriented toward computer based solutions. In such case simplicity of the governing equations is of less importance. As a consequence, interest in the Donnell equations has diminished.

The complete derivation for the buckling of circular rings and tubes under uniform external pressure and the buckling of a tube of finite length under uniform external pressure, torsion and tension is used as a starting point in some of the work presented here. The appropriate analysis is presented again in Appendix A.1. The principal result from this analysis is the critical external pressure, q_{cr} for buckling of a circular ring is:

$$q_{cr} = \frac{E}{4(1-\nu^2)}\left(\frac{h}{R}\right)^3 . \tag{2.5.1}$$

where R is the mean radius of the ring, h is the wall thickness, E is the Young's modulus and ν is the Poisson ratio of the wall material. This very well-known result demonstrates that the collapse pressure of such structure is proportional to the cubic ratio of the wall thickness to the mean radius. Another form of the above result is:

$$q_{cr} = \frac{3EI}{(1-\nu^2)R^3} . \tag{2.5.2}$$

where I is the second moment of cross-section area about its centroid. When written in this form, it is clear that the critical pressure of a long tube is directly proportional to the second moment of area of the wall and cubically to the inverse of the mean radius. Therefore, a multi-layered pipe, which implies a significant increase in this second moment of area, should as a first approximation, deliver a greater collapse pressure.

The pitfall in this first approximation is that the above solution was derived based on a thin wall (membrane theory) with the whole structural system behaving elastically thus the stresses induced through the walls during the axissymmetric pressure loading must remain below the yielding stress, σ_y. If the external pressure q_y, at which yielding in the extreme fibre begins is to be calculated, including an ovality w_1, the following equation from Appendix A.1 can be used:

$$q_y^2 - \left[\frac{\sigma_y}{m} + (1+6mn)q_{cr}\right]q_{cr} + \frac{\sigma_y}{m}q_{cr} = 0 . \tag{2.5.3}$$

where, $m = R/h$, and $n = w_1/R$, where w_1 is the maximum initial radial deviation from a circular form, R is the mean radius of the ring, h is the wall thickness, q_y is the external pressure at which yielding begins, and σ_y is the yielding stress.

These formulations give a good insight into the problem of the buckling of cylindrical shells. Among the main parameters that govern the buckling load is the initial ovality. Small variations of ovality leads to a very large drop in the collapse pressure as pointed out by Timoshenko /73/, figure 7-9 page 293.

The solution for tubes of finite length also presented in Appendix 2 uses the same basic assumptions as elastic membrane theory. This solution was originally proposed by Flugge /27/, 1973, for the buckling of a cylinder with finite length subjected to uniform external pressure, axial load, and torsion. Several key points come out from this analysis. Finally, the external pressure capacity of the pipe increases considerably when it is subjected to axial tension. In addition, an increase in internal pressure does not perceptibly improve the axial load. For external pressure loads only, the formulation also demonstrates that for very long pipes, the solution converges asymptotically to the solution of rings, equation (2.5.2). In addition, when the pipe is shortened, (length smaller than 50 times the mean radius) the critical external pressure increases and the wave mode of failure would be greater than 2. Figures A.2.7 and A.2.8 from Flugge /27/ and reproduced in Appendix 2 and illustrate these tends.

The classic approach for multi-layered pipe with finite length was developed by Raville /65/, 1955. These results have the same general tend, see Appendix 4 section A.4.3. On the other hand, multi-layered pipes that incorporate an intermediate material need a methodology that brings in the interaction of the intermediate layer.

The basic work of Raville /63/, 1954, addresses the problem of a long sandwich pipe. Because of the relevance of this methodology, Raville's derivation is also presented in Appendix 4. He derives the following relationship

$$P_{cr}\frac{a\left(1-\nu_f^2\right)}{E_f f}=\frac{3(1-b/a)^2}{1+(b/a)^2}. \qquad (2.5.4)$$

where E_f and ν_f are respectively the Young's modulus and Poisson ratio of the

faces, f is the thickness of the faces, a and b are respectively the mean radius of the outer and inner faces. The principal assumption of Raville is that the Young's Modulus, E_c and shear modulus, $G_{r\theta}$ of the core are infinite. This leads to the above simple relationship of equation (2.5.4). However, it should be noted that his work includes also the effects of finite E_c and $G_{r\theta}$ – see Appendix 4.

3. Stress analysis of multi-layered cylinder with internal pressure

3.1 Introduction

The objective of this part of the thesis is to investigate the stress distribution in multi-layered long cylinders with an intermediate layer of a different material subjected to an axisymmetric loading due to internal pressure. Using axisymmetric loading on a cylinder under internal pressure considerably simplifies the resultant stress and strain analysis. In particular, the work compares the structural performance of a single pipe and an equivalent double walled pipe utilising the same weight of steel in terms of the von Mises stress per unit pressure difference between the inner and outer surfaces. This is done for a wide variation of pipe geometry and stiffness of the annular inner layer. Section 3 gives the methodology developed for this whereas the results are presented in section 6.

First, the single layer cylinder problem is reviewed. The solution is then extended for multi-layered cylinders by using deformation compatibility relationships between the layer interfaces. A computer program, using FORTRAN code, was then written to perform all the analyses presented here. The analytical solution has also been compared with results obtained from the finite element package called ABAQUS.

The main assumption employed in the analysis is that the multi-layered cylinder has inner and outer layers or faces made from a material of high Young's Modulus such as steel with the intermediate layer or core made of a less stiff material. Thus the core is taken to have a Young's Modulus E_c that is less than that of the faces E_s. The comparisons of internal stress are made between the multi-layered pipe and a single layer pipe using the same amount of material of high Young's Modulus. It means that the material of the single layer is split into two thinner layers that will constitute the faces of the equivalent multi-layered pipe.

In considering the stresses on an element of the pipe wall, it is assumed that there are no axial forces on the pipe. There are, therefore, only two main stress components: the hoop or circumferential stress and the radial stress. However, to have a better representation of the actual stress state of the element, the von Mises criterion is used. This can be written as

$$\sigma_{Mises} = \sqrt{\sigma_{hoop}^{\ 2} + \sigma_{Radial}^{\ 2} + \sigma_{hoop} \cdot \sigma_{Radial}} \,. \qquad (3.1.1)$$

Comparisons between the multi-layered pipe and an equivalent single walled pipe are made for a range of parameter ratios. The first of these is the ratio *m*, of the Young's Modulus of the core material (E_c) to the high Young's Modulus material (E_s) then $m = E_s/E_c$. The other parameter ratios used are the outside diameter to wall thickness ratio for the single layer pipe OD/t, the thickness ratio of the core to the inner face $\eta = co/f_1$ and position of the core relative to the inner and outer faces as described by ratio $\chi = f_1/t$ and generic position in the wall thickness $\rho = (r-a)/t$. Figure 3.3.1 shows the pipe radius nomenclature, see also the Table 3.11

	Symbol	Value
Inner face thickness	f_1	*b-a*
Core thickness	*co*	*c-b*
Outer face thickness	f_2	*d-c*
Total thickness	*t*	*d-a*
Core thickness ratio	η	(*c-b*)/(*b-a*)
Core position	χ	(*b-a*)/(*d-a*)
Radial position	ρ	(r-a)/(d-a)

Table 3.1.1 Ratios nomenclature for multi-layered pipe.

The comparisons are made considering variations on the Young's modulus relationship betweethe materials used in the faces and the sandwiched materials$m = E_s/E_c$, the diameter to thickness ratio for the single layer pipe OD/t, and the thickness ratio of the core to the faces η and position of the core χ .

The results are summarised graphically. The radial position *r*, along the wall of the single cylinder as well as for the composite cylinder was also normalised with the total wall thickness. Therefore, the parameter ρ is zero for the inner radius position and one for the outer radius position.

3.2. The single layer pipe

Consider a two dimensional element of a long, thick walled single layer cylinder of uniform material strength under internal pressure, as shown in Figure 3.2.1. There are

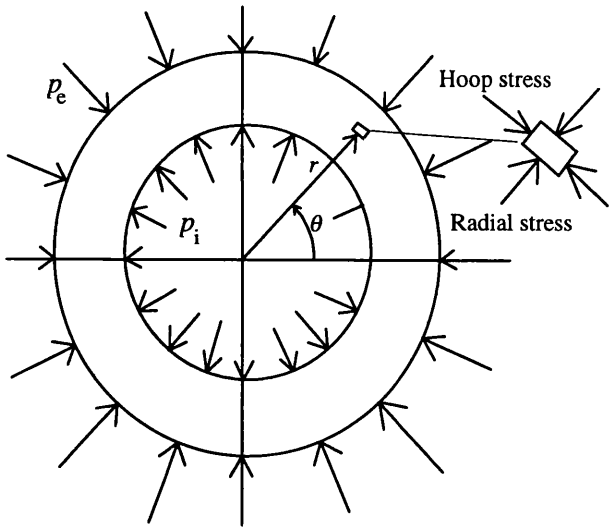

Fig. 3.2.1 - Single walled pipe cross-section.

no axial forces or forces parallel to the cylinder axis. Therefore, no stresses act in that direction. The hoop stress σ_h, will act on both radial surfaces of the element in the circumferential direction along with the radial stress σ_r. Since the weight of the element is neglected in the force system acting on the element both these stresses will vary with radial position, but are constant with angular position θ. This is a standard thick cylinder analytical solution that can be written as

$$\sigma_h = \frac{a^2 p_i - b^2 p_e}{b^2 - a^2} + \frac{(p_i - p_e)a^2 b^2}{(b^2 - a^2)r^2},$$
$$\sigma_r = \frac{a^2 p_i - b^2 p_e}{b^2 - a^2} - \frac{(p_i - p_e)a^2 b^2}{(b^2 - a^2)r^2}. \qquad (3.2.1)$$

where p_i and p_e are respectively the internal and the external pressures, a and b are respectively the inner and the outer radius of the cylinder, and r is the generic radial position. Figure 3.2.1 illustrate this nomenclature. These results are well known as Lame's equations, available in standard structural textbook such as Boresi, Schmidt and Sidebottom, 1932 (fifth edition 1993) - Advanced Mechanics of Materials, page 440. Note that the sum of the stresses is always a constant. This is a consequence of the two dimensional nature of the loading. The deformation relation can also be written as

$$u(r) = \left(\frac{1-\nu_s}{E}\right)\left(\frac{a^2 p_i - b^2 p_e}{b^2 - a^2}\right)r + \left(\frac{1+\nu_s}{E}\right)\left(\frac{p_i - p_e}{b^2 - a^2}\right)a^2 b^2 \frac{1}{r}. \qquad (3.2.2)$$

Where, u is the radial strain, E and ν_s are respectively the Young's Modulus and Poisson ratio of the cylinder material.

3.3. The multi-layered cylinder – analytical model

Relationships for stresses and strains may be developed for the multi-layered cylinder in the same fashion as carried out above for the single layer cylinder. The geometry of such a cylinder can be defined by the inner face radius a, the outer face

radius d, the intermediate layer having as inner radius b and outer radius c. The internal and external pressures will have the same nomenclature of p_i and p_e respectively. In this case, two more pressures need to be defined that will be acting on the two internal interfaces of the pipe. These are defined by p_1 and p_2 as shown in Figure 3.3.1.

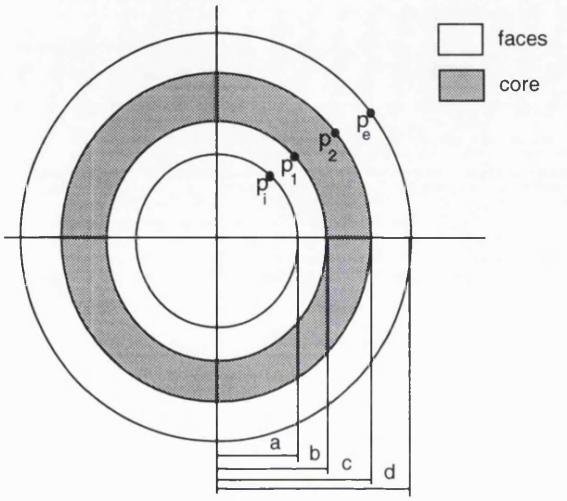

Fig 3.3.1 Multi-layered pipe cross-section.

The expressions for the stresses along the radius are similar to the expressions of (3.2.1) as function of the internal and external radii and the pressures on the layer. The solution for the double walled cylinder is obtained by determining the pressure on the intermediate layer. These pressures are obtained by using the strain compatibility relationships for the displacement of the cylinder surfaces at the boundaries of outer and inner layers and the intermediate layer.

Using δ_1 and δ_2 as the displacements of the cylinder surfaces of the intermediate layer at its inner and outer boundaries, at radius b and c respectively, three cylinders with the following geometry and pressures can be defined as described in Table 3.3.1 below:

Cylinder layer		Young's modulus	Inner radius	Outer radius	Inner pressure	Outer pressure	Inner displacement	Outer displacement
1	inner layer	E_s	a	b	p_i	p_1	u_i	u_1
2	core layer	E_c	b	c	p_1	p_2	δ_1	δ_2
3	outer layer	E_s	c	d	p_2	p_e	u_2	u_e

Table 3.3.1 Nomenclature for multi-layered pipe.

Using, this nomenclature the compatibility equations can be determined. Note that the displacements at the boundaries of each layer are evaluated:

$$u_1 = \delta_1 \ , \quad u_2 = \delta_2 . \tag{3.3.1}$$

Combining the displacement given by equation (3.2.2) with compatibility equations (3.3.1) gives:

$$\frac{2a^2p_i - (a^2+b^2)p_1}{b^2-a^2} + p_1v_s = \left[\frac{(b^2+c^2)p_1 - 2c^2p_2}{c^2-b^2} + p_1v_c\right]m,$$

$$\frac{2b^2p_1 - (b^2+c^2)p_2}{c^2-b^2} + p_2v_c = \left[\frac{(c^2+d^2)p_1 - 2d^2p_e}{d^2-c^2} + p_2v_s\right]\frac{1}{m}, \qquad (3.3.2)$$

where m is the ratio E_s/E_c defined above. This is a system of two equations and two unknown variables p_1 and p_2. Rearranging in matrix form gives:

$$M = \begin{bmatrix} \frac{2\cdot b^2\cdot m}{b^2-c^2} & \frac{c^2+d^2}{d^2-c^2} + \frac{b^2+c^2}{c^2-b^2}\cdot m + v_s - mv_c \\ \frac{a^2+b^2}{b^2-a^2} + \frac{b^2+c^2}{c^2-b^2}\cdot m + mv_c - v_s & \frac{2\cdot c^2\cdot m}{b^2-c^2} \end{bmatrix},$$

$$p = \begin{bmatrix} p_1 \\ p_2 \end{bmatrix}, \qquad b = \begin{bmatrix} \frac{2\cdot d^2}{d^2-c^2}p_e \\ \frac{2\cdot a^2}{b^2-a^2}p_i \end{bmatrix}, \qquad (3.3.3)$$

$$M\cdot p = b \quad \Rightarrow \quad p = M^{-1}\cdot b,$$

These equations may be solved with simple FORTRAN computer program.

Based on this solution a comparison between the structural performance of the multi-layered pipe and the conventional single walled pipe subjected to internal pressure is carried out for a wide range of pipe geometry and stiffness of the intermediate material.

The objective is to evaluate the level of the stresses along the wall of the multi-layered which has the same amount of steel as a single walled pipe subjected to the same internal pressure. This means that the conventional single walled pipe will have its wall split in two thinner walls and an intermediate material is placed into the annulus space. Obviously, the intermediate material being examined should have lower strength and thus cost in comparison with the skins.

The structural performance is measured as the ratio between the von Mises stresses reached in the radial direction (normalised by the wall thickness) in both pipes, i.e. the multi-layered pipe construction and the conventional single walled pipe.

The main presentation of the results and the discussion of these are in section 6.1. However, in general terms the comparison demonstrated lower level of stresses in

the skins of the double walled pipe than that seen in the single walled pipe. It suggests that the multi-layered pipe configuration improves the structural performance of the pipe by withstanding the same amount of internal pressure and yet reducing the stress level in the skins.

3.4 ABAQUS Modelling

The finite element package ABAQUS /1/ version 5.5, 1995 was used to perform the internal pressure stress and strain analysis for the validation of the analytical model described in the previous section.

The ABAQUS system includes a general purpose finite element program, an interactive pre-processor used to create models for ABAQUS and an interactive post-processing program which displays and output lists from restart and results files written by ABAQUS.

Since the ABAQUS analysis modules are batch programs, the objective is to assemble an input file which describes a problem so that ABAQUS can provide an analysis. Input files for complex simulations can be large, but can be managed without too much difficulty by using the convenience features built into the program's input structure.

An input file for ABAQUS contains model data and history data. Model data define a finite element model, the element nodes, element properties, material definitions, and so on. History data define what happens to the model - the sequence of events or loading. The definition of a step includes the procedure type such as static analysis, the modelling of transients as well as control parameters for time integration or for the non-linear solution methodology, the loading, and output options.

First, the single walled cross-section was solved based on the well-know analytical solution for the stress and strain distribution along the radius of a single walled cross-section. After that a finite element model was prepared to perform the comparison with the analytical results. The construction of the input file will be described later in this section. Figure 6.1.1 in Section 6 illustrates a comparison between the results obtained from the finite element model and the analytical solution. This

figure indicates excellent agreement as is to be expected.

The input file for ABAQUS follows a standard procedure. There are five blocks which define the problem to be solved by the program. The first is the node definition and generation; the second defines the element mesh or the way the nodes are connected to form the elements that will compose the whole finite element model. The third block is the material or materials definition, which has to be linked with a set of elements. The fourth block defines the loading case and the boundary conditions. Finally, the fifth block establishes the form and variables that will be printed in the output file.

The selection of the element type is one of the key decisions of a finite element problem. ABAQUS offers a huge range of element types. After considering the merits and drawbacks of very many of these, it was decided to perform this analysis using two types of elements – the axisymmetric element CAX8H and the plane strain element CPE8H. The problem was solved with both element types and gave almost exactly the same results. However of these two, the axisymmetric element CAX8H was used to produce the results of several geometries because the nodes and element mesh for this element type is much easier to define.

Based on the input file of Listing number 3.2.6-A, the multi-layered ABAQUS model was built, solved and verified against the analytical model developed in section 3. In this file, it was necessary to define another material set to represent the different material properties of the core and a new element mesh to model core thickness as three layers. To perform analysis using the plane strain element, a FORTRAN code was written to generate the node mesh which was used later to form the elements and consequently the finite element model. This model could selectively be represented by half or a quarter of the cylinder. Using suitable boundary conditions, the symmetry of the half or quarter cylinder is exploited to reduce both computer time and disk space. A simple FORTRAN code was produced for the mesh generation to calculate the cartesian co-ordinates of each node in a cylindrical form and write the results in a suitable format to be input directly in the ABAQUS input file. This code gives the node numbers with the comma separation added to comply with ABAQUS standard input format. The basic input

data for this program are the inner and outer radius of each layer, the number of nodes in each layer, the generation angle and the total angle. The relation between the total angle and the generation angle will be the number of nodes in the circumferential direction. It used 10 degrees for generation angle and 180 degrees for the total angle. The number of elements in the thickness was fixed in 100. Figure 6.1.2 in section 6 presents a comparison between the results obtained with the input file for multi-layered cross-sections and the analytical model developed in section 3. Good agreement is demonstrated by the comparison.

The input file for the multi-layered analysis is described in detail below. The lines starting with an asterisk (*) denote a command line which demands a specific action from ABAQUS. The first block of the input file contains the information to define the finite element node mesh. The command *HEADING is reserved to input the title of the input file. The commands *NODE and *NGEN are used to define the co-ordinates of the nodes. The command *NODE defines for each node number a co-ordinate associated with it. The command *NGEN generates several nodes between two nodes already defined using equal distances between them. It is useful to use the *NSET command to give a name to a given node set.

- First block:

```
*HEADING
 THICK CYLINDER - INTERNAL PRESSURE - COMPOSITE
*RESTART,WRITE,OVERLAY
*NODE
1,10.
201,20.
1001,10.,0.05
1201,20.,0.05
2001,10.,0.1
2201,20.,0.1
*NGEN,NSET=SIDE
1,201
*NGEN
1001,1201
2001,2201
```

The second block defines the element mesh. The *ELEMENT command defines the type of the element among those described in the element library of ABAQUS.

There are several types and the selection of the element is the most important information to be input to the finite element system. The element type is directly related with the solution of the problem. For this analysis the axisymmetric element CAX8H. The reasons to use the axisymmetric element type CAX8H are two. First, the node mesh and element mesh can be easily defined without using a node mesh generator, ABAQUS has built in all necessary features to generate the axisymmetric mesh. Secondly, the results showed for the single walled cylinder with a mesh composed of axisymmetric elements CAX8H demonstrated a good agreement with the analytical solution.

In addition, the selection of the element type is a difficult task and only experienced engineers are able to do so. Therefore, this analysis was performed based on recommended and tested element type.

The command *ELGEN is used in the second block to generate the elements that will compose the structural model. This command has several features and properties to make the mesh generation more user friendly. The command *ELSET is similar to the command *NSET, although, it is used only to define a name for a set of elements rather than nodes.

- Second block:

```
*ELEMENT,TYPE=CAX8H
1,1,3,2003,2001,2,1003,2002,1001
*ELGEN
1,100,2
*ELSET,ELSET=INNER
1
*ELSET,ELSET=OUTER
100
*ELSET,ELSET=STE,GENERATE
1,40
81,100
*ELSET,ELSET=COM,GENERATE
41,80
```

The third block is to define the material properties associated with element numbers. This block starts with the command *SOLID SECTION where the material name and the element set is defined. The next command is *MATERIAL and *ELASTIC

which define the material elastic properties for a given element set. An isotropic material is assumed if nothing is specified. In this multi-layered analysis, two elastic materials sets have been defined to represent the material of the skins (STEEL) and the core(COMPOS). The analysis is applied only to the elastic regime of the materials.

- Third block:

```
*SOLID SECTION,MATERIAL=STEEL,ELSET=STE
*MATERIAL,NAME=STEEL
*ELASTIC
30.E6,.3
*SOLID SECTION,MATERIAL=COMPOS,ELSET=COM
*MATERIAL,NAME=COMPOS
*ELASTIC
30.E4,.3
```

The fourth block is to impose the boundary conditions and the loading parameters. The command *BOUNDARY defines the constraints applied to the model based on a set of nodes. The constraints could be for displacement and rotation in any direction according to the three dimensional system of co-ordinates of the problem. The loading parameters start with the command *STEP which define a loading case. This problem uses only one loading case which is the internal pressure applied in the inner surface. The pressure used is 15,000 at the inner surface and zero at the outer surface. The command *STATIC defines a ramp to gradually build the load defined in the command *DLOAD.

- Fourth block:

```
*BOUNDARY
SIDE,2
*STEP,NLGEOM,INC=50
*STATIC
.1,1.
*DLOAD
INNER,P4,15000
OUTER,P2,0
```

The last block of commands is to define the output file. The finite element program ABAQUS allows several combinations of output. For this analysis, the output was prepared to output the radial and hoop stresses along the radius as well as the strain

in the centroidal position of each node.

- Fifth block:

```
*PRINT,RESIDUAL=NO
*NODE PRINT
U
*EL PRINT,POSITION=NODES,SUMMARY=NO
S
*EL FILE,POSITION=CENTROIDAL,SUMMARY=NO
S
*END STEP
```

4. External pressure analysis

4.1 Overview of approach

4.1.1 Summary of techniques

This chapter is concerned with a comparative investigation of analytical methods for determining the collapse pressure of multi-layered cylindrical pipes. The work uses three analytical models. Two of these - the elastic foundation model and a classic elastic collapse model - are based on analyses developed by others but applied here for the range of parameters typical of the offshore application of multi-layered pipes. The third analytical model is a further development of an elasto-plastic analysis proposed by Montague (1975). Montague used two dimensional Tresca and Mises criteria for his analysis of a structure with thin outer and inner shells. Because of the presence and importance of axial forces in offshore multi-layer pipes, it is necessary to use a three dimensional von Mises criterion and also develop the analysis further to apply for thicker walled shells. This is done here and the results of the updated criterion and enhanced analysis are compared against Montague's original experimental results.

The comparative investigation also includes finite element analysis using two and three dimensional analysis.

The three analytical models and the finite element approach are first summarised below:

(1) The Elastic Foundation Model

This model is based on the conventional theory for the buckling analysis of rings. It has been developed to apply to multi-layered pipes by considering each layer of the pipe as a stand alone layer linked to the other two layers by a set of springs. The characteristics of the boundaries and their interactions are not considered. The elastic collapse pressure and the wave failure modes are then evaluated for each layer.

(2) A Classic Elastic Analysis for Collapse

This classic elastic method is a further development of an approach originally reported by Raville (1954) in a set of papers. The main assumption of this

analysis is that the multi-layered pipe wall is continuous although shear stresses along the layers are considered. The boundaries between the layers are treated as a continuous link.

(3) An Elastic-Plastic Collapse Model

This analytical model is substantially developed further based partly on the ideas originally proposed by Montague (1975). This work examined submerged pressure vessels with very thin faces and based collapse on a two dimensional Tresca failure criteria only. The further development of the analysis described in this section considers the onset of plastic stresses in all layers of the multi-layered pipe with the analytical model has been extended further to apply to thicker faces and uses a failure criterion based on three dimensional von Mises stresses. Thus, as also explained above, axial pressures can also be taken into account.

(4) Finite Element Analysis

Finally, the ultimate model in terms of accuracy , finite element analysis (FEA) was also used. The ABAQUS FEA package was utilised with two approaches. The first used a two dimensional model assuming that axial deformations did not influence the stress state of each element. This is a representative model for very long lengths of pipe. The second approach used a three dimensional model to ensure that the collapse pressure evaluated was the best estimate available.

This section refers to the existing analytical methods that are used for this comparative evolution of collapse pressures and also presents the development of the extended methods.

The results of the comparative evaluation are presented at a later stage in section 6.2.

4.1.2 Basic Properties of Sandwich Structures

This subsection describes two fundamental properties of sandwich structure that apply to multi-layered pipes. The issues raised arose from the background research

into the mechanics of sandwich structures. It was discovered that work on the mechanics of sandwich structures has not been sufficiently widely reported in the usual sources of research literature. Plantema (1966) and Allen (1969) give particularly good and complete overviews of this field.

The definition of sandwich structure is a three-layer consisting of two skins or faces of dense and high-strength material separated by a thick intermediate layer of low density material which have a much lower Young's Modulus and tensile strength. The intermediate material layer is called the core of the sandwich. Obviously, the bending stiffness of this construction is greater than that of a single construction of the same total weight made of the same material as the faces.

The core has to guarantee the following important characteristics. It has to possess a sufficient stiffness in the direction perpendicular to the skins in order to ensure that they remain parallel and at a fixed distance from each other. It should be stiff enough in shear to avoid the structure behaving as two independent beams under bending loads. Moreover, the core must also keep the faces flat avoiding the possibility of the faces locally buckling in their own plane or wrinkling under the influence of compressive stress. In addition, it is also important that the adhesive between the faces and the core does not allow substantial relative movements between the contact surface.

Aeroplane and missile structures were the main application during the early development of sandwich type construction. They employ sandwiches with metal faces and honeycomb and corrugated cores. Building panels are used as a semi structural application and can be designed to deliver a better insulation for sound and heat. The building panels, like aircraft panels, should be light in weight but, unlike aircraft panels, they must be cheap. In the offshore industry the sandwich structure is still not routinely utilised. However, considering the new demands for deep water applications where weight and collapse resistance play an important role such sandwich structures have an obvious future.

This subsection uses two examples below to illustrate two key properties of

sandwich structures which affects the structural strength and elastic collapse of multi-layered pipes presented in the remaining sections of this chapter.

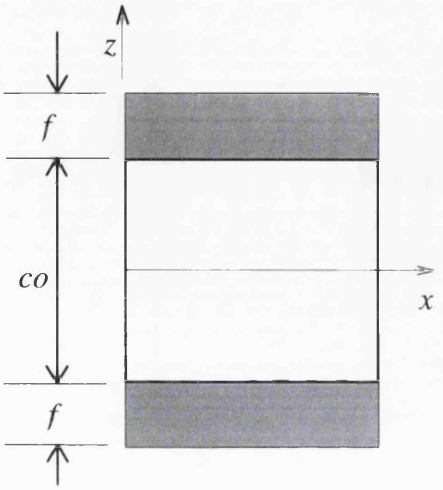

Fig. 4.1.1 Element of a sandwich beam.

The first of these is concerned with the role of the core material in keeping the faces a set distance apart.

An element of a typical cross-section of a sandwich construction is presen 1 in Figure 4.1.1. The faces are taken with equal thickness, f, and the core thickness is co. The sandwich section is taken of unit width, which is, no restriction.

Considering a hinged beam with such a cross-section, the stresses and strain are determined, by the use of ordinary theory of bending. The well-know relationship between the bending moment M and the curvature $1/R$ is $M = -EI/R$. Using the notation for flexural rigidity $D = EI$, the flexural rigidity of a sandwich beam is

$$D = E_s \frac{f^3}{6} + E_s \frac{f(co+f)^2}{2} + E_c \frac{co^3}{12}, \qquad (4.1.1)$$

where E_s and E_c are the Young's Modulus of the faces and the core respectively. On the right hand side of this equation, the first two terms represent the stiffness of the faces and the third the stiffness of the core. In practical sandwich structures the second term is dominant. The first term amounts to less than 1% of the second term when $co/f > 4.77$. The third term would be less than 1% of the second term when $E_s/E_c > 54$, provided $co/f > 4.77$.

The second example analysis below is used to illustrate the role of shear in the sandwich core material in maintaining the structural integrity of the sandwich strut column in bending and buckling.

In literature, bookssuch as Allen /2/, 1969 and Plantema /58/, 1966 treat total deflection of a sandwich strut column, w, as a sum of two partial deflections – those due to bending w_b and due to shear w_s.

The buckling of a sandwich strut column can be determined using this principle. Assuming a flexural rigidity D, and a length L. The Euler load, $P_E = \pi^2 D/L^2$, represents the smallest thrust at which the strut column will reach the neutral equilibrium or becomes unstable after being given some lateral displacement. In the case of sandwich strut column, shear deformations occur in the core. These reduce the stiffness of the strut column and the critical load would be less than the Euler load defined above.

Consider a sandwich strut column, shown in Figure 4.1.2. The flexural stiffness is shown in equation (4.1.1). Neglecting the first and the third term the bending rigidity of the sandwich strut column becomes: $D = E_s f(co+f)^2/2$. When the thrust P reaches the critical axial load two superimposed displacements, w_b – the ordinary bending displacement and, w_s – the additional displacement associated with the shear deformation of the core, occur. At a typical section x along the strut column, the bending moment is

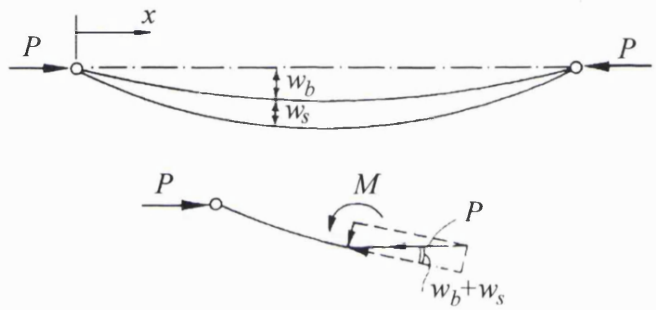

Fig. 4.1.2 Hinged sandwich strut column

$$M = P(w_b + w_s) = -Dw_b'' . \tag{4.1.2}$$

The thrust P at the section x is $P(w_b' + w_s')$ and is acting perpendicular to the mean axis of the sandwich strut column. This represents the shear force that is related to the shear deflection by

$$w_s' = \frac{P(w_b' + w_s')}{S} , \tag{4.1.3}$$

where S is the shear stiffness is given by (see Allen /2/, 1969, page 17 - equation (2.15a))

$$S = \frac{Q}{w_s'} = G\frac{(co+f)^2}{co} , \tag{4.1.4}$$

where Q is the normal shear force on the section, and G is the core material shear rigidity. The term w_s may be eliminated from (4.1.2) after differentiating once to yield a differential equation in w_b:

$$w_b''' + k^2 w_b' = 0\ , \tag{4.1.5}$$

where $$k^2 = \frac{P}{D(1-P/S)}.$$

The solution is

$$w_b = C_1 \sin a_1 x + C_2 \cos a_1 x + C_3\,. \tag{4.1.6}$$

The total deflection, w_b+w_s may be obtained from equation (4.1.2) by differentiating (4.1.6) twice and inserting the result in the right hand side to yield:

$$w_b + w_s = -\frac{D}{P}\left(-C_1 a_1{}^2 \sin ax - C_2 a_1{}^2 \cos a_1 x\right) = \frac{C_1 \sin a_1 x - C_2 \cos a_1 x}{1+P/S}. \tag{4.1.7}$$

The boundary conditions are w=0 at x=0. This gives $C_2 = 0$. The condition w=0 at x=L requires that C_1 vanishes, in this case the strut column remains straight. For the stability criterion where C_1 is non-zero, the strut column buckles since $\sin kx = 0$. The buckling loads therefore correspond to the values $k = n \cdot \pi/L$ and can be shown to be

$$P = \frac{n^2\pi^2\, D/L^2}{1+n^2\pi^2\, D/L^2\, S} \qquad \text{or} \qquad P = \frac{S}{1+s/n^2}\ , \qquad \text{n=1,2,...,} \tag{4.1.8}$$

where $s = L^2 S/\pi^2 D$. Considering the two extreme cases when the shear stiffness is infinite and when the bending stiffness is infinite, respectively, it is found from equation (4.1.8) that the smallest buckling loads are

$$P_E = \frac{\pi^2 D}{L^2}\ , \qquad \text{for} \qquad S \to \infty\,, \tag{4.1.9}$$

$$P_S = S\ , \qquad \text{for} \qquad D \to \infty\,. \tag{4.1.10}$$

P_E is the Euler load, and so for infinite bending stiffness, the buckling load is equal to the shear stiffness. Equation (4.1.8) can now be written in an alternative form:

$$\frac{1}{P} = \frac{1}{P_E} + \frac{1}{P_S}. \tag{4.1.11}$$

The above basic analysis, also given in the referred literature, gives an overview of the structural behaviour of multi-layered constructions. It illustrates how important is the core material role in the buckling resistance. Therefore, the core material should perform elastically and has to be at the same time strong enough in shear to keep the faces apart and avoid local wrinkling. For hydrostatic pressure loading, the deformation would be axisymmetric and will induce compressive

stresses on the component layers. In that sense, depending on the application, the core could be of soft (plastic) or hard (ceramic) material. The latter would significantly increase the buckling pressure. On the other hand, it will impose restrictions on the bending characteristics of the pipe. The plastic material, would not significantly improve the buckling resistance, and would need special attention for shear and face wrinkling.

The aeronautics industry has solved the wrinkling problem using metallic honeycomb cores. This solution could also be applied in offshore pipes. The intermediate spaces of the metallic honeycomb can be filled with expanded plastic with good insulation characteristics and the honeycomb structure would guarantee the sandwich structural performance.

The books of Allen /2/, 1969 and Plantema /58/, 1966 give a complete derivation and discussion of the bending and buckling of sandwich strut beams. It should be pointed out that the behaviour and response of sandwich construction is fundamentally based on the mechanics characteristics of the core material.

4.2 The elastic foundation model

4.2.1 Introduction

The principle of rings on elastic foundation to model distributed reactions loads is well established in engineering stress analysis. This principle can be used to derive a simple mathematical model for the elastic buckling of each layer of a multi-layered pipe.

4.2.2 Circular ring buckling under external fluid pressure

A modern version of the classical circular ring buckling problem is presented by Brush and Almroth, 1975. Their derivation is repeated in Appendix 3 to give the reader a more complete development of the theory for its application to multi-layered pipes. The fundamental equation arising from this work [equation (A.3.37)] is repeated below. The collapse pressure q is given by

$$q = \left(n^2 - 1\right) \cdot \frac{EI}{a^3} \qquad n = 2,3,4,\ldots, \tag{4.2.1}$$

where n is the wave mode, E is the Young's modulus of the wall material, I is the second moment of the area of the ring wall about an axis through the mean radius, and a is the mean radius of the ring.

4.2.3 Circular ring on elastic foundation

The solution given in (4.2.1) can be extended to include the stabilising influence of an elastic foundation. The ring is considered completely filled with a soft elastic medium that is treated as an infinite set of uncoupled radial springs. For such a foundation the pressure q_f, per unit length, between ring and foundation is given by

$$q_f = -k_f w, \tag{4.2.1}$$

where k_f, is a known constant representing the foundation elasticity modulus. This solution is also developed in Appendix 3 [see equation (A.3.49)]. The expression derived from this for the collapse pressure q_{cr} is:

$$q_{cr} = \left(n^2 - 1\right) \cdot \frac{EI}{a^3} + \frac{1}{\left(n^2 - 1\right)} k_f a, \qquad n = 2,3,4,\ldots \tag{4.2.2}$$

For $k_f = 0$, equation (4.2.2) reduces to equation (4.2.1). For given values of EI, k_f,

and a, the value of n may be determined by trial and error to give the smallest q_{cr}.

The result from equation(4.2.2) will be explored in the next section and used as the basis of the elastic foundation multi-layered pipe collapse model.

4.2.4 Elastic layer approach for multi-layered pipe

This analysis has been developed by the author by following the approach described in the last two sections.

A multi-layered pipe is taken to be composed of three elastic layers. Using this approach, a critical pressure for each layer can be found provided the other layers deform radially only and elastically. Therefore, according to the material and geometric characteristics of each layer it will act as an infinite set of uncoupled radial springs with specific elastic modulus.

For determination of the radial elastic modulus of the layer consider the multi-layered pipe of Figure 4.2.1 (a). Using the nomenclature given, Figure 4.2.1 (b), (c), and (d) show the elastic foundation model. The radial displacement of the first or inner layer u_1 as a function of the radial position is given by

$$u_1(r) = C_1 r + \frac{C_2}{r}, \quad b \geq r \geq a. \tag{4.2.3}$$

where r is the radial position and a, b are the inner and outer radius of the inner layer. The constants C_1 and C_2 are functions of the material, geometric dimensions, and radial pressures applied on the layer boundaries. E_1 and ν_1 are the Young's modulus and the Poisson ratio respectively of the inner layer material. The radial pressures p_i and p_1 are the inner pipe pressure and the radial contact pressure on the boundary between the inner and the intermediate layers. Thus

$$C_1 = \frac{1-\nu_1}{E_1}\left(\frac{a^2 p_i - b^2 p_1}{b^2 - a^2}\right), \quad C_2 = \frac{1+\nu_1}{E_1}\left(\frac{p_i - p_1}{b^2 - a^2}\right)a^2 b^2. \tag{4.2.4}$$

In order to find the elastic modulus K_1 equation (4.2.3) is re-written to isolate the contact pressure for $r = b$. This gives

$$p_1 = K_1 \cdot u_1(b) + F_1(p_i). \tag{4.2.5}$$

Where K_1 is the elastic foundation modulus of the inner layer and F_1 is a function only of the inner pressure. Thus

$$K_1 = \frac{E_1(b^2 - a^2)}{b\left[a^2(1+\nu_1) + b^2(1-\nu_1)\right]}, \quad F_1 = \frac{2a^2 p_i}{a^2(1+\nu_1) + b^2(1-\nu_1)}. \tag{4.2.6}$$

In the same fashion, the radial displacement in the second or intermediate layer u_2 and in the third or outer layer u_3 can be written as a function of the radial position

$$u_2(r) = C_3 r + \frac{C_4}{r}, \quad c \geq r \geq b, \tag{4.2.7}$$

$$C_3 = \frac{1-\nu_2}{E_2}\left(\frac{b^2 p_1 - c^2 p_2}{c^2 - b^2}\right), \quad C_4 = \frac{1+\nu_2}{E_2}\left(\frac{p_1 - p_2}{c^2 - b^2}\right) b^2 c^2,$$

$$u_3(r) = C_5 r + \frac{C_6}{r}, \quad d \geq r \geq c, \tag{4.2.8}$$

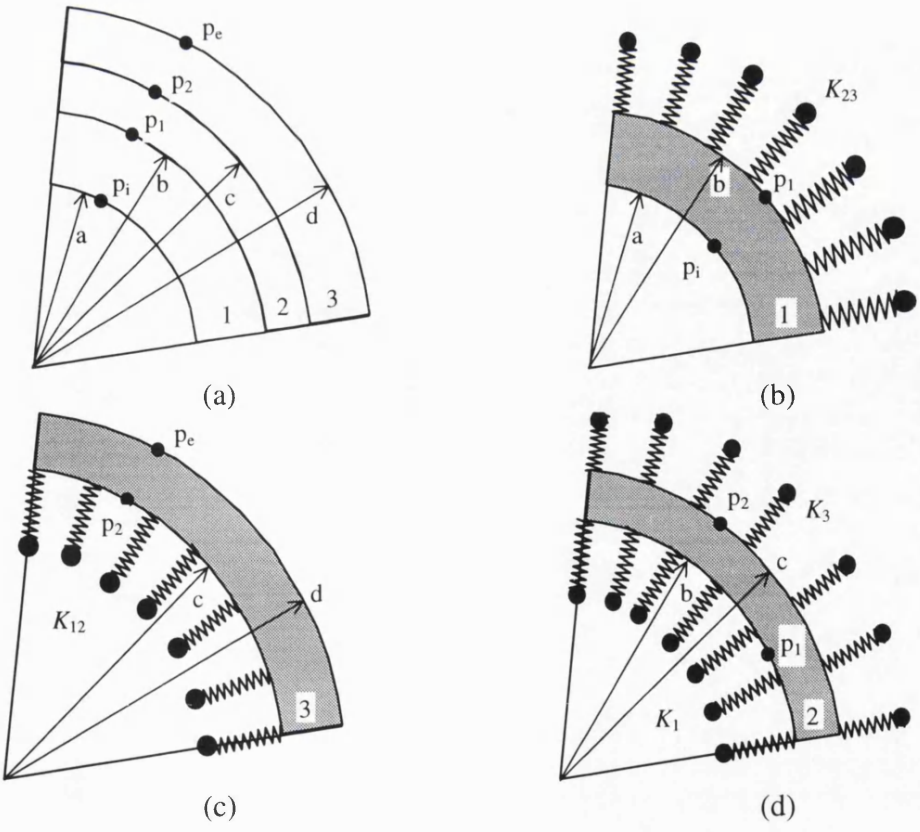

Fig. 4.2.1 Elastic foundation model.

$$C_5 = \frac{1-\nu_3}{E_3}\left(\frac{c^2 p_2 - d^2 p_e}{d^2 - c^2}\right), \quad C_6 = \frac{1+\nu_3}{E_3}\left(\frac{p_2 - p_e}{d^2 - c^2}\right)c^2 d^2.$$

According to Figure 4.2.1, a is the pipe inner radius, b and c are respectively the outer radius of the inner layer or the inner radius of the intermediate layer and the outer radius of the intermediate layer or the inner radius of the outer layer, d is the outer radius of the pipe; p_1 and p_2 are respectively the radial contact pressures between the intermediate layer and the inner layer and the intermediate layer and the outer layer; p_i is the inner pressure of the pipe and p_e is the external pressure on the pipe. Equations (4.2.7) and (4.2.8) may also be written in the same fashion:

$$p_1 = K_{23} \cdot u_2(b) + F_{23}(p_e), \tag{4.2.9}$$

$$p_2 = K_{12} \cdot u_2(c) + F_{12}(p_i), \tag{4.2.10}$$

$$p_2 = K_3 \cdot u_3(c) + F_3(p_e). \tag{4.2.11}$$

Where K_{23} is the elastic foundation modulus of the combination of the intermediate and the outer layers and F_{23} is a function only of the external pressure; K_{12} is the elastic foundation modulus of the combination of the inner and intermediate layers, and F_{12} is a function only of internal pressure. However, equations (4.2.9) and (4.2.10) have respectively the terms p_2 and p_1, therefore, these terms have to be substituted by functions. In the first case (p_1, p_i) and in the latter (p_2, p_e). Using compatibility relations, see section 3:

$$p_1 = \frac{\dfrac{2a^2 p_i}{b^2 - a^2} + \dfrac{2c^2 m p_2}{c^2 - b^2}}{\dfrac{a^2 + b^2}{b^2 - a^2} + \dfrac{b^2 + c^2}{c^2 - b^2}m - \nu_1 + m\nu_2}, \tag{4.2.12}$$

$$p_2 = \frac{\dfrac{2b^2 p_1}{c^2 - b^2} + \dfrac{2d^2 p_e}{d^2 - c^2} \cdot \dfrac{1}{m}}{\dfrac{b^2 + c^2}{c^2 - b^2} + \dfrac{c^2 + d^2}{d^2 - c^2} \cdot \dfrac{1}{m} - \nu_2 + \nu_1 \cdot \dfrac{1}{m}}. \tag{4.2.13}$$

Assuming the following change of variables the elastic foundation modulus may be written as follow,

$$\begin{cases} A = a^2 - b^2, \quad B = b^2 - c^2, \quad C = b^2 + c^2, \\ D = c^2 + d^2, \quad E = c^2 - d^2. \end{cases} \tag{4.2.14}$$

$$K_{23} = \frac{[(m - \nu_3 m + \nu_2 m)E + D]B + mED + mE^2}{\left[\left(m - m\nu_2{}^2 - \nu_3 + \nu_2\nu_3\right)E + (1 - \nu_2)D\right]\ B - \nu_3 E^2 + (1 - \nu_3)DE - D^2} \cdot \frac{E_c}{b},$$

$$F_{23}=\frac{(D^2-E^2)p_e}{\left[(m-mv_2{}^2-v_3+v_2v_3)E+(1-v_2)D\right]\ B-v_3E^2+(1-v_3)DE-D^2},$$

$$K_{12}=\frac{\left\{\left[(mv_2-1-v_1)B-mC\right]A-BC-B^2\right\}}{\left\{\left[(m-mv_2{}^2+v_2+v_1v_2)B+(1+v_1)C\right]\ A+v_2B^2+(1+v_2)CB-C^2\right\}}\cdot\frac{E_c}{c},$$

$$F_{12}=\frac{(B+C)(2A+B+C)p_i}{\left[(m-mv_2{}^2+v_2+v_1v_2)B+(1+v_1)C\right]\ A+v_2B^2+(1+v_2)CB-C^2},$$

$$K_3=\frac{mE}{v_3E-D}\cdot\frac{E_c}{c},\qquad F_3=\frac{(E-D)p_e}{v_3E-D}. \tag{4.2.15}$$

Using these results for specific material and geometric parameters the buckling pressure and the buckling mode may be determined based on an equation similar to (4.2.2). This is done here using the following notation, q_{12} is the buckling load and n_{12} is the buckling mode of the outer layer with the inner and the intermediate layers acting as an elastic foundation. In the same way, q_{23} and n_{23} are respectively the buckling load and buckling mode for the inner layer with the intermediate and outer layers acting as an elastic foundation. Finally, q_{13} and n_{13} are respectively the buckling load and buckling mode of the intermediate layer assuming that the outer and inner layers act as elastic foundations (see Figure 4.2.5 for reference). Then

$$\begin{aligned}
q_{12}&=(n_{12}{}^2-1)\cdot\frac{E_3I_3}{[(c+d)/2]^3}+\frac{1}{(n_{12}{}^2-1)}K_{12}\left(\frac{c+d}{2}\right)\\
q_{23}&=(n_{23}{}^2-1)\cdot\frac{E_1I_1}{[(a+b)/2]^3}+\frac{1}{(n_{23}{}^2-1)}K_{23}\left(\frac{a+b}{2}\right)\qquad n=2,3,4,\ldots\\
q_{13}&=(n_{13}{}^2-1)\cdot\frac{E_3I_3}{[(b+c)/2]^3}+\frac{1}{(n_{13}{}^2-1)}K_{13}\left(\frac{b+c}{2}\right)
\end{aligned} \tag{4.2.16}$$

Based on equations (4.2.16) the three buckling loads and their respective buckling modes may be found by incrementing the values of the buckling mode n=2,3,4,... and minimising the value of q. The solutions of these equations, depending on the parameters of the multi-layered pipe, may differ. However, a good design should optimise layer performance to obtain a better buckling resistance.

It should be pointed out that here this model assumes completely elastic behaviour of all layers immediately before buckling. In addition, there is no consideration of

the nature and behaviour of the boundaries, which are fully connected during the whole axisymmetric deformation. This may be too unrepresentative an assumption. However, for a range of multi-layered pipe geometries, the method can give a good indication of the elastic collapse load. Also, this approach may yield a means of optimising the thickness of each layer of the multi-layered pipe provided the layer thicknesses were chosen to have similar collapse pressures to each other. Based on this model, when the external pressure reaches the collapse load, all layers would fail simultaneously rather than individually.

4.3 Combined buckling of multi-layered cylinders

4.3.1 Introduction.

The buckling model presented in this section was originally presented by Raville, 1954 in a series of papers. Initially, some aspects of Raville's work are reproduced here and then used as a basis for a method to predict the collapse pressure of multi-layered pipes. The complete review of Raville's papers is included in Appendix A.3.

There are not many works published in the literature related to bending and collapse of sandwich shell structures that possess cores rigid enough to deliver a significant contribution to the bending stiffness of the structure. The complexity of such a problem is still under researched. There are the particular problem of sandwich shell structures with an anti-plane core, one which take into account only the stiffness in the cross-section plane in which the shear stress normal to the faces throughout the depth of the core is assumed constant. Such shells differ from ordinary homogeneous plates because the bending deformations are enhanced by the addition of a non-zero shear strain in the core and of direct strains in the core, perpendicular to the faces. These shear strains and the direct strains in the core are directly related to the possibility of wrinkling or instability of the faces in its own plane.

The problem of sandwich shell structures has been addressed in the literature by two methods. In the first method equations are established to define the equilibrium of the separate faces and of the core to prescribe the necessary continuity between them. The result is a set of differential equations that are solved in particular cases for the transverse deformations of the shell. In the second method, the problem is divided into two separate parts which may be called the bending problem and the wrinkling problem. In the bending problem, it is assumed that the core is anti-plane and also infinitely stiff in the direction perpendicular to the faces. This excludes the possibility of wrinkling instability in the faces, but it allows the evaluation of the effect of core shear deformation on the deflections and stresses in the shell structure. In the wrinkling problem, the core elastic properties are considered but the task is simplified by permitting the mean planes of the faces to deflect in the

longitudinal direction only, not in their own planes. Therefore, overall bending of the shell is not considered, but wrinkling and local distortion under concentrated load can be analysed.

4.3.2 A long cylinder under uniform fluid pressure.

Consider a multi-layered cylinder with thin, isotropic walls of stiff material separated by an orthotropic core of weak material. It means that the bending and shear in the walls or faces may be neglected, and the only stress components present in the core are the normal stresses on surfaces parallel to the faces and the transverse shear stress. The solution is not limited with respect to core thickness, since elastic theory is used. The result based on the assumption of membrane theory for the faces is repeated below (see Appendix 4 section A.4.1).

$$\left(\frac{p^2}{E_c^2}\right)\kappa(1-\kappa)\left\{4\frac{(1-b/a)^2}{(b/a)^2}+\left[\left(\frac{E_c}{2G_{r\theta}}+2\right)\left(\frac{1-(b/a)^2}{(b/a)^2}\right)\right.\right.$$

$$\left.+\frac{E_c a(1-\nu_f^2)}{4E_f f}\left(\frac{1+b/a}{b/a}\right)\right]\ln\frac{b}{a}\Bigg\}-\frac{p}{E_c}\left\{\frac{(1-b/a)^2}{(b/a)^2}\left[\frac{b}{a}-\kappa\left(1+\frac{b}{a}\right)\right]\right.$$

$$+\frac{3}{4}\left[1-\kappa(1-b/a)\right]\frac{\ln b/a}{b/a}-\frac{1}{3}\left[\frac{b}{a}+\kappa(1-b/a)\right]$$

$$\left.\left[\left(\frac{E_c}{2G_{r\theta}}-1\right)\left(\frac{1-(b/a)^2}{(b/a)^2}\right)+\frac{E_c a(1-\nu_f^2)}{4E_f f}\left(\frac{1+b/a}{b/a}\right)\right]\right\}-\frac{1}{4}\frac{(1-b/a)^2}{b/a}=0. \quad (4.3.1)$$

where p is the critical external uniform pressure, E_c and $G_{r\theta}$ are respectively the Young's modulus and the shear modulus of the core material, E_f and ν_f are respectively the Young's modulus and the Poisson ratio of the faces material, f is the thickness of the faces, a and b are respectively the mean radius of outer and inner faces, and κ is a numeric factor given by:

$$\kappa=\frac{1}{1+\frac{b}{a}-\frac{E_f f}{E_c a}\log\frac{b}{a}}.$$

Equation (4.3.1) yields two positive roots for p being largely separated one from the other. The lower root corresponds to the critical pressure p_{cr}. Consequently, p_{cr} can be obtained with good accuracy if the terms containing p^2 are neglected.

Examining results from equation (4.3.1) for certain limiting cases demonstrates that, if either E_c or $G_{r\theta}$ is set to zero the critical pressure becomes also equal to zero. This is to be expected in view of the assumption of membrane faces. On the other hand, if either E_c or $G_{r\theta}$ are taken to be infinite, equation (4.3.1) becomes

$$P_{cr}\frac{a\left(1-v_f^2\right)}{E_f f}=\frac{3(1-b/a)^2}{1+(b/a)^2}. \tag{4.3.2}$$

The value of P_{cr} obtained from (4.3.2) should be compared to the value obtained from the formula for the critical pressure on a long homogeneous cylinder if the second moment of area used is equal to the second moment of area of the spaced faces of the sandwich cylinder. The formula for the critical pressure on a long homogeneous thin cylinder is

$$P_{cr}=\frac{3EI}{R^3\left(1-v_f{}^2\right)}. \tag{4.3.3}$$

If the mean radius, R is taken equal to the mean radius of the sandwich cylinder, $R=(a+b)/2$, and I is made equal to the second moment of area of the spaced multi-layered cylinder faces, $I=f(a-b)^2/2$, equation (4.3.2) may be written as

$$P_{cr}\frac{a\left(1-v_f^2\right)}{E_f f}=\frac{3(1-b/a)^2}{(1+b/a)^3/4}. \tag{4.3.4}$$

Comparison of equations (4.3.2) and (4.3.4) shows that they would be equal if both denominators of the right-hand sides are equal:

$$1+\frac{b^2}{a^2}\approx\frac{\left(1+b/a\right)^3}{4}, \text{ when } b/a\approx 1. \tag{4.3.5}$$

For thin cylinders the ratio $b/a\approx 1$. As this ratio decreases from a value of 1, as can be seen in Figure 4.3.5, equation (4.3.2) become less accurate since it is derived on the basis of it being a thin cylinder with the pressure applied on the middle surface and thus fails to represent a thick cylinder with pressure applied on the outer surface only.

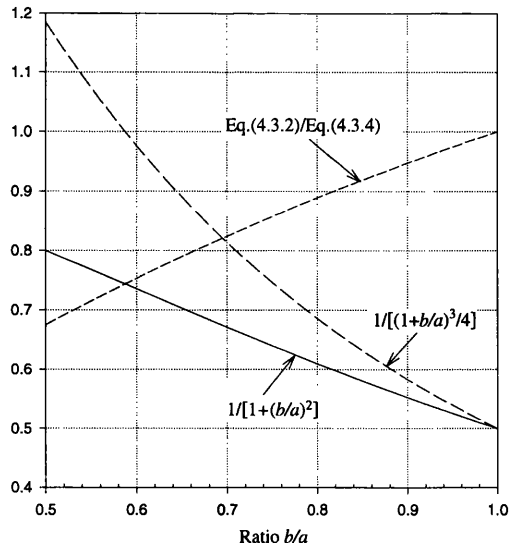

Fig. 4.3.1 Comparison between (4.3.2) and (4.3.4)

The solution presented by Raville /63/, 1954 is accurate for multi-layered cylinders with materials and dimensions in accordance with the basic assumptions applicable. The core assumptions are sufficiently representative of a typical honeycomb sandwich construction. The range of applicability of this solution could be increased if the effect of the thickness of the faces on the overall stiffness of the cylinder were considered in the stability analysis. This could be performed by the use of shell theory rather than membrane theory with regard to the faces. Raville's next work /64/, 1955 has also addressed this latter problem.

4.3.3 Buckling of multi-layered cylinder with face stiffnesses

The last section refers to a long cylinder with thin faces where the membrane theory has been employed and a simplified solution was obtained with faces of equal thickness. Raville /64/, 1955 issued a supplementary development of his previous work to present a solution for the stresses and critical pressure that apply to sandwich cylinders having moderately thick faces of unequal thickness. In this case, bending moment and transverse shear in the individual faces were considered. It was assumed, as before, that buckling takes place at stresses below the elastic limit of the sandwich materials.

The faces are assumed to be homogeneous and isotropic and are analysed on the basis of shell theory rather than membrane theory.

The solution is further described according to Raville /64/ in Appendix 4 section A.4.2. However, the results are summarised below.

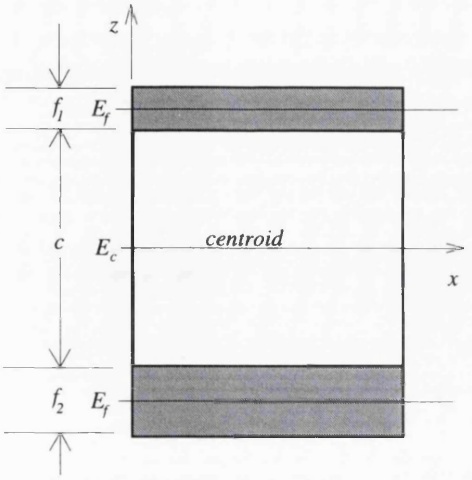

Fig. 4.3.2 Dimensions of the cross-section of a sandwich with faces of unequal thickness.

In his work Raville /64/, 1955 evaluated the collapse pressure based on a polynomial, which results from an expansion of the determinant of a fourth order matrix, where the critical pressure was a function of γ_{cr}, see Appendix 4. Therefore, the lower root of γ_{cr} corresponds to the critical load on the cylinder. The critical load is

$$q_{cr} = \frac{E_f f_1}{a\left(1-\nu_f^2\right)}\gamma_{cr} . \qquad (4.3.6)$$

where E_f and ν_f are respectively the Young's Modulus and the Poisson ratio of the skins, a and f_1 are respectively the radius of the mean surface and the thickness of the outer skin, γ_{cr} is a numerical factor that corresponds to the critical pressure in the solution of the determinant of the characteristic matrix.

A simpler expression for this determinant is obtained if the modulus of elasticity of the core in the radial direction is assumed to be infinite. Under this assumption, the value of γ_{cr} may be written as:

$$\gamma_{cr} = \left(1-n^2\right)\frac{1+\dfrac{b f_1}{a f_2}}{1+\dfrac{b^2 f_1}{a^2 f_2}}\left\{\frac{\left(1-\dfrac{b}{a}\right)^2+\left(\phi_1\dfrac{f_1}{f_2}+\phi_2\dfrac{b}{a}\right)\left(\dfrac{f_1}{f_2}+\dfrac{b}{a}\right)+n^2\psi\left[\phi_1\left(1+\phi_2\right)\dfrac{b}{a}+\phi_2\left(1+\phi_1\right)\dfrac{f_1}{f_2}\right]}{\left(1+\phi_1\right)\dfrac{f_1}{f_2}+\left(1+\phi_2\right)\dfrac{b}{a}+n^2\psi\left(1+\phi_1\right)\left(1+\phi_2\right)}\right\}$$

$$\text{where } \psi = \frac{E_f f_1\left(1-\dfrac{b^2}{a^2}\right)}{2G_{r\theta}b\left(1-\nu_f^2\right)},\ \phi_1 = \frac{f_1^2}{12a^2},\ \phi_2 = \frac{f_2^2}{12b^2} . \qquad (4.3.7)$$

This equation with n=2, yields values of γ_{cr} within 3% of the values obtained from the whole expansion of the determinant for normal sandwich constructions. For cylinders having very thin faces (membrane faces assumption) of equal thickness, the values of ϕ_1 and ϕ_2 are assumed to be zero, and for n=2, the above equation reduces to

$$\gamma_{cr} = -\frac{3(1-b/a)^2}{\left(1+\frac{b^2}{a^2}\right)\left[1+\frac{2E_f f(1-b/a)}{G_{r\theta} b(1-v_f^2)}\right]}. \qquad (4.3.8)$$

The value of critical load is then determined from the definition (4.3.6). Equation (4.3.8) can be used as a good approximation to the critical load on cylinders with membrane faces.

4.3.4 Buckling of multi-layered cylinder of finite length

The theoretical analysis of the buckling of a circular cylinder of multi-layer construction subjected to fluid pressure with finite length is reviewed in Appendix A.4.3. This work was based on the previous work of Raville (1955) /63/, and Norris and Zahn (1963) /54/.

The solution obtained is based on the assumption that the multi-layered cylinder elements are composed of isotropic, membrane faces and an orthotropic core. The mathematical solution of the problem , which is in the form a characteristic determinant of sixth order, is applicable to multi-layered cylinders of any length and of any core thickness. The core is considered to have such low load carrying capacity in the tangential and longitudinal directions as compared to the faces that the normal stress in the core in these directions and the shear in the core planes perpendicular to the faces and in these directions may be neglected. This assumption is likely to represent the annular cores of most practical multi-layered pipe construction. The action of the core and faces is related by the assumption that their displacements are equal at the interfaces between the core and faces. It means that the pipe wall is considered to buckle and behaves as an elastic continuum.

The solution is obtained solving the matrix denoted by N [see Appendix 4 section A.4.3]. The lowest negative value of α for which this determinant equals zero is proportional to the critical pressure on the sandwich cylinder; this value of α will be referred to as α_{cr}. After this value is found, the value of the critical pressure is obtained from the definition as:

$$q_{cr} = \frac{E_f f}{a\left(1-v_f^2\right)}\alpha_{cr}. \tag{4.3.9}$$

Norris and Zahn /54/, 1963 presented a paper referred to as FPL-07 which contains curves and formulae for calculation of the critical external pressure of finite length, circular cylindrical shells with sandwich walls. The skins are isotropic and their individual stiffness is not taken into account. The core is orthotropic, i.e. only normal stresses perpendicular to the faces and shear stresses in the cross-section plane are taken into account.This work is based on the solution of equation (51) on page 23 of the Raville's report 1844-B /65/, 1955 for buckling coefficient. The determinant of this equation was simplified by assuming that transverse Young's Modulus of the core (E_c) was infinite. Their paper includes a change in the variables and gives the following formula for collapse pressure:

$$q_{cr} = \frac{2E_f f}{\left(1-v_f^2\right)r}k. \tag{4.3.10}$$

$$k = \frac{\frac{8}{9}+\alpha^2\left(n^2-1\right)\left(3+\frac{n^2}{\beta}\right)\left[\left(\frac{n^2}{\beta}-\frac{1}{3}\right)\left(n^2-1+\beta\right)-\frac{2}{3}\right]+\frac{32}{9}V\alpha\left(n^2+\frac{\beta}{3}\right)}{\left[\left(n^2-1\right)\left(1+\frac{n^2}{\beta}\right)^2+\frac{1}{3}\right]\left[1+4V\alpha\left(n^2+\frac{\beta}{3}\right)\right]}$$

where, L is the cylinder length, h is the distance between the skins mean surfaces, r is the mean radius of the sandwich cylinder, d is the thickness of the sandwich, $\Phi = \frac{4r}{d}$, $\phi = \frac{2h}{d}$, $\beta = \left(\frac{\pi r}{L}\right)^2$, $\alpha = \frac{\phi}{\Phi} = \frac{h}{2r}$ and $V = \frac{E_f f}{4r\left(1-v_f^2\right)G_{r\theta}}$ are numerical factors, and the Poisson ratio material of the faces, v_f is assumed to be equal to 1/3.

This approach allows a quick assessment of the critical external pressure and was used to generate the curves, included in section 6.3, for comparison with other methods.

4.4 Buckling of multi-layered cylinder using an elastic plastic approach

4.4.1 Introduction

The work by Montague /47/, /48/, and /49/ has shown through experimental results that a double-skinned composite circular cylindrical shell under external pressure may have the buckling pressure predicted based on elastic plastic theory. This work assumes that the multi-layered construction has two thin skins and the core is isotropic. Moreover, Montague concludes that the construction reduces the sensitivity to initial imperfections because the wall has greater resistance to the formation of circumferential lobes. In addition, the elastic instability pressure of the shell is correspondingly increased. Because both elastic instability and instability following local yielding are unlikely, the failure of the shell will be due to material strength failure. Unlike instability, material failure is highly predictable.

In Montague's /47/, 1975 work the collapse consists of a totally elastic stage which ends when the steel skins reach a yield stress condition in the circumferential direction. This occurs approximately at the steel boiler pressure, i.e. at the pressure which would cause circumferential membrane yielding if the shell wall of the two skins combined into a single thickness. The shell then proceeds to withstand increased external pressure with a reduced radial stiffness until failure eventually takes place when the core material reaches a yield or ultimate stress condition. Because the core is more flexible, it will withstand high strains before this happens.

The theory proposed by Montague has been extended and modified here to cope with offshore multi-layered pipes. The assumption of thin wall is removed and the method extended so as to be applicable to a large range of multi-layered pipe sizes. In addition, the boundary conditions have been generalised to allow the input of a generic axial stress. Moreover, the bucking or collapse has been obtained from a three dimensional von Mises failure criterion rather than two dimensional Tresca as used by Montague.

The method predicts the buckling or collapse pressure assuming that the pipe will fail after all its layers have reached the plastic condition. For a range of large wall thicknesses, this approach always gives a smaller buckling load than that predicted

by elastic models. It is often mentioned in the literature as the lower bound buckling value. A comparison of results using this method is presented in section 6.

4.4.2 Elastic plastic model

Consider a multi-layered pipe as shown in Figure 4.4.1. The inner and outer layers are made of a high strength material like steel. The core or intermediate layer is made of an isotropic material. The main stress and strain relationships for the system are derived here for three stress/strain states - firstly when all three layers behave elastically and secondly when the inner or outer layer reach the yield stress but the core remains elastic. Finally, both inner and outer layer in the yielding condition and the core remaining elastic are considered.

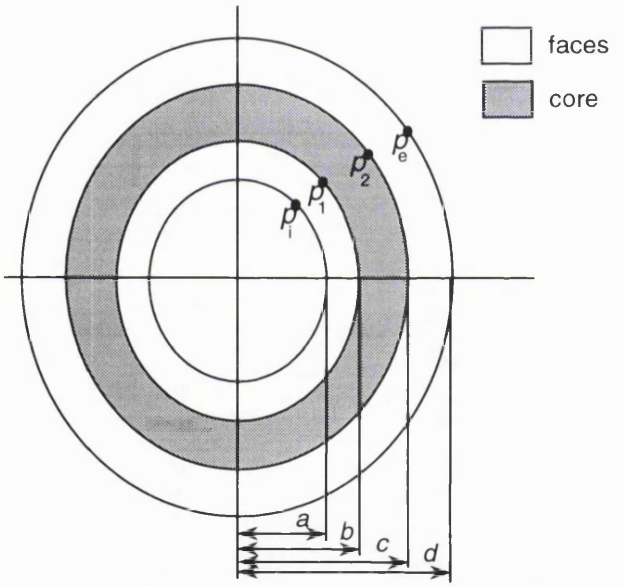

Fig. 4.4.1 Multi-layered pipe cross-section

The auxiliary relations from pipe geometry are:

$$
\begin{aligned}
m &= \frac{E_s}{E_f}, \\
a_1 &= c^2 + b^2, \\
a_2 &= c^2 - b^2, \\
a_3 &= d^2 + c^2, \\
a_4 &= d^2 - c^2, \\
a_5 &= b^2 + a^2, \\
a_6 &= b^2 - a^2, \\
a_7 &= \nu_s - m\nu_c .
\end{aligned}
\qquad (4.4.1)
$$

The multi-layered pipe showed in Figure 4.4.1 has three layers. The faces comprise the first or inner layer and the second or outer layer. They are made of the same material, with Young's modulus E_s and Poisson ratio ν_s. The core is made of a different material with Young's modulus E_c and Poisson ratio ν_c. The nomenclature for radii, stresses and pressures are presented below:

Layer	Position	Radius	Hoop stress	Radial stress	Axial stress	Pressure
1st layer or skin	inner surface	a	σ_{h1i}	σ_{r1i}	σ_{x1}	p_i
	outer surface	b	σ_{h1o}	σ_{r1o}	σ_{x1}	p_1
Core	inner surface	b	σ_{hci}	σ_{rci}	σ_{xc}	p_1
	outer surface	c	σ_{hco}	σ_{rco}	σ_{xc}	p_2
2nd layer or skin	inner surface	c	σ_{h2i}	σ_{r2i}	σ_{x2}	p_2
	outer surface	d	σ_{h2o}	σ_{r2o}	σ_{x2}	p_e

Table 4.4.1 Multi-layered pipe stress nomenclature.

For all layers in the elastic regime the constitutive equations (Lamé equations) can be written to supply the stresses in radial and circumferential directions. The axial stresses are taken to be constant through the thickness of each layer. The hoop stresses (in the circumferential direction) will have the subscript h and radial stresses will have the subscript r. A radial generic position point will be denoted by r. It is obvious that the radial stresses acting on the surfaces of each layer are equal to the negative value of the correspondent pressure. For the first layer the stresses are:

$$\sigma_{h1} = \frac{a^2 p_i - b^2 p_1}{b^2 - a^2} - \frac{(p_1 - p_i)a^2 b^2}{(b^2 - a^2)\, r^2}, \quad \sigma_{r1} = \frac{a^2 p_i - b^2 p_1}{b^2 - a^2} + \frac{(p_1 - p_i)a^2 b^2}{(b^2 - a^2)\, r^2}, \quad b \geq r \geq a. \tag{4.4.2}$$

Stresses in the first layer evaluated at the outer surface, $r = b$ are:

$$\sigma_{h1o} = \frac{2a^2 p_i - (b^2 + a^2)p_1}{b^2 - a^2}, \qquad \sigma_{r1o} = -p_1. \tag{4.4.3}$$

Stresses in first layer evaluated at the inner surface, $r = a$ are:

$$\sigma_{h1i} = \frac{(b^2 + a^2)p_i - 2b^2 p_1}{b^2 - a^2}, \qquad \sigma_{r1i} = -p_i. \tag{4.4.4}$$

Constitutive equations for the second layer or outer layer are:

$$\sigma_{h2} = \frac{c^2 p_2 - d^2 p_e}{d^2 - c^2} - \frac{(p_e - p_2)c^2 d^2}{(d^2 - c^2)\, r^2}, \quad \sigma_{r2} = \frac{c^2 p_2 - d^2 p_e}{d^2 - c^2} + \frac{(p_e - p_2)c^2 d^2}{(d^2 - c^2)\, r^2}, \quad d \geq r \geq c. \tag{4.4.5}$$

Stresses in second layer evaluated at the inner surface, $r = c$ are:

$$\sigma_{h2i} = \frac{(d^2 + c^2)p_2 - 2d^2 p_e}{d^2 - c^2}, \qquad \sigma_{r2i} = -p_2. \tag{4.4.6}$$

Stresses in second layer evaluated at the outer surface, $r = d$ are:

$$\sigma_{h2o} = \frac{2c^2 p_2 - (d^2 + c^2) p_e}{d^2 - c^2}, \qquad \sigma_{r2o} = -p_e . \tag{4.4.7}$$

Constitutive equations for the core or intermediate layer are:

$$\sigma_{hf} = \frac{b^2 p_1 - c^2 p_2}{c^2 - b^2} - \frac{(p_2 - p_1) b^2 c^2}{(c^2 - b^2) r^2}, \quad \sigma_{rf} = \frac{b^2 p_1 - c^2 p_2}{c^2 - b^2} + \frac{(p_2 - p_1) b^2 c^2}{(c^2 - b^2) r^2}, \quad c \geq r \geq b. \tag{4.4.8}$$

Stresses in core evaluated at the inner surface, $r = b$ are:

$$\sigma_{hfi} = \frac{(c^2 + b^2) p_1 - 2c^2 p_2}{c^2 - b^2}, \qquad \sigma_{rfi} = -p_1 . \tag{4.4.9}$$

Stresses in core evaluated at the outer surface, $r = c$ are:

$$\sigma_{hfo} = \frac{2b^2 p_1 - (c^2 + b^2) p_2}{c^2 - b^2}, \qquad \sigma_{rfo} = -p_2 . \tag{4.4.10}$$

Provided that geometry and external pressure are known and the internal pressure is assumed to be zero stress equations show two unknowns p_1 and p_2. Therefore, once they are determined the hoop and radial stresses on the whole wall thickness may be evaluated directly. In order to determine these pressures compatibility equations have to be written. Table 4.4.2 shows the nomenclature used for strains:

Layer	Position	Hoop stain	Radial strain	Axial strain
1st layer or skin	inner surface	ε_{h1i}	ε_{r1i}	ε_{x1i}
	outer surface	ε_{h1o}	ε_{r1o}	ε_{x1o}
Core	inner surface	ε_{hci}	ε_{rci}	ε_{xci}
	outer surface	ε_{hco}	ε_{rco}	ε_{xco}
2nd layer or skin	inner surface	ε_{h2i}	ε_{r2i}	ε_{x2i}
	outer surface	ε_{h2o}	ε_{r2o}	ε_{x2o}

Table 4.4.2 Multi-layered pipe strain nomenclature.

The axial and circumferential strain relations for the three layers are given below with the radial compressive stresses having been substituted by the corresponding negative boundary pressure.

$$
\begin{aligned}
\varepsilon_{x1i} &= \frac{\sigma_{x1} - \nu_s(\sigma_{h1i} - p_i)}{E_s}, \quad \varepsilon_{x1o} = \frac{\sigma_{x1} - \nu_s(\sigma_{h1o} - p_1)}{E_s}, \quad (a)\\
\varepsilon_{x2i} &= \frac{\sigma_{x2} - \nu_s(\sigma_{h2i} - p_2)}{E_s}, \quad \varepsilon_{x2o} = \frac{\sigma_{x2} - \nu_s(\sigma_{h2o} - p_e)}{E_s}, \quad (b)\\
\varepsilon_{xci} &= \frac{\sigma_{xc} - \nu_c(\sigma_{hci} - p_1)}{E_c}, \quad \varepsilon_{xco} = \frac{\sigma_{xc} - \nu_c(\sigma_{hco} - p_2)}{E_c}, \quad (c)\\
\varepsilon_{h1i} &= \frac{\sigma_{h1i} - \nu_s(\sigma_{x1} - p_i)}{E_s}, \quad \varepsilon_{h1o} = \frac{\sigma_{h1o} - \nu_s(\sigma_{x1} - p_1)}{E_s}, \quad (d)\\
\varepsilon_{h2i} &= \frac{\sigma_{hci} - \nu_s(\sigma_{x2} - p_2)}{E_s}, \quad \varepsilon_{h2o} = \frac{\sigma_{hco} - \nu_s(\sigma_{x2} - p_e)}{E_s}, \quad (e)\\
\varepsilon_{hci} &= \frac{\sigma_{hci} - \nu_c(\sigma_{xc} - p_1)}{E_c}, \quad \varepsilon_{hco} = \frac{\sigma_{hco} - \nu_c(\sigma_{xc} - p_2)}{E_c}. \quad (f)
\end{aligned}
\tag{4.4.11}
$$

The axial strain equations should be equal to each other. However, based on the previous assumptions, only two equations among them are linearly independent. The independent equations are

$$\varepsilon_{x1o} = \varepsilon_{xci}, \quad \varepsilon_{x2i} = \varepsilon_{xco}, \tag{4.4.12}$$

and represent continuity on contact boundaries of the intermediate layer. In other words, the outer surface of the inner layer will displace by the same amount as the inner surface of the intermediate layer. In the same way the displacements of the outer surface of the intermediate layer have to be equal to the displacement of the inner surface of the outer layer. Therefore, the circumferential compatibility equations are

$$\varepsilon_{h1o} = \varepsilon_{hci}, \quad \varepsilon_{h2i} = \varepsilon_{hco}. \tag{4.4.13}$$

The longitudinal stress equilibrium offers two alternatives. The first is for a pipe under a tension or compression T. The second is for a pipe with a blind flange on one end. It means that the same external pressure is acting on the flange. This boundary condition affects only the right hand side of the following equation. In the first case it would be equal to T/π and in the second to $-d^2 p_e$. Then

$$(b^2 - a^2)\sigma_{x1} + (c^2 - b^2)\sigma_{xf} + (d^2 - c^2)\sigma_{x2} = -d^2 p_e \text{ or } T/\pi. \tag{4.4.14}$$

Circumferential equilibrium gives two equations - the first being for the outer layer and the second for the inner layer:

$$
\begin{aligned}
-dp_e &= -cp_2 + (d-c)\sigma_{h2m},\\
-bp_1 &= (b-a)\sigma_{h1m}.
\end{aligned}
\tag{4.4.15}
$$

Where $\sigma_{h1m} = \int_a^b \sigma_{h1} dr = \frac{-bp_1}{(b-a)}$, and $\sigma_{h2m} = \int_c^d \sigma_{h2} dr = \frac{-bp_e + cp_2}{(d-c)}$ are the average hoop stresses on the inner and outer layers.

Consider that the yielding stress of the inner and outer layer material is σ_{sy}. In order to determine the external pressure which the inner or outer layer reaches the yielding limit should be investigated in both cases. In the first case, the inner layer yields and the outer and intermediate layers remain in the elastic zone. In this case the external pressure p_{e1} may be found by combining eleven equations in matrix form. These equations are one for longitudinal stress equilibrium (4.4.14), two for circumferential equilibrium (4.4.15), four for compatibility (4.4.12) and (4.4.13), and the four hoop stress relations (4.4.3), (4.4.6), (4.4.9) and (4.4.10). Taking the average Mises stress σ_{M1} in the inner layer to be equal to the yield stress of the material the value of the external pressure p_{e1} may be determined by the linear system of equations. The average Mises stress in the first layer is given by

$$\begin{aligned} \sigma_{M1o} &= \sqrt{\sigma_{h1o}^{\,2} - \sigma_{h1o}\sigma_{x1} + \sigma_{x1}^{\,2} + \sigma_{h1o}p_1 + p_1^{\,2} + \sigma_{x1}p_1}\,, \\ \sigma_{M1i} &= \sqrt{\sigma_{h1i}^{\,2} - \sigma_{h1i}\sigma_{x1} + \sigma_{x1}^{\,2} + \sigma_{h1i}p_i + p_i^{\,2} + \sigma_{x1}p_i}\,, \\ \sigma_{M1} &= \frac{\sigma_{M1o} + \sigma_{M1i}}{2}. \end{aligned} \qquad (4.4.16)$$

Grouping these eleven equations setting the eleven unknowns to $\{\sigma_{x1}, \sigma_{x2}, \sigma_{xc}, \sigma_{h1o}, \sigma_{h2i}, \sigma_{h2m}, \sigma_{hco}, \sigma_{hci}, p_1, p_2, p_{e1}\}$ and rearranging in matrix form yields:

$$\begin{bmatrix} a_6 & a_4 & a_2 & 0 & 0 & 0 & 0 & 0 & 0 & 0 & 0 \\ -v_s & 0 & mv_c & 1 & 0 & 0 & 0 & 0 & -m & a_7 & 0 \\ 0 & 1 & -m & 0 & 0 & -v_s & 0 & mv_c & 0 & 0 & a_7 \\ 0 & 0 & 0 & 0 & 0 & a_4 & 0 & 0 & 0 & 0 & -a_3 \\ 1 & 0 & -m & -v_s & 0 & 0 & 0 & 0 & mv_c & a_7 & 0 \\ 0 & 0 & 0 & a_6 & 0 & 0 & 0 & 0 & 0 & a_5 & 0 \\ 0 & -v_s & mv_c & 0 & 0 & 1 & 0 & -m & 0 & 0 & a_7 \\ 0 & 0 & 0 & 0 & 0 & 0 & 0 & a_2 & 0 & -2b^2 & a_1 \\ 0 & 0 & 0 & 0 & 0 & 0 & c-d & 0 & 0 & 0 & c \\ 0 & 0 & 0 & 0 & a-b & 0 & 0 & 0 & 0 & -b & 0 \\ 0 & 0 & 0 & 0 & 0 & 0 & 0 & 0 & a_2 & -a_1 & 2c^2 \end{bmatrix} \cdot \begin{bmatrix} \sigma_{x1} \\ \sigma_{x2} \\ \sigma_{xc} \\ \sigma_{h1o} \\ \sigma_{h1m} \\ \sigma_{h2i} \\ \sigma_{h2m} \\ \sigma_{hco} \\ \sigma_{hci} \\ p_2 \\ p_2 \end{bmatrix} = \begin{bmatrix} -d^2 p_e * \\ 0 \\ 0 \\ -2d^2 p_e \\ 0 \\ 0 \\ 0 \\ 0 \\ 2dp_e \\ 0 \\ 0 \end{bmatrix}$$

(*) Boundary condition on the pipe's end. (4.4.17)

Setting external pressure to unity (p_e=1) and assuming the internal pressure is zero (p_i=0), equation (4.4.17) is solved. This procedure makes all unknown variables proportional to p_e. To evaluate the actual value of p_e, the average Mises stress in the inner layer should be taken to reach the yield stress value. Substituting the value of p_1 in equation (4.4.4) the value of σ_{h1i} is obtained. Using this σ_{h1i} value and the result of (4.4.17) in (4.4.16) the average Mises stress in the inner layer σ_{M1} may be obtained per unit of external pressure. The actual external pressure is $p_{el} = \sigma_{sy}/\sigma_{M1}$. With these results, all stresses and strains on the multi-layered pipe may be determined.

The radial displacements of the boundary surfaces of the core follow from the strain relation as follows:

$$w_{ci} = \varepsilon_{hci} \cdot b, \quad w_{co} = \varepsilon_{hco} \cdot c. \tag{4.4.18}$$

The change in thickness of the core is (w_{co}-w_{ci}). This will be negative, indicating that the core becomes thicker with the application of external pressure to the shell. The solution of equation (4.4.17) describes the total elastic behaviour of the multi-layered pipe. However, at external pressure p_{el}, the average Mises stresses in the inner face will reach the elastic limit. The elastic limit could be reached by the

outer layer rather than the inner. In this case equations (4.4.16) should be changed to allow the second layer average Mises stresses to reach the yielding condition:

$$\sigma_{M2o} = \sqrt{\sigma_{h2o}^{\ 2} - \sigma_{h2o}\sigma_{x2} + \sigma_{x2}^{\ 2} + \sigma_{h2o}p_2 + p_e^{\ 2} + \sigma_{x2}p_e}\ ,$$
$$\sigma_{M2i} = \sqrt{\sigma_{h2i}^{\ 2} - \sigma_{h2i}\sigma_{x2} + \sigma_{x2}^{\ 2} + \sigma_{h2i}p_2 + p_2^{\ 2} + \sigma_{x2}p_2}\ , \qquad (4.4.19)$$
$$\sigma_{M2} = \frac{\sigma_{M2o} + \sigma_{M2i}}{2}.$$

In the same fashion the system of linear equations in (4.4.17) is solved for an external pressure unity of (p_e=1). The value of σ_{h2o} is obtained from (4.4.7) and then substituted in (4.4.19). The value of p_{e2} is determined based on the average Mises stress in the outer layer σ_{M2} and the yielding stress is, therefore,

$$p_{e2} = \sigma_{sy}/\sigma_{M2}\ .$$

Following the determination of the external pressure, depending on whatever layer had reached the yielding condition first, all the stresses on the multi-layered pipe can be obtained.

On the other hand, when this happens the constitutive equations previusly used cease to be true for whichever face has yielded. There is no doubt that, normally, the yield of the outer layer follows quickly after yield of the inner, see Figure 4.4.2 - assuming that the elastic modulus of the core is small compared with that of the faces, and any subsequently higher pressure will be sustained by a sandwich wall with plastic faces and an elastic core. Assuming that no form of instability takes place, the eventual failure of the shell will follow due to failure of the core material.

This process will now be followed step by step but, before doing so, it is necessary to establish constitutive relations for the faces after loss of elasticity. These are performed using the three dimensional form of the von Mises criterion.

Suppose that at external pressure, p_e=p_{e1}, the inner face reaches the yield condition. It is supposed that the other face is still elastic as well as the core. Without referring to a particular example, it is not known whether the inside skin or outside skin will first reach the yield condition. Suppose that the inside layer yields first, it

follows that, at p_e=p_{e1}. For the first increment of external pressure $\hat{p}_{e1}$, where $p_e = p_{e1} + \hat{p}_{e1}$. Assuming that the yielding limit is reached by the 3D-Mises stress condition of the first layer all strains would be plastic. Denoting any increments in the variables with a hat symbol, when the external pressure is incremented by $\hat{p}_{e1}$ the increment in hoop stress in the inner layer will be *zero* , as will be the increment in radial and axial stresses. Thus,

$$\hat{\sigma}_{h1} = 0, \quad \hat{\sigma}_{x1} = 0, \quad \hat{p}_1 = 0. \tag{4.4.20}$$

Also, if it is assumed that the strain rate is the sum of the elastic and plastic components, the strain equation for the inner layer in incremental form (4.4.11) may be replaced by

$$\hat{\varepsilon}_{h1o} = \varepsilon_{h1op}, \tag{4.4.21}$$

where ε_{h1op} is the plastic component of the circumferential strain rate in the outer surface of the inner layer. It is assumed that the inner layer is completely plastic. Apart from these adjustments, previous equations, written now in incremental form, will describe the wall behaviour whilst the inside layer is plastic and the outside face and core are elastic. The equation (4.4.17) should be modified to give the incremental variables, including the plastic deformation ε_{h1op}. Therefore, using (4.4.19) the incremental pressure ($\hat{p}_{e1}$) that allows the outer face to reach the elastic limit may be determined interactively. Dropping one of the equations (4.4.15) and equation (4.4.3) the matrix has now only nine equations and unknowns.

The solution of (4.4.22) describes the incremental stresses and strains appropriate to the outer layer and the core in the elastic condition and the inner layer in the plastic condition. The equation remains valid as long as, in the inner layer, the von Mises stress is equal to the yield stress ($\sigma_{M1} = \sigma_{sy}$).

$$\begin{bmatrix} a_4 & a_2 & 0 & 0 & 0 & 0 & 0 & 0 & 0 \\ 0 & mv_c & 0 & 0 & 0 & -m & 0 & E_s & 0 \\ 0 & -m & 0 & 0 & 0 & mv_c & 0 & 0 & E_s \\ -v_s & mv_c & 1 & 0 & -m & 0 & a_7 & 0 & 0 \\ 1 & -m & -v_s & 0 & mv_c & 0 & a_7 & 0 & 0 \\ 0 & 0 & 0 & 0 & 0 & a_2 & a_1 & 0 & 0 \\ 0 & 0 & a_4 & 0 & 0 & 0 & -a_3 & 0 & 0 \\ 0 & 0 & 0 & 0 & a_2 & 0 & a_1 & 0 & 0 \\ 0 & 0 & 0 & c-d & 0 & 0 & 2c & 0 & 0 \end{bmatrix} \cdot \begin{bmatrix} \hat{\sigma}_{x2} \\ \hat{\sigma}_{xc} \\ \hat{\sigma}_{h2i} \\ \hat{\sigma}_{h2m} \\ \hat{\sigma}_{hco} \\ \hat{\sigma}_{hci} \\ \hat{p}_2 \\ \varepsilon_{h1op} \\ \varepsilon_{x1op} \end{bmatrix} = \begin{bmatrix} d^2\hat{p}_{e1}* \\ 0 \\ 0 \\ 0 \\ 0 \\ 0 \\ -2d^2\hat{p}_{e1} \\ 0 \\ 2d\hat{p}_{e1} \end{bmatrix} \quad (4.4.22)$$

(*) Boundary condition on the pipe's end.

Using an iterative numerical procedure such as Secant or Regula falsi methods the value of $\hat{p}_{e1}$ is determined. Solving $F(p_{e1}) = \sigma_{sy} - \sigma_{M2} = 0 \pm tolerance$, the value of p_{e1} is found for very small tolerances (10^{-5}) within a few iterations. Following this solution, the average von Mises stress in the outer layer and as well as in the inner layer have reached the yielding limit.

However, if during this pressure increment, the second layer had reached the plastic limit rather than the first. The increment in hoop, axial, and radial stresses in the outer layer are taken as *zero*. The pressure $\hat{p}_2$ on the outer layer of the core will be proportional to the increase in the external pressure. Therefore,

$$\hat{\sigma}_{h2} = 0, \quad \hat{\sigma}_{x2} = 0, \quad \hat{p}_2 = \frac{d}{c}\hat{p}_{e2}. \tag{4.4.23}$$

The strain rate is now plastic. The strain equation for the inner layer in (4.4.11) may be replaced by

$$\hat{\varepsilon}_{h2i} = \varepsilon_{h2ip}, \tag{4.4.24}$$

where ε_{h2ip} is the plastic component of the strain rate in the inner surface of the outer layer. The following equations, written in incremental form, will describe the wall behaviour whilst the outside layer is plastic and the inside layer and core are

elastic. Therefore, the increment now will be $p_e = p_{e2} + \hat{p}_{e2}$, being ($\hat{p}_{e2}$) the incremental pressure that allows the inner face to reach the elastic limit whilst the outer layer is in the plastic condition. In the same fashion dropping one of equations (4.4.15) and (4.4.6) the matrix has also nine equations and unknowns including the plastic deformations ε_{h2ip} and ε_{x2ip}.

Using the same procedure, the value of $\hat{p}_{e2}$ is determined iteratively. Solving $F(p_{e2}) = \sigma_{sy} - \sigma_{M1} = 0 \pm tolerance$ the value of p_{e2} is determined. Following this solution, the average von Mises stresses in the outer layer and as well as in the inner layer have reached the yielding limit.

$$\begin{bmatrix} a_6 & a_2 & 0 & 0 & 0 & 0 & 0 & 0 & 0 \\ -v_s & mv_c & 1 & 0 & 0 & -m & a_7 & 0 & 0 \\ 0 & -m & 0 & 0 & mv_c & 0 & 0 & 0 & E_s \\ -v_s & mv_c & 1 & 0 & 0 & -m & a_7 & 0 & 0 \\ 0 & 0 & 0 & a-b & 0 & 0 & -b & 0 & 0 \\ 0 & mv_c & 0 & 0 & -m & 0 & 0 & E_s & 0 \\ 0 & 0 & 0 & 0 & 0 & a_2 & -a_1 & 0 & 0 \\ 0 & 0 & 0 & 0 & a_2 & 0 & -2b^2 & 0 & 0 \\ 0 & 0 & a_6 & 0 & 0 & 0 & a_5 & 0 & 0 \end{bmatrix} \cdot \begin{bmatrix} \hat{\sigma}_{x1} \\ \hat{\sigma}_{xc} \\ \hat{\sigma}_{h1o} \\ \hat{\sigma}_{h1m} \\ \hat{\sigma}_{hco} \\ \hat{\sigma}_{hci} \\ \hat{p}_1 \\ \varepsilon_{h2ip} \\ \varepsilon_{x2ip} \end{bmatrix} = \begin{bmatrix} -d^2\hat{p}_{e2} * \\ 0 \\ -a_7 d\hat{p}_{e2}/c \\ 0 \\ 0 \\ -a_7 d\hat{p}_{e2}/c \\ -2cd\hat{p}_{e2} \\ -a_1 d\hat{p}_{e2}/ca_2 \\ 0 \end{bmatrix} \quad (4.4.25)$$

(*) Boundary condition on the pipe's end.

In practice, whichever layer becomes plastic first, the other will follow after a relatively small increase in pressure and both layers will be in the plastic condition. Suppose that this case happens for the increment $\hat{p}_e$ when $p_e = p_{1e} + \hat{p}_{1e} + \hat{p}_e$ then:

$$\hat{\sigma}_{h1i} = \hat{\sigma}_{h1o} = \hat{\sigma}_{h2i} = \hat{\sigma}_{h2o} = \hat{p}_1 = 0, \quad \hat{p}_2 = \hat{p}_e d/c. \tag{4.4.26}$$

Substituting this in the previous stress relations for the core

$$\hat{\sigma}_{hco} = -\frac{da_1}{ca_2}\hat{p}_e, \quad \hat{\sigma}_{hci} = -\frac{2cd}{a_2}\hat{p}_e. \tag{4.4.27}$$

The strains relations become

$$\hat{\varepsilon}_x = \frac{\hat{\sigma}_{xc} - v_c(\hat{\sigma}_{hco} - \hat{p}_e\, d/c)}{E_c} = \frac{\hat{\sigma}_{xc} - v_c\hat{\sigma}_{hci}}{E_c},\ \hat{\varepsilon}_{h2i} = \hat{\varepsilon}_{h2ip},\ \hat{\varepsilon}_{h1o} = \hat{\varepsilon}_{h1op},$$

$$\hat{\varepsilon}_{hci} = \frac{\hat{\sigma}_{hci} - v_c\hat{\sigma}_{xc}}{E_c},\ \hat{\varepsilon}_{hco} = \frac{\hat{\sigma}_{hco} - v_c(\hat{\sigma}_{xc} - \hat{p}_e\, d/c)}{E_c}, \tag{4.4.28}$$

where, $\hat{\varepsilon}_x = \hat{\varepsilon}_{x1} = \hat{\varepsilon}_{x2} = \hat{\varepsilon}_{xc}$, $\hat{\varepsilon}_{h1o} = \hat{\varepsilon}_{h1op} = \hat{\varepsilon}_{hci}$, and $\hat{\varepsilon}_{h2i} = \hat{\varepsilon}_{h2ip} = \hat{\varepsilon}_{hco}$. The increment to the hoop, axial, and radial stresses for both faces vanishes. For core failure the von Mises stress average in the core should reach the yield point. Following the 3-D von Mises criterion:

$$\sigma_{Mco} = \sqrt{\sigma_{hco}^{\ 2} - \sigma_{hco}\sigma_{xc} + \sigma_{xc}^{\ 2} + \sigma_{hco}p_1 + p_1^{\ 2} + \sigma_{xc}p_1},$$

$$\sigma_{Mci} = \sqrt{\sigma_{hci}^{\ 2} - \sigma_{hci}\sigma_{xc} + \sigma_{xc}^{\ 2} + \sigma_{hci}p_2 + p_2^{\ 2} + \sigma_{xc}p_2}, \tag{4.4.29}$$

$$\sigma_{Mc} = \frac{\sigma_{Mco} + \sigma_{Mci}}{2}.$$

Where $-p_1$ and $-p_2$ are the radial stresses in the inner and outer surfaces of the core respectively during the last pressure increment with both faces plastic and only the core in the elastic regime. During this external pressure increment, all stresses in inner and outer layers will remain unchanged once they are in the plastic condition. Then dropping the equations related to these pressures, the incremental form reduces to the matrix in equation (4.4.30).

In the same way, the system of linear equations in (4.4.30) is solved iterative. The increments in p_1 and p_2 are *zero*. However, the compressive radial stress on the outer surface of the core will be proportional to the increment of the external pressure according to the circumferential equilibrium equation (4.4.15), therefore, $p_2 = p_e\, d/c$. The pipe continues to behave in a stable manner with increasing pressure as long as the core remains in the elastic condition. The design of the pipe structure should be such as to ensure that buckling eventually takes place due to strength failure of the core material. It is a simple matter, knowing the yield stress of the core, to estimate the value of external pressure at which its stress state will reach some failure criteria based either on Tresca or von Mises.

$$\begin{bmatrix} a_2 & 0 & 0 & 0 & 0 & 0 \\ -m & 0 & mv_c & 0 & 0 & E_s \\ mv_c & -m & 0 & 0 & E_s & 0 \\ mv_c & 0 & -m & E_s & 0 & 0 \\ 0 & 0 & 1 & 0 & 0 & 0 \\ 0 & 1 & 0 & 0 & 0 & 0 \end{bmatrix} \cdot \begin{bmatrix} \hat{\sigma}_x \\ \hat{\sigma}_{hco} \\ \hat{\sigma}_{hci} \\ \hat{\varepsilon}_{h1op} \\ \hat{\varepsilon}_{h2ip} \\ \hat{\varepsilon}_x \end{bmatrix} = \begin{bmatrix} -d^2\hat{p}_e * \\ 0 \\ -a_7\hat{p}_e d/c \\ 0 \\ -2cd\hat{p}_e/a_2 \\ -a_1 d\hat{p}_e/a_2 c \end{bmatrix} \quad (4.4.30)$$

(*) Boundary condition on the pipe's end.

Apart from the average von Mises stress on each layer other criteria may be used such as Tresca by changing the step by step relations accordingly. However, by applying von Mises criteria for all layers, the results showed a better match with experimental results, see Figure 4.4.2. In this Figure, the theoretical result using Tresca the present work model and the experimental results are presented. The experimental data were obtained by Montague, 1975.

A computer code has been developed by the author to perform the analysis described above using the experimental data included in Montague, 1975. The multi-layered pipe characteristics are:

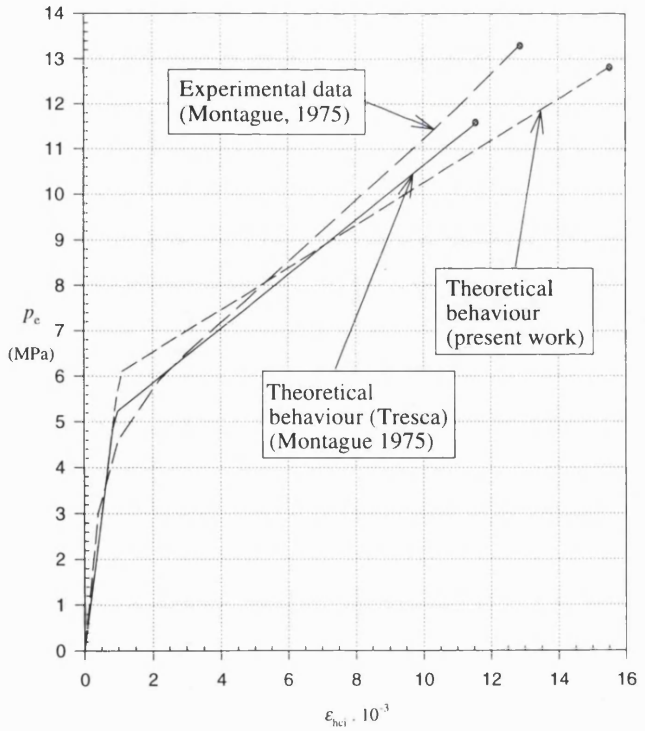

Fig. 4.4.2 Comparison of theoretical and experimental; external pressure behaviour with hoop strain inner surface of the core.

- Geometry
  a=59.7 mm, b=60.5 mm,
  c=68.0 mm, d=68.8 mm.
- Material
  E_s=200 GPa, $\nu_s = 0.28$, $\sigma_{sy} = 193.1$ MPa,
  E_c=4.38 GPa, $\nu_c = 0.38$, $\sigma_{cy} = 61.5$ MPa.

Table 4.4.3 shows the results obtained. Figure 4.4.2 presents a comparison between the external pressure behaviour with experimental data from Montague, 1975 and his Tresca approach. It can be seen that the von Mises approach predicts the experimental buckle pressures more closely. It should be stressed that this example is for very thin layers or skins. For thicker layers, the von Mises approach would give better results.

	Yield of inner layer	Yield of outer layer	Yield of core
	p_e=5.6 MPa	p_e=6.1 MPa	p_e=12.9 MPa
Pressures			
Boundary inner layer/core (MPa)	3.41	3.52	10.34
Boundary core/outer layer (MPa)	5.60	6.11	12.85
Inner layer			
Axial Stress (MPa)	-110.4	-110.4	-110.4
Hoop Stress inner surface (MPa)	-225.9	-137.0	-137.0
Hoop Stress outer surface (MPa)	-223.0	-223.0	-223.0
Radial Stress inner surface (MPa)	0	0	0
Radial Stress outer surface (MPa)	-2.97	-2.97	-2.97
Mises Stress inner surface (MPa)	195.7	195.7	195.7
Mises Stress outer surface (MPa)	190.5	190.5	190.5
Mises Stress aver. surface (MPa)	193.1	193.1	193.1
Outer layer			
Axial Stress (MPa)	-102.2	-137.0	-137.0
Hoop Stress inner surface (MPa)	-193.2	-227.7	-227.7
Hoop Stress outer surface (MPa)	-191.0	-225.1	-225.1
Radial Stress inner surface (MPa)	-3.41	-3.52	-10.34
Radial Stress outer surface (MPa)	-5.60	-6.11	-12.85
Mises Stress inner surface (MPa)	164.4	195.3	195.3
Mises Stress outer surface (MPa)	160.6	190.9	190.9
Mises Stress aver. surface (MPa)	162.5	193.1	193.1
Core			
Axial Stress (MPa)	-4.89	-5.84	-10.7
Hoop Stress inner surface (MPa)	-7.17	-8.23	-73.7
Hoop Stress outer surface (MPa)	-6.73	-7.68	-66.3
Radial Stress inner surface (MPa)	-2.97	-2.97	-2.97
Radial Stress outer surface (MPa)	-3.41	-3.52	-10.34
Mises Stress inner surface (MPa)	3.82	4.74	67.2
Mises Stress outer surface (MPa)	2.89	3.61	55.8
Mises Stress aver. surface (MPa)	3.35	4.18	61.5
Strains			
Axial - all layers (10^{-3})	-0.236	-0.361	4.199
Hoop - at radius=b (10^{-3})	-0.956	-1.114	-15.640
Hoop - at radius=c (10^{-3})	-0.818	-0.942	-13.318
Displacements			
At radius=b (mm . 10^{-3})	-0.0578	-0.0674	-0.946
At radius=c (mm . 10^{-3})	-0.0556	-0.0640	-0.906
Core thickness (mm)	7.502	7.503	7.541

Table 4.4.3 Theoretical stress and strain results based on Montague (1975) experimental data.

4.5 ABAQUS analysis

As has been done before, the finite element package ABAQUS /1/, was used to predict the buckling pressure for multi-layered pipes. The idea was to have results from an independent and well-known commercial structural analysis program to compare with results from the three analytical models described above.

The ABAQUS buckling prediction based on eigenvalue assessment is described in detail in section 2.2.3 of the User's Manual /1/ with the buckling analysis procedures given in section 10.2.2. The two dimensional numerical solution described here followed conventional practices in such analysis. However, the three dimensional approach had to be developed from scratch. ABAQUS uses the classical eigenvalue analysis to estimate the critical (buckling) load for structures that carry their design loads primarily by axial or membrane action rather than by bending action. Their response often involves very small deformations prior to buckling.

The classic eigenvalue buckling problem, in the finite element context, is stated as follow:

1) Given a structure with an elastic stiffness matrix, $K_{(b)}^{MN}$;

2) Loading pattern defined by the vector Q^M;

3) Initial stresses and load stiffness matrix, $K_{(Q)}^{NM}$

where the superscripts N and M refers to degrees of freedom of the whole model and the subscript i represents the i^{th} mode. The solution is to find load multipliers (eigenvalues), λ_i, and buckling mode shapes (eigenvectors), ϕ_i^M, which satisfy

$$\left[K_{(b)}^{NM} + \lambda_i K_{(Q)}^{NM}\right]\phi_i^M = 0$$

The critical loads are given by $\lambda_i Q^M$.The smallest load multiplier and the associated mode shape correspond to the critical load and failure shape mode of the structure.

This built in feature for evaluation of the eigenvalues of a loaded structure described above was then used for the prediction of the critical external pressure on multi-layered pipes.

The set of command lines for ABAQUS input to solve this three dimensional problem is described as follows: First, a node generation facility was developed. This is one of the most important tasks since the whole element mesh needs to be generated based on node co-ordinates, which have to be defined in this step. After that the element type is defined and based on the node numbers and their co-ordinates the elements mesh can be generated to build the complete finite element model. The material definition command and the element generation command are used to set the materials properties and the corresponding element material definition. Once the model is ready and its mechanical properties are defined, definition of boundary constraints and loading enables the analysis to be performed. The definition of the boundary constraints and loads is based on element or node groups which are constrained to deform in particular directions. The loads are defined based on program features and special commands that allow the user to define loading in several forms. Another feature in the ABAQUS input is the *BUCKLE command that defines the eigenvalue problem.

The command that defines an hydrostatic pressure load combined with the command that defines the eigenvalue problem sets the input to solve the critical pressure on the multi-layered pipe. At least half of the cylinder has to be considered otherwise the buckling shape modes would be restricted to only those that will fit in the structural section supplied by the user. Therefore, it was necessary to build a 180 degrees mesh to allow a complete eigenvalue analysis of the multi-layered pipe composed of three layers.

Following the standard procedure to generate the input file for ABAQUS analysis, it was necessary to generate a mesh of nodes which represents the whole multi-layer cylinder. A FORTRAN code was developed to perform this task. In addition, boundary conditions have to define the symmetric behaviour of the other half of the multi-layered cylinder that was not included in the mesh.

A FORTRAN code was developed to generate the node mesh for each geometry. The program builds the node set for one half of an entire multi-layered cylinder in a form that is formatted and ready to be included in an ABAQUS input file. In addition, a suitable command generates the elements of each layer in a systematic way. Each layer has to be defined as a group of elements that will have its material properties defined and input. Finally, the loading and the type of problem is defined - in particular the external pressure is defined as acting on the outer layer only and the eigenvalue problem is also defined including the highest mode shape to be calculated.

Another similar FORTRAN code was also produced to generate the two dimensional node mesh to analyse the difference between the solutions for a ABAQUS two dimensional and a three dimensional computation. The two dimensional model is intended to simulate a very long pipe. On the other hand, the three dimensional model had to be calibrated in order to define the minimum length of multi-layered pipe model that needed to be used. This length was defined after several runs where the collapse pressure mode becomes independent of the length. In other words, the collapse is characterised by the same cross-section pattern along the length.

Another important issue in finite element analysis is the definition of the element. The element types selected for this work were CPE8 for the two dimensional model and the C3D20 type for the three dimensional model. The CPE8 element type has eight nodes arranged as a plane squared box where each wall contains three nodes. The C3D20 element type has twenty nodes arranged as a cubic squared box where each face contains eight nodes.

In both, two and three dimensional models each element extended circumferentially over a ten degree arc around the 180 degrees of the half pipe. The half cylinder was used to allow ABAQUS to evaluate the even and odd eigenvalues and the deformation pattern of each mode shape. The ten degree sector angle was obtained after testing for an acceptable compromise between ABAQUS memory usage and speed compared to accuracy of results.

It is a standard result for ABAQUS that the first eigenvalue (failure in two lobes, n=2) is the smallest, and is therefore, the elastic buckling pressure. With the increase in the Young's modulus ratio between the face material and the core material. E_s/E_c , the values of the higher failure modes tend to be of the same order of magnitude. However, the two lobes failure always gives the smallest value.

The result of the three dimensional model agrees with the analytical combined elastic solution posed by Raville (1954), which uses the same basic assumptions. Although, the two dimensional model gives results close to the three dimensional model they tend to be more conservative. This statement is elaborated on further in section 6.2 with graphical comparisons of the collapse pressure obtained from different prediction methods.

The selection of the element type was done using the same criteria used in the first analysis with ABAQUS described in section 3.4. The axisymmetric elements were disregarded from the very beginning because they do not allow the solution for higher buckling modes. Using axisymmetric element type the whole cylinder is represented by repetition of a simple slice. This way, the element mesh was developed for 180 degrees sector and the symmetry of such a sector was defined in the boundary conditions. The element selection follows a stepped approach with the comparison of the best match of the ABAQUS buckling result and the analytical solution of the perfect single walled cylinder.

In this case there is the necessity to generate the co-ordinates of the nodes in order to prepare an input file suitable for ABAQUS. This mesh generation was performed by developing a FORTRAN code which has a specific output format that can be input directly under the *NODE and *NGEN commands into the ABAQUS input file. The output includes the node numbers and its corresponding co-ordinates. This FORTRAN code is a program which calculates the cartesian co-ordinates of each node in a cylindrical form based on the geometric parameters that are input. The basic input data for this program are the inner and outer radius of each layer, the number of nodes in each layer, the generation angle and the total angle and also the sinusoidal imperfection. The geometry of the layers can be defined by the inner

radius and the values of α and β, these parameters define the thickness of each layer assuming that the skins have equal thickness. These parameters are also used in the comparison graphs presented in Section 6 . The relation between the total angle and the generation angle will be the number of nodes in the circumferential direction. 10 degrees was used for the generation angle and 180 degrees for the total angle, giving 9 elements in the circumferential direction. The number of elements in the radial direction for each layer was fixed at 3. This value was defined after several tests aimed at reducing the computer time but maintaining the accuracy of the results. The number of elements in the longitudinal direction for the three dimensional model was fixed at one. The analysis was aimed at evaluating the buckling pressure due to external pressure loading. Therefore, it is not necessary to have more than one element in the longitudinal direction. Boundary conditions were also established at the nodes in the base of the half cylinder in order to have them behaving symmetrically with the other half of the cylinder. The sinusoidal imperfection was introduced to induce the buckling mode with very small ovality. It was observed that the elastic buckling (eigenvalue evaluation) always follows the two lobes mode even though an imperfection in other modes was input.

Section 6 shows a series of graphs presenting the results obtained from the finite element model and the analytical solutions. It has been noted that the ABAQUS results show similar trends to those obtained from the elastic models for a range of geometric parameters.

The input file for the multi-layered analysis is described in detail below. The lines starting with an asterisk (*) denote a command line which demands a specific action from ABAQUS. The first block of the input file contains the information to define the finite element node mesh. The command *HEADING is reserved to input the title of the input file. The commands *NODE and *NGEN are used to define the co-ordinates of the nodes. The command *NODE defines for each node number a co-ordinate associated with it. The command *NGEN generates several nodes between two nodes already defined using equal distances between them. It is useful to use the *NSET command to give a name to a given node set.

The analysis developed for this buckling problem has to define a half cylinder finite element model as explained before. Therefore, two codes were written to generate the mesh for the two and the three dimensional node mesh.

- First block:

```
*HEADING
 MULTI-LAYER CYLINDER - BUCKLING PRESSURE - ELASTIC
*RESTART,WRITE,OVERLAY
*NODE
  ....
  ....
  ....
*NGEN,NSET=ALL
  ....
  ....
  ....
*NGEN,NSET=SIDE
  ....
  ....
  ....
*NGEN,NSET=BASE
  ....
  ....
  ....
```

The second block defines the element mesh. The *ELEMENT command defines the type of the element among those described in the element library of ABAQUS. There are several types and the selection of the element is the most important information for the finite element system. For this analysis the plane strain element CPE8 was used for the two dimensional analysis and C3D20 for the three dimensional analysis.

The command *ELGEN is used to generate the elements that will make up the structural model. This command has several features and properties to make the mesh generation more user friendly. The command *ELSET is similar to the

command *NSET, however, it is used only to define a name for a set of elements rather than nodes.

- Second block:

```
*ELEMENT,TYPE=C3D20
 ....
 ....
 ....
*ELGEN
 ....
 ....
 ....
*ELSET,ELSET=INNER
 ....
 ....
 ....
*ELSET,ELSET=OUTER
 ....
 ....
 ....
*ELSET,ELSET=STE,GENERATE
 ....
 ....
 ....
*ELSET,ELSET=COM,GENERATE
 ....
 ....
 ....
```

The third block is to define the material properties associated with element numbers. This block starts with the command *SOLID SECTION where the material name and the element set is defined. The next command is *MATERIAL and *ELASTIC which define the material elastic properties for a given element set. Isotropic material is assumed if nothing is specified. In this multi-layered analysis two elastic material sets have been defined to represent the material of the skins (STEEL) and the core (COMPOS). The analysis is limited to the elastic regime of the materials.

- Third block:

```
*SOLID SECTION,MATERIAL=STEEL,ELSET=STE
*MATERIAL,NAME=STEEL
*ELASTIC
30.E6,.3
*SOLID SECTION,MATERIAL=COMPOS,ELSET=COM
*MATERIAL,NAME=COMPOS
*ELASTIC
30.E4,.3
```

The fourth block imposes boundary conditions and the loading parameters. The command *BOUNDARY defines the constraints applied to the model based on a set of nodes. The constraints could be for displacement and rotation in any direction according to the three dimensional system of co-ordinates of the problem. The loading parameters start with the command *STEP which defines a loading case. This problem uses only one loading case which is the unit external pressure applied on the outer surface. The command *BUCKLE is then introduced with an additional parameter which is the maximum buckling mode that should be evaluated. The command *DLOAD defines the unit loading applied on the external surface.

- Fourth block:

```
*STEP
*BUCKLE
 4,
*BOUNDARY
 SIDE,2
 BASE,1
*DLOAD
 OUTER,P4,1
```

The last block of commands is to define the output file. The finite element program ABAQUS allows several combinations of output. For this analysis, the output was set to give the radial and hoop stresses along the radius as well as the strains in the centroidal position of each element.

- Fifth block:

```
*EL PRINT,FREQUENCY=0
*NODE PRINT, SUMMARY=NO
U, RF
*MODAL PRINT
*MODAL FILE
*END STEP
```

5. Multi-layered pipes in catenary configuration

5.1 Overview

This section now considers the global analysis of a multi-layered pipe in a catenary configuration in deep water. The purpose of this part of the work is to apply the local internal and external pressure models developed earlier to a practical offshore requirement of a catenary riser in deep water. The multi-layered cross-section pipe in a catenary must withstand not only the internal and external pressure loads but also those due to tension and bending. This section compares the multi-layered pipe cross-section with an equivalent single walled pipe subjected to all of the above loads. A quasi-static analysis is used to carry out the comparison. The work in this section was developed by the author based on the previously established catenary equations.

A simple and therefore economic configuration for production risers is the single free catenary. This geometry is very simple; the riser top connection is attached to the platform and then the riser length is laid on the sea bed starting from an appropriate top angle. There are also other possible configurations such as the lazy S, lazy wave, steep S, and so on, as shown inFigure 5.1.1. However, all of them

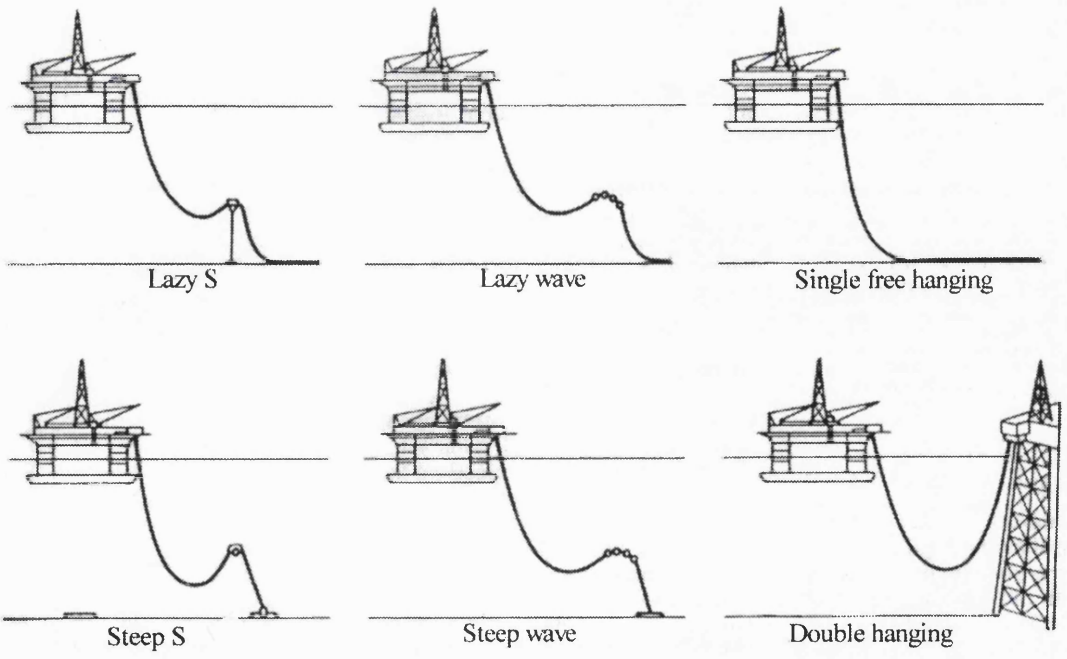

Fig. 5.1.1 Risers configuration.

require additional equipment, such as buoyancy units, and therefore will imply additional costs and installation procedures. The only reason for using other configurations, rather than the single free catenary, is connected with special requirements such as tension load limit of the top connection or to increase allowable platform horizontal motions or to reduce touch down point motions. There are several commercial packages for analysing flexible and rigid riser behaviour due to hydrodynamic loads, self weight and surface vessel motions. Most of them compute a numerical solution based on finite difference or finite element methods. The numerical approach has to be used in order to solve the non-linearities which arise from the hydrodynamic loads and the catenary configuration.

On the other hand, when the water depth increases the static geometry and structural behaviour of a riser in free catenary configuration approaches that of a single cable. It means that bending moments can be neglected - in other words the transmission of moments along the riser does not affect its geometry. Therefore, for deep water (water depths more than 300 meters), the static configuration can be evaluated and optimised more easily using an analytical model based on the assumption that the bending stiffness is neglected and the riser treated as a cable.

5.2 Static analytical model

A static analysis is presented here for a riser in deep water whose bending moment induced loads are negligibly small compared to the loads due to tension and self weight. This assumption is demonstrated to have small errors as will be shown later based on comparison with a finite difference based commercial analysis program FLEXRISER version 4.2 /26/, 1994. Another assumption is that the axial elasticity of the riser is not considered. This assumption also does not introduce a significant error in the model.

The fluid drag force, that is the hydrodynamic resistance due to the flow past the riser element has both normal and parallel components of force. Both of these are proportional to the square of current speed. It is clear that if these loads are to be considered, they will introduce a non-linearity into the equations. This non linearity will not allow straight forward integration, and therefore, the solution would have to

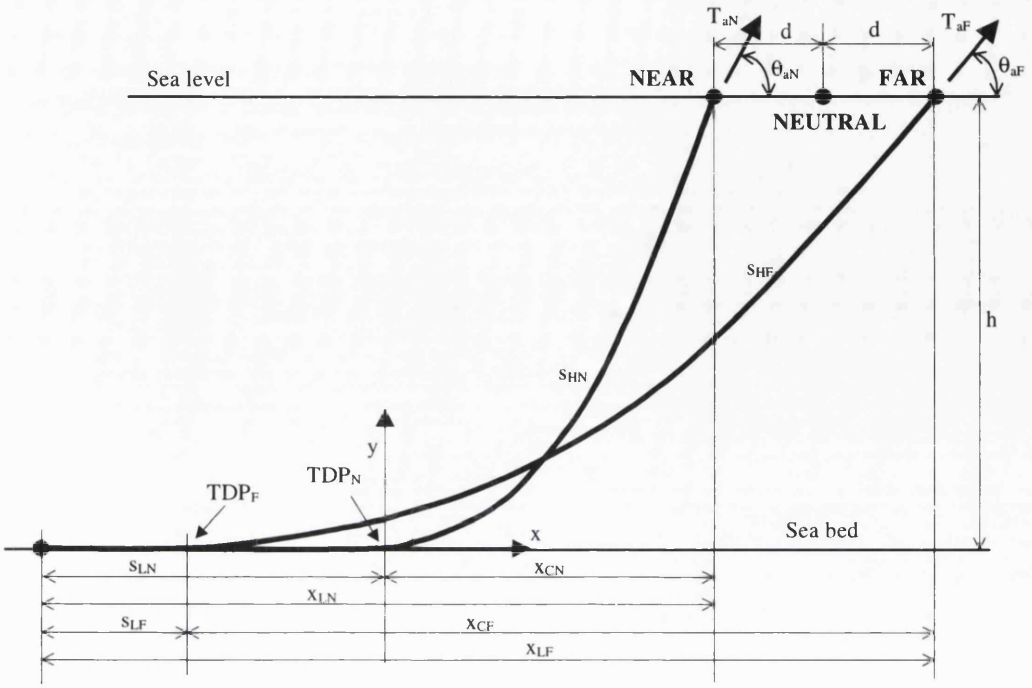

Fig. 5.2.1 Free hanging riser nomenclature.

be obtained only by numerical methods. The static model below, therefore, only considers the zero current still water case.

Consider a single free hanging configuration as shown in figure 5.2.1 and the cable element showed in figure 5.2.2. The rectangular co-ordinates system is fixed at the touch down point, the weight per unit length is w, the top tension is T_a, the horizontal tension is H, and the angle measured between the riser axis and the horizontal is denoted by θ.

For static analysis the equilibrium equations for the element of length ds can be assembled based on the sum of the forces in the vertical and horizontal directions. In this case, the drag and lift forces are not considered:

$$\begin{cases} dT\sin\theta = wds\,, \\ dT\cos\theta = 0\,. \end{cases} \tag{5.2.1}$$

From (5.2.1) integrating the second equation yields

$$T\cos\theta = Const. = H\,. \tag{5.2.2}$$

Once there are no other horizontal loads in the whole system the horizontal projection of the top tension should be equal to the horizontal load at the touch down point. This way the top tension may be written as $T = H / \cos\theta$. Substituting this in

the first equation of (5.2.1) and using the relation $\tan\theta = dy/dx$ gives

$$\frac{d}{dx}(H\tan\theta) = H\frac{d}{dx}\left(\frac{dy}{dx}\right) = w\frac{ds}{dx}. \tag{5.2.3}$$

Integrating the above equation and using the boundary conditions that for $x = 0$, $y = 0$ and $dy/dx = 0$, the solution is

$$y = \frac{H}{w}\left[\cosh\left(\frac{wx}{H}\right) - 1\right]. \tag{5.2.4}$$

From this solution several important relations can be written for the riser as:

$$y'' = \frac{w}{H}\sqrt{1+y'^2}\ ,\ s = \frac{H}{w}\sinh\left(\frac{wx}{H}\right),\ h = \frac{H}{w}\left(\cosh\left(\frac{wx}{H}\right) - 1\right),$$

$$T = H + wh = H\cosh\left(\frac{wx}{H}\right) = \frac{hw}{1-\cos\theta} = \frac{wx}{\sinh^{-1}(\tan\theta)},$$

$$x = \frac{H}{w}\sinh^{-1}\left(\frac{sw}{H}\right) = \frac{H}{w}D = \frac{h}{1/\cos\theta - 1}\sinh^{-1}(\tan\theta). \tag{5.2.5}$$

These results will now be compared with the finite difference commercial package for riser analysis called FLEXRISER /26/. The aim is to find the error made on the assumption that the bending stiffness was neglected. Figure 5.2.3 presents these comparisons. The main parameters for design are top tension at far position and radius of curvature at near position. These are critical points because they are subjected to the maximum stresses. It has been assumed that the top connection offset is 10% of the water depth from the neutral position.

Figure 5.2.3 shows that the error made, for this range, is small and conservative. The top tension on the simplified model is around 2% greater than the FLEXRISER /26/ result at 300m and approaches zero as the water depth increases. The radius of curvature is around 2% smaller than the FLEXRISER /26/ result and grows to about

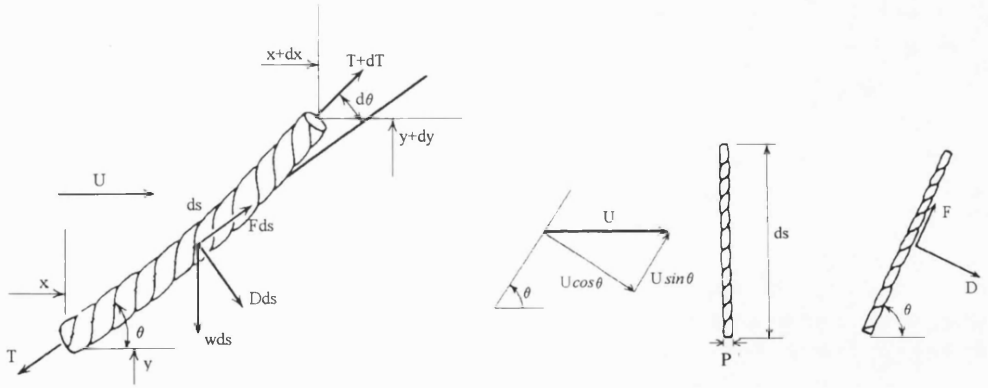

Fig. 5.2.2 Riser element.

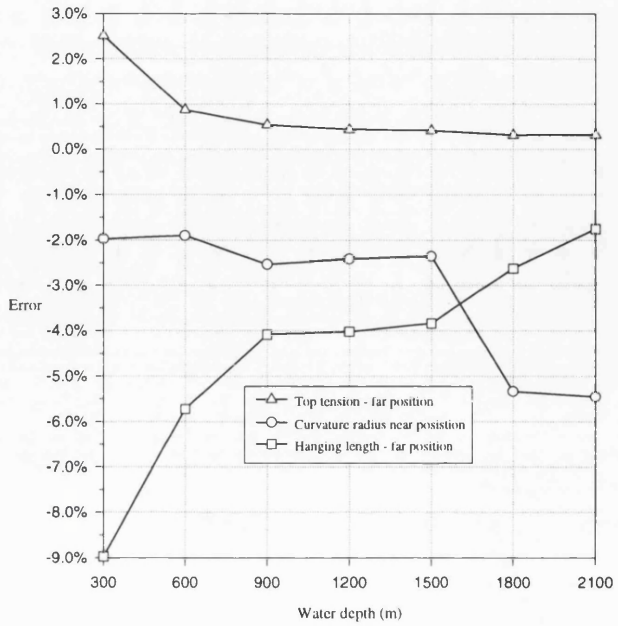

Fig. 5.2.3 Cable approach versus FLEXRISER.

5% as the water depth increases. Geometric parameters such as hanging length and horizontal projection show errors of less than 4% for water depths greater than 900m.

The varying error behaviour is explained by the fact that FLEXRISER is a non-linear finite difference code with the extent of non-linearity dependent on curvature which arises from water depth. The difference in the radius of curvature between the analytic result and FLEXRISER appearing around 1700 m water depth is, therefore, likely to be due to the effect of curvature based non-linear behaviour in the prediction from FLEXRISER.

Based on these results, one can quickly analyse and optimise the static design of a catenary riser using the simplified cable model. It is well known that the riser should be designed to cope with dynamic loads. Bearing this scenario in mind, the static design should be carried out allowing a safety stress margin to be used to withstand dynamic loading.

5.3 Assessment of critical stresses

The catenary configuration has two critical points in terms of stress. The top connection at the far position and the touch down point at the near position. The first

arises because at the far position the top connection will be subjected to the maximum top tension. The second, because at the near position the sag bend will reach the minimum radius of curvature and therefore the maximum bending moment.

Consider the subscript a to denote the top connection and b for the touch down point, and also take the subscript N for near position and F for far position. Using the notation $D = wx/H$, the top tension may then be written as:

$$\frac{T_a}{wh} = 1 + \frac{H_a}{wh}. \tag{5.3.1}$$

But $H_a = T_a \cos\theta_a$, so

$$\frac{T_a}{wh} = \frac{1}{1-\cos\theta}. \tag{5.3.2}$$

The maximum top stress will be reached at the far position and is equal to the top tension divided by the area A_s. Using the yield stress σ_y for the wall material, the maximum axial stress of the riser can be represented by α_{aF} which is the relation between the maximum top stress at far position and the wall material yield stress. Thus,

$$\sigma_{aF} = \frac{T_{aF}}{A_s},\ \alpha_{aF} = \frac{\sigma_{aF}}{\sigma_y} = \frac{T_{aF}}{\sigma_y A_s}. \tag{5.3.3}$$

Using (5.3.2) gives:

$$\frac{\alpha_{aF}}{\left(\frac{wh}{\sigma_y A_s}\right)} = \frac{1}{1-\cos\theta_a}. \tag{5.3.4}$$

Defining the reference ratio α_R in terms of the top stress reached when $\theta_a = 90^o$, leads to the fact that when the riser is in the up right vertical position, the top tension equals own weight or the mass per unit of length w times the water depth h. Then:

$$\alpha_R = \frac{wh}{\sigma_y A_s}. \tag{5.3.5}$$

Therefore, the dimensionless relation α_{aF}/α_R denotes the ratio of the far position axial top tension stress to the slack vertical axial top tension stress and will always be greater than unity. This ratio given in equation (5.3.6) is plotted in figure 5.3.1,

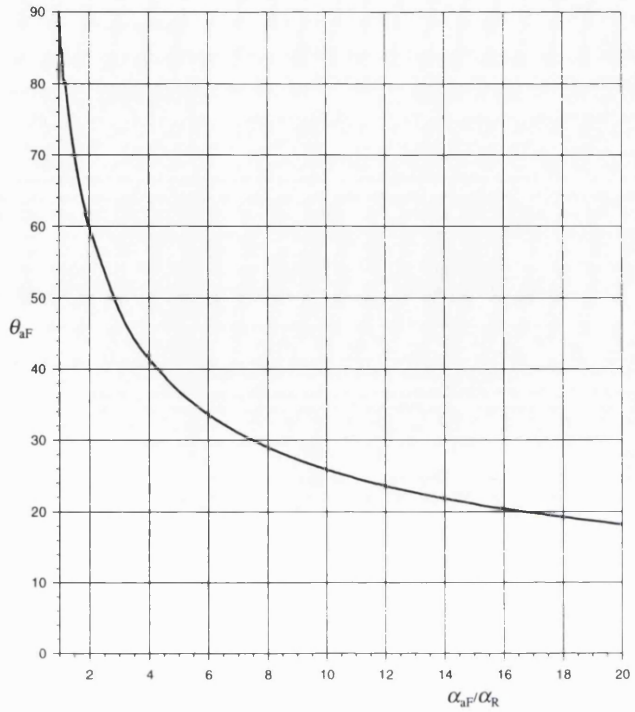

Fig. 5.3.1 Top angle versus stress rate at far position.

$$\frac{\alpha_{aF}}{\alpha_R} = \frac{1}{1-\cos\theta_{aF}}. \tag{5.3.6}$$

It is seen that if the far point stress ratio grows to infinity, the top angle approaches zero. Another interesting conclusion is that reasonable values for this stress ratio should be larger than say 3 but less than 10. In this range, the top angle from the horizontal will be between 50 and 25 degrees.

Considering a single walled steel pipe, and keeping the riser content density and the wall yield stress fixed, the reference ratio is a function only of the ratio between the outside diameter and the wall thickness, OD/*t*. The reference ratio is given by

$$\alpha_R = \frac{g}{\sigma_y}\left[(\rho_m - \rho_o) + \left(\frac{\rho_o - \rho_w}{4}\right)\cdot\left(\frac{(OD/t)^2}{(OD/t-1)}\right)\right], \tag{5.3.7}$$

where g is the acceleration due to gravity, ρ_m is the wall material density, ρ_o is the riser contents density, and ρ_w is the sea water density. It can be seen from figure 5.3.2(a) that the reference ratio α_R has a slight variation with *OD/t* for content density close to the sea water density. This figure was prepared by considering a pipe made of steel grade API 5LX60 and contents density for oil and gas. If the riser content density is low, filled with gas for example, the α_R value varies accordingly.

Next the near position parameters are analysed. The main parameter is the maximum offset of the floating unit - typical by between 5% and 15%. The following equations follow from the catenary solution of (5.2.5):

$$s = \frac{H}{w}\sinh D, \quad h = \frac{H}{w}(\cosh D - 1), \text{ and } x = \frac{H}{w}D. \tag{5.3.8}$$

Therefore,

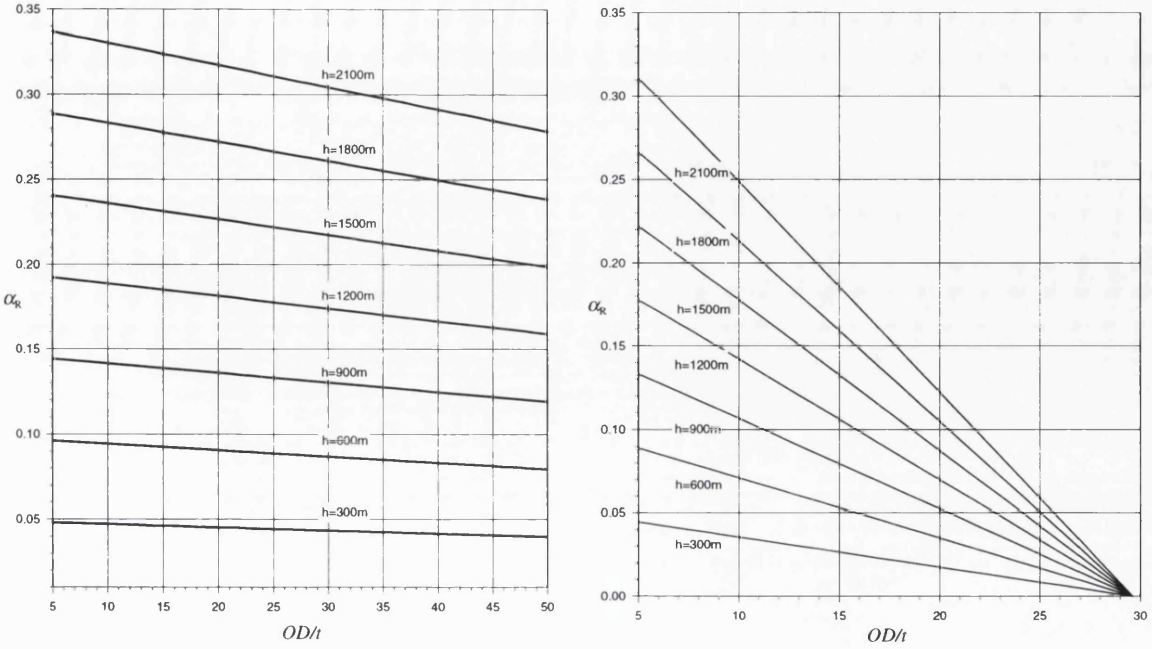

(a) Oil content (920 kg/m^3). (b) Gas content (1.3 kg/m^3).

Fig. 5.3.2 Variation of reference ratio α_R with *OD/t*.

$$\frac{s}{h}=\frac{\sinh D}{\cosh D-1},\quad \frac{x}{h}=\frac{D}{\cosh D-1},\text{ and }\frac{s-x}{h}=\frac{\sinh D-D}{\cosh D-1}. \tag{5.3.9}$$

From figure 5.2.1 based on the following nomenclature, and remembering that the subscript *F* is for far position and *N* for near position. The variables are as following

$s \rightarrow$ total length of the riser;

$s_h \rightarrow$ free hanging length of the riser;

$s_L \rightarrow$ length of riser laid on sea bed;

$x_c \rightarrow$ horizontal projection of the free hanging length;

$x_L \rightarrow$ horizontal projection of the whole riser length;

$h \rightarrow$ water depth;

$d \rightarrow$ maximum horizontal offset of the top connection.

The following relationships can then be posed:

$$\begin{cases} s = s_{hF} + s_{LF}\,, \\ x_{LN} = x_{LF} - 2d\,, \\ x_{LF} = x_{cF} + s_{LF}\,. \end{cases} \tag{5.3.10}$$

Using (5.3.9) and (5.3.10) gives

$$\frac{s - x_{LN}}{h} = \frac{s_{hF} - x_{cF} + 2d}{h} = \frac{s_{hN} - x_{cN}}{h} = \frac{\sinh D_N - D_N}{\cosh D_N - 1}. \qquad (5.3.11)$$

Then,

$$B = \frac{s_{hF} - x_{cF}}{h} = \frac{\sinh D_F - D_F}{\cosh D_F - 1}. \qquad (5.3.12)$$

Substituting and assuming that $\delta = d / h$ and $A = B + 2\delta$ gives

$$\frac{\sinh D_N - D_N}{\cosh D_N - 1} = B + 2\delta = A. \qquad (5.3.13)$$

The value of D_N can be evaluated with negligible error by substituting the hyperbolic functions in (5.3.13) for Taylor series around zero up to fifth order: $\sinh D_N = D_N + {D_N}^3/6$, and $\cosh D_N = 1 + {D_N}^2/2 + 24$, to yield

$$D_N = \frac{2}{A}\left[1 - \sqrt{1 - 3A^2}\right] \qquad (5.3.14)$$

From these results and remembering that $\tan\theta = \sinh D$, the top angle at near position can be found provided that the value of A is known. It means, when the top angle at far position θ_{aF} is known D_F can be evaluated using $D_F = \sinh^{-1}(\tan\theta_{aF})$.

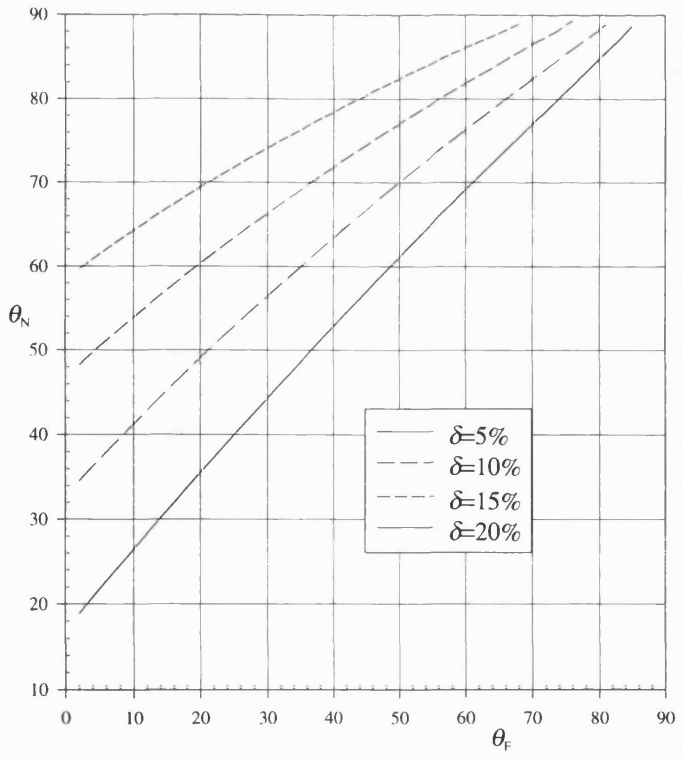

Fig. 5.3.3 Values of top angle near position θ_N as a function of θ_F and maximum offset δ.

Substituting D_F in equation (5.3.12) the value of B is calculated. Now, A is obtained by adding to B twice the maximum excursion δ. From equation (5.3.14) D_N is finally determined. So, $\theta_N = \tan^{-1}(\sinh D_N)$. Figure 5.3.3 shows the relationship between these angles as a function of the offset.

In order to optimise the design, the bending stress

condition reached by the pipe wall at the touch down point region (*TDP*) should be examined. The region where the minimum radius of curvature r_c is reached can be obtained using equation (5.2.5), with $y''_{TDP} = 1/r_c$. At the touch down point, the slope is $y'_{TDP} = 0$. Therefore,

$$y''_{TDP} = \frac{w}{H}\sqrt{1+y'^{2}_{TDP}} = \frac{1}{r_c} = \frac{w}{H}. \tag{5.3.15}$$

From bending theory the bending moment is

$$M = -EIy'' = -\frac{EI}{r_c}. \tag{5.3.16}$$

The maximum bending stress in a pipe is reached when y is maximum or equal to half of the pipe outside diameter *OD/2*. Thus, at *TDP* the maximum bending stress is

$$(\sigma_b)_{MAX} = \frac{M}{I}\cdot\frac{OD}{2} = \frac{E}{r_c}\cdot\frac{OD}{2}. \tag{5.3.17}$$

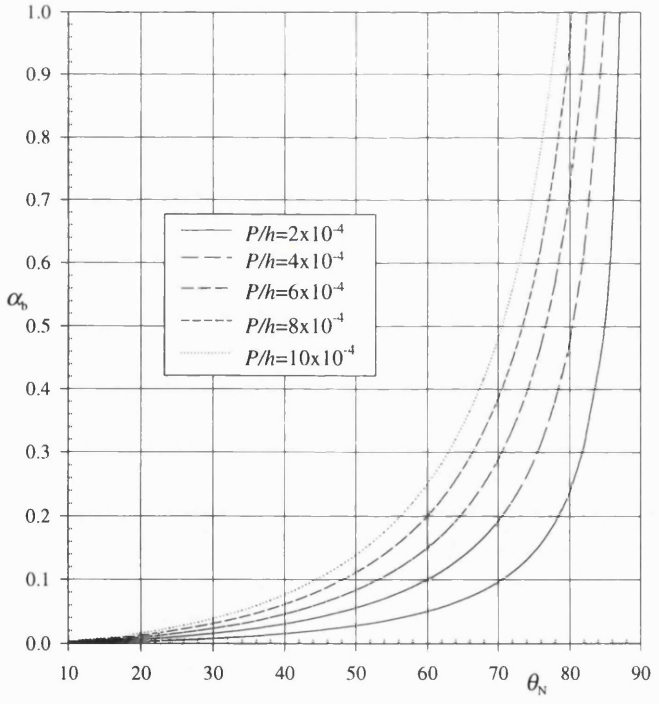

Fig. 5.3.4 Values of touch down point stress condition α_b as a function of θ_N and the dimensionless OD/*h*.

It should be pointed out that the second moment of area (*I*) from equation (5.3.16) when substituted in (5.3.17) is dropped. It means that the pipe second moment of area has no influence in the maximum stress reached at the touch down point. Therefore, whatever the geometry of the pipe, the bending stress at touch down point will be a function only of the radius of curvature, the outside diameter and material properties. This simplification arises because the radius of curvature is not a function of the pipe bending rigidity (*EI*) due to the fact that the riser is being treated as a cable. With α_b being the ratio between the maximum bending stress and the yield

stress of the pipe wall material ($\sigma_y = E \cdot \varepsilon_y$). Thus,

$$\alpha_b = \frac{\sigma_b}{\sigma_y} = \frac{1}{2 \cdot \varepsilon_y} \cdot \frac{1}{r_c/h} \cdot \frac{OD}{h}. \tag{5.3.18}$$

From (5.3.8) and (5.3.15), the minimum radius of curvature r_c may be written as a function of top angle at near position. Thus,

$$\frac{H}{w} = \frac{h}{\cosh D_N - 1}, \qquad \frac{r_c}{h} = \frac{1}{\cosh D_N - 1}. \tag{5.3.19}$$

Based on (5.3.18) and (5.3.19), the bending stress ratio (α_b) is obtained as a function of the top angle at near position and the non-dimensional variable *P/h*. Figure 5.3.4 shows this relation graphically. Thus,

$$\alpha_b = \frac{(\cosh D_N - 1)}{2\varepsilon_y} \cdot \frac{OD}{h}. \tag{5.3.20}$$

Although the bending stress is the most important stress, the real stress condition of the touch down point has to incorporate the axial stresses σ_A, due to horizontal tension, and the hoop stresses σ_H, due to hydrostatic pressure. Combining these stresses using the von Mises criteria the value of the stress condition can be obtained more accurately:

$$\sigma_{MISES} = \sqrt{\tfrac{1}{2}\left[(\sigma_x - \sigma_y)^2 + (\sigma_x - \sigma_z)^2 + (\sigma_y - \sigma_z)^2\right]}. \tag{5.3.21}$$

Considering the element, of figure 5.3.5 and the axis convention, the bending stresses are acting in the same direction than the axial stresses. Then, they should be summed. Therefore, the stresses acting on the element are:

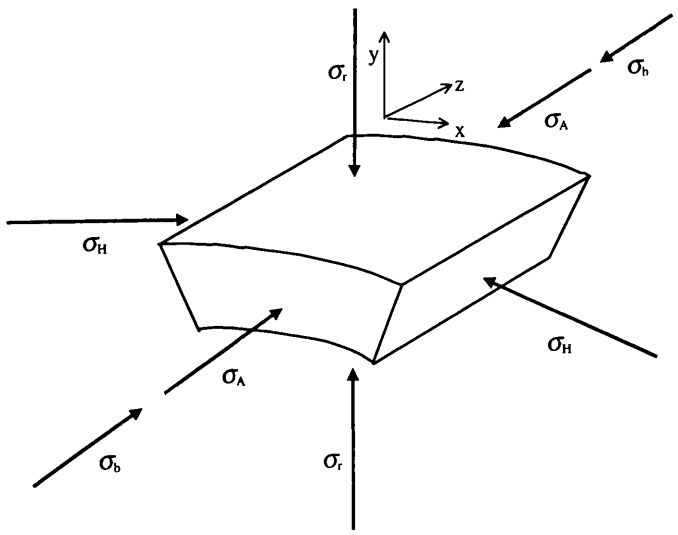

Fig. 5.3.5 Wall element at touch down point.

$$\sigma_x = \sigma_A + \sigma_b, \quad \sigma_y = \sigma_r = -p_e, \quad \sigma_2 = 0 \tag{5.3.22}$$

The value of the bending stress and axial stress is a function of the riser configuration, pipe geometry, and material properties. On the other hand, the hoop and radial stresses are function of water depth, pipe geometry, and also material properties.

So, considering *a* the inner radius and *b* the outer radius for a single walled pipe,

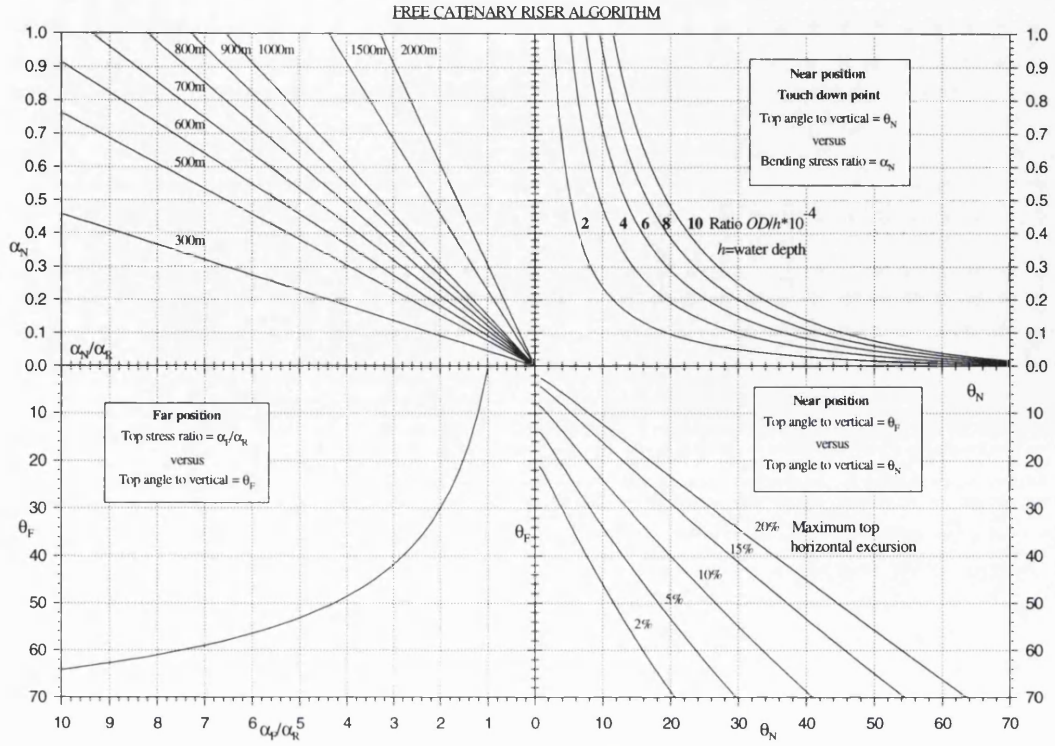

Fig. 5.3.6 Free catenary riser algorithm.

give the equations

$$\sigma_A = \frac{H}{A_s} = \frac{H}{\pi\left(b^2 - a^2\right)},\ \sigma_b = E \cdot \frac{w}{H} \cdot b,\ \sigma_H = \frac{2a^2 p_i - \left(a^2 + b^2\right) p_e}{\left(b^2 - a^2\right)}. \quad (5.3.23)$$

Based on this approach an algorithm to optimise the design of a catenary riser may be built. Figure 5.3.6 shows this algorithm. The aim is to determine the optimised top angle at far and near position. Using the free catenary riser algorthm the designer can chose and optimise the top angle for near and far position of a steel catenarty riser based on the maximum stress reached on these positions. Next an application of the algorthm will illustrate its utility.

These angles will determine the whole catenary riser configuration provided the bending stiffness is neglected. Bearing in mind that the maximum pipe stresses have to comply with standards, the optimised top angles can be easily determined. For example, considering the following pipe geometry:

- Inside diameter = 10 inch
- Wall thickness = 0.7692 inch
- *P/t* ratio = 15
- Water depth = 1000 m
- Content density:
- Steel API 5LX60
- Yield stress = 4.137 10^8 Pa
- Yield strain = 0.2%
- Young Modulus = 2.07 10^{11} Pa
- Poisson ratio = 0.29

- Oil 920 Kg/m^3
- Sea water 1025 Kg/m^3
- Gas 1.3 Kg/m^3
- Density = 7850 Kg/m^3
- Excursion = 10%
- *OD/h* = 2.93 10^{-4}

From the data above, the steel pipe area and the submerged weight per unit of length can be evaluated. Substituting water depth and the yield stress into (5.3.5) gives the top axial reference stress ratio α_R=15.43%. It means that this pipe in a vertical position and just hanging will reach 15.43% of the yield stress in the axial direction. Using figure 5.3.6, the optimised design may be found based on the curves for 10% excursion; *OD/h*=2.9 10^{-4}; and 1000 m water depth. With a top ratio of 2.02, which means an axial stress at far position of 2.02 times the reference axial stress ratio or 31.24% of the yield stress. This value gives a top angle with the vertical at far position of 30.41 degrees. On the next graph, using 10% excursion yields a top angle at near position equal to 13.91 degrees. Going up to the next graph with *OD/h*, gives a bending stress ratio at touch down point equal to 23.15%. Combining the bending stress ratio with axial, radial and hoop stresses at touch down point with von Mises criterion gives 31.24%. In other words the same stress state of the top connection at the far position.

OD/t	25	20	15	10
α_R	14.81%	15.12%	15.43%	15.74%
Far position				
Top angle w/vertical (degree)	30.62	30.42	30.41	30.92
Top Axial stress/yield	30.18%	30.62%	31.24%	32.37%
Near position				
Top angle w/vertical (degree)	14.04	13.92	13.91	14.23
TDP Mises	30.18%	30.62%	31.24%	32.36%
TDP bending stress	21.54%	22.28%	23.15%	24.35%
TDP Hoop stress/yield	5.17%	4.55%	3.93%	3.31%
TDP Radial stress/yield	2.43%	2.43%	2.43%	2.43%
TDP Axial stress/yield	4.74%	4.79%	4.88%	5.13%

Table 5.3.1 Effect of changes in *OD/t*, content oil, water depth 1000m.

Water depth (m)	300	500	1000	1500	2000
α_R	4.63%	7.71%	15.43%	23.14%	30.86%
Far position					
Top angle w/vertical (degree)	56.88	46.44	30.41	21.68	16.70
Top Axial stress/yield	28.48%	28.02%	31.24%	36.70%	43.30%
Near position					
Top angle w/vertical (degree)	31.35	24.22	13.91	8.59	5.66
TDP Mises	28.49%	28.03%	31.24%	36.69%	43.31%
TDP bending stress	22.51%	21.07%	23.15%	27.80%	33.50%
TDP Hoop stress/yield	1.18%	1.97%	3.93%	5.90%	7.86%
TDP Radial stress/yield	0.73%	1.21%	2.43%	3.64%	4.86%
TDP Axial stress/yield	5.02%	5.37%	4.88%	4.07%	3.37%

Table 5.3.2 Effect of change in water depth, *OD/t*=15, content oil.

Riser content	Gas	Oil	Water
α_R	8.85%	15.43%	16.18%
Far position			
Top angle w/vertical (degree)	44.60	28.72	27.08
Top Axial stress/yield	29.70%	29.70%	29.70%
Near position			
Top angle w/vertical (degree)	23.00	12.87	11.86
TDP Mises	29.71%	33.20%	34.94%
TDP bending stress	11.43%	25.57%	28.32%
TDP Hoop stress/yield	17.10%	3.93%	2.43%
TDP Radial stress/yield	2.43%	2.43%	2.43%
TDP Axial stress/yield	5.67%	4.42%	4.19%

Table 5.3.3 Effect of change in riser content, OD/t=15, water depth 1000m.

The following tables have been obtained using the optimisation method aiming always to maintain the same stress level for the far and near position.

5.4 Comparison between multi-layered and single walled pipes

The free catenary riser design applying multi-layered pipes rather than single walled pipes will demand the same design procedure. However, due to its characteristics the multi-layered riser will allow much more design flexibility; since the density of the intermediate layer material can be selected to induce less submerged weight per unit of length in the pipe structure. Therefore, the induced stresses will drop in the same fashion. On the other hand, in order to match the single walled pipe hydrostatic pressure resistance the multi-layered pipe will need a bigger outside diameter. It implies according to (5.3.18), that the maximum bending stress will increase in direct proportion to the outside diameter. It means that the equivalent multi-layered walled pipe should be designed bearing in mind that the outside diameter should be kept as low as possible.

A rough comparison of the drop of top tension due to the higher wall thickness of the multi-layered pipe is shown in figure 5.4.1. The percentage represents the rate between the double walled pipe top tension and the single walled pipe. The density of the intermediate material was taken to be 50% of the sea water; the pipes were designed to 1000m water depth, using 30% of yield stress at the top connection in far position, and 10% offset. The geometric structural equivalence was met by equating the theoretical buckling pressure to $\beta = 1$.

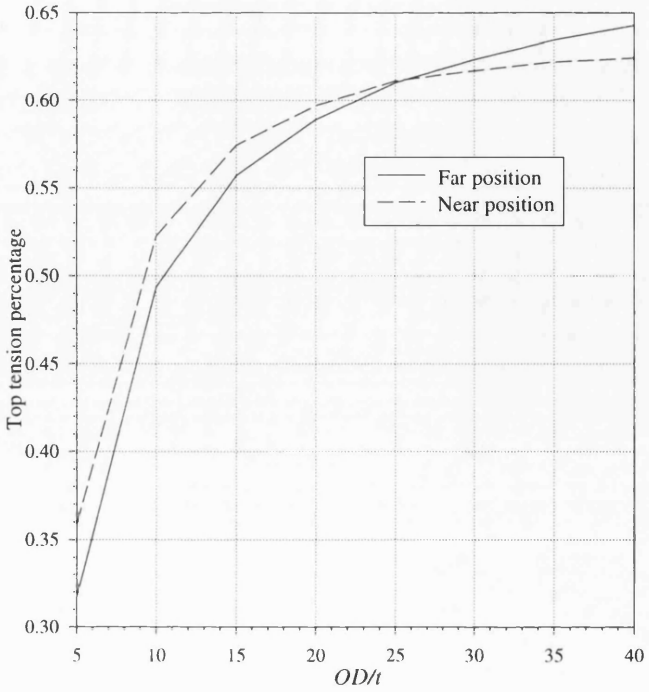

Fig 5.4.1 Top tension percentage of using multi-layered pipe rather than single walled pipe.

To achieve an equivalent multi-layered pipe design the theoretical hydrostatic buckling pressure was equalised. To simplify, the multi-layered pipe will have its geometric characteristics reduced to two parameters provided the inside diameter is kept the same as of the single wall pipe. The theoretical well known equation for the critical external pressure $(p_{SW})_{cr}$ of single walled pipe is

$$(p_{SW})_{cr} = \frac{E_s}{4\left(1-\nu_s^{\,2}\right)}\left(\frac{t}{R}\right)^3 = \frac{E_s}{4\left(1-\nu_s^{\,2}\right)}\left(\frac{2}{OD/t-1}\right)^3. \qquad (5.4.1)$$

Where E_s is the Young's modulus, and ν_s the Poisson's ratio of the wall material, t is the wall thickness, and R is the wall mean radius. The multi-layered pipe elastic buckling pressure for long cylinders is evaluated assuming the approximation of Raville (1954) /62/. The faces are of equal thickness f, the core thickness is co, and the Young's modulus and shear modulus of the core material is to be infinite. Then

$$(p_{MP})_{cr} = \frac{E_s f}{a\left(1-\nu_s^{\,2}\right)} \cdot \frac{3\left[\left(1-b/a\right)^2 + \frac{f^2}{12ab}\left(1+b/a\right)^2\right]}{\left(1+\frac{b^2}{a^2}\right)}, \qquad (5.4.2)$$

where a is the mean radius of the first face, and b is mean radius of the second face.

Simplifying the equation (5.4.2) considering thin faces or membrane facing, and assuming the two dimensionless parameters for defining the geometry of the double walled pipe $\alpha = b/a$ and $\beta = co/f$ gives

$$(p_{MP})_{cr} = \frac{E_s}{(1-\nu_s^2)} \cdot \frac{3(1-\alpha)^3}{(\beta+1)(1+\alpha^2)}. \qquad (5.4.3)$$

Equating (5.4.1) and (5.4.3) but keeping the inside diameter the same, the equivalent equation obtained is

$$OD/t = 1+\left[\frac{1}{1-\alpha}\sqrt[3]{\frac{2}{3}(1+\beta)(1+\alpha^2)}\right]. \qquad (5.4.4)$$

This equivalence is only valid for a limited range of values of α and β. That is values where the faces are thin compared with core thickness $c/f \geq 5$. In addition, the material of the core should have sufficient strength to keep the faces apart and do not wrinkle just before buckling.

The elastic theoretical solution for double walled buckling pressure can be refined. However, this will lead to a very complicated equivalence equation with no practical application. Here the margins where the simplification used on equation (5.4.3) is acceptable, is evaluated. If moderately thick faces is used, the bending rigidity and shear in the faces have to be considered, equation (5.4.3) would become

$$(p_{MP})^*_{cr} = \frac{E_s}{(1-\nu_s^2)} \cdot \left[\frac{3(1-\alpha)^3}{(\beta+1)(1+\alpha^2)} + \frac{(1-\alpha^2)^2(1-\alpha)}{12\alpha(1+\alpha^2)(\beta+1)^3}\right]. \qquad (5.4.5)$$

Table 5.4.1 shows the comparison between (5.4.3) and (5.4.5) as a function of α and

α	β	$(p_{MP})_{cr} \cdot \frac{(1-\nu_s^2)}{E_s}$		Differ.
		(5.4.3)$*10^3$	(5.4.5)$*10^3$	
0.7	1	27.181	27.961	+2.87%
0.8	1	7.317	7.523	+2.81%
0.9	1	0.829	0.852	+2.79%
0.7	5	9.060	9.089	+0.32%
0.8	5	2.439	2.447	+0.31%
0.9	5	0.276	0.277	+0.31%
0.7	10	4.942	4.947	+0.09%
0.8	10	1.330	1.332	+0.09%
0.9	10	0.151	0.151	0.09%

Table 5.4.1 Buckling pressure for thick faces.

β values. For values of $c/f > 5$ membrane theory leads to almost the same value for the thick faces. For values of $c/f \geq 1$ the error is less than 3% and the difference is almost independent of the values of α. Therefore, the equivalence equation (5.4.4) may be used over a quite wide range.

If finite values for Young's modulus and Shear modulus were introduced in the evaluation, the critical pressure, p'_{CM} is obtained by determining the biggest roots of the following second degree equation, which is result of the determinant evaluation – see Raville (1954):

$$\left(\frac{p'_{CM}{}^2}{E_c^2}\right)\kappa(1-\kappa)\left\{4\frac{(1-b/a)^2}{(b/a)^2}+\left[\left(\frac{E_c}{2G_{r\theta}}+2\right)\left(\frac{1-(b/a)^2}{(b/a)^2}\right)\right.\right.$$

$$\left.+\frac{E_c a(1-\nu_s^2)}{4E_f f}\left(\frac{1+b/a}{b/a}\right)\right]\ln\frac{b}{a}\Bigg\}-\frac{p'_{CM}}{E_c}\left\{\frac{(1-b/a)^2}{(b/a)^2}\left[\frac{b}{a}-\kappa\left(1+\frac{b}{a}\right)\right]\right.$$

$$+\frac{3}{4}[1-\kappa(1-b/a)]\frac{\ln b/a}{b/a}-\frac{1}{3}\left[\frac{b}{a}+\kappa(1-b/a)\right]\left[\left(\frac{E_c}{2G_{r\theta}}-1\right)\left(\frac{1-(b/a)^2}{(b/a)^2}\right)\right.$$

$$\left.\left.\left.+\frac{E_c a(1-\nu_f^2)}{4E_f f}\left(\frac{1-b/a}{b/a}\right)\right]\right\}-\frac{1}{4}\frac{(1-b/a)^2}{b/a}=0, \qquad (5.4.6)$$

where E_c, $G_{r\theta}$ are the Young's modulus and Shear modulus of the core material respectively, p is the critical pressure, and

$$\kappa=\frac{1}{\left(1+\frac{b}{a}\right)-\frac{E_f f \ln b/a}{E_c a}}. \qquad (5.4.7)$$

The difference between equation (5.4.6) and the simplified equation (5.4.3) is shown in figure 5.4.2 as a function of the strength of the core material and the geometric parameters α and β. The core material is considered isotropic, therefore, $G_{r\theta} = E_c/2(1+\nu_c)$. The Young's modulus of the core material is represented by the dimensionless number m, which is the ratio between the Young's modulus of the faces and the Young's modulus of the core, so $m = E_f/E_c$. Figure 5.4.2 shows the range of values for α, β, and m where the simplified equation can be used within a minor error. From this figure one can see that this simplified assumption leads to an overestimated value of the buckle pressure. In other words the simplified approach

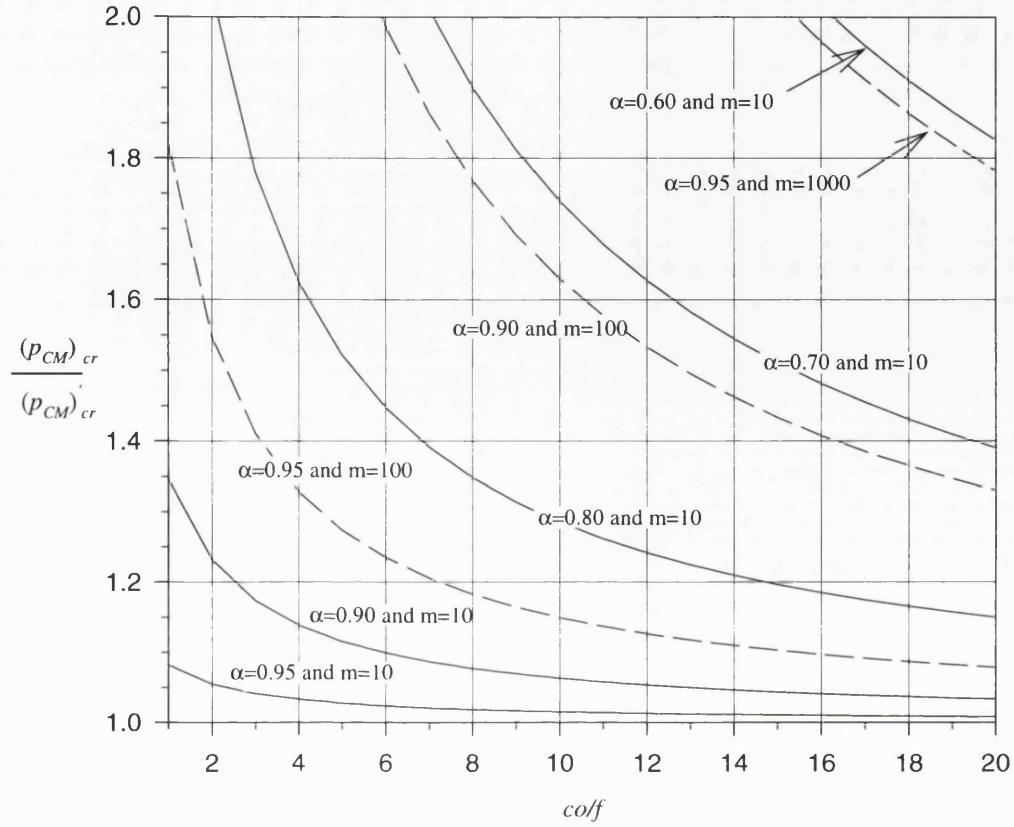

Fig. 5.4.2 Muilti-layered pipe buckle pressure comparison by considering the Young's Modulus and Shear Modulus of the core $(p_{CM})'_{cr}$ eq. (5.4.6) and $(p_{CM})_{cr}$ eq. (5.4.3).

leads to a bigger value for the buckling pressure. For values of $\alpha = 0.95$ and $m = 10$ equation (5.4.3) and (5.4.6) give almost the same values. As long as the double walled pipe becomes thicker $\alpha < 0.95$ or the intermediate material becomes softer $m > 10$ the difference between them rises.

The equivalence approach in equation (5.4.4) is a good starting point for the design of equivalent multi-layered pipes. However, after the core material has been chosen, the whole equation (5.4.6) for bucking assessment should be computed to allow a safe design. For a better evaluation of the benefits of multi-layered construction, the figures 5.4.3(a) and 5.4.3(b) show the equivalence between the single walled and multi-layered construction for the same theoretical buckling pressure based on equation (5.4.4). One of the parameters α or β has to be fixed in order to determine the other for a specific single walled pipe as defined by its ratio P/t.

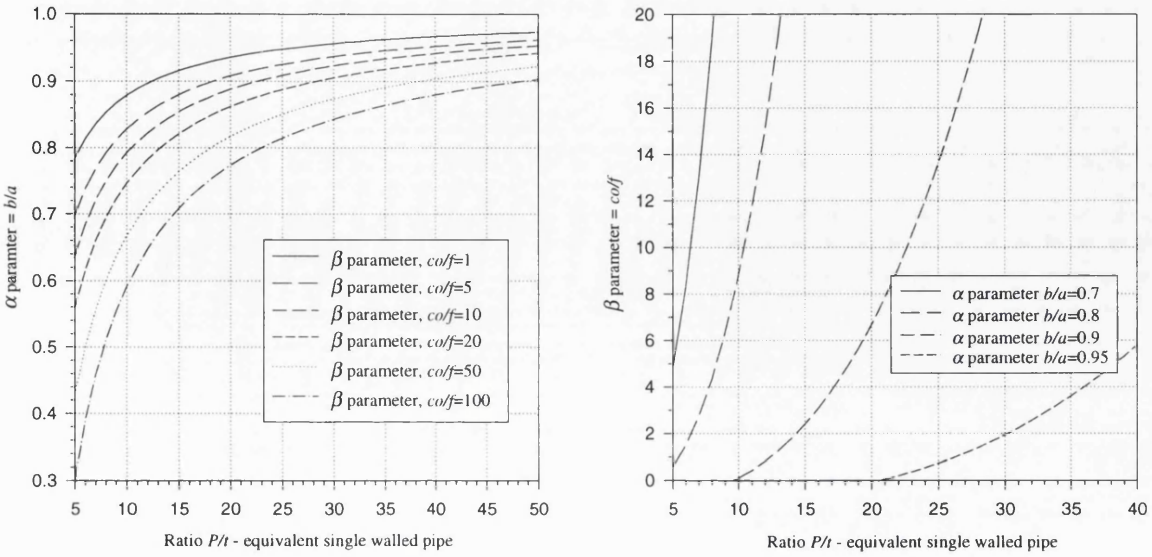

(a) (b)

Fig. 5.4.3 Buckling equivalence of multi-layered pipe with singe walled pipe, same internal diameter.

Besides the buckling pressure, the bending stress at touch down point (*TDP*) in the near position has to be checked. As has been pointed out before, when outside diameter increases the bending stress grows proportionally. The maximum stresses achieved on the wall for a typical free catenary configuration should be investigated. Of course, the multi-layered pipe can considerably reduce the top tension by using a light material in the core. However, it will lead to the design of a buckling equivalent

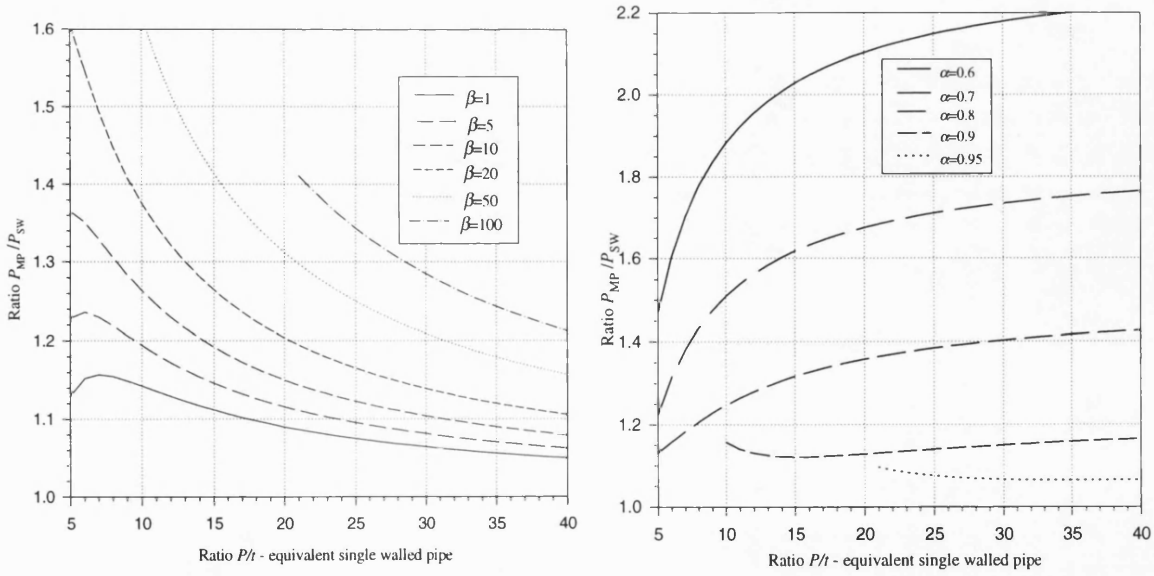

(a) (b)

Fig 5.4.4 Outside diameter ratio equivalent multi-layered to single walled pipe.

multi-layered pipe with bigger outside diameter. Figures 5.4.4(a) and 5.4.4(b) show the ratio of outside diameter for a equivalent multi-layered pipe (P_P) to the outside diameter of a single walled pipe (P_W). It can be seen that using the multi-layered construction will induce more bending stresses at touch down point in near position. For α>0.90 the outside diameter increases less than 20% for the whole range. For typical offshore applications (10>OD/t>30) it is possible to find a suitable combination of parameters to avoid big increases in the outside diameter.

6. Application studies

6.1 Multi-layered cylinder solution for internal pressure and ABAQUS.

In order to verify the solution achieved by the analytical approach presented in section 3, results from this analysis were compared with results from the finite element solid modelling package ABAQUS for several configurations. In these comparisons, an internal pressure of 103440 MPa (15000 psi) and a zero external pressure were used. The comparison is made between a single layer steel pipe and a multi-layered pipe with a core with material of Young's Modulus given by $E_c = E_s/m$. The single cylinder geometry is 0.254m (10-inch) internal radius and 0.508m (20-inch) outer radius.

Figure 6.1.1 presents the radial strain, hoop, and radial stress distributions along the thickness for the single layer steel cylinder. Figure 6.1.2 shows the solution for a multi-layered pipe. In this case, the pressure gap and the internal and external radius are the same. However, the intermediate layer is 40% (co/t=0.4) of the wall thickness with an inner radius of b=0.3556m (14-inch) and an outer radius of c=0.4572 m (18-inch). The ratio m between the steel and intermediate material Young's modulus is 500. The analytical derived stresses as well as the strains match accurately with equivalent results from ABAQUS as would be expected.

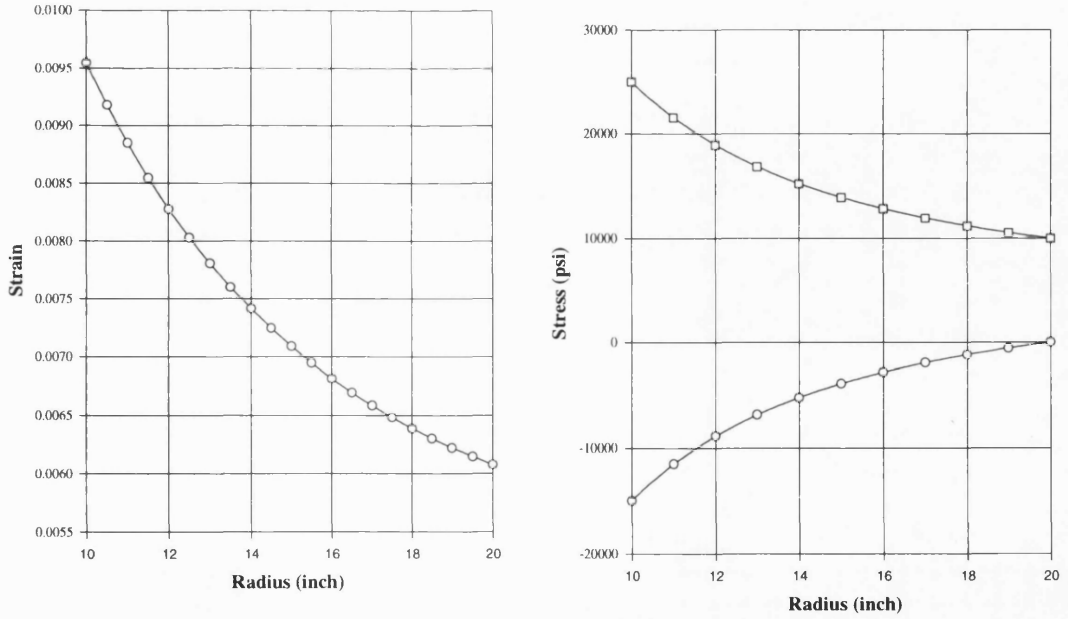

Fig. 6.1.1 Comparison between the analytical model (continuous line) and ABAQUS solution (symbols) for a single walled steel pipe - Stresses (hoop and radial) and strain in radial direction.

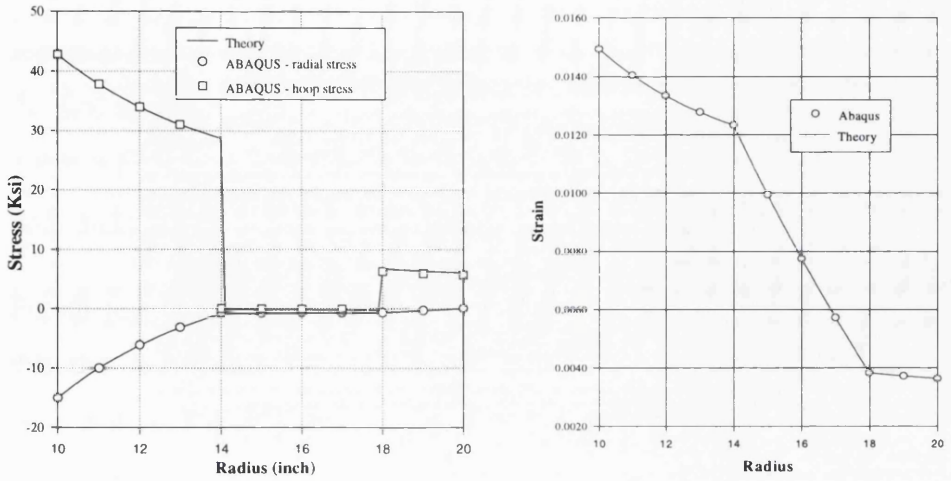

Fig. 6.1.2 Comparison between the analytical model (continuous line) and ABAQUS solution (symbols) for the multi-layered pipe - Stresses (hoop and radial) and strain in radial direction, m=500.

6.2 Parametric results for multi-layered pipes under internal pressure.

This section presents a parametric study of analyses carried out to investigate the behaviour of the stresses and strains of different multi-layered pipe cross-sections under internal pressure loading. The case considered is a pipe made of steel inner and outer layers with the internal core layer being of smaller Young's Modulus. The results are presented in graphical form.

To achieve a better understanding of the structural behaviour of multi-layered pipes, their stress and strain performance is presented in comparison with the equivalent isotropic single walled pipe. The basic criterion for this comparison is that the amount of steel in both pipes is the same. The multi-layered pipe differs only by the inclusion of an intermediate layer that splits the steel into two thinner faces. The graphical results from the parametric analysis are classified into three groups corresponding to the diameter and thickness relation of the equivalent single walled steel pipe. An outside diameter to wall thickness ratio OD/t equal to 10, 20 and 30 represents the range from thick to thin wall pipes. The intermediate material stiffness is given as the ratio between the steel and the intermediate material Young's Modulus, that is $m = E_s / E_c$. The geometry of the multi-layered pipe is also defined in terms of the thickness and the position of the intermediate layer. The thickness of the intermediate layer corresponds to the ratio η, between the actual intermediate

layer thickness and the total thickness of the pipe wall. The position of the intermediate layer defined as ratio χ, gives the relationship between the thickness of the first steel layer with the total thickness of the pipe wall, see Figure 3.3.1 and Table 3.1.1. It means that if χ was equal to $(1-\eta)/2$ the core is in the centre and both inner and outer steel faces have the same thickness.

For all cases presented, the inner radius of the pipe thickness is 5-inches. Beyond this, the various changes in geometry are given in terms of the ratios given above. Note that the second steel layer has thickness $t(1-\eta-\chi)$ where t is the total wall thickness. Tables 6.2.1, 6.2.2, and 6.2.3 present the geometrical parameters used to plot the graphs for $OD/t=10$, 20, and 30. The first row of values correspond to the single walled steel pipe geometry based on the parameter OD/t. These are followed by the values for the geometry of the multi-layered pipe including the intermediate layer dimensions with all dimensions in inches. The Table presents values for four cases each case representing a particular core material thickness denoted by η with this parameter assuming values of 80%, 60%, 40% and 20% of the total wall thickness. The value of χ as explained above denotes the position of the intermediate layer, which in this case is always centred in the pipe total wall thickness.

***OD/t*=10**	**Radius (inches)**	χ / η	**80% 10%**	**60% 20%**	**40% 30%**	**20% 40%**
single walled pipe	inner thickness outer		5.000 1.250 6.250	5.000 1.250 6.250	5.000 1.250 6.250	5.000 1.250 6.250
inner layer	inner thickness outer		5.000 0.476 5.476	5.000 0.551 5.551	5.000 0.588 5.588	5.000 0.610 5.610
core layer	inner thickness outer		5.476 3.810 9.286	5.551 1.654 7.205	5.558 0.784 6.372	5.610 0.305 5.915
outer layer	inner thickness outer		9.286 0.476 9.762	7.205 0.551 7.756	6.372 0.588 6.960	5.915 0.610 6.525
Total thickness			**4.762**	**2.756**	**1.960**	**1.525**

Table 6.2.1 - Pipe dimensions (in inches) for $OD/t=10$.

All graphs of Figure 6.2.1 were obtained for intermediate layer centred in the pipe wall. It means that the internal and external layers have the same thickness. Here the aim is to understand the behaviour of the multi-layered pipe with core intermediate

layer material which is less stiff than steel. The Young's Modulus ratio as $m=E_s/E_c$ of 2, 5 and 10 were used.

The results presented on the graphs as the von Mises Stress Ratio μ which is a ratio of the von Mises stress reached at a point in the radial direction for the multi-layered pipe with respect to that reached in the equivalent single walled pipe. As explained before, the equivalent single walled pipe is that using the same amount of steel as the multi-layered pipe. The non-dimensional radius parameter ρ is the ratio between the radial position divided to the total thickness. The ratio μ plotted for the intermediate core layer is not relevant since it is the ratio of the stresses reached in the core material with the stresses reached in the equivalent isotropic steel pipe. Of course the stresses in the steel will be very much greater than these in the less stiff intermediate material.

OD/t=20	Radius (inches)	χ / η	80% 10%	60% 20%	40% 30%	20% 40%
single walled pipe	inner		5.000	5.000	5.000	5.000
	thick.		0.556	0.556	0.556	0.556
	outer		5.556	5.556	5.556	5.556
inner layer	inner		5.000	5.000	5.000	5.000
	thickness		0.237	0.260	0.269	0.274
	outer		5.237	5.260	5.269	5.274
core layer	inner		5.237	5.260	5.269	5.274
	thickness		1.896	0.778	0.359	0.137
	outer		7.133	6.038	5.628	5.412
outer layer	inner		7.133	6.038	5.628	5.412
	thickness		0.237	0.260	0.269	0.274
	outer		7.370	6.298	5.897	5.686
Total thickness			**2.370**	**1.298**	**0.897**	**0.686**

Table 6.2.2 - Pipe dimensions (in inches) for *OD/t*=0.

The most important result, therefore, is the value of the von Mises Stress Ratio, μ, through the outer and inner steel faces. Values of μ greater than unity mean that the equivalent steel pipe is subjected to greater stresses than the equivalent multi-layered pipe, for the same internal pressure condition. Thus μ denotes the amount of over-stress an homogeneous single walled pipe has to withstand to achieve the same performance as the double walled pipe facing the same pressure loading. Another interpretation of μ is that it is a measure of the greater structural efficiency achievable by moving from a single walled pipe to an equivalent multi-layered pipe with the same steel weight.

OD/t=30	Radius (inches)	χ η	80% 10%	60% 20%	40% 30%	20% 40%
single walled pipe	inner thickness outer		5.000 0.357 5.357	5.000 0.357 5.357	5.000 0.357 5.357	5.000 0.357 5.357
inner layer	inner thickness outer		5.000 0.160 5.160	5.000 0.170 5.170	5.000 0.202 5.202	5.000 0.177 5.177
core layer	inner thickness outer		5.160 1.276 6.435	5.170 0.512 5.682	5.202 0.150 5.352	5.177 0.089 5.266
outer layer	inner thickness outer		6.435 0.160 6.595	5.682 0.170 5.852	5.352 0.202 5.504	5.266 0.177 5.443
Total thickness			**1.595**	**0.852**	**0.504**	**0.443**

Table 6.2.3 - Pipe dimensions (in inches) for *OD/t*=0.

Another parameter plotted in Figure 6.2.1 is Mises stress along the radial direction divided by the difference between internal and external pressures. This ratio has been plotted against the same radius parameter ρ in order to visualise the stresses

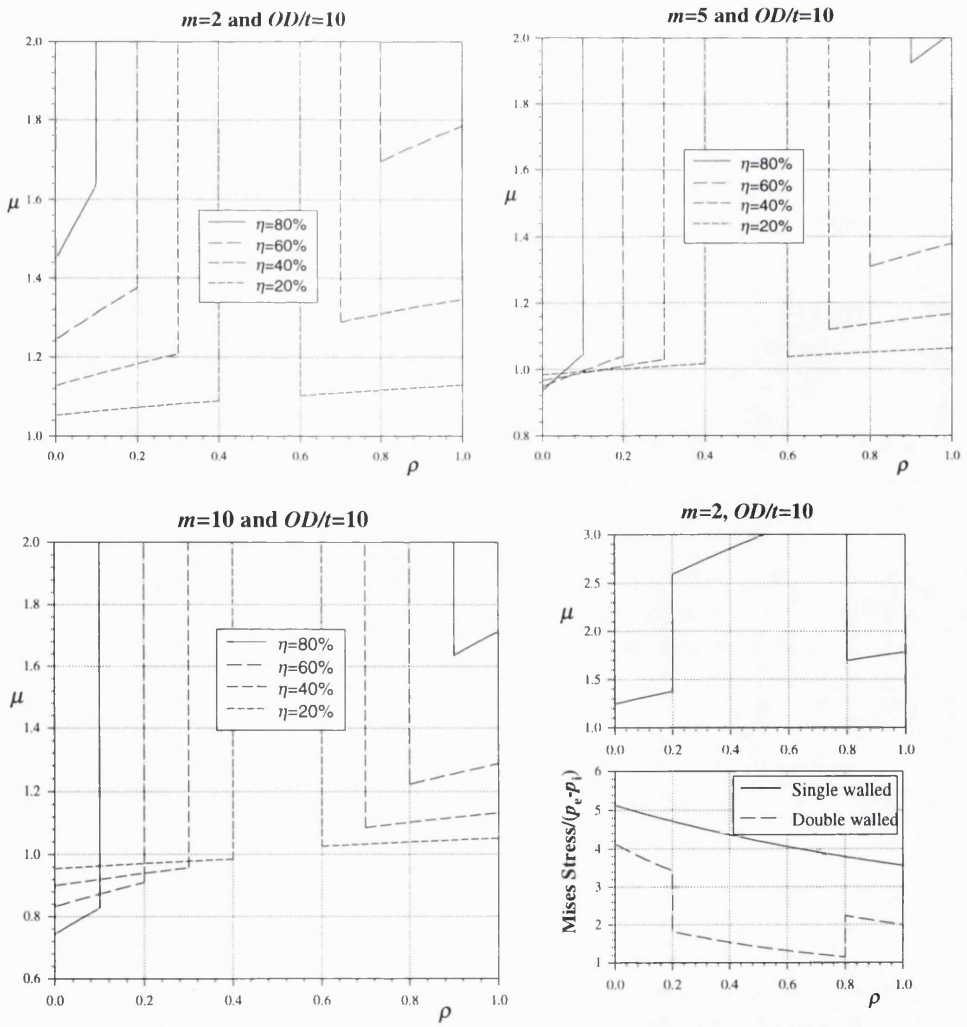

Fig. 6.2.1 The μ Mises Stresses Ratio parameter with multi-layered pipes for core materials with m=2, m=5 and m=10.

achieved in both pipes. For this case the Mises stresses for the single walled construction are around 20% greater than for the double walled construction for the same internal pressure. In other words, using the same amount of steel and the same pressure gap the multi-layered construction leads to a lower stress level.

It can be observed in the graphs of Figure 6.2.1 that for an intermediate core material Young's Modulus that is half of that of steel (m=2), the stress parameter μ is greater than unity. It means that in this case the multi-layered pipe is demanding less strength of the steel than the single walled pipe.

Figures 6.2.2 (a), (b) and (c) present calculation that show the behaviour of the multi-layered pipe using thin walled steel pipe inner and outer layers. The ratios OD/t equal 20 and 30 and the Young's modulus parameter m is equal to 2, 5 and 10.

It can be observed that as the intermediate material is made less stiff, the stress performance parameter μ reduces. The significance of the μ value falling below unity is that there is no improvement in the structural performance. However, the multi-layered pipes stress performance improves as the inner and outer wall thickness are reduced. For OD/t equal 30 the stress performance is better than that of the equivalent steel pipe for all values of m. For relation OD/t=20, the parameter μ is greater than unity only for intermediate stiffer materials or with m less than 5.

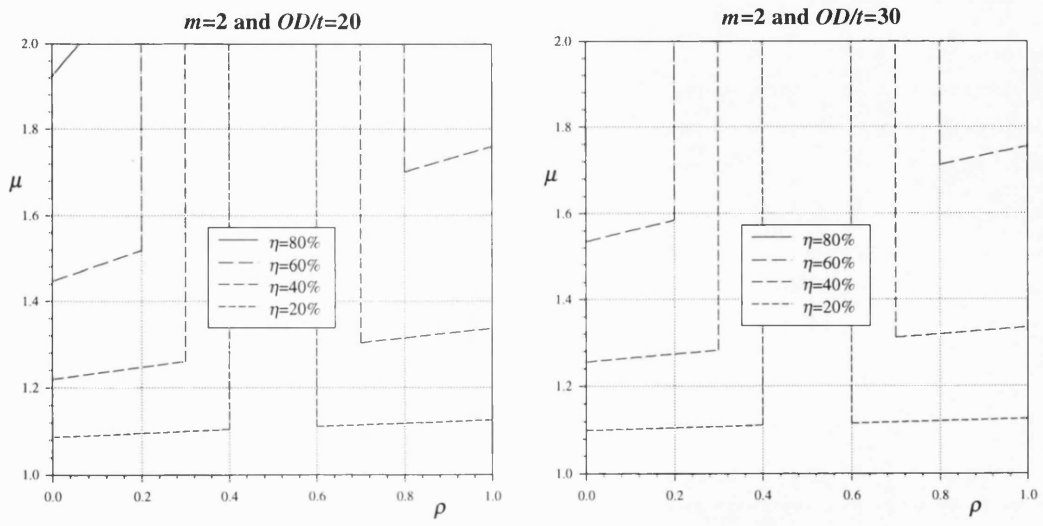

Fig. 6.2.2(a) Single walled pipes with OD/t equal to 20 and 30. Mises Stresses Ratio parameter for intermediate materials with m=2.

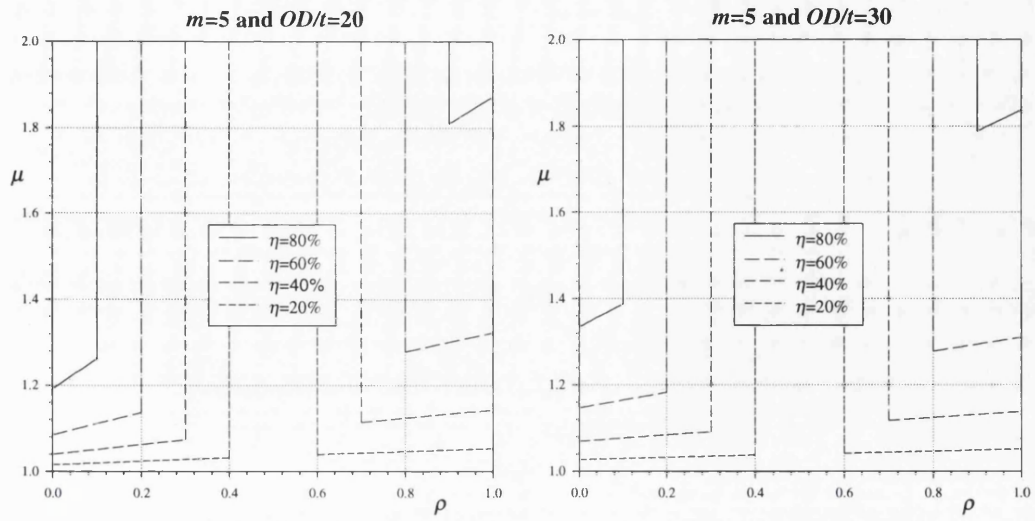

Fig. 6.2.2(b) Single walled pipe with *OD/t* equal to 20 and 30. Mises Stresses Ratio parameter for intermediate materials with m=5.

Having demonstrated that the inclusion of an intermediate material layer improves the performance of multi-layered pipe when subjected to internal pressure. It is worthwhile investigations structural performance due to moving the intermediate layer away from the centre of the wall. That is with a non centred construction. In this case, the multi-layered pipes will have their inner layer thicker than the external layer. It should be pointed out here that the case of inner steel layer being thinner than the outer layer has not been presented because in these cases, all μ values were less than 1.0 giving reduced performance compared to the equivalent single walled pipe. This feature has been analysed for two cases. The first with the inner layer equal to 30% of the total wall thickness and the second case with the inner layer

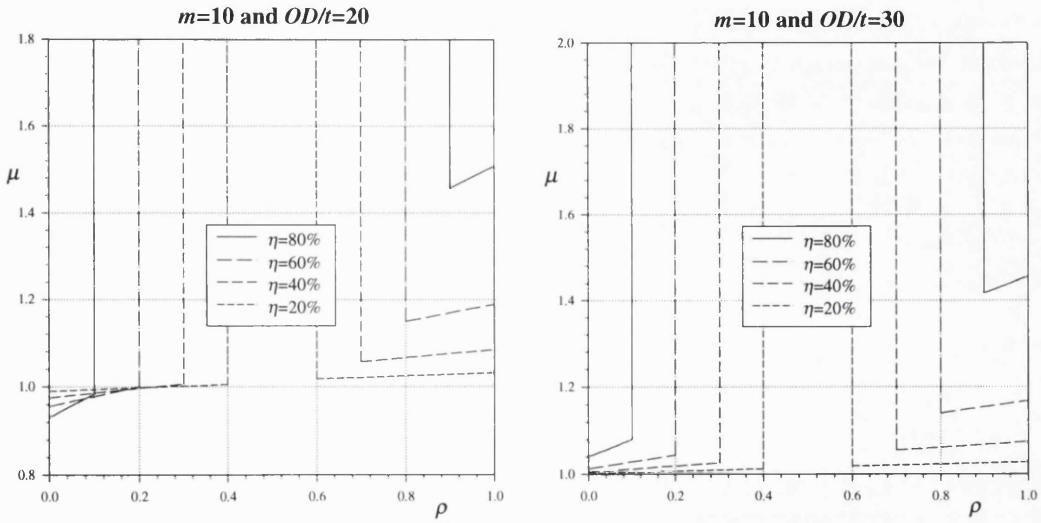

Fig. 6.2.2(c) Single walled pipe with *OD/t* equal to 20 and 30. Mises Stresses Ratio parameter for intermediate materials with m=10.

equal to 40% of the total wall thickness. In both cases, the Mises Stress Ratio parameter μ has been evaluated for several intermediate material thickness.

The graphs in Figures 6.2.3 (a), (b), and (c) show the performance ratio μ for three single walled OD/t values of 10, 20 and 30. Note that the multi-layered pipe performance is better as thickness of the core layer is increased.

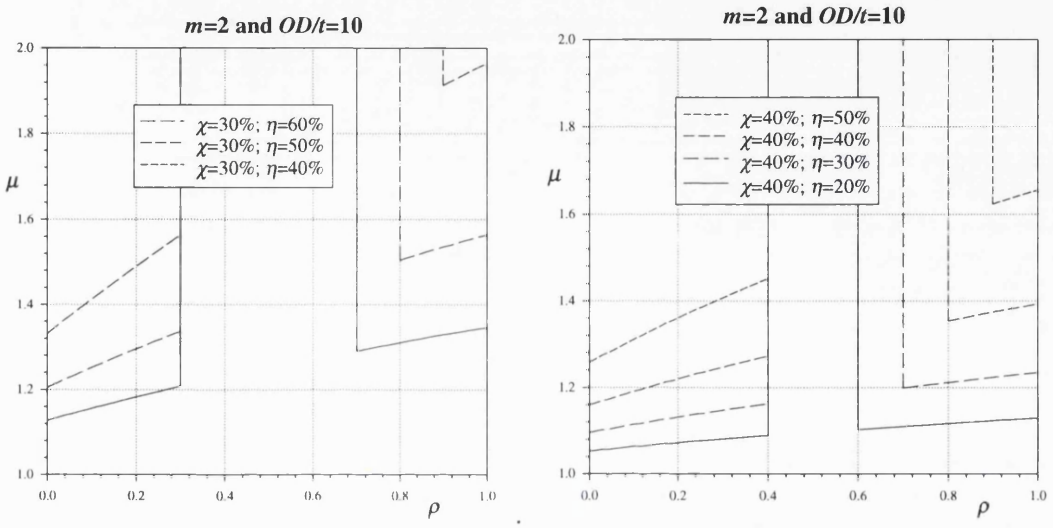

Fig. 6.2.3(a) - Non-centred construction effect.

It is useful, in conclusion, to present the above result in a specific manner though the ratio of the Von Mises stress to the pressure difference $(p_i - p_e)$ for both the multi-layered and single walled pipe. One case is plotted in this way in Figure 6.2.4 for m=2 and OD/t=10. This figure demonstrates that both steel layers of the multi-layered pipe have lower stresses than the equivalent single steel layer pipe.

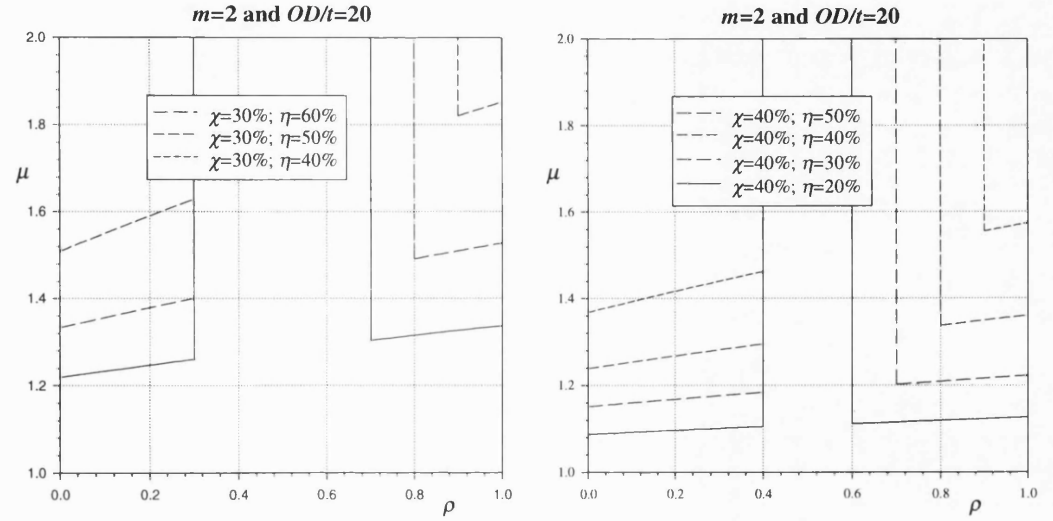

Fig. 6.2.3(b) - Non-centred construction effect.

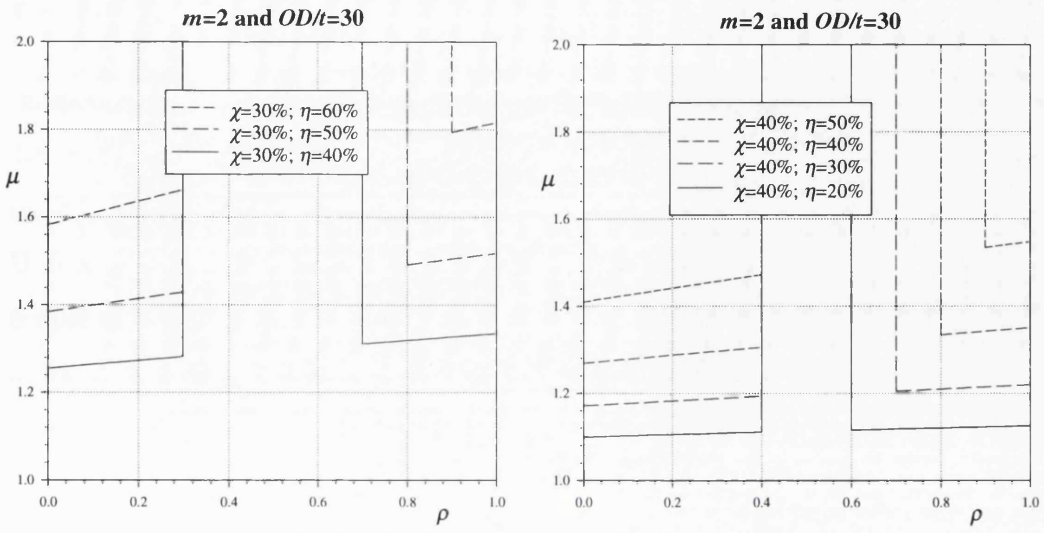

Fig. 6.2.3(c) - Non-centred construction effect.

Also, the stress reached in the inner boundary of the first steel layer for the multi-layered pipe is 4.5 times the pressure gap of 103440 MPa (15000 psi). On the other hand, the stress reached in the inner boundary of the single steel pipe is 5.1 times the same pressure gap. Therefore, the ratio parameter μ in this case is 1.13. It means that the full steel pipe is bearing 13% more stress than the multi-layered pipe for the same pressure gradient in the inner boundary of the pipe.

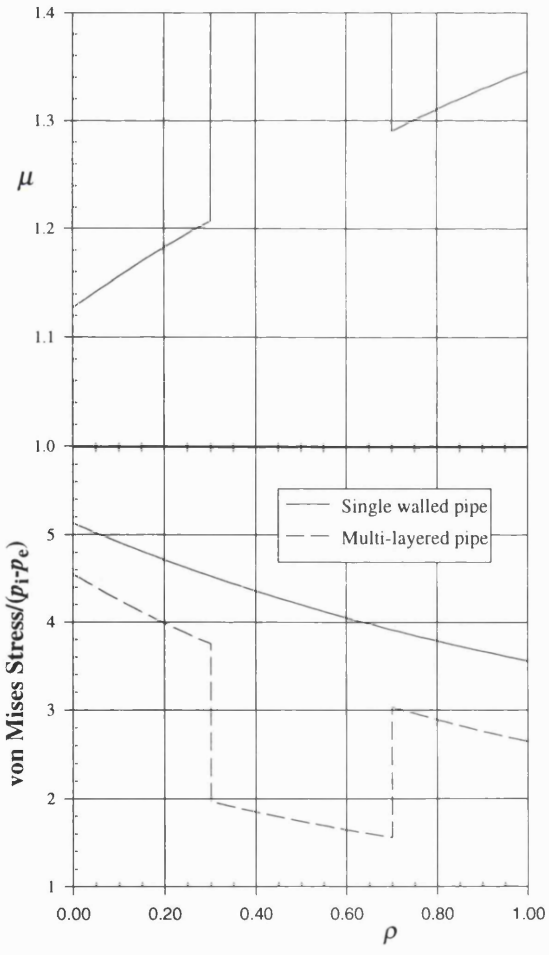

Fig. 6.2.4 Comparison Mises stresses normalised by the pressure gap $(p_i - p_e)$.

6.3 Multi-layered pipes under external pressure

In section 4, three analytical models for external pressure have been presented for the multi-layered pipe. These are the elastic foundation model, the classic elastic model, and the elastic-plastic model. Each model has its merits and drawbacks. Unfortunately, experimental data are not available so as to calibrate and define the proper range of validity of each model. However, based on the comparison of results of those models between each other and with finite element analysis some insights into the buckling problem of such non conventional construction can be obtained.

In order to present a comparison between the external buckling pressure for the multi-layered pipe, a comprehensive study has been carried out. A comparison between results from the three methods and the finite element method package ABAQUS is performed. A large range of wall thicknesses and diameters have been considered based on the two basic parameters for the multi-layered pipe; but with the restriction that the inner and outer layers or faces have the same thickness (*b-a=d-c*), see Figure 3.3.1.

The following graphs were produced by fixing the parameter β, which is the ratio between the core layer thickness and the face thickness, $\beta = (c-b)/(b-a)$ and varying the parameter α, which is the ratio between the mean radius of the outer and inner layers $\alpha = (c+d)/(a+b)$.

β stands for the magnitude of the core thickness. The α parameter is related to the slenderness of the constructions, i.e. when it approaches unity, it implies that the total wall thickness in becoming small compared with the mean radius. Table 6.3.1 shows the values of the multi-layered pipe geometry *a*, *b*, *c*, *d*, *co*, *f* and *t* for a range of α and β values based on a 20-inch inside diameter pipe (*a*=10-inch). Here *f* is the face thickness, *co* is the core thickness and *t* is the total wall thickness. The radii *a*, *b*, *c*, and *d* are shown in Figure 3.3.1.

α	β	a	b	c	d	f	co	t
0.95	1	10.000	10.267	10.533	10.800	0.267	0.267	0.800
	3	10.000	10.132	10.530	10.662	0.132	0.397	0.662
	5	10.000	10.088	10.529	10.617	0.088	0.441	0.617
	10	10.000	10.048	10.528	10.567	0.048	0.480	0.576
0.90	1	10.000	10.571	11.143	11.714	0.571	0.571	1.714
	3	10.000	10.282	11.127	11.408	0.282	0.845	1.408
	5	10.000	10.187	11.121	11.308	0.187	0.935	1.308
	10	10.000	10.102	11.117	11.218	0.102	1.015	1.218
0.80	1	10.000	11.333	12.667	14.000	1.333	1.333	4.000
	3	10.000	10.645	12.581	13.226	0.645	1.935	3.226
	5	10.000	10.426	12.553	12.979	0.426	2.128	2.979
	10	10.000	10.230	12.529	12.759	0.230	2.299	2.759
0.7	1	10.000	12.400	14.800	17.200	2.400	2.400	7.200
	3	10.000	11.132	14.528	15.660	1.132	3.396	5.660
	5	10.000	10.741	14.444	15.185	0.741	3.704	5.185
	10	10.000	10.397	14.371	14.768	0.397	3.974	4.768

Table 6.3.1 Multi-layered geometry as function of α and β (all dimensions in inches).

The comparison graphs include five continuous curves and two sets of symbols. The buckling pressure is presented in kilopounds force per square inch, (1 ksi= 6.895 MPa). The continuous and thicker curves represents the elastic plastic behaviour of the multi-layered pipe. In this case, the buckling pressure is estimated as the pressure achieved when the core reaches elastically the strength limit after the two faces have already been in plastic condition. In addition, the yield stress for the faces and the ultimate stress for the core are the main parameters in the estimated buckling pressure. This approach was developed by the author in section 4.4.

The other continuous but single curve represents the elastic buckling based on elastic instability of the multi-layered wall failing on the second mode. This model assumes that the wall behaves as an elastic continuous layer and also that the wall thickness is small in comparison with the pipe radius. In addition, the core ratio β, should be relatively high ($\beta > 5$) and the core Shear Modulus is considered. These results were based on the elastic approach formulation of Norris and Zahn /54/, 1963 (section 4.3.4).

The three segmented curves represent the elastic foundation model also developed by the author, which is described in section 4.2. Each curve is related to the failure of one of the three layer considering the other two layers as an elastic foundation. It is clear that the smaller bucking value identifies the layer that would reach the

instability condition first while the others still behaving elastically. Moreover, on the right of the graphs there is an extra y-axis that presents the correspondent wave mode for the elastic instability.

Finally, there are two sets of symbols. The black square symbols represents the ABAQUS results for a 2-D cylinder model and the black bullet symbols represents the 3-D cylinder model. The ABAQUS results were obtained for the second wave mode failure, elastic instability i.e. by evaluating the eigenvalues. Figure 6.3.1(a) include the key for the curves and points shown on the following figures. The graphs were produced for two main cases. For Young's modulus ratio between the faces and core material m=10 and m=100. Figure 6.3.1(a) to Figure 6.3.1(e) give results for a smaller ratio between the Young's modulus of the faces and the core (m=10) and the core thickness parameter β is set to 1, 3, 5, 8 and 10 respectively. Figure 6.3.1(f) to Figure 6.3.1(j) are results with the Young's modulus parameter increased ten times (m=100) and the thickness parameter varies in the same way as before.

It should be pointed out that the elastic buckling model curve shows good agreement with the ABAQUS results mainly for β>5 and α>0.8. This implies that the elastic theoretical model agrees with the finite element package in the range that encompasses its basic assumptions as would be expected. In the elastic foundation approach the assumption is that each layer should have a small thickness in comparison with its mean radius. From the range shown in Figure 6.3.1 the elastic foundation model has a bigger range of agreement with ABAQUS than the elastic model of section 4.2. Finally, the elastic plastic approach, which is not based on loss of stability, presents a quite linear behaviour. The greater the yield limit of the faces and the limit strength of the core the greater the estimated buckling pressure.

It needs to be stressed that the elastic plastic approach leads to smaller predictions of the buckling pressure. This can be considered as a lower bound. On the other hand, Figures 6.3.1 present a quite big range of parameters. For a slender pipe, that means high values of α, during hydrostatic pressure loading the structure is more prone to buckle due to loss of stability. In that sense the stresses developed in the walls would not exceed the material yield stresses of the individual layers of the multi-layered

pipe. Moreover, for a quite thick wall, that means small values of α, the multi-layered pipe would develop a higher strength to hydrostatic pressure. Due to this extra strength, the cylinder will reach the elastic limit of its individual layers before the loss of stability.

This can be compared to a single bar-column with a compressive axial load. If the bar has a square cross section of sides h, and a length L, the Euler load would be $P_e = EI\,\pi^2/L^2$. If the yield stress of the bar-column material is $\sigma_y = E\varepsilon_y$ the axial load to reach the yield condition is $P_y = Eh^2\varepsilon_y$. Therefore, for the bar slender ratio $h/L > \sqrt{12\varepsilon_y}/\pi$, the bar-column will reach the yield condition before the unstable Euler load during axial loading. For typical steel $\varepsilon_y = 0.2\%$, than $h/L > 4.93\%$.

This behaviour can be extended to the multi-layered pipe. For thick pipes the layers would reach the yield condition before loss of stability during hydrostatic loading. Figures 6.3.1 shows a predominant lower values for elastic plastic approach for values of α<0.9. It does not mean that thick wall multi-layered pipe would not fail by loss of stability. There are imperfections that would trigger the instability at smaller loads.

Another important factor that must be considered is the boundaries between the layers. It is assumed in the theoretical models that the layers remain fully linked during their axisymmetric deformations. It means that there is no slip or friction on the boundaries immediately before failure. In addition, the existence of imperfections on the individual layers is not considered in the models. The imperfections could be the trigger for a the loss of stability and would bring the buckling pressure down as demonstrated by Donnell (1956) in /1/ for single walled cylinders.

There are no experimental results available for the data presented here to be plotted against and compared with. However, for multi-layered cylinders with thin skins and a thick core, the experimental data from Montague show a good agreement with the elastic plastic model, see Figure 4.4.2.

Figure 6.3.1(a) shows a comparison between the models for a small thickness ratio ($\beta = 1$) and for a relatively hard core, such as concrete ($m = 10$), represented by the ratio between the Young's Modulus of the materials of the faces and core. From the graph, it is clear that all the models converge to the same solution when the total wall thickness of the cylinder is diminishing, i.e. for values of $\alpha > 0.95$. On the other hand, as the cross-section wall becomes thicker, the classic elastic solution, represented by the formulation posed by Norris and Zahn /54/, 1963 gives the smaller prediction of the critical external pressure. It is of interest to note that the elastic foundation solution for intermediate layer buckling shows the smaller

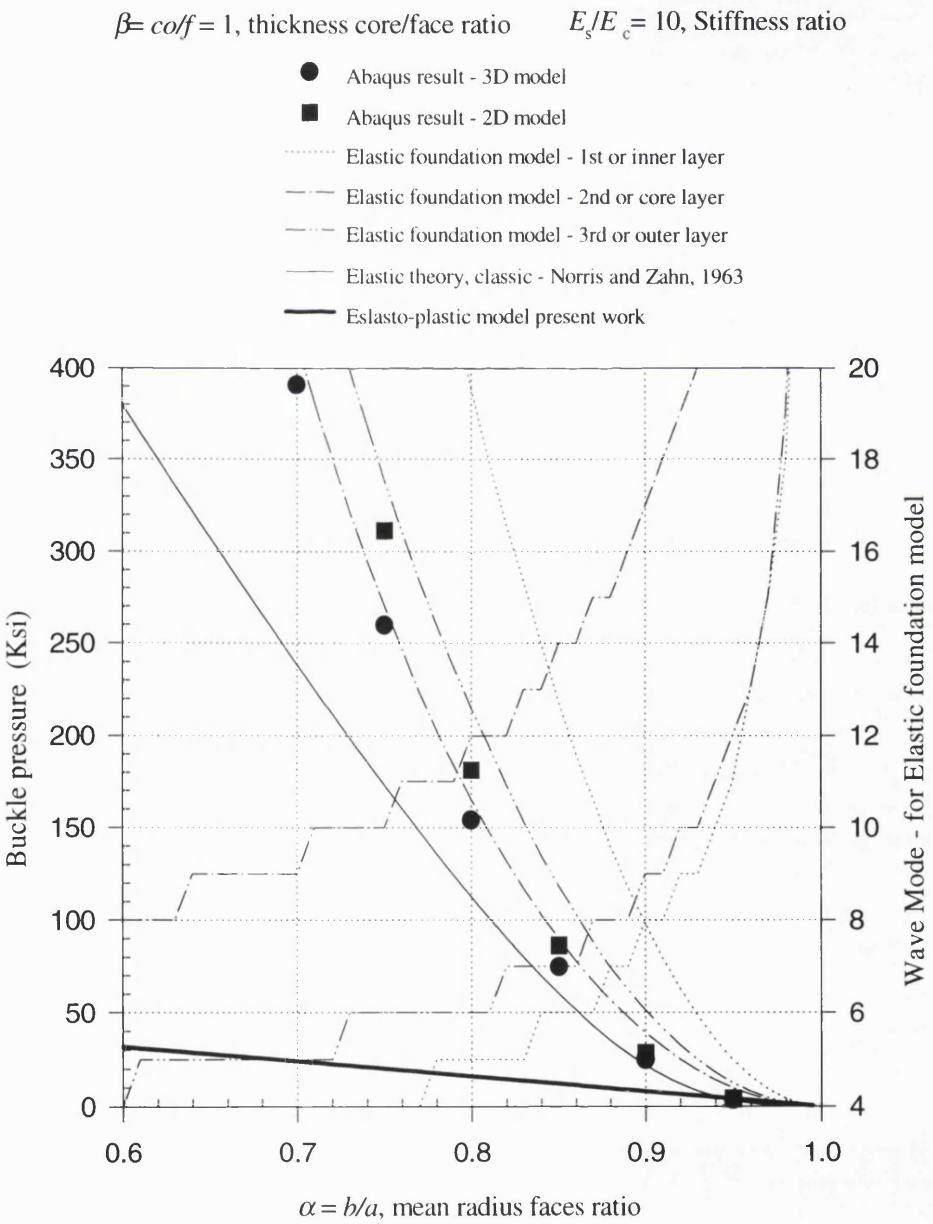

Fig. 6.3.1(a) Comparison of external pressure models.

solution among the elastic foundation models and at the same time gives better agreement with the finite element solution obtained out ABAQUS. It should be pointed out here that the finite element solution implies a collapse mode shape with $n = 2$ or the cylinder is buckling in the well know form of two lobes. As expected, the elasto-plastic model always gives smaller predictions across almost the full range of α. It means that for the cylinder with thicker wall, in this case identified as $\alpha<0.9$, the theoretical models for elastic collapse cylinder do not give the lowest critical pressure. In addition, the elasto-plastic solution indicates a possible collapse by plasticity of its skins and reaching a limiting stress in the core rather than a loss of instability.

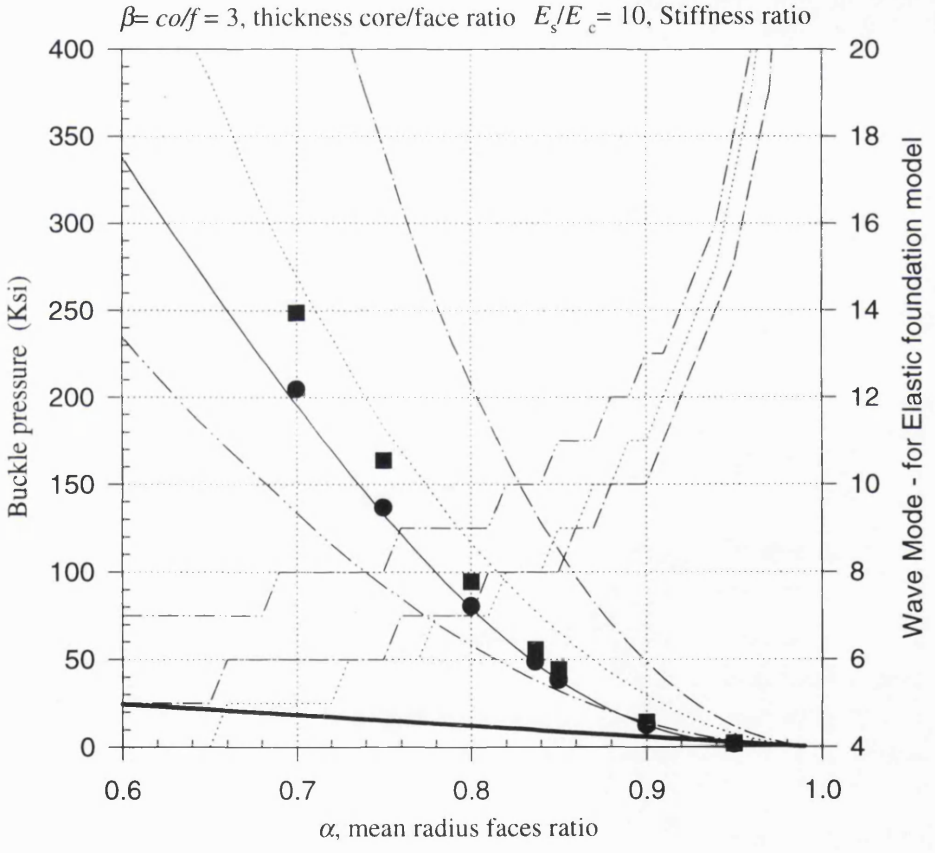

Fig 6.3.1(b)

Figure 6.3.2(b) differs from the former only by an increase in the thickness ratio, therefore, now $\beta = 3$. This means that the core thickness has increased relative to the total thickness, and the total wall thickness has diminished for the same value of α – see table 6.3.1. The results show the same trend as Fig. 6.3.1(a) when the abscissa parameter α approaches towards the right. However, the elastic solution that leads

to the smaller collapse prediction is now the elastic foundation model for the outer layer. The classic elastic solution is now in better agreement with the 3-D FEA results. It should be stressed that the classic solution also assumes that the cylinder is collapsing with a mode shape corresponding to $n = 2$.

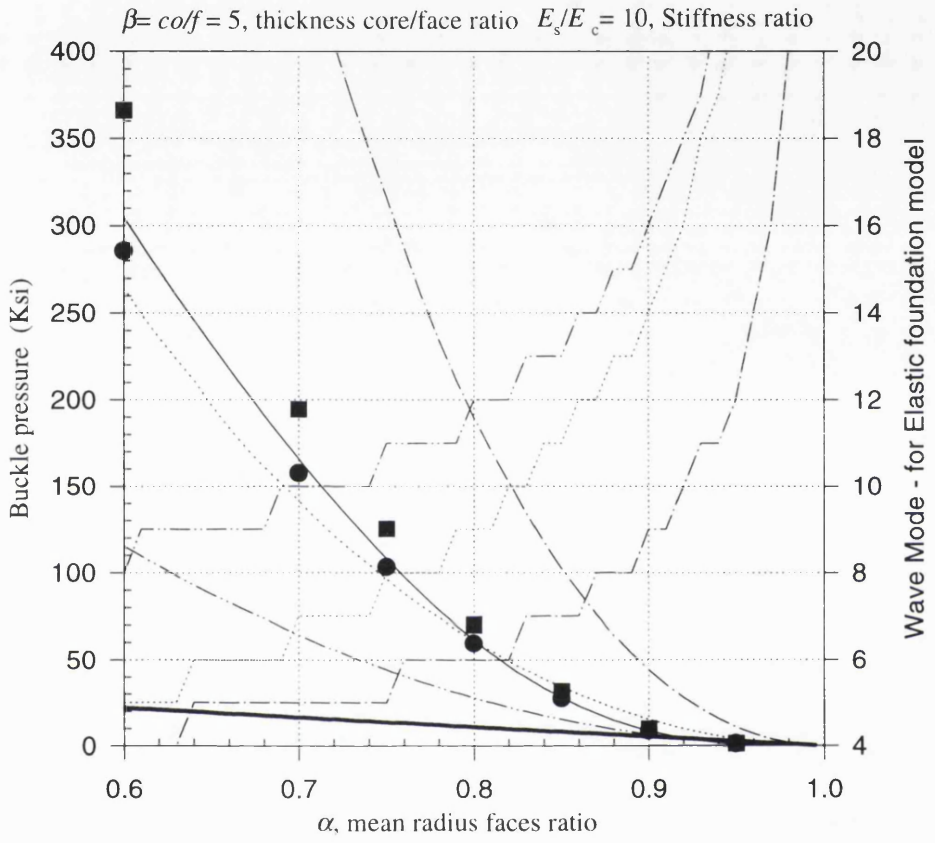

Fig 6.3.1(c)

Again Figure 6.3.1(c) has approximately the same behaviour as Figure 6.3.1(b). In this case, the difference is again only in the thickness ratio that has been increased, now to a value $\beta = 5$. As before, the smallest solution among the elastic solutions is from the elastic foundation collapse for the outer layer. The classic elastic solution, the elastic foundation model for inner layer and the FEA have predictions of the same magnitude. Another interesting observation from this result is that the elasto-plastic result has a larger range of reasonable agreement with the elastic solution (in the range $0.9<\alpha<1$).

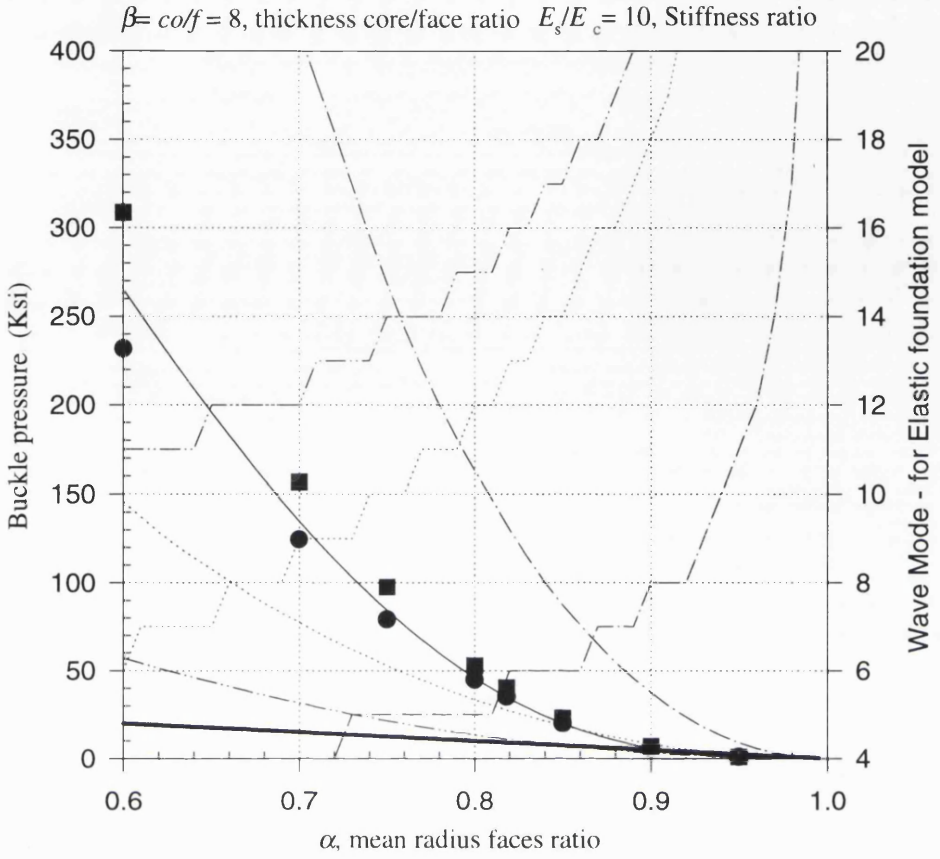

Fig 6.3.1(d)

Figure 6.3.1(d) has been produced by changing only the thickness ratio – this now being $\beta = 8$. Again, the elastic foundation model for the outer layer leads to the smaller prediction of the critical external pressure among the elastic models. It should be observed that the elasto-plastic result, based on the present work, shows very good agreement with the elastic foundation model for the outer layer in the range $0.8<\alpha<1$. The FEA solution also present a good match with the classic elastic approach. This trend has been observed in almost all of the cases considered here.

The next Figure, 6.3.1(e), shows the same trend observed in Figure 6.3.1(d). In this case the value of thickness ratio have been pushed even further, now to $\beta = 10$. The elastic foundation model for the outer layer also leads to the smaller predictions in terms of loss of stability. The elasto-plastic result now shows a larger range of agreement with the elastic foundation model for the outer layer over the range $0.75 < \alpha < 1$. The 3-D finite element analysis continues to show good agreement with the classic solution.

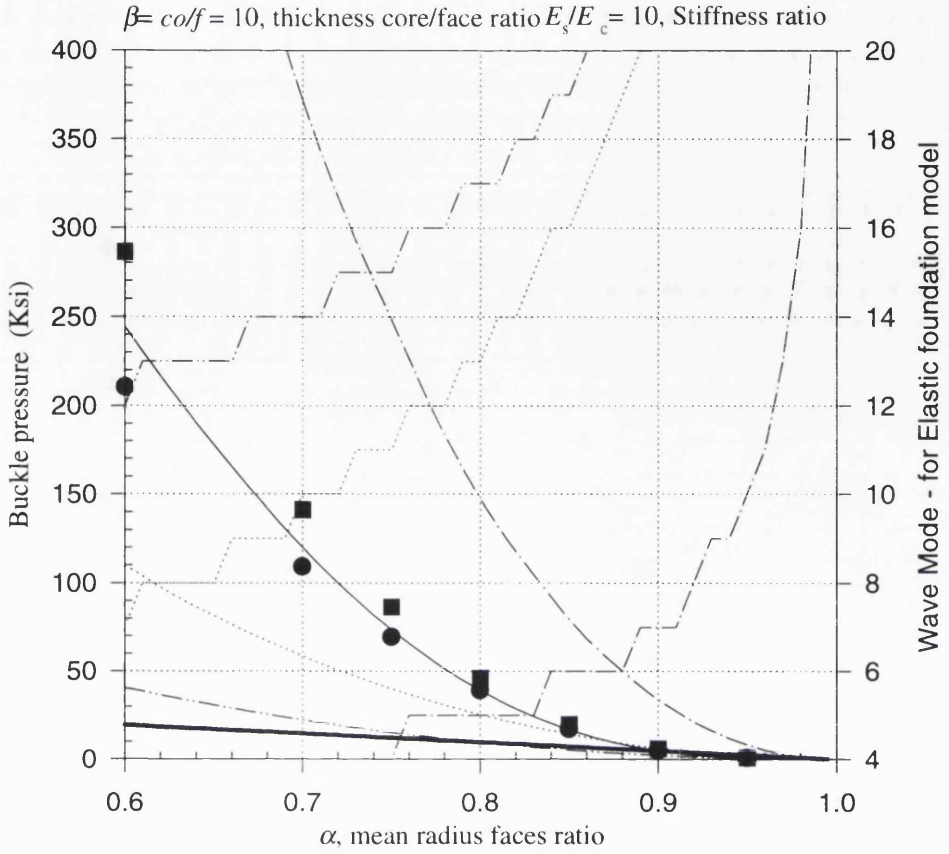

Fig 6.3.1(e)

Several important observations can be deduced from Figures 6.3.1(a) to 6.3.1(e).

It has required a relatively stiff core material (m = 10) such as concrete to demonstrate the better external pressure performance of the multi-layered construction. The most important observation from these figures is that collapse of a multi-layered cylinder with a relatively stiff core tends to have an elasto-plastic nature very close to the loss of stability obtained with increase of the thickness ratio β. It means that a multi-layered pipe with this characteristic would probably collapse in a combined manner somewhere between elasto-plastic type and loss of stability of the outer layer possibly triggered by imperfections. Unfortunately, there is currently no known experimental data available to support this statement. However, an inspection of the above figures shows that this is likely to happen.

In the next set of results, the effect of a soft (less stiff) core will be considered for the same range of thickness ratios.

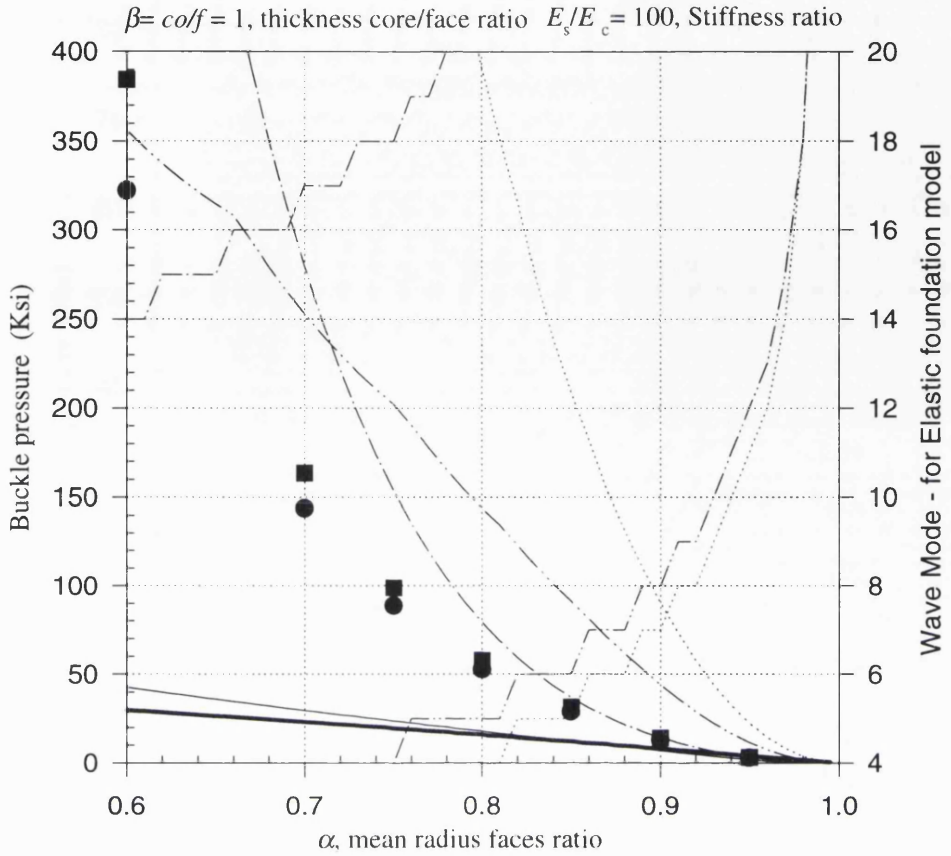

Fig 6.3.1(f)

Figure 6.3.1(f) shows a comparison between the models for a small thickness ratio (β = 1) and for a relatively soft core, such as polypropylene (m = 100), represented by the ratio between the Young's Modulus of the materials of the faces and core. In this case, the classic solution shows better agreement with the elasto-plastic approach and represents the smaller prediction of the critical pressure among the elastic models. The elastic foundation solution gives a very high prediction for thicker cylinders or $\alpha < 0.9$. On the other hand, for thin walls, $\alpha > 0.9$, the elastic foundation model for the outer layer shows agreement with the elasto-plastic model. The difference between the classic elastic solution and the FEA results in this range of parameters may be explained by the simplification included in the Norris and Zahn formulation that assumes an orthotropic core rather than the isotropic behaviour assumed by the FEA solution.

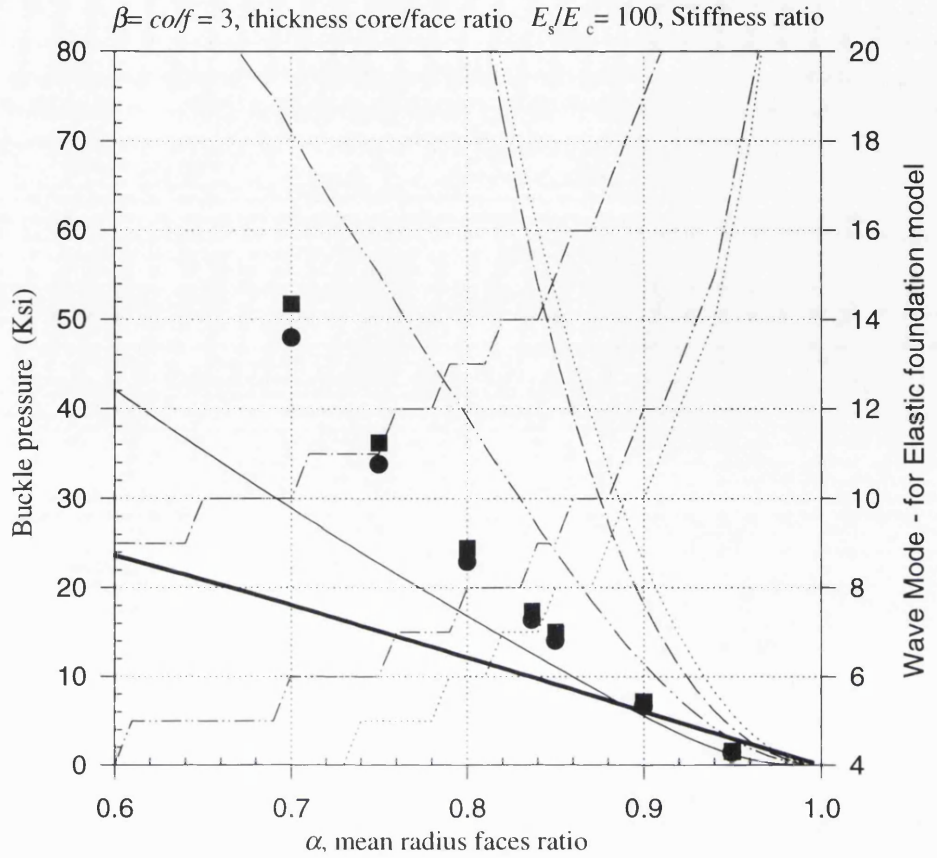

Fig 6.3.1(g)

Figure 6.3.1(g) differs from the former only by an increase in the thickness ratio – therefore, now $\beta = 3$. The core thickness has increased relatively to the total thickness, and the total wall thickness has diminished for the same value of α – see table 6.3.1. The elastic foundation solutions show larger values for the critical pressure. The classic elastic solution, formulation of Norris and Zahn, is the smaller result for the whøle range among the elastic models. In this case there is an important observation, for thin multi-layered walls (value of $\alpha > 0.9$). In this case, the classic solution gives a smaller critical pressure than the elasto-plastic approach. There seems to be a transition point between the collapse due to elasto-plastic limit deformation and lost of stability under uniform external pressure loading for the multi-layered cylinder construction. The FEA agrees with this trend and the result shown for $\alpha = 0.95$ falls clearly below the elasto-plastic solution line. The solution from the FEA and the classic solution are now getting closer to each other. This may be due the fact that relatively speaking, the total wall thickness is becoming smaller and the effects of the simplified assumptions of the classic approach are also small .

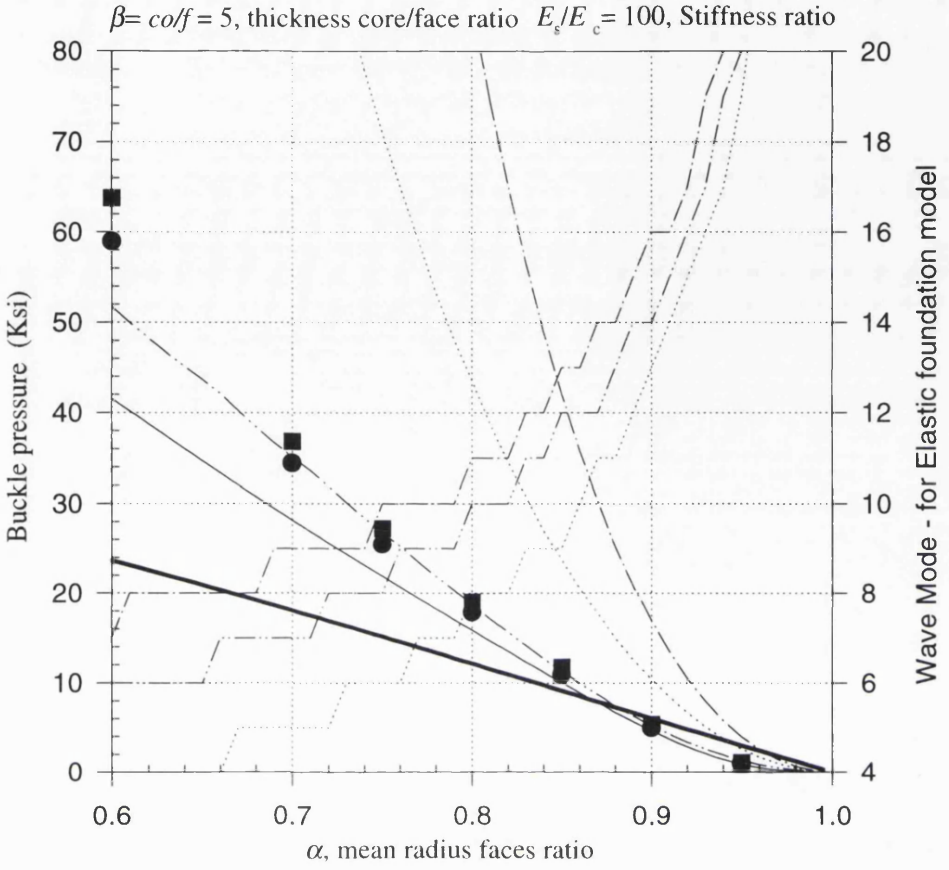

Fig 6.3.1(h)

Figure 6.3.1(h) has approximately the same trend as Figure 6.3.1(g). In this case, the difference is again only in the thickness ratio which has been increased to $\beta = 5$. The elastic foundation solution for the outer layer shows a agreement with the FEA results. The others elastic foundation solutions gives a very high prediction. The trend of lost of stability for $\alpha > 0.88$ is also clear. The elastic foundation model for the outer layer, the classic solution and the FEA results coincide in the range $0.88 < \alpha < 1$. This means that the multi-layered construction for this range will collapse from loss of stability. In addition, the transition point where this change in behaviour is likely to take place is $\alpha = 0.88$. However, for $\alpha < 0.88$ the elasto-plastic solution also gives the smaller critical pressure prediction. The FEA and the classic solution are now closer for the whole range. As pointed out before, the simplified assumptions in the classic model approach is becoming less important when the total thickness of the wall is relatively smaller.

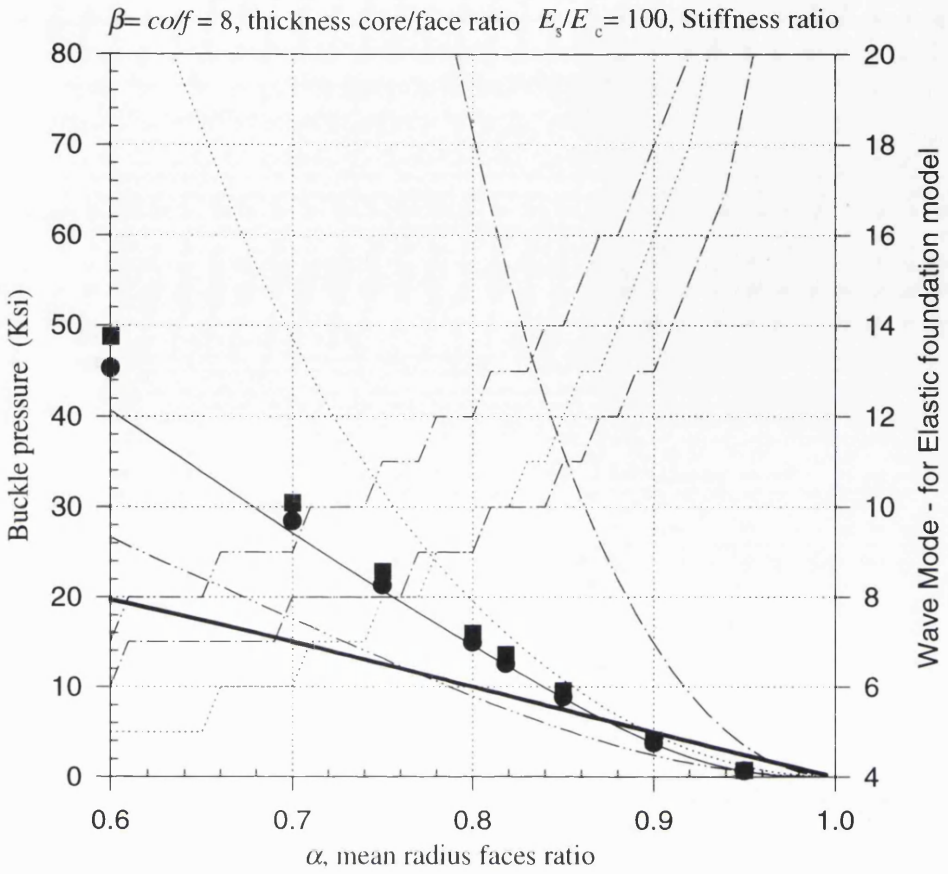

Fig 6.3.1(i)

Figure 6.3.1(i) is produced using $\beta = 8$ and keeping all other parameters the same. In this case, the elastic foundation model for the outer layer gives the smaller critical pressures for $\alpha > 0.78$. The 3-D FEA and the classic solution are coincident for the whole range of α. The elastic models clearly show that the collapse for $\alpha > 0.9$ would occur by lost of stability rather than elasto-plastic deformation. The elastic foundation prediction for the inner layer also falls below the elasto-plastic line. The trend of large values from results of the elastic foundation for the core layer may be explained as its thickness relative to the other two layers is increasing when the thickness ratio β increases (see table 6.3.1). Therefore, the loss of stability of a thicker core should not be expected to happen at low external pressure.

Figure 6.3.1(j) corresponds to $\beta = 10$. The same general behaviour observed in the last figure is also present. In this particular case, the elastic foundation model prediction for the inner layer shows agreement with the classic solution and the FEA results for **a**

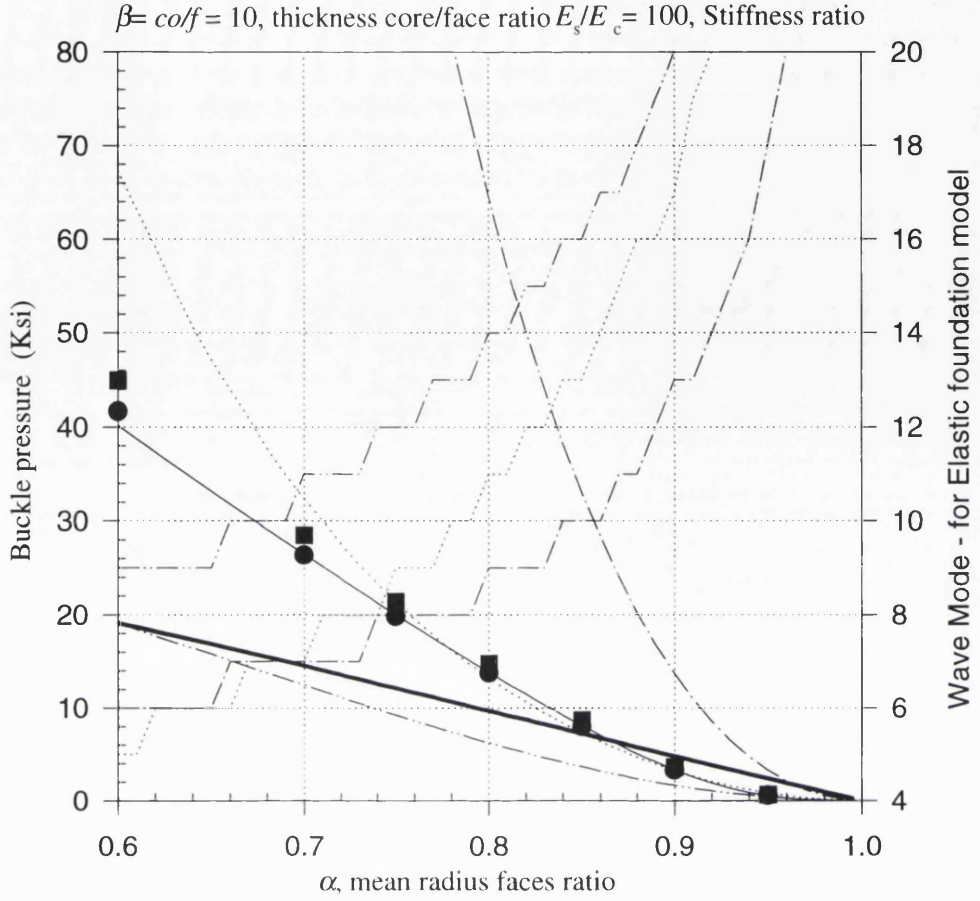

Fig 6.3.1(j)

large proportion of the range ($\alpha > 0.74$). The elastic foundation for the outer layer gives the smaller prediction of critical pressure for the whole range. This indicate that this combination of parameters would always lead to a collapse by loss of stability. On the other hand, results from the classic elastic solution, the FEA results and the elastic foundation for the inner layer show a transition point at $\alpha = 0.86$. For values outside this range, the collapse would occur by elasto-plastic deformation.

Figures 6.3.1(f) to 6.3.1(j) lead to several observations for relatively soft cores (m = 100) such as polypropylene on the effects of a softer core material on the external pressure performance of the multi-layered construction. The main observation from these figures is that collapse of a multi-layered cylinder with a relatively soft core and thin walls ($\alpha > 0.9$) tends to have an elastic solution or that it will collapse by loss of stability. This trend increases with increase in the thickness ratio β. In the selection of parameters used here, it is clear that there is a transition point which is not exactly a point but a range of values of α where the collapse will

take place by a combination of behaviours. Therefore, a combination of loss of stability and a catastrophic local plastic deformation should govern the failure mode of these multi-layered construction. Unfortunately, insufficient experimental data are available to support this statement. However, these points can be concluded from inspection of the figures presented.

6.4 Catenary riser

It is important to consider during this work, a range of materials that can be used in the core. It is quite clear that the faces of the multi-layered pipe should be made of steel or other metallic or ductile material. The steel is far the less expensive and allows a huge range of alloys to provide specific applications requirements. In addition, the faces will need to withstand contact with the conducted fluid and the external environment. On the other hand, the core material presents a bigger range of options. The aeronautical industry has used aluminium honeycomb to ensure high strength and less weight at the same time. However, the deep water offshore industry

	E (GPa)	G (GPa)	ν (Poisson)	σ_y (MPa)	ρ (kg/m^3)
1 - Expanded plastics					
PVC	0.0552	0.0093	-	1.03	66
Phenolic	0.0069	0.0034	-	0.17	56
Polyurethane	0.0186	0.0048	-	0.52	72
Polystyrene	0.0110	0.0045	-	0.28	42
2 - US commercial aluminium honeycomb, 1/4" cell size					
.002-in foil	1.79	0.33	-	3.29	63
.003-in foil	3.01	0.52	-	6.20	94
.004-in foil	3.69	0.75	-	9.56	123
3 - Reinforced plastic honeycomb, 3/16" cell size					
Phenolic/Glass	1.23	0.44	0.41	11.51	140
Phenolic/asbestos	1.37	0.43	0.60	10.77	149
Silicone/Asbestos	1.01	0.36	0.39	4.85	139
4 - Polymeric material					
Polyethylene (LDPE)	0.25	0.088	0.42	16	940
Polyethylene (HDPE)	1.40	0.48	0.45	38	970
Polypropylene (PP)	1.90	0.68	0.40	40	910
Polystyrene (PS)	3.50	1.25	0.40	85	1,100
Rigid PVC	3.50	1.24	0.41	70	1,400
Acrylic	3.20	1.14	0.40	80	1,200
Nylons	2.80	1.00	0.40	100	1,150
5 - Metallic material					
Steel	209	82	0.29	200-1800	7,850
Cast Iron nodular	175	69	0.26	735	7,352
Aluminium alloy	70	27	0.33	250	2,790
Titanium alloy	106	40	0.33	910	1,900
6 - Ceramic					
Alumina	360	142	0.23	2,750.00	3,980
Low-polytype sialon (glassy phase)	300	122	0.27	3,500.00	3,245
Hot-pressed silicon nitrite	310	122	0.27	3,500.00	3,200
Reaction-bonded silicon nitrite	200	79	0.19	1,000.00	2,500
Sintered silicon carbide	410	172	0.27	2,000.00	3,100
Partially stabilized zirconia	200	81	0.23	1,850.00	5,780
7 - Other materials					
Balsa wood	2.41	0.10	-	6.21	96
Concrete	18.50	7.71	0.20	43	2,450
Araldite	4.40	1.60	0.43	61.5	840

Table 6.4.1 Core material properties (several sources).

has other kinds of demands. The main one is the requirement for high hydrostatic pressure resistance. This implies the use of high compressive strength materials such as ceramic. Another interesting issue is the additional control of thermal insulation and the submerged pipe weight. These could be more important than the hydrostatic resistance itself for shallow water application. The multi-layered pipe construction may also be extended for application in surface pipelines. The properties required here are high tolerance to internal pressure and the possibility of achieving high internal diameters. In addition, the core material may be selected to deliver thermal insulation, weight and structural functions.

Table 6.4.1 presents a range of data for possible core material. Some materials with density smaller than sea water (1025 kg/m^3) will provide buoyancy and, therefore, some relief in top tension. However, for big diameter gas pipelines, a heavy core would provide the additional weight necessary to keep the pipeline stable on the sea bed.

The multi-layered pipe can be used as a riser or pipeline. In the first case, the submerged weight (top tension) and the capability to withstanding bending and cyclic loads would be paramount to guarantee a stresses level within the safety margin specified during the service life. In the latter, the bending and cyclic loads will act only during installation. The pipeline should be designed to withstand only hydrostatic pressure during its service life.

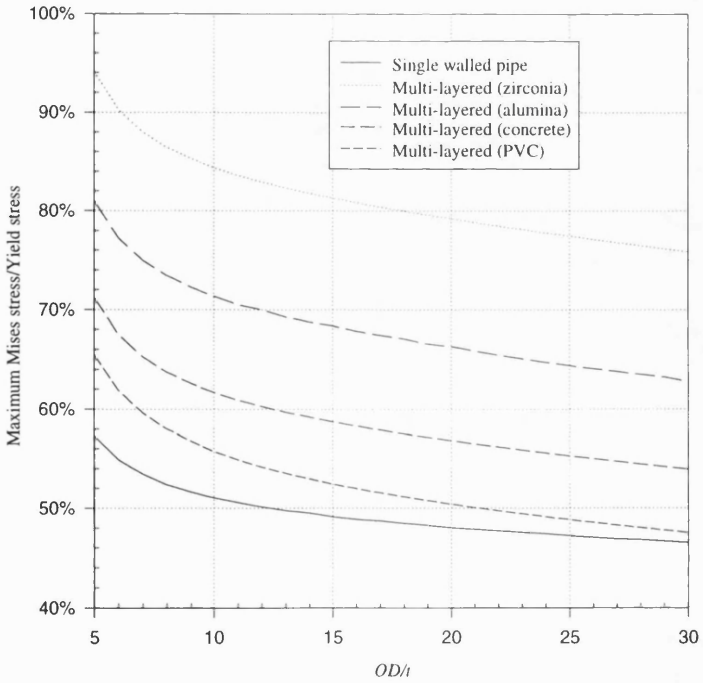

Fig 6.4.1 Comparison for equivalent multi-layered varying core material

Based on section 5, figure 6.4.1, presents a comparison between multi-layered and

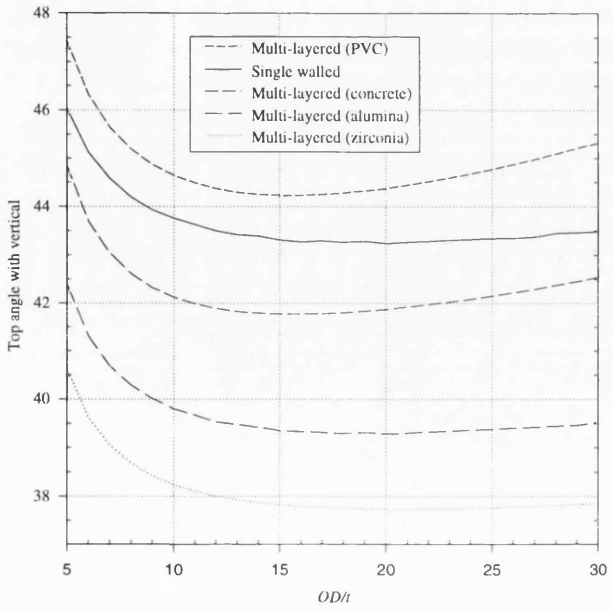

Fig. 6.4.2 Comparison of top angle with vertical far position.

single walled pipes for different core materials in a free catenary configuration in 1000 meters water depth, core thickness ratio β=3, 10-inch internal diameter and top connection excursion of 10% of the water depth. The equivalent multi-layered pipe geometry is computed based on equation (5.4.4). The maximum ratio between the von Mises stress and yield stress for each configuration is optimised by ensuring that the top connection axial stress at far position is at the same value of the von Mises stress in touch down point at near position. The latter includes radial hydrostatic, bending, and axial stresses. Figure 6.4.1 shows that for this particular application, if the stress level is kept below 70%, the core material can not be made of zirconia and for alumina the equivalent *OD/t* ratio single walled pipe have to be greater than 12. Figure 6.4.2 shows correspondent top angle with the vertical and figure 6.4.3 shows the top tension ratio between the multi-layered and the single walled pipe for the corresponding configurations. It can be seen that all core material leads to a smaller top tension than the single walled pipe.

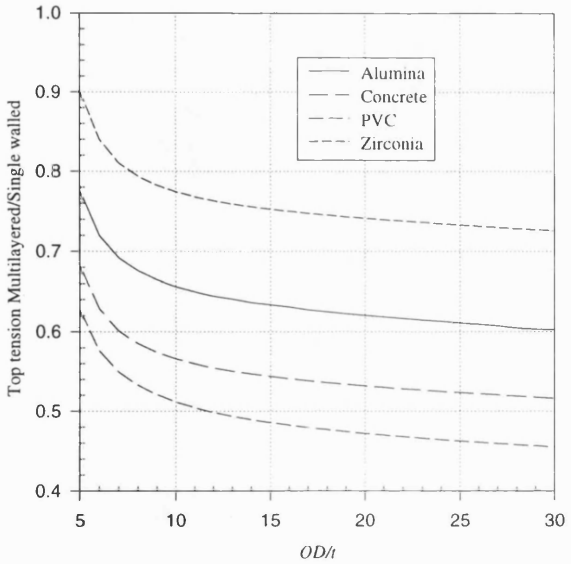

Fig. 6.4.3 Comparison of top tension ratio at far position.

For a better understanding of the multi-layered pipes in several catenary configurations, concrete has been investigated as the core

material. The following figures show the possible configurations that can replace a typical single steel walled pipe, which will be denoted by its internal diameter and *OD/t* ratio. The figures are divided in groups. The figure 6.4.4 group are for internal diameter of 10-inch and oil content. These figures are subdivided by letters (a), (b)..., these subdivisions represents different water depths and core ratios. The multi-layered pipe equivalence was determined again by equation (5.4.4). Therefore, the curves corresponding to the multi-layered pipe represents the performance of the buckling equivalent multi-layered pipe to the single walled pipe. The *x*-axis of all figures is the outside diameter to thickness ratio, *OD/t*, of the equivalent single steel walled pipe.

The figures show the maximum von Mises stress ratio normalised by the steel yield stress reached on both critical points. It is assumed that the single walled pipe wall and the multi-layered pipe faces are made of the same steel with yield stress equal to 60 ksi. The two critical points are the top connection at far position and the touch down point at near position. The figures also include the top tension and top angle with vertical for far position. The values presented on these figures were results from

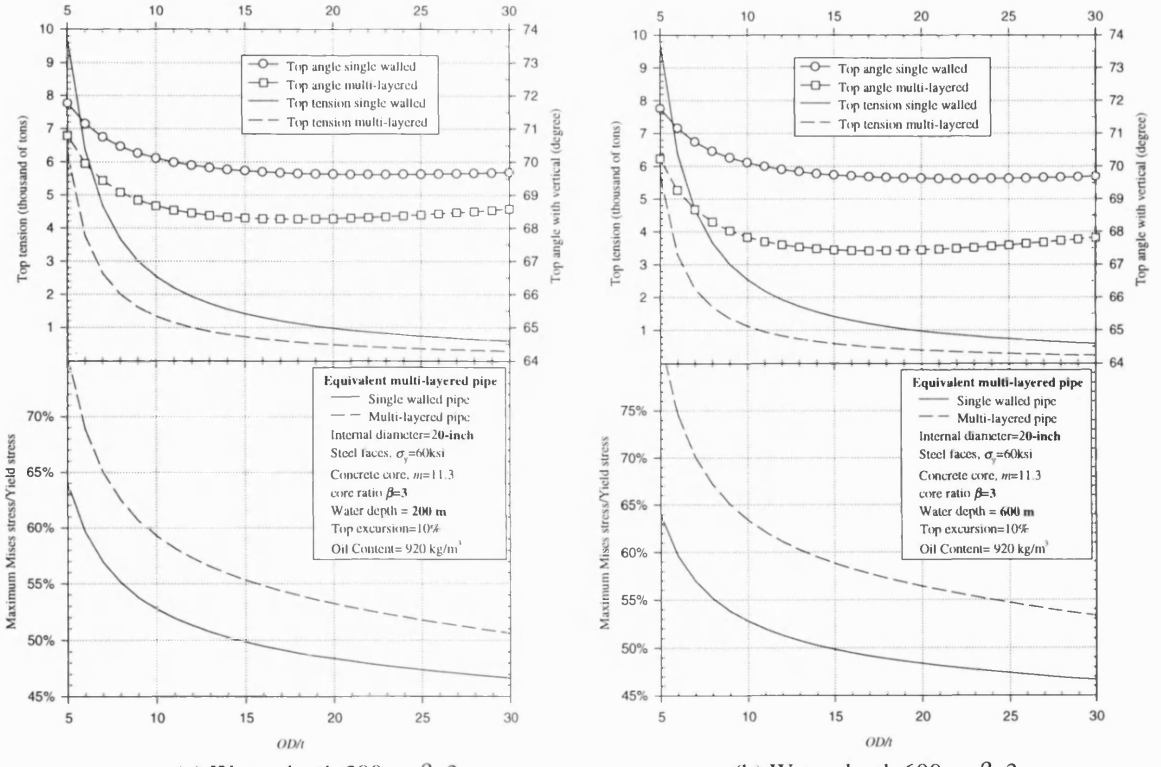

(a) Water depth 200m; β=3 (b) Water depth 600m; β=3

Fig. 6.4.4 Comparison for multi-layered, concrete core internal diameter 20-inch, oil content.

a FORTRAN code based on the catenary model developed in section 5. The catenary configuration is optimised by making the stress condition at both critical points to be equal.

For the equivalent multi-layered pipe the values of top tension are always smaller. However, due to its bigger outside radius the bending stresses push the von Mises stress at touch down point to a greater value. Therefore, the designer should pay particular attention to the touch down point stresses. Assuming a typical value of 70% of the yield stress in figure 6.4.4 only for configurations of β=10, figures 6.4.4(g) and (h), is there some restrictions for the multi-layered alternative.

Let us examine the effect of increasing the internal diameter of the pipe. Figure 6.4.5 show the configurations for a 20-inch internal diameter pipe. It can be seen that the concrete core alternative for big diameter pipes are not recommended for shallow water applications. Only from 600m water depth are there feasible alternatives for a specific range of *OD/t*. The increase in the core ratio β for this case will worsen the stress problem at touch down point.

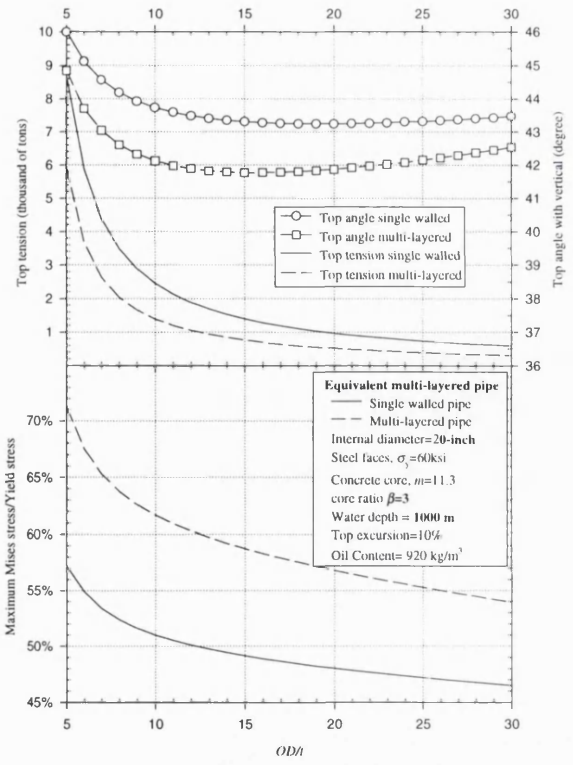

(c) Water depth 1000m; β=3

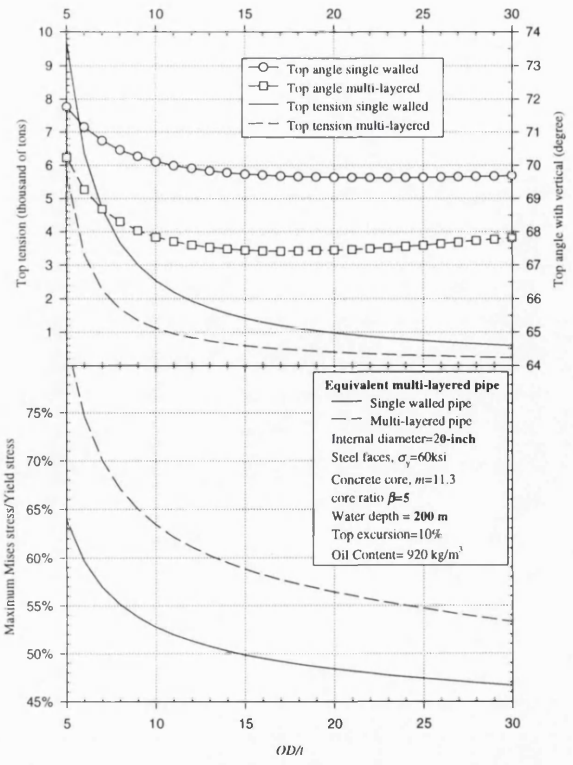

(d) Water depth 200m; β=5

Fig. 6.4.4 Comparison for multi-layered, concrete core internal diameter 20-inch, oil content.

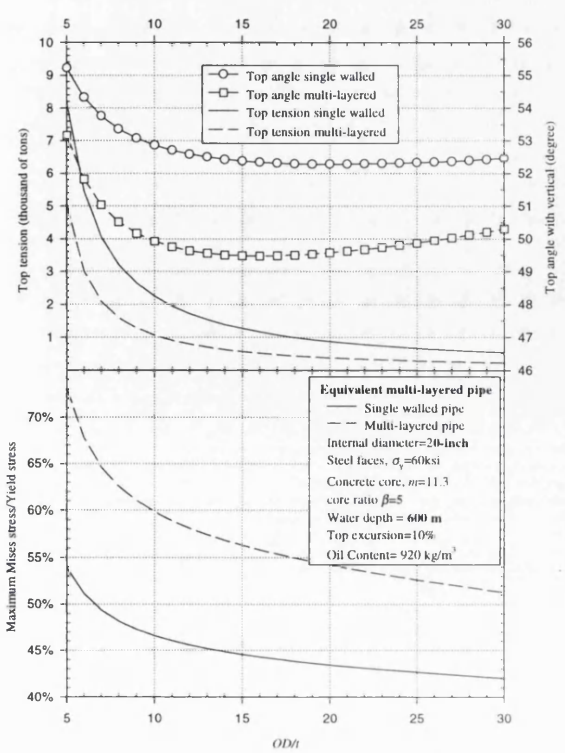

(e) Water depth 600m; β=5

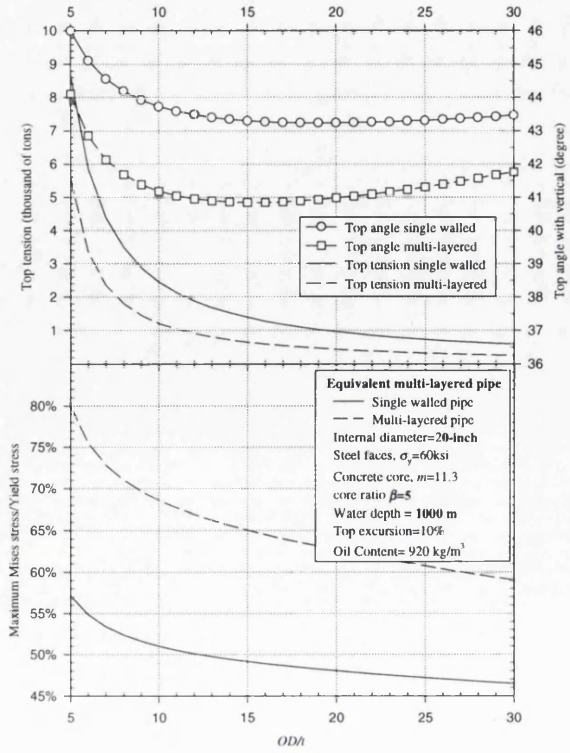

(f) Water depth 1000m; β=5

Fig. 6.4.4 Comparison for multi-layered, concrete core internal diameter 20-inch, oil content.

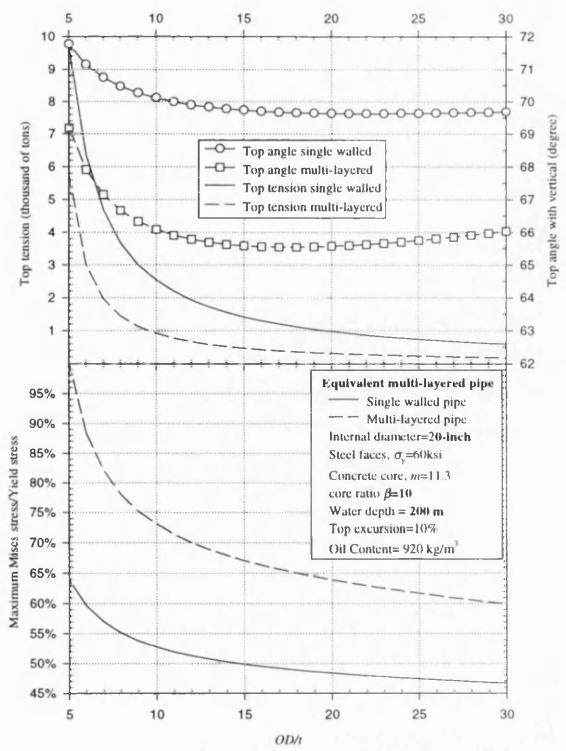

(g) Water depth 200m; β=10

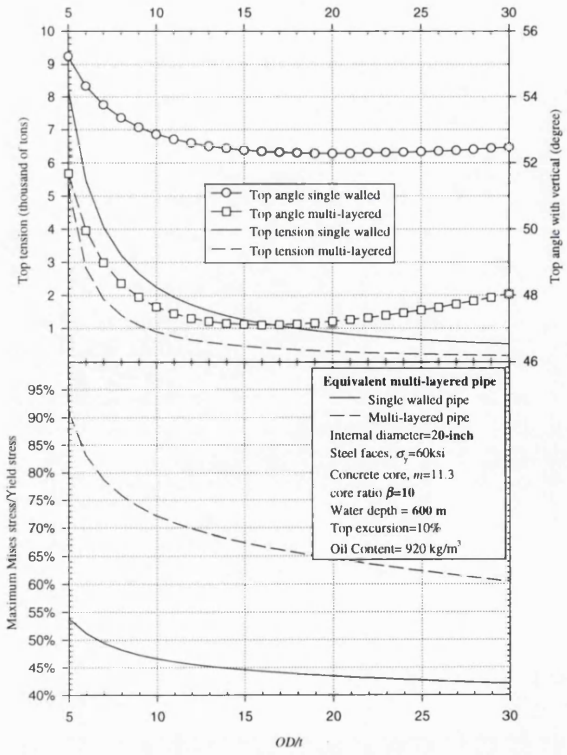

(h) Water depth 600m; β=10

Fig. 6.4.4 Comparison for multi-layered, concrete core internal diameter 20-inch, oil content.

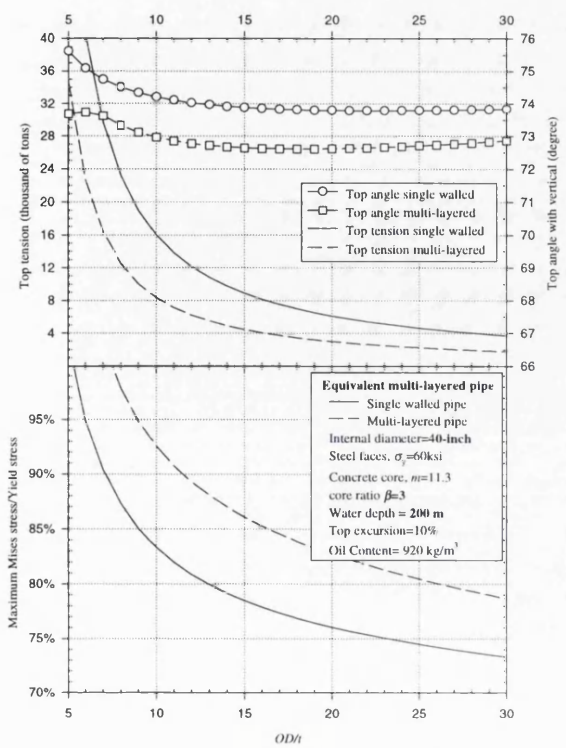

(a) Water depth 200m; β=3

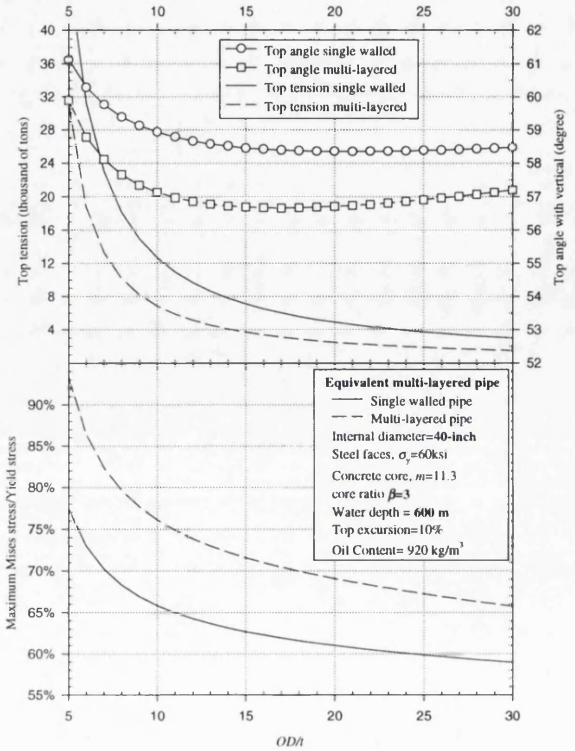

(b) Water depth 600m; β=3

Fig. 6.4.5 Comparison for multi-layered, concrete core internal diameter 40-inch, oil content.

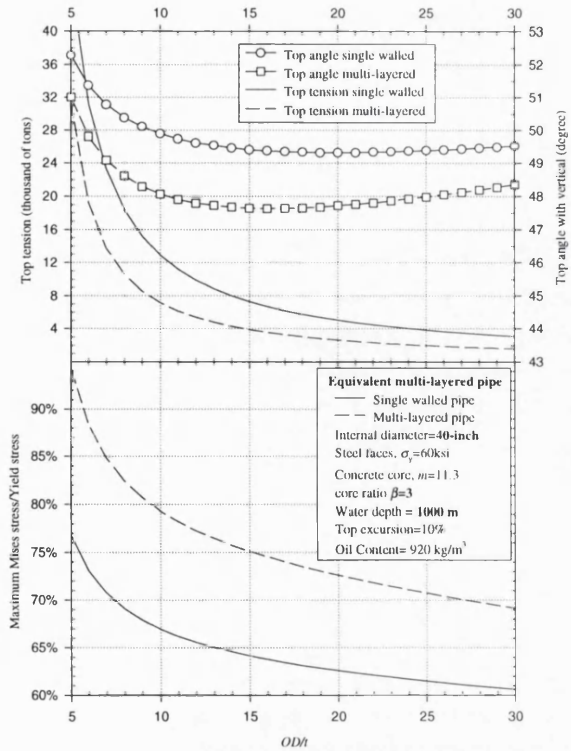

(c) Water depth 1000m; β=3

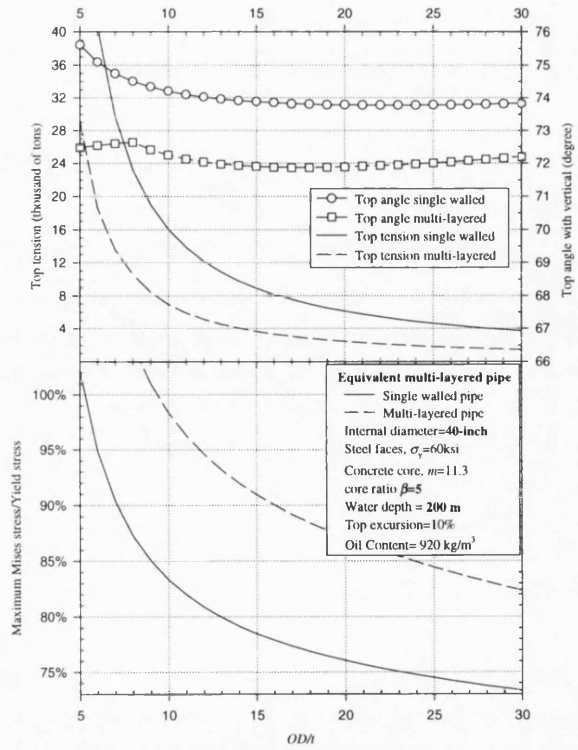

(d) Water depth 200m; β=5

Fig. 6.4.5 Comparison for multi-layered, concrete core internal diameter 40-inch, oil content.

All configurations examined until now were for oil content. Changing the content to gas introduces a change in the stress distribution. The next set of figures will demonstrate that multi-layered pipe alternative becomes even more attractive in this case. However, there is a limitation for $OD/t>18$ the multi-layered pipe start to float, i.e. the up-thrust is greater than its submerged weigh. Therefore, figure 6.4.6 was built only for $OD/t<18$. An interesting fact arises in figure 6.4.6 – there are specific situations where the von Mises stress at touch down point for the multi-layered alternative is smaller than that for the single walled pipe. The explanation is that in spite of the bending stress increment induced by a greater outside radius, the reduction in top tension relief the axial stresses causes the observed change. It means that multi-layered alternatives for catenary gas pipes would reduce not only the top tension but also the von Mises stress at touch down point.

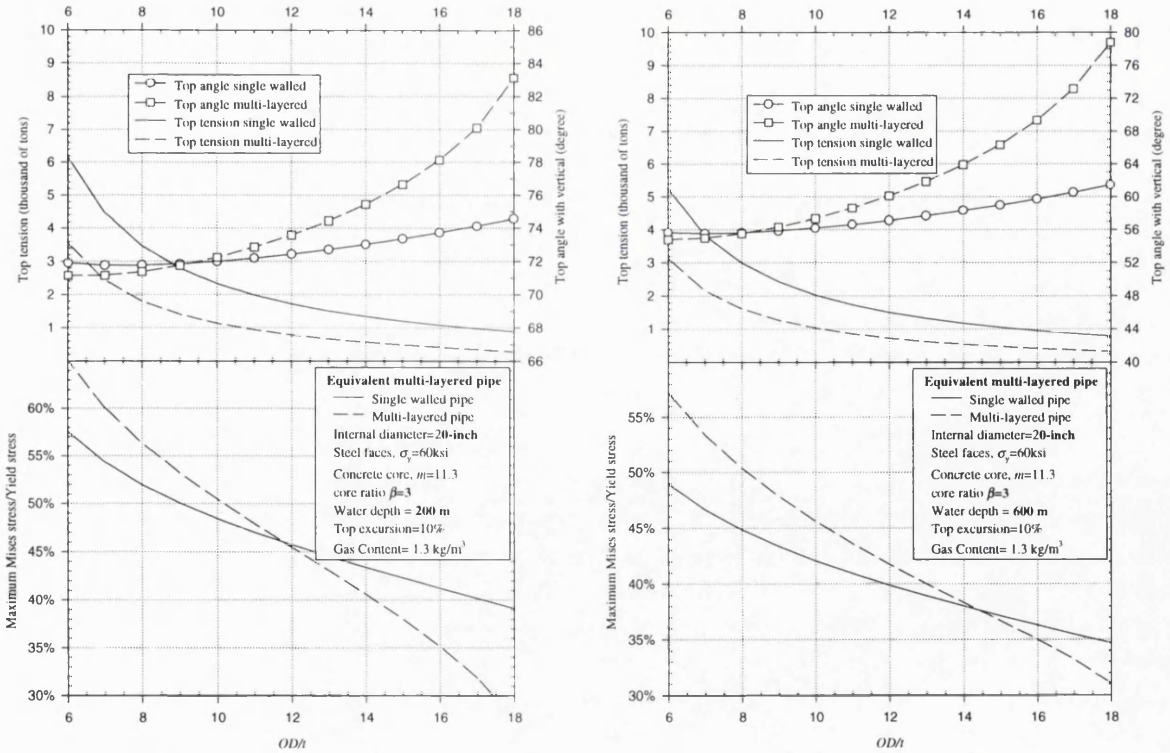

(a) Water depth 200m; β=3, ID=20-inch (b) Water depth 600m; β=3, ID=20-inch

Fig. 6.4.6 Comparison for multi-layered, concrete core, gas content.

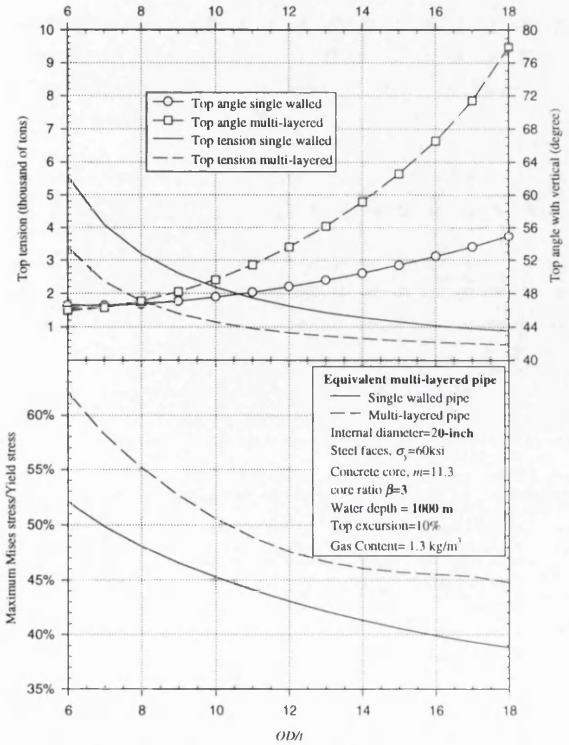

(c) Water depth 1000m; β=3, ID=20-inch

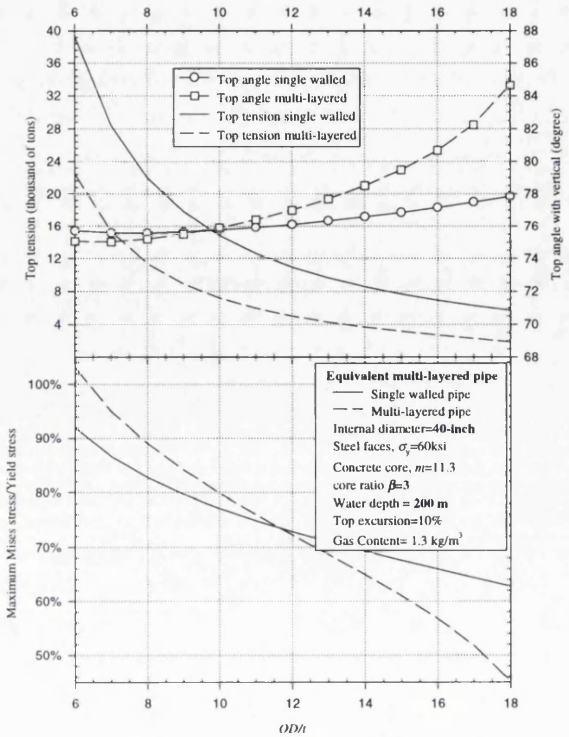

(d) Water depth 200m; β=3, ID=40-inch

Fig. 6.4.6 Comparison for multi-layered, concrete core, gas content.

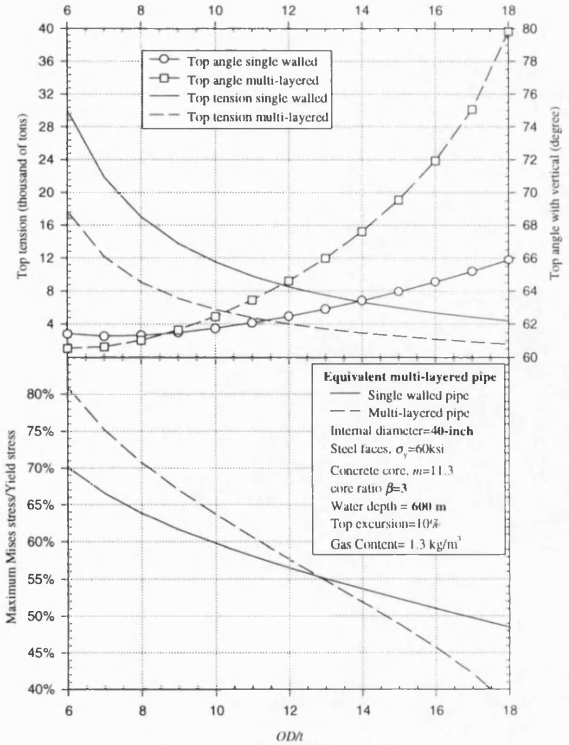

(e) Water depth 600m; β=3, ID=40-inch

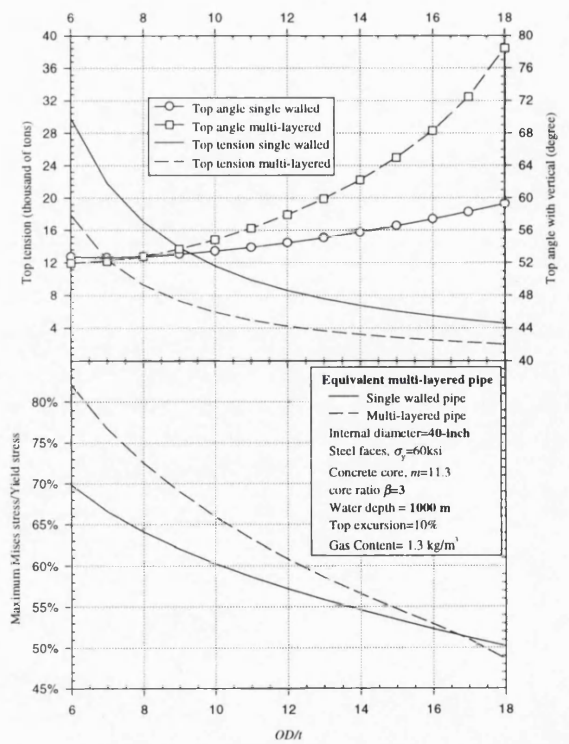

(f) Water depth 1000m; β=3, ID=40-inch

Fig. 6.4.6 Comparison for multi-layered, concrete core, gas content.

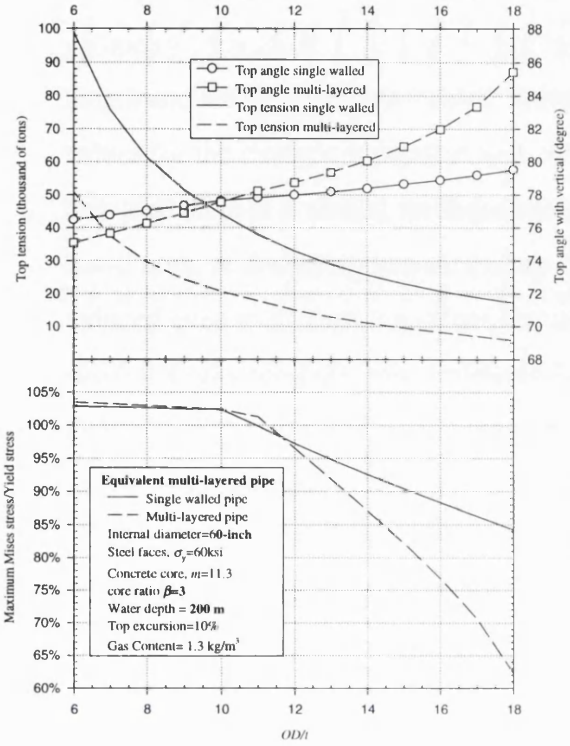

(g) Water depth 200m; β=3, *ID*=60-inch

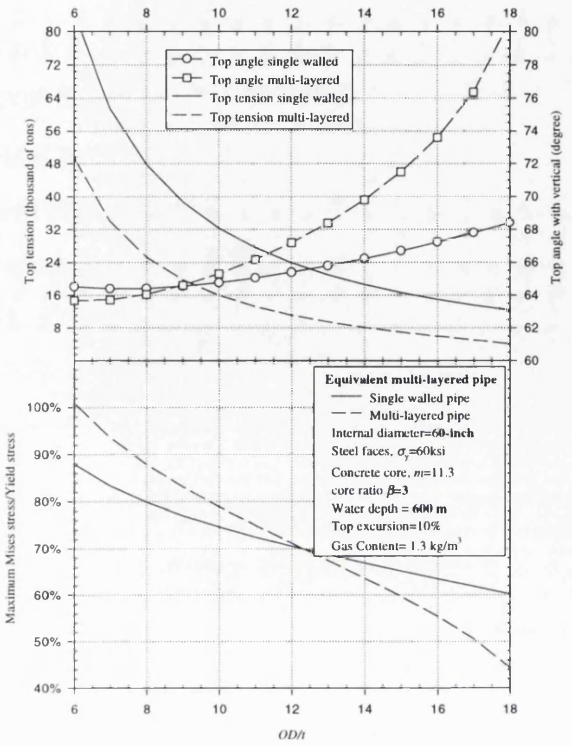

(h) Water depth 600m; β=3, *ID*=60-inch

Fig. 6.4.6 Comparison for multi-layered, concrete core, gas content.

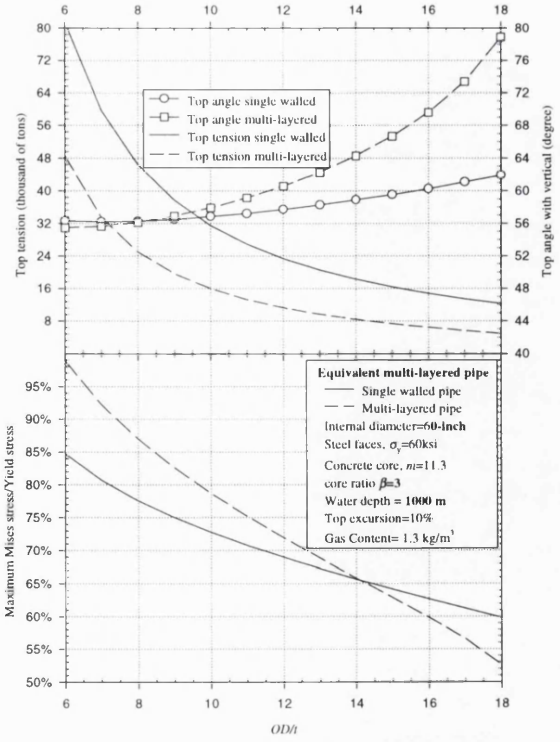

(i) Water depth 1000m; β=3, *ID*=60-inch

Fig. 6.4.6 Comparison for multi-layered, concrete core, gas content.

During the design of a multi-layered pipe it is possible to optimise the catenary geometry with smaller top angle with vertical that will demand a smaller hanging length and also smaller top tension. However, this optimisation will imply different values for the stresses reached at both critical points. With the aid of figure 6.4.7, provided there is a margin for these stresses, increasing the von Mises stress in touch down point at the near position, the top tension and top angle with the vertical can be reduced even more than the values showed in figures 6.4.6. Figures 6.4.7 (oil content) and 6.4.8 (gas content) were produced for a fixed single walled pipe geometry OD/t=15. The x-axis is the ratio between the axial stress at the far position normalised by the yield stress. The other curves give the top tension and top angle at the far position, the von Mises stress ratio at touch down point normalised to yield stress and the top angle at near position. Finally, these tools will allow the designer to select and understand the benefits of the multi-layered alternative for riser and pipeline applications in the offshore industry.

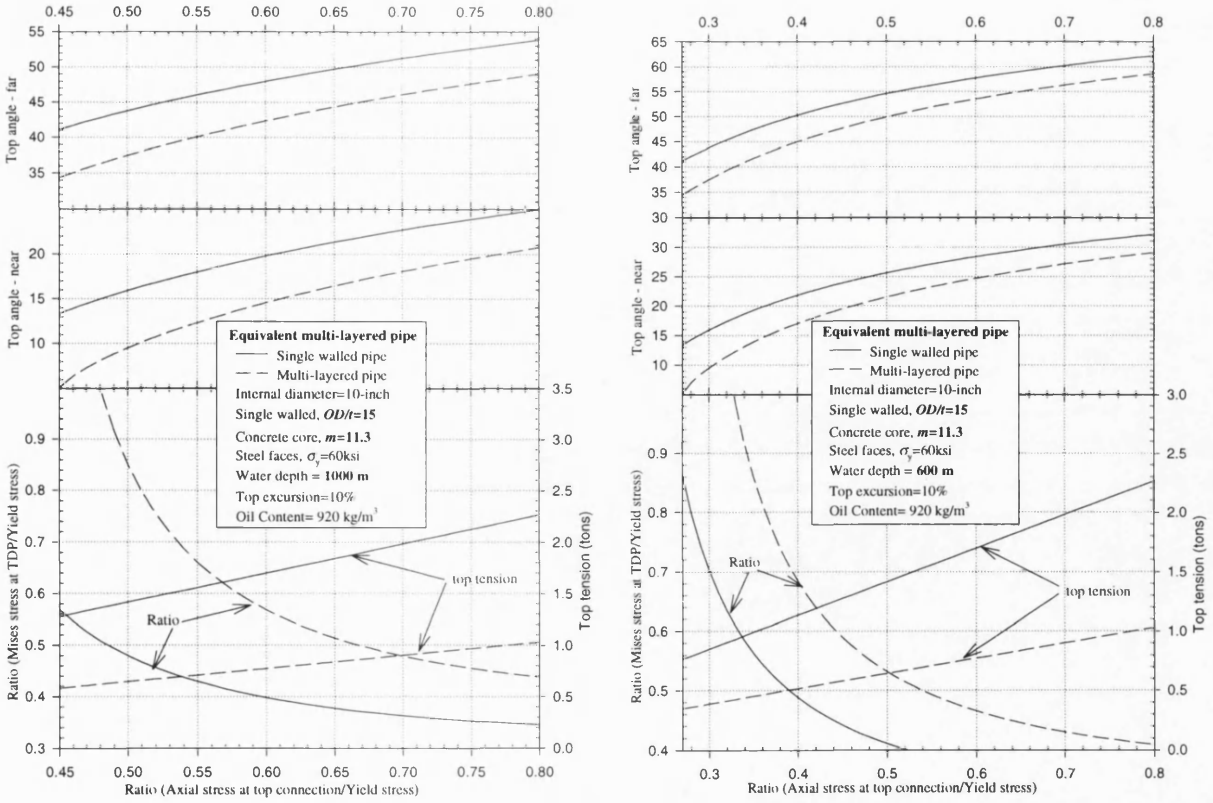

(a) 1000m water depth, ID=10-inch. (b) 600m water depth, ID=10-inch.

Fig. 6.4.7 Comparison for buckling equivalent multi-layered, concrete core, single walled pipe OD/t=15

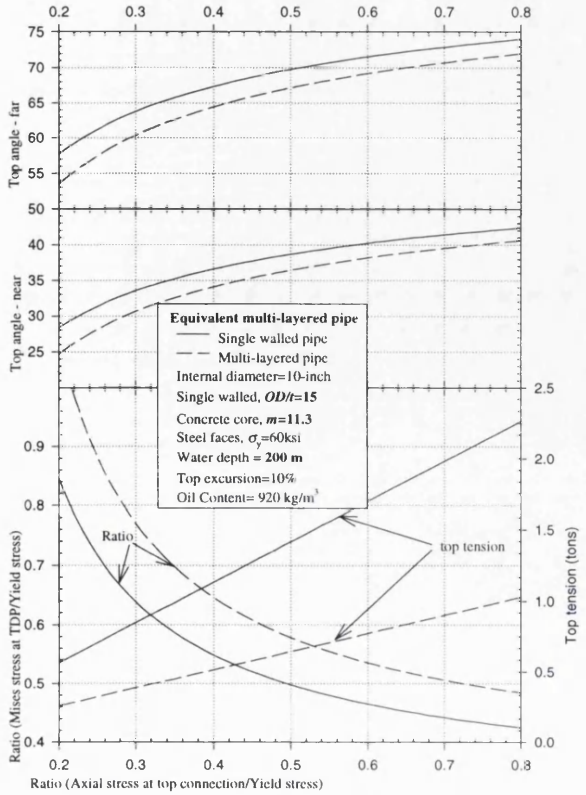

(c) Water depth 200m; β=3, *ID*=10-inch

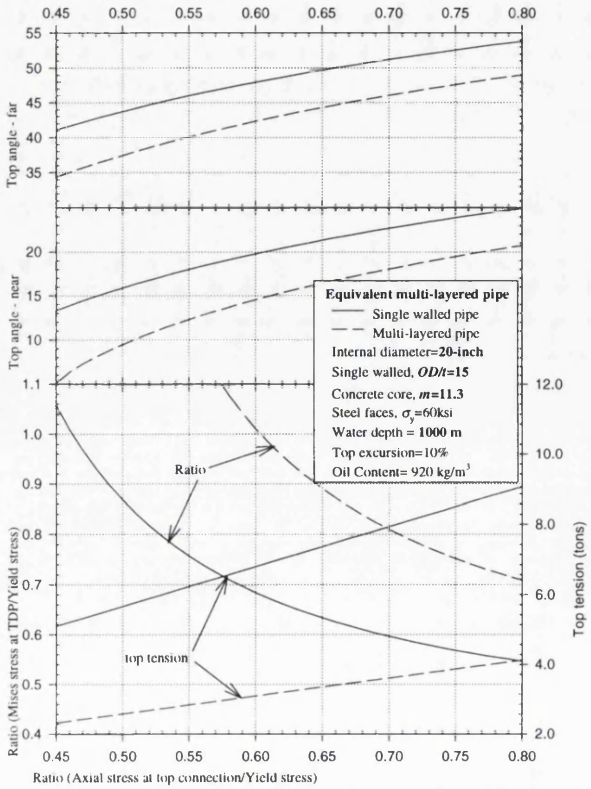

(d) Water depth 1000m; β=3, *ID*=20-inch

Fig. 6.4.7 Comparison for multi-layered, concrete core, oil content, single walled pipe *OD/t*=15

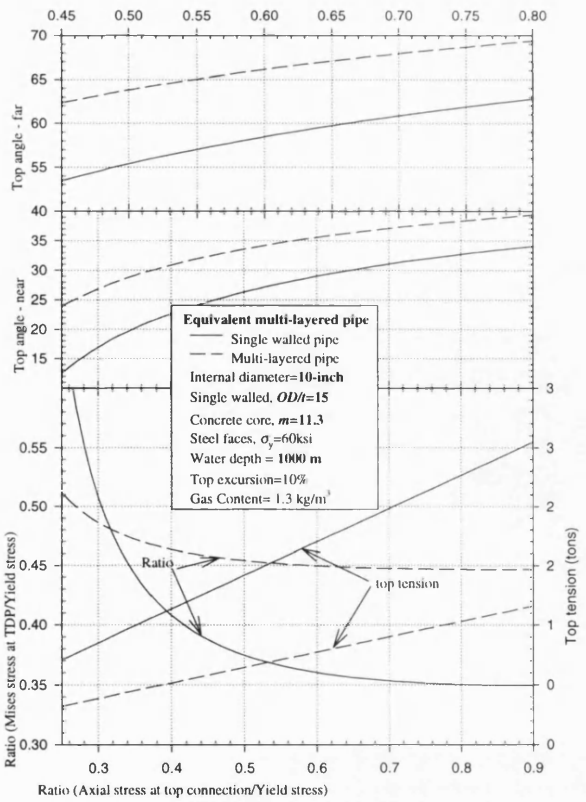

(a) Water depth 1000m; β=3, *ID*=10-inch

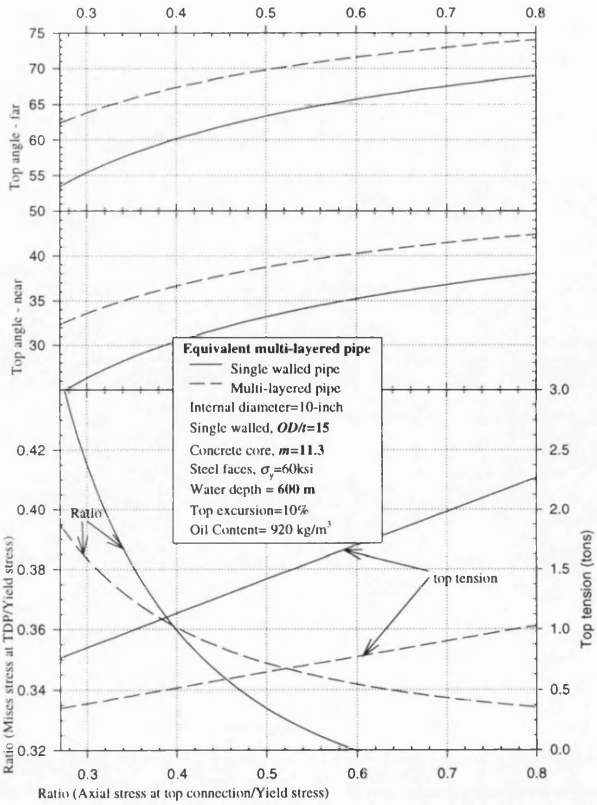

(b) Water depth 600m; β=3, *ID*=10-inch

Fig. 6.4.8 Comparison for multi-layered, concrete core, gas content, single walled pipe *OD/t*=15

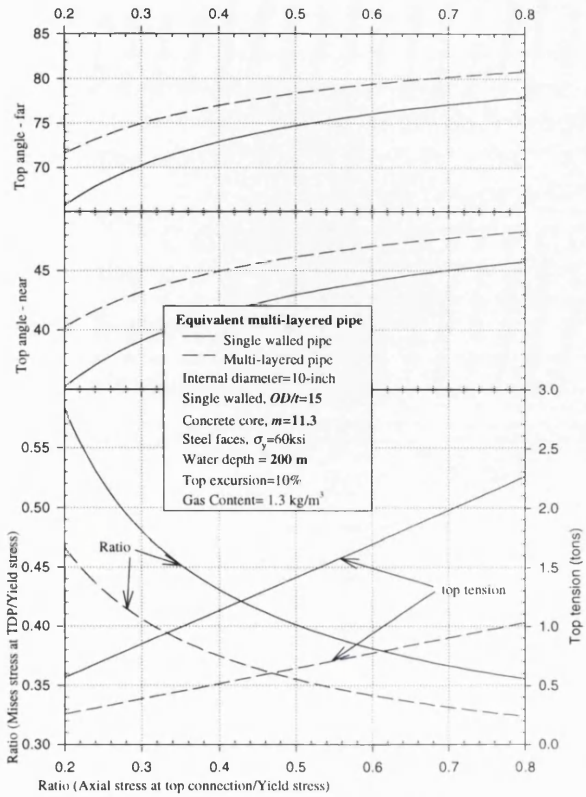

(c) Water depth 200m; β=3, *ID*=10-inch

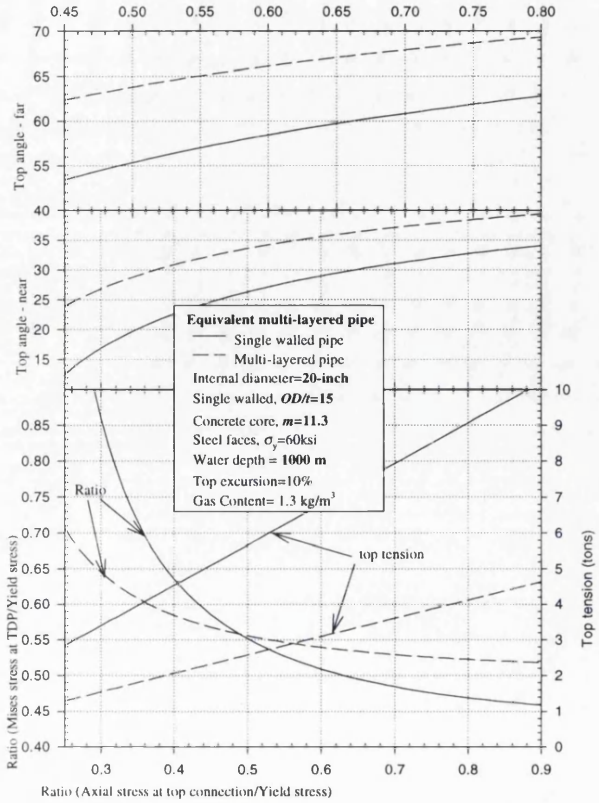

(d) Water depth 1000m; β=3, *ID*=20-inch

Fig. 6.4.8 Comparison for multi-layered, concrete core, gas content, single walled pipe *OD/t*=15

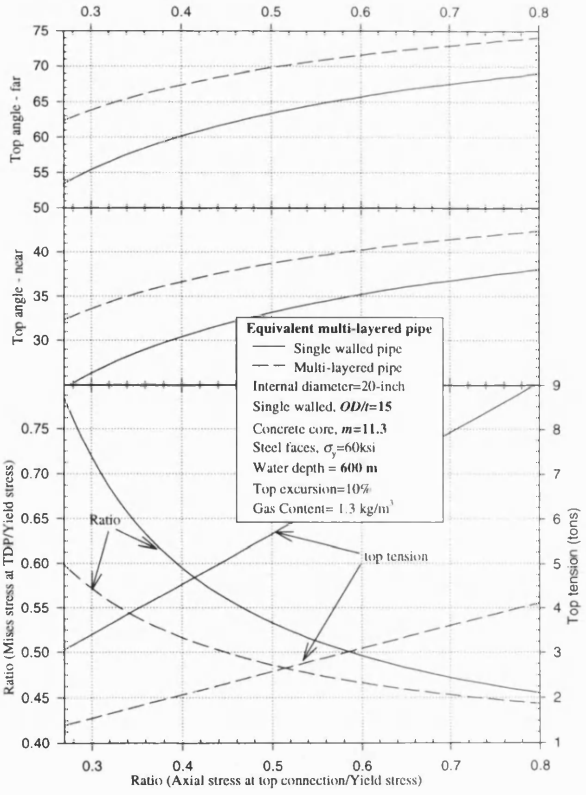

(e) Water depth 600m; β=3, *ID*=20-inch

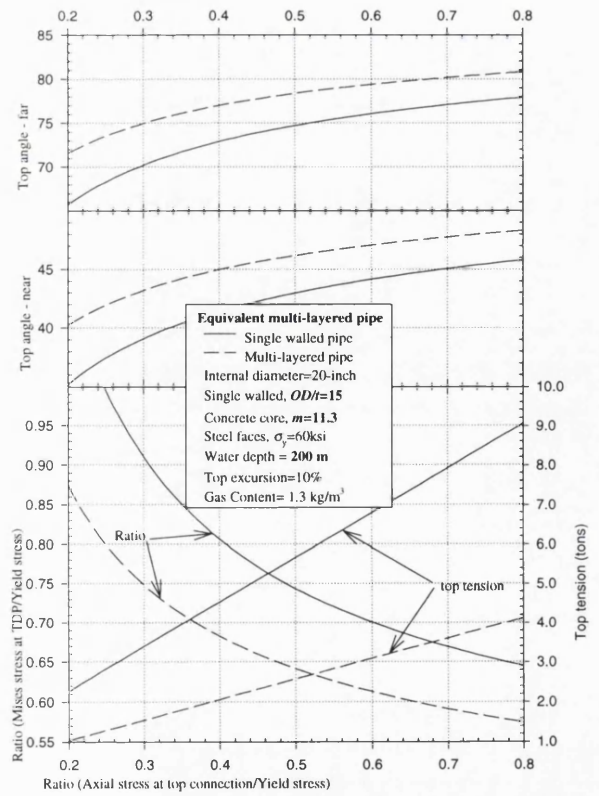

(f) Water depth 200m; β=3, *ID*=20-inch

Fig. 6.4.8 Comparison for multi-layered, concrete core, gas content, single walled pipe *OD/t*=15

7. Discussion and conclusions

7.1 Research objectives

The objectives of this research were to investigate and build a set of tools for analysing and verifying the application of multi-layered pipe structures as an alternative to single walled pipes for deep water application in the offshore industry. In particular, the work was aimed at carrying out analytical investigations of the structural mechanics of multi-layered pipes in an attempt to understand the way in which such pipes withstand internal and external hydrostatic pressures. Finite element analysis has only been used as a confirmation tool with none of the basic research relying on such analysis. One potential application of a multi-layered pipe in deep water – the catenary riser – was also investigated.

7.2 Development of analysis techniques

Two approaches have been used for the structural analysis of multi-layered pipes in deep water. First, a local analysis has been used to investigate the stress and strain distribution through layers of multi-layered pipes of different materials and cross sections. This analysis has considered both internal and external pressure loading. Secondly, the global behaviour of the multi-layered pipe was investigated in a deep water catenary riser application to demonstrate that a multi-layered pipe could bring significant practical benefits as an alternative to single walled pipes.

In terms of local analysis, a set of equations have been developed in section 3 to predict the stress and strain distribution in the walls and intermediate material of a multi-layered pipe subjected to internal pressure loading. The results have been compared with those from the finite element program ABAQUS and have shown very good agreement.

In addition, for external pressure loading four methods have been used and developed further in section 4. The first, the elastic foundation method, considers that the collapse would arises as a loss of elastic stability. A second elastic approach, originally proposed by Raville (1954), has also been used. A third method, based on elastic-plastic behaviour, is than used to estimate collapse pressures when all layers have reached the plastic condition based on a von Mises criterion. Finally, a fourth

method uses results from the finite element program ABAQUS to obtain a wide range of comparisons between results from the above methods. A comparison of results is presented in section 6.

The global behaviour of a multi-layered pipe in deep water catenary riser application is described in section 5. A static catenary based configuration analysis tool was developed to optimise typical designs and demonstrate the benefits of the multi-layered pipes in comparison to equivalent single walled pipes.

7.3 Conclusions

Several important conclusions arise from this investigation. The main issue, however, is that multi-layered pipes would be a better choice, for the stand point of structural integrity, than single walled pipes for the majority of deep water installations. If there are any special demand such as high internal pressure and insulation, the multi-layered pipe would also perform better than conventional single walled pipe. On the other hand, a multi-layered pipe would also demand more expenses and the connection between pipe sections will require special attention. Of course, these issues would need to be balanced by the designer during a feasibility study.

The conclusion of this investigation are summarised below.

(1) Multi-layered pipes are feasible alternatives for application where conventional solutions are not feasible, such as for:

- high internal pressure requirement;
- high external pressure for deep water applications;
- submerged weight restrictions;
- top tension restrictions;
- large wall thickness as a function of high hydrostatic pressure requirement;

Other favourable properties of multi-layered pipes such as high thermal insulation properties, better dumping properties, and good impact resistance are present but have not been addressed in this work.

(2) Multi-layered pipe can be used very effectively as catenary risers and perform better than single walled pipe. Multi-layered pipes used in this offer a significant reduction in top tension. However, as has been pointed out before, there are many other considerations to be taken into account during riser design.

(3) A multi-layered pipe generally provides a better internal distribution of stresses than the equivalent single walled pipe when it is subjected to internal pressure. In section 6, figure 6.2.4 shows the comparison between the stresses in the wall of a single walled pipe and a multi-layered pipe.

(4) The collapse analysis of multi-layered pipes due to external pressure presents a very complex problem. Much previous work in this field has addressed aerospace and non-offshore sandwich structures. The investigation of this thesis has applied and extended three analytical based methods to apply to the deep water offshore multi-layered pipe. These methods are:

- an elastic foundation model based on application of conventional elastic foundation theory;
- the classic elastic interaction model originally proposed by Raville (1954);
- an elasto-plastic extension to the interaction model above.

(5) The principal conclusion of the above work on collapse can be split up between multi-layered pipes with soft and hard cores – this parameter being defined by the ratio, $m = E_f / E_c$, of the Young's Modulus of the faces (E_f) and of the core (E_c). Values of m of around 100 or more are regarded as a 'soft' core whereas those around 10 are considered to be 'hard' core.

For soft cores, the elastic models (elastic foundation and extension of Raville's work (1954)) lead to smaller collapse pressure estimates for thin walled multi-layered pipes ($\alpha > 0.90$, where α is the ratio between the mean radius of the multi-layered pipe faces $\alpha = b/a$) than the elasto-plastic approach. These elastic methods also give the better estimates of collapse pressures for thin walled multi-layered shells as employed in aircraft design. However, for thicker pipes used in offshore applications ($\alpha < 0.90$), the elasto-plastic model gives smaller estimates

for collapse pressure, and is therefore, the best technique to be used in design. Figures 6.3.1(f) to 6.3.1(j) illustrate these conclusions. For hard cores, with values of m around 10, the elasto-plastic model gives the smaller prediction for collapse pressure, see figures 6.3.1(a) to 6.3.1(e).

(5) The finite element program ABAQUS gives better estimates of collapse pressure for multi-layered pipes using 3D rather than 2D element modelling. Figures 6.3.1 shows that the 3D analysis model gives smaller values which are closes to the analytical elastic solutions than the 2D model.

(6) For relatively hard core (m = 10) such as concrete, based on figures 6.3.1(a) to 6.3.1(e) the collapse of a multi-layered cylinder tends to have an elasto-plastic solution very close to the loss of stability with increase of the thickness ratio β. It means that a multi-layered pipe with this characteristics would collapse in a combined behaviour between elasto-plastic and loss of stability of the outer layer possibly triggered by imperfections. Unfortunately, no experimental data are available to support this statement.

(7) For a relatively soft core (m = 100) such as polypropylene, principal observation from Figures 6.3.1(f) to 6.3.1(j) is that the collapse of a multi-layered pipe with thin walls ($\alpha > 0.9$) tends to be an elastic nature due to loss of stability. This trend increases with increase of thickness ratio β.

7.4 Future investigations

This thesis was aimed at examining the structural mechanics of multi-layered pipes in depth. By necessity this meant that many additional and related issues were not covered.

It should be said at the outset that there are still significant theoretical, experimental and practical design research areas that remain to be addressed for multi-layered pipes. Several specific areas of further investigation arises from this research are described below.

The layer interface problem needs to be addressed more deeply. The combined

elastic approach assumes that all layers work together as an integrated sandwich wall. The elastic-plastic analysis uses compatibility equations that impose continuous contact between the core boundaries during hydrostatic pressure loading. The elastic foundation approach replaces these layers by a set of elastic foundation springs. All assure that the interfaces between layers remain in continuous contact and are effectively very strongly bonded together. This clearly need not be the case in practice and the structural effects of it need to be investigated.

All three analysis approaches used here have their merits and drawbacks and they all give a prediction for the collapse load. However, they need to be composed with experimental results and the background of experimental observed structural failure needs to be compared with the theories. The failure mode of a multi-layered pipe is important. Its collapse can be completely elastic following a theoretical wave mode or can be elastic-plastic and triggered by an imperfection, which will grow at a particular point around the pipe surface or more likely due to a combination of these. The behaviour of the interfaces, mainly on the post-buckling deformations also needs to be addressed.

Another possible future development is to perform an elastic-plastic finite element assessment to compare results with the 3-D elastic-plastic method included in this present work. Obviously, some physical tests would improve such analysis and give more understanding of the significance of this approach. In addition, experimental tests would also give a clarify the physical significance of the elastic foundation model, in particular when the model indicates that the core layer loss stability before the two faces.

Recent new features in finite element analysis could also be explored to simulate the boundaries interaction of the multi-layered cylinder. This important interaction will produce a better understanding of the physics of the failure mode including the post-buckling behaviour of multi-layered cylinders. Of course, some experimental results have also to be pursued in order to calibrate the element contact properties to be inputted into the finite element package.

The material alternatives available for use as the core material should also be

narrowed down for specific applications such as for pure insulation or weight and insulation and so on. In addition, more understanding of the behaviour of core materials subjected to compression is required.

The free catenary model in this investigation was developed for a static configuration only. There are additional dynamic loads to be considered. Future work needs to address the more complete problem with the application of current profile and wave induced loads on the catenary.

References

1. ABAQUS - Finite Element Analysis Package - version 5.5, Hibbitt, Karlsson & Sorensen, inc., 1995.
2. Allen, H.G., *Analysis and Design of Structural Sandwich Panels*, Oxford: Pergamon 1969.
3. Bai Y., Igland R., Moan, T., *Collapse of thick tubes under combined tension and bending*, Journal of Constructional Steel Research, 1995, vol. 32, pp. 233-257.
4. Baker, E.H., Kovalevsky, L., Rish, F.L., *Structural Analysis of Shells*, MacGraw-Hill book co, 1972.
5. Bandyopadhyay K., Xu J., Shteyngart S., Eckert H., *Plastic buckling of cylindrical shells*, American Society of Mechanical Engineers, Pressure Vessels and Piping Division (Publication) PVP, 1994, vol. 271, pp. 33-36.
6. Berak E. G., Gerdeen J. C., *A Finite Element Technique for Limit Analysis of Structures, Journal of Pressure Vessel Technology*, 1990, vol. 112, pp. 138-144.
7. Bonanni, D.L., *Stability analysis of thick-section composite cylinders under hydrostatic-pressure including 3-dimensional effects and non-linear material response*, Compression Response Of Composite Structures, 1994, 1185, pp. 7-33.
8. Brown, T.L., Hyer, M.W., *Effects of layer waviness on the stresses and failure in hydrostatically loaded cylinders*, Compression Response Of Composite Structures, 1994, 1185, pp. 78-94.
9. Brush, D.O., Almroth, B.O., *Buckling of Bars, Plates and Shells*, MacGraw-Hill Book Company, 1975.
10. Corona, E., Kyriakides, S., *Experimental investigation of the degradation and buckling of circular tubes under cyclic bending and external pressure*, Thin-Walled Structures, 1991, vol. 12, pp. 229-263.
11. Choo, Y.S., Horne, M., *Limit strength of composite sandwich cylinders subjected to external- pressure*, Composite Steel Structures : Recent Research And Developments, 1991, pp. 40-51.
12. Chryssostomidis, C., Papadakis N.A., *Buckling analysis of sandwich shell structures subjected to hydrostatic load*, Marine Technology, 1994, vol. 31, pp. 106-115.
13. DiSciuva, M., Carrera, E., *Static buckling of moderately thick, anisotropic laminated and sandwich cylindrical shell panels*, AIAA Journal, 1990, vol. 28, pp. 1782-1793.
14. Dong, S.B., Etitum, P., *Three-dimensional stability analysis of laminated anisotropic circular cylinders*, International Journal of Solids and Structures, 1995, vol. 32, pp. 1211-1230.
15. Donnell, L. H., *Effect of Imperfections on Buckling of Thin Cylinders Under External Pressure*, Journal of Applied Mechanics, 1956, vol. 23, pp 569-575.
16. Donnell, L. H., Wan, C.C., *Effect of Imperfections on Buckling of Thin Cylinders and Columns Under Axial Compression*, Journal of Applied Mechanics, Trans. ASME, 1950, vol. 72, pp 73.

17.Donnell, L.H., *Beams, Plates and Shells*, MacGraw-Hill Inc, 1976.

18.Dorninger, K., Rammerstorfer, F.G., *Layered composite shell element for elastic and thermoelastic stress and stability analysis at large deformations*, International Journal for Numerical Methods in Engineering, 1990, vol. 30, pp. 833-858.

19.Dyau, J.Y., Kyriakides, S., *On the localisation of collapse in cylindrical shells under external pressure*, International Journal of Solids and Structures, 1993, vol. 30, pp. 463-482.

20. Durban, D., Kubi, M., *General Solution for the Pressurised Elastoplastic Tube*, Journal of Applied Mechanics, 1992, vol. 59, pp. 20-26.

21.Dyau J.Y., Kyriakides S., *On the propagation pressure of long cylindrical shells under external pressure*, International Journal of Mechanical Sciences, 1993, vol. 35, pp. 675-713.

22.Dyau, J.Y., Kyriakides, S., *On the response of elastic-plastic tubes under combined bending and tension*, Journal of Offshore Mechanics and Arctic Engineering, 1992, vol. 114, pp. 50-62.

23.Ellinas, C., Croll, J., *Elastic-Plastic buckling design of cylindrical shells subject to combined axial compression and pressure loading*, Journal of Solids Structures, 1986, vol. 22, pp. 1007-1017.

24.Estefen, S.F., *Ultimate Strength Behaviour of Submarine Pipelines Under External Pressure and Bending*, Journal Construction Steel Research, 1994, vol. 28, pp. 137-151.

25.Fang, J., Lyons G.J., *Material Damping of free hanging pipes: Theoretical and experimental studies*, Journal of Sound and Vibration, 1994, 173(3), pp 371-389.

26.FLEXRISER - Riser Analysis Package - version 4.2, Zentech Consultants ltd, 1994.

27.Flugge, W., *Stress in Shells*, Springer-Verlag, 1973.

28.Hamidzadeh, H.R., Chandler, D.E., *Circumferential vibrations of three layered sandwich cylinders*, American Society of Mechanical Engineers, Design Engineering Division (Publication) DE, 1991, vol. 36, pp. 233-237.

29.Heinen, A., Hennenberg, H.M., Fischer, O., Kinetische Stabilitaet elastischer Schalentragwerke, *Kinetic stability of elastic shell structures*, Archive of Applied Mechanics, 1994, vol. 64, pp. 457-471.

30.Jones, I.W., Salermo, V.L., *The effect of damping on the forced vibration of cylindrical sandwich shells*, Transaction of ASME, Journal of Engineering for Industry, Aug 1966, pp. 318-324.

31.Ju, G.T., Kyriakides, S., *Bifurcation buckling versus limit load instabilities of elastic-plastic tubes under bending and external pressure*, Journal of Offshore Mechanics and Arctic Engineering, 1991, vol. 113, pp. 43-52.

32.Ju G.T., Kyriakides S., *Bifurcation and localisation instabilities in cylindrical shells under bending. II. Predictions*, International Journal of Solids and Structures, 1992, vol. 29, pp. 1143-1171.

33.Kiciman, M.O., Konishi, D. Y., *Stability of Honeycomb Sandwich Cylinders*, ASME Paper, 61-AV-36, 1961.

34.Kuenzi, E., Bohannan, B., Stevens, G., *Buckling Coefficients for Sandwich Cylinders of Finite Length Under Uniform External Lateral Pressure*, Forest Products Laboratory, Note FPL-0104, September 1965.

35.Kuriyama, Y., Mimaki, T., *Finite-element analysis of collapse strength and burst strength of double-walled cra pipe*, Computer Aided Innovation Of New Materials , Parts 1 and 2, 1993, pp. 1523-1526.

36.Kyriakides S., Chang Y.C., *On the effect of axial tension on the propagation pressure of long cylindrical shells*, International Journal of Mechanical Sciences, 1992, vol. 34, pp. 3-15.

37.Kyriakides S., Youn S.K., *On the Collapse of circular confined rings under external pressure*, International Journal of Solids and Structures, 1984, vol. 20, pp. 699-713.

38.Kyriakides, S., Ju, G.T., *Bifurcation and localisation instabilities in cylindrical shells under bending. I-Experiments*, International Journal of Solids and Structures, 1992, vol. 29, pp. 1117-1142.

39.Kyriakides S., Yeh, M., Roach, D., *On the Determination of the propagation pressure of long circular tubes*, Journal of Pressure Vessel Technology, 1984, vol. 106, pp. 150-1.

40.Kyriakides, S., Babcock, C., Elyada, D., *Initiation of propagation buckles from local pipeline damages*, Journal of Energy Resources Technology, 1984, vol. 106, pp. 79-87.

41.Leissa, A.W., Iyer, K.M., *Modal response of circular cylindrical shells with structural damping*, Journal of Sound and Vibration, 1981, vol. 77(1), pp. 1-10.

42.Li, F.S., Kyriakides, S., *On the response and stability of two concentric contacting rings under external pressure*, International Journal of Solids and Structures, 1991, vol. 27, pp. 1-14.

43.March, H. W., Kuenzi, E. W., *Buckling of Sandwich Cylinders in Torsion*, Forest Products Laboratory, Report 184, January 1958.

44.Mackenzie, D., Nadrajah, C., Shi, J., Boyle, J.T., *Simple Bounds on Limit Loads by Elastic Finite Elements Analysis, Journal of Pressure Vessel Technology*, 1993, vol. 115, pp. 138-144.

45.Mackenzie, D., Nadrajah, C., Shi, J.,Boyle, J.T., *A Method of Estimating Limit Loads by Iterative Elastic Analysis, I and II*, International Journal of Pressure Vessels and Piping, 1993, vol. 53.

46.Moan, T., Estefen, S., Saevik, S., Zimmer, R.A., *Limits States for the Ultimate Strength of Tubular Subjected to Pressure, Bending and Tension Loads*, Marine Structures, 1994, vol. 7, pp. 323-344.

47.Montague, P., *A Simple composite construction for cylindrical shells subjected to external pressure*, Journal Mechanical Engineering Science, (c) IMechE 1975, Vol. 17(2), pp. 105-113.

48.Montague, P., *The experimental behaviour of double skinned, composite, circular cylindrical shells under external pressure*, Journal Mechanical Engineering Science, (c) IMechE 1978, Vol. 20(1), pp. 21-34.

49.Montague, P., *Some aspects of double-skin composite construction for sub-sea pressure chambers*, Boss/79-Second International conference on behaviour of off-shore structures, paper 76, pp. 415-424.

50.Montague, P., Sang, Y., Choo, *Double-skin construction of large pressure vessels for sub-sea systems*, OTC-1981, Offshore Technology Conference, paper 4106, pp. 361-368.

51.Montague, P., *Experimental behaviour of thin-walled cylindrical shells subjected to external pressure*, Journal of Mechanical Engineering Science, 1969, vol. 11(1), pp 40-56.

52.Murphey, C.E., Langner, C.G., *Ultimate pipe strength under bending collapse and fatigue*, Offshore Mechanics and Arctic Engineering Symposium, 1985, February 1985, pp 467-477.

53.Nashif, A.D., Jones, D.I.G., Henderson, J.P., *Vibration Damping*, John Wiley & Sons - 1985.

54.Norris, C.B., Zahn, J.J., *Design curves for the buckling of sandwich cylinders of finite length under uniform external lateral pressure*, Forest Products Laboratory, Forest Service, United States Department of Agriculture, Report No. FPL-07, May 1963.

55.Palmer, Martin, *Buckle Propagation in Submarine Pipelines*, Nature 1975, Vol. 1, pp. 46-48

56.Palchevskii, A.S., *Stability of a multi-layer cylindrical shell in interlayer pressure*, Soviet Applied Mechanics (English Translation of Prikladnaya Mekhanika), 1988, pp. 358-362.

57.Piche, R., *Lower Bound for Critical Buckling Load Using Matrix Norms*, Journal of Engineering Mechanics, 1993, vol. 119.

58.Plantema, F.J., *Sandwich Construction - The Bending and Buckling of Sandwich Beams, Plates, and Shells*, John Wiley & Sons - 1966.

59.Polizzoto C., *On the Conditions to Prevent Plastic Shakedown of Structures Part-I and II* , Journal of Applied Mechanics, 1993, vol. 60, pp. 15-25.

60.Poston, T., Stewart, I., *Catastrophe Theory and its Applications*, Pitman publishing ltd, 1978.

61.Ramesh, T.C., Ganesan, N., *Influence of constrained damping layer on the resonant response of orthotropic cylindrical shells*, Journal of Sound and Vibration, 1995, vol. 185(3), pp. 483-500.

62.Ramesh, T.C., Ganesan, N., *Orthotropic cylindrical shells with a viscoelastic core: a vibration and damping analysis*, Journal of Sound and Vibration, 1994, vol. 175(4), pp. 535-555.

63.Raville, M.E., *Analysis of long cylinders of sandwich construction under uniform external lateral pressure*, Forest Products Laboratory, Forest Service, United States Department of Agriculture, Report No. 1844, November 1954.

64.Raville, M.E., *Analysis of long cylinders of sandwich construction under uniform external lateral pressure - facings of moderate and unequal thicknesses*, Forest Products Laboratory, Forest Service, United States Department of Agriculture, Report No. 1844-A, February 1955.

65.Raville, M.E., *Buckling of sandwich cylindres of finite length under uniform external lateral pressure*, Forest Products Laboratory, Forest Service, United States Department of Agriculture, Report No. 1844-B, May 1955.

66.Reissner, E., *Small bending and stretching of sandwich-type shells*, National Advisory Committee on Aeronautics, Tech. Note 1832, 1949.

67.Roy, A.K, Tsai, S.W., *Design of thick composite cylinders*, Design and Analysis of Composite Material Vessels, 1987, pp 75-85.

68.Ryder, G.H., *Strength of Materials*, Macmillian press ltd, 1969.

69.Saunders, P.T., *An Introduction to Catastrophe Theory*, Cambridge University press, 1980.

70.Starbuck, J.M., Blake, H.W., *Failure of thick composite cylinders subjected to external hydrostatic-pressure*, Compression Response Of Composite Structures, 1994, 1185, pp 159-174.

71.Thompson, J.M.T., *A General Theory of Elastic Stability*, John Wiley & Sons,1973.

72.Timosheko, S.P., Krieger, S.W., *Theory of Plates and Shells*, McGraw-Hill int book co, 1940.

73.Timoshenko, S.P., Gere, J.M., *Theory of Elastic Stability*, McGraw-Hill int. book co, 1936, (ed.1961).

74.Yeh, M.K., Kyriakides, S., *On the collapse of inelastic thick-walled tubes under external pressure*, Journal of Energy Resources Technology, Trans. ASME, 1986, 108, pp 35-47.

75.Yeh, M.K., Kyriakides, S., *Collapse of deep water pipelines*, Journal of Energy Resources Technology, Transactions of the ASME, 1988, 110., pp. 1-11.

76.Wierzbicki, T., Bhat, S., *Initiation and propagation of buckles in pipelines*, International Journal of Solids Structures, 1986, 22, pp 985-1005.

77.Warburton, G.B., Soni, S.R., *Resonant response of orthotropic cylindrical shells*, Journal of Sound and Vibration, 1977, 53(1), pp 1-23 .

78.Ward, I.M., *Mechanical Properties of Solid Polymers*, 1990.

79.Zahn, J., Kuenzi, E., *Classical Buckling of Cylinders for Sandwich Construction in Axial Compression-Orthotropic Cores*, Forest Products Laboratory, FPL-018, 1963.

80.Zhou, C.T., Zhou, C.B., *The computation of non-linear instability for multi-layered composite cylindrical-shells*, Fifth International Conference On Composite Materials ICCM-V. 1985, pp 1135-1144.

Appendix 1

A.1 Analysis of external pressure for a ring

This appendix include the derivation of the buckling of circular rings and tubes under uniform external pressure. The ring solution was originally presented in Timoshenko's book Theory of Elastic Stability /73/, 1936 pages 289 to 296. The nomenclature are the same as used in Timoshenko's book.

In figure A.1.1, the thin line indicates the initial circular shape of the ring, and the other line represents the slightly deflected ring on which a uniformly distributed pressure is acting. The lower half of the ring has been removed and the action on the upper half is represented by a longitudinal compressive force S and by a bending moment M_0 acting on each of the cross sections A and B. The uniform normal pressure per unit of length is given by q. The generic ring radial displacement is w and the displacemnet at A and B centre line of the ring is w_0.

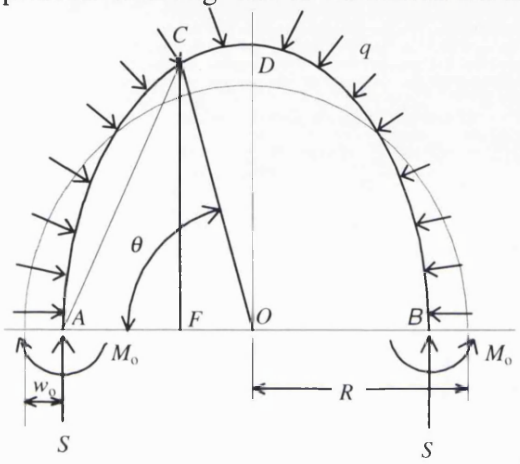

Fig. A.1.1 - Ring or tube under external pressure.

The bending moment, neglecting squares of small quantity w and w_0, becomes:

$$M = M_o - qR(w_o - w), \quad \text{(A.1.1)}$$

with this expression for bending moment, the differential equation for the deflection curve is (see 7-4, page 291, Timoshenko /73/, 1936):

$$\frac{d^2w}{d\theta^2} + w\left(1 + \frac{12q(1-\nu^2)R^3}{Eh^3}\right) = \frac{12(1-\nu^2)(-M_0R^2 + qR^3w_0)}{Eh^3}. \quad \text{(A.1.2)}$$

Considering the notation:

$$k^2 = 1 + \frac{12q(1-\nu^2)}{E}\left(\frac{R}{h}\right)^3. \quad \text{(A.1.3)}$$

The general solution is

$$w = A_1 \sin k\theta + A_2 \cos k\theta + \frac{-M_0R^2 + qR^3w_0}{EI + qR^3}. \quad \text{(A.1.4)}$$

Let us consider the condition at the cross sections A and D of the buckled ring, see figure A.1.1. From symmetry it is clear that

$$\left(\frac{dw}{d\theta}\right)_{\theta=0} = 0, \qquad \left(\frac{dw}{d\theta}\right)_{\theta=\pi/2} = 0. \quad \text{(A.1.5)}$$

From the first of these conditions it follows that $A_1=0$, and from the second

$$\sin\frac{k\pi}{2} = 0. \quad \text{(A.1.6)}$$

The smallest, non-trivial, root of this equation is $k\pi/2 = \pi$ and $k=2$. Substituting in the previous expression equation (A.1.3) the value of the critical pressure is

obtained:

$$q_{cr} = \frac{E}{4(1-\nu^2)}\left(\frac{h}{R}\right)^3. \qquad \text{(A.1.7)}$$

The radial deflections of the buckled tube, from (A.1.4) are:

$$w = \frac{1}{4}\left(\frac{M_0(1-\nu^2)R^2}{EI} + w_0\right)\cos 2\theta - \frac{M_0(1-\nu^2)R^2}{4EI} + \frac{3}{4}w_0. \qquad \text{(A.1.8)}$$

Considering the inextensible condition which requires that v, the tangential displacement, vanishes at $\theta = 0$ and $\theta = \pi/2$:

$$M_0 = \frac{3w_0 EI}{(1-\nu^2)R^2} = q_{cr} w_0 R. \qquad \text{(A.1.9)}$$

Substituting this result, the displacements become

$$w = w_0 \cos 2\theta, \text{ and } v = \frac{1}{2}w_0 \sin 2\theta. \qquad \text{(A.1.10)}$$

From equation (A.1.9) the moment M_0 can be produced by applying the compressive force S at A and B (see figure A.1.1) with an eccentricity w_0. The same result is obtained by substituting expression (A.1.9) into equation , (A.1.1). For $\theta = \pm\pi/4$ and $\theta = \pm 3\pi/4$ the radial displacement w is zero and the bending moment vanishes.

The solution corresponding to the smallest root k=2 has been discussed. The values of k=4, 6... and so on a series of other shapes of a buckled tube section with larger number of wave shapes in them associated with a larger critical pressure can be produced.

The condition of symmetry of the collapsed ring introduced a limitation in this solution. As a result of this assumption only even numbers have been obtained as solution for k. By assuming only one axis of symmetry, for instance, the horizontal axis AB, solutions with odd numbers k, namely, k=3, 5... and so on are obtained. The case k=1 represents a translation of the ring as a rigid body and should not be considered. Thus k=2 is the smallest root and the corresponding distributed load is the critical pressure. The buckling forms of higher order associated with larger roots can be obtained by introducing additional constraints in the ring. Without those, buckling will always be in two lobes pattern as shown in figure A.1.1.

This result assumes a perfect cylinder or that there are no imperfections. However, failure of tubes under external pressure depends very much upon the various kinds of inaccuracies. The typical imperfection in tubes is an initial ellipticity, the limiting value of which is usually known for each type of tube from numerous inspection measurements. The deviation of the shape of the tube from a perfect circular form can be defined by the initial radial deflections w_i. These deflections are simplified by assuming them to be of the form $w_i = w_1 \cos 2\theta$. In which w_1 is the maximum initial radial deviation from a circle and θ is the central angle. Under the action of an external pressure q, there will be additional flattening of the tube. The corresponding radial displacements will be called w. Thus the bending moment is $M = qR(w + w_1 \cos 2\theta)$. Substituting into the differential equation:

$$\frac{d^2 w}{d\theta^2} + w\left[1 + \frac{12(1-\nu^2)}{Eh^3}qR^3\right] = -\frac{12(1-\nu^2)}{Eh^3}qR^3 w_1 \cos 2\theta. \qquad \text{(A.1.11)}$$

The solution which satisfy the conditions of continuity at the boundaries is

$$w = \frac{w_1 q}{q_{cr} - q} \cos 2\theta , \qquad \text{(A.1.12)}$$

where q_{cr} is the critical value of the uniform pressure given in (A.1.7). It is seen that at points where $\theta = 0$ or $\theta = \pi$ the moment reaches a maximum, where

$$M_{max} = qR \frac{w_1}{1 - q/q_{cr}} . \qquad \text{(A.1.13)}$$

For small values of the ratio q/q_{cr} the change in the ellipticity due to external pressure q is neglegible and the maximum bending moment is qR times the initial amplitude deflection w_1. When the ratio q/q_{cr} is not small, the change in the initial ellipticity should be considered. The maximum compressive stress is then obtained by adding to the maximum compressive stress due to the bending moment M_{max} the stress produced by the compressive force qR

$$\sigma_{max} = \frac{qR}{h} + \frac{6qR}{h^2} \frac{w_1}{1 - q/q_{cr}} . \qquad \text{(A.1.14)}$$

This equation can be used with sufficient accuracy provided the stresses are kept below the yield-point of the material. The value of the external pressure, at which yielding in the wall starts, can be calculated. The notation, $R/h=m$ and $w_1/R=n$ is used, the equation for calculating the yielding pressure q_y becomes:

$$q_y^{\,2} - \left[\frac{\sigma_y}{m} + (1 + 6mn) q_{cr} \right] q_{cr} + \frac{\sigma_y}{m} q_{cr} = 0 . \qquad \text{(A.1.20)}$$

The pressure q_y determined above is smaller than the pressure at which collapse of the tube occurs, and it becomes equal to that of a perfect round tube when $n=0$.

Appendix 2

A.2 Analysis of external pressure for a pipe

This solution for a tube with limited length was originally published by Flugge /27/, 1973, section 8.2, pages 439 to 452. The nomenclature used was the same used in Flugge's book.

Flugge's approach consider a shell shaped as a circular cylinder of length l, radius a, subjected simultaneously to three simple loads: a uniform normal pressure on its wall, p_r=-p, an axial compression applied at the edges as force P per unit of circumference and a shear load T per unity of circumference applied at the same edges so as to produce a torque in the cylinder. The axial axis is x, and the angular position is denoted by the angle ϕ (see figure A.2.1). The derivatives with respect to the dimensionless co-ordinates x/a and ϕ will be indicated by primes and dots:

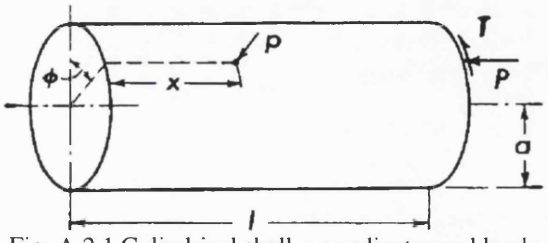

Fig. A.2.1 Cylindrical shell, co-ordinates and loads.

$$a\frac{\partial(\,)}{\partial x}=(\,)',\qquad \frac{\partial(\,)}{\partial\phi}=(\,)^{\bullet}. \tag{A.2.1}$$

From Flugge /27/, 1973 page 448 the following set of three equations can be written as:

$$\begin{aligned}
&aN_x'+aN_{\phi x}^{\bullet}-pa(u^{\bullet\bullet}-w')-Pu''-2Tu'^{\bullet}=0,\\
&aN_{\phi}^{\bullet}+aN_{x\phi}'-M_{\phi}^{\bullet}-M_{x\phi}'-pa(v^{\bullet\bullet}+w^{\bullet})-Pv''-2T(v'^{\bullet}+w')=0,\\
&M_{\phi}^{\bullet\bullet}+M_{\phi x}'^{\bullet}+M_{x\phi}'^{\bullet}+M_x''+aN_{\phi}+pa(u'-v^{\bullet}+w^{\bullet\bullet})+Pw''-2T(v'-w'^{\bullet})=0.
\end{aligned} \tag{A.2.2}$$

The elastic law will be used to express the forces N and moments M by u, v, w and their derivatives. The extensional rigidity D and the flexural rigidity K are defined below. Introducing the dimensionless parameters k, q_1, q_2, q_3 and dividing them by D:

$$\begin{gathered}
D=\frac{Et}{1-\nu^2},\quad K=\frac{Et^3}{12(1-\nu^2)},\quad k=\frac{K}{Da^2}=\frac{t^2}{12a^2},\\
q_1=\frac{pa}{D},\quad q_2=\frac{P}{D},\quad q_3=\frac{T}{D}.
\end{gathered} \tag{A.2.3}$$

Thus, the differential equations of the buckling problem assume the following form:

$$\begin{aligned}
&u''+\frac{1+\nu}{2}u^{\bullet\bullet}+\frac{1+\nu}{2}v'^{\bullet}+\nu\,w'+k\left(\frac{1-\nu}{2}u^{\bullet\bullet}-w'''+\frac{1-\nu}{2}w'^{\bullet\bullet}\right)-\\
&\qquad -q_1(u^{\bullet\bullet}-w')-q_2u''-2q_3u'^{\bullet}=0,
\end{aligned} \tag{A.2.4a}$$

$$\begin{aligned}
&\frac{1+\nu}{2}u'^{\bullet}+v^{\bullet\bullet}+\frac{1-\nu}{2}v''+w^{\bullet}+k\left(\frac{3}{2}(1-\nu)v''-\frac{3-\nu}{2}w''^{\bullet}\right)\\
&\qquad -q_1(v^{\bullet\bullet}+w^{\bullet})-q_2v''-2q_3(v'^{\bullet}+w')=0,
\end{aligned} \tag{A.2.4b}$$

$$\begin{aligned}
&\nu\,u'+v^{\bullet}+w+k\left(\frac{1-\nu}{2}u'^{\bullet\bullet}-u'''-\frac{3-\nu}{2}v''^{\bullet}+w''''+2w''^{\bullet\bullet}+w^{\bullet\bullet}+2w^{\bullet\bullet}+w\right)+\\
&\qquad q_1(u'-v^{\bullet}+w^{\bullet\bullet})+q_2w''-2q_3(v'-w'^{\bullet})=0.
\end{aligned} \tag{A.2.4c}$$

These equations describe the collapse of a cylindrical shell under the most general homogeneous membrane stress action. The three load parameters q are the elastic strains caused by the corresponding basic loads, and since this theory is based on the assumption that such strains are small compared with unity q_1, q_2, and q_3 should be neglected compared with unity in any particular case.

When there is no shear load ($T=0$, hence $q_3=0$), the differential equations admit a solution of the form:

$$\begin{cases}
u=A\cos m\phi\cos\dfrac{\lambda x}{a},\\
v=B\sin m\phi\sin\dfrac{\lambda x}{a},\\
w=C\cos m\phi\sin\dfrac{\lambda x}{a},
\end{cases} \tag{A.2.5a}$$

where

$$\lambda=\frac{n\pi\ a}{l}, \tag{A.2.5b}$$

and n is an integer. The solution describes a buckling mode with n half waves along the length of the cylinder and $2m$ half waves around its circumference. This is not the most general solution, however, it fulfils the boundary conditions and can be considered as a good approxiamtion. The boundary conditions at the ends of the cylinder are $x=0$ and $x=l$, and also $N_x = 0, M_x = 0$. Thus the solution represents the collapse of a shell whose ends are supported in tangential and radial directions but are not clamped or restricted in the axial direction. When this solution is introduced in the differential equations, the trigonometric functions drop out and the following equations are obtained:

$$A\left[\lambda^2+\frac{1-\nu}{2}m^2(1+k)-q_1m^2-q_2\lambda^2\right]+B\left[-\frac{1+\nu}{2}\lambda m\right]+ \\ +C\left[-\nu\lambda-k\left(\lambda^3-\frac{1-\nu}{2}\lambda m^2\right)-q_1\lambda\right]=0, \tag{A.2.6a}$$

$$A\left[-\frac{1+\nu}{2}\lambda m\right]+B\left[m^2+\frac{1-\nu}{2}\lambda^2(1+3k)-q_1m^2-q_2\lambda^2\right]+ \\ +C\left[m+\frac{3-\nu}{2}k\lambda^2 m-q_1m\right]=0, \tag{A.2.6b}$$

$$A\left[-\nu\lambda-k\left(\lambda^3-\frac{1-\nu}{2}\lambda m^2\right)-q_1\lambda\right]+B\left[m+\frac{3-\nu}{2}k\lambda^2 m-q_1m\right]+ \\ +C\left[1+k\left(\lambda^4+2\lambda^2m^2+m^4-2m^2+1\right)-q_1m^2-q_2\lambda^2\right]=0. \tag{A.2.6c}$$

In these equations the buckling amplitudes A, B, C are unknowns and the coefficients between brackets form a the characteristic matrix of the collapse problem. Since these equations are homogeneous, they admit, in general, only the trivial solution $A=B=C=0$ indicating that the shell is not in neutral equilibrium. Only if the determinant of the characteristic matrix equals zero a non trivial solution for A,B,C is possible. Thus the vanishing of the determinant is the collapse condition of the shell. When the collapse condition is fulfilled a correspondent buckling mode according to the values of m and n is obtained. In all cases of neutral equilibrium, the magnitude of the deformation are arbitrary.

In collapse condition the dimensionless loads q_1 and q_2 and the modal parameters m and λ are unknows. Of m it is known that must be an integer (m=0,1,2...); of λ, that it must be a multiple of $n\pi a/l$ (n=1,2...). The buckling condition may be written separately for every pair m and λ fulfilling these requirements and consider it as a relation between q_1 and q_2 that describes those combinations of two loads for which the shell is in neutral equilibrium. When these equations are plotted as curves in a q_1 and q_2 plane, a diagram shown in figure A.2.2 is obtained, which can be interpreted as follow. The origin $q_1 = q_2 = 0$ represents the unloaded shell.

When a load is applied, the point moves along some path, as show in figure A.2.2 by the dotted line. As long as it does not cross any of the curves, the shell is in stable equilibrium; but as soon as one of the curves is reached, equilibrium becomes neutral, with the buckling mode defined by the parameters m and λ of this curve. The stable domain in the q_1 and q_2 plane is, therefore, bounded by the envelope of all curves, which is shown in the diagram by heavy line.

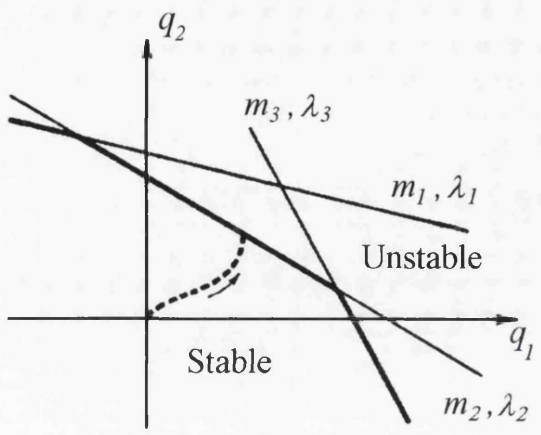

Fig. A.2.2 Stable and unstable regions in the q_1, q_2 plane.

The expanded determinant is a polynomial of the third degree in these parameters. Since they are very small quantities, it is sufficient to keep only the linear terms and to write the buckling condition as:

$$c_1 + c_2 k = c_3 q_1 + c_4 q_2 . \quad \text{(A.2.7)}$$

This equation describes a straight line in the q_1 and q_2 plane, and the limit of the stable domain, as show in the figure A.2.3, is a polygon consisting of sections of straight lines for different pairs m and λ.

The coefficients c_1, c_2, c_3, c_4 may be determined by expanding the determinant. Since c_1 turns out to be proportional to λ^4, the term with λ^4 may be dropped in all other coefficients, and it is obtained:

$$\begin{aligned} c_1 &= (1-\nu^2)\lambda^4, \\ c_2 &= (\lambda^2+m^2)^4 - 2\left[\nu\lambda^6 + 3\lambda^4 m^2 + (4-\nu)\lambda^2 m^4 + m^6\right] + 2(2-\nu)\lambda^2 m^2 + m^4, \\ c_3 &= m^2(\lambda^2+m^2)^2 - m^2(3\lambda^2+m^2), \\ c_4 &= \lambda^2(\lambda^2+m^2)^2 + \lambda^2 m^2. \end{aligned} \quad \text{(A.2.8)}$$

From equation (A.2.8) the stability curve can be determined provided l and k are given. Some examples are shown in figure A.2.3, and the some conclusions are drawn. Although the load and the basic stress system have axial symmetry, the buckling mode does not ($m \neq 0$) but develops nodal generators. Their number increases as q_1 increases and is higher for thinner shells. In the right-hand part of the diagrams the curves for shells of different lengths are so arranged that the shorter shell has higher critical pressures. For this reason nodal circles can not occur. Somewhere close to the q_2 axis the curves from different λ intersect, and from there on toward the left long shells can buckle at the smaller load of shorter shells by adopting a mode with nodal circles. As a consequence, an internal pressure $(q_1 < 0)$ does not perceptibly increase the axial load q_2, while an axial tension $(q_2 < 0)$ increases considerably the resistance offered to an external pressure.

For the case of external pressure only, i.e. one-parametric loading and assume that $q_2 = 0$. Equation (A.2.7) and (A.2.8) then yield:

$$q_1 = \frac{(1-\nu^2)\lambda^4 + kA}{m^2(\lambda^2+m^2)^2 - m^2(3\lambda^2+m^2)} \quad \text{(A.2.9)}$$

where, $A = (\lambda^2+m^2)^4 - 2(\nu\lambda^6 + 3\lambda^4 m^2 + (4-\nu)\lambda^2 m^4 + m^6) + 2(2-\nu)\lambda^2 m^2 + m^4$.

With l / na as abscissa and q_1 as ordinate every integer m yields one curve, and from these a festoon curve is derived. The result is curves, which rise monotonic toward the

left, there is no doubt as to the choice of $n = 1$, and the abscissa may be written simply as l / a.

The festoon curves end with the arc corresponding to $m = 2$ and on the right approach a horizontal asymptote giving the buckling load for a cylinder of infinite length. When in (A.2.9) putting $m = 2$ and $\lambda \to 0$, it is found the asymptotic value to be $q_1 = 3k$. This result may be easily be interpreted in the following way. The solution presented in (A.2.5a) from which all preceding buckling formulas have been derived, assumes that at the ends of the cylinder $w = 0$, i.e. that there are bulkheads which prevent deflection. If the cylinder is very long, its central part is little influenced by the stiffening effect of these bulkheads. A circular strip of width dx, which may be isolate here, behaves much like a circular ring of cross section $t \cdot dx$.

The second moment of area of this cross section is $I = t^3 dx / 12$, and the load per unit circumference is pdx. When such a ring buckles in its plane, it gets oval according to (A.2.5a) with $m = 2$ and $B = -C$, and the buckling load is known to be:

$$pdx = \frac{3EI}{a^3} = \frac{3Et^3 dx}{12a^3} \qquad \text{(A.2.10)}$$

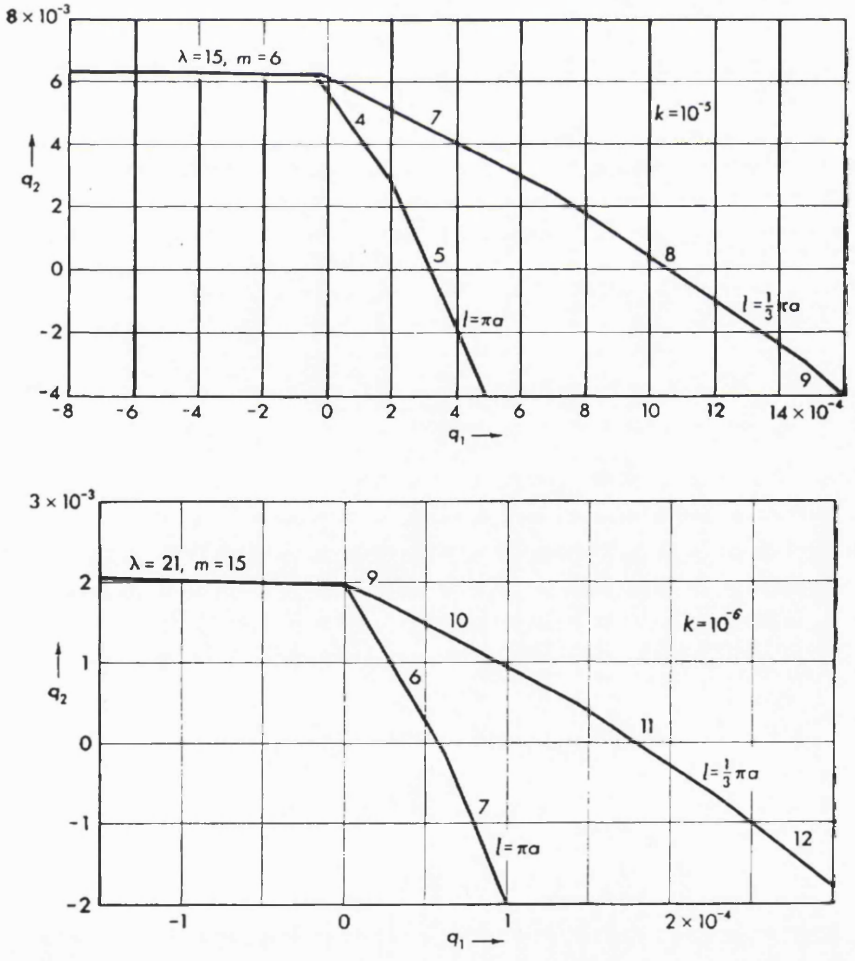

Fig. A.2.3 Buckling diagrams for a cylindrical shell subjected to two-way thrust.

When E is replaced by $E/(1-\nu^2)$, we may bring this into the form $q_1 = 3k$ in perfect agreement with the asymptotic value for the long shell. It may be seen that $m = 0$ cannot yield a finite value to q_1 since the denominator in (A.2.9) contains a factor m^2. With $m = 1$ equation (A.2.8) simplifies considerably because many terms cancel.

$$q_1 = \frac{(1-\nu^2)\lambda^2 + k\lambda^4\left[\lambda^2 + 2(2-\nu)\right]}{\lambda^2 - 1} \qquad \text{(A.2.11)}$$

For $\lambda > 1$ this equation yields values of q_1 which are larger than those obtained with $m \neq 1$ and therefore there is no arc $m = 1$ in the festoon curves showed in figure A.2.4. But for $\lambda < 1$, i.e. for $l > \pi a$, (A.2.11) yields a negative value for q_1, corresponding to an internal pressure in the shell. If λ is small enough we may neglect λ^2 compared with unit and have:

$$q_1 = -(1-\nu^2)\lambda^2 - k\lambda^6 \approx -(1-\nu^2)\lambda^2 \quad \text{or} \quad p = -\pi^2 E\frac{at}{l^2}, \qquad \text{(A.2.12)}$$

This buckling of a shell whose basic stress system consists of nothing but a tensile hoop force.

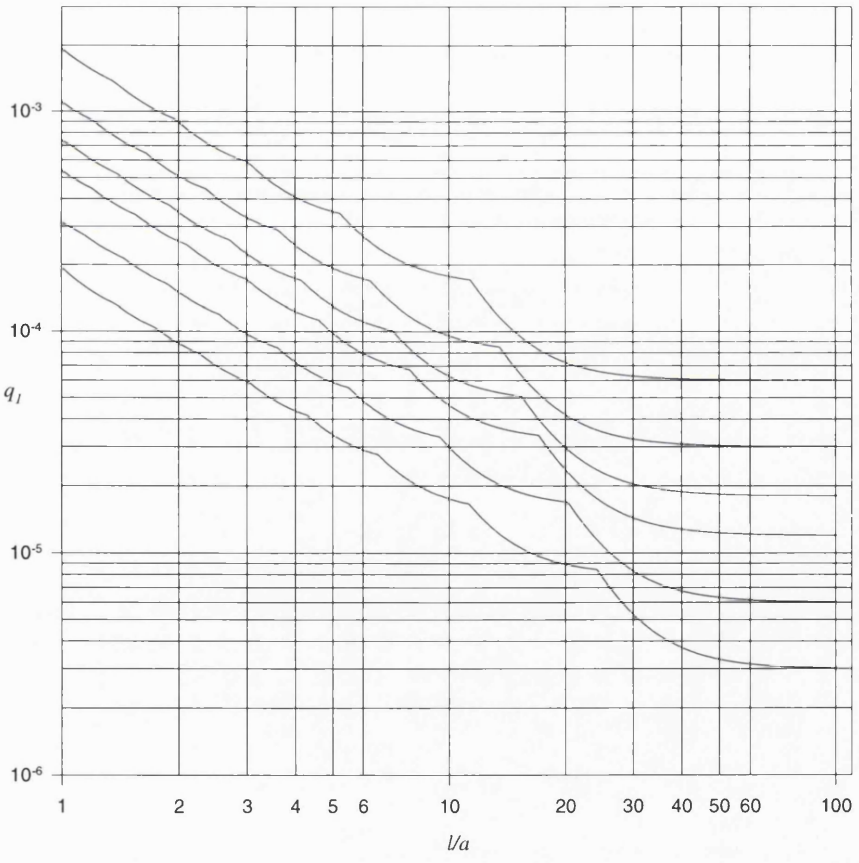

Figure A.2.4 Single walled pipe buckling pressure.

Apendix 3 Circular ring buckling under external fluid pressure

A.3.1 Circular ring buckling

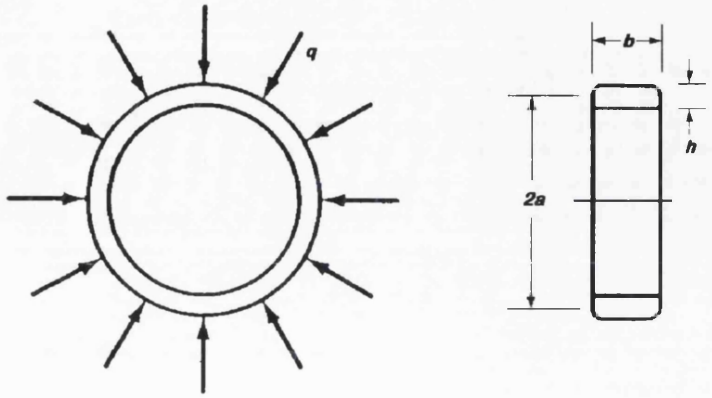

Fig. A.3.1 Circular ring subjected to uniform external pressure.

The classical circular ring buckling problem is presented by Brush and Almroth, /9/ 1975. The basis and main results are repeated as follow:

Consider a ring subjected to external fluid pressure. Following the usual notation p is the pressure or load per unit of area and q is the load per unit circumferential length. For a ring of width b, as in figure A.3.1, $|q| = |bp|$. Equations for equilibrium of a ring element in a slightly deformed configuration are derived from the principles of stationary potential energy, as follows. The total potential energy is the sum of the strain energy U of the ring itself and the potential energy Ω of the applied pressure. The strain energy of the ring may be written as

$$U = \frac{EAa}{2}\int \varepsilon^2 d\theta + \frac{EIa}{2}\int \kappa^2 d\theta \,. \qquad \text{(A.3.1)}$$

The two terms are the membrane and bending strain energies, respectively, for the ring. A ring subjected to uniform external pressure is a conservative system. **As such** the change in potential energy of the applied loads as the structure deforms is the negative of the work done by the loads during the deformation. For fluid-pressure loading the pressure at each point on the ring surface remains normal to the surface as the ring deforms. Thus the potential energy of the applied pressure may be expressed in terms of the product of the pressure q times the change in the area enclosed by the outer surface of the ring. Since the ring thickness h does not change appreciably during deformation, the change in area enclosed by the outer surface is approximately

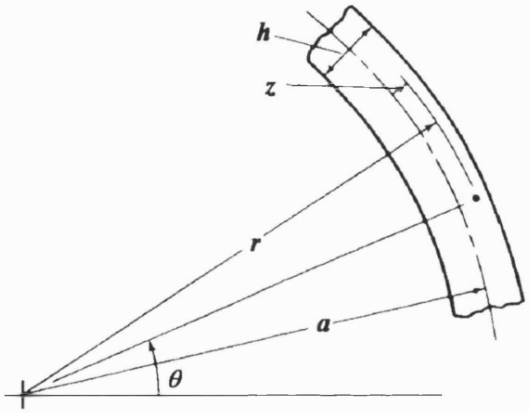

Fig. A.3.2 Polar co-ordinate system.

equal to the change in area enclosed by the median surface. Consequently, the expression for the potential energy Ω is, approximately,

$$\Omega = -q(\pi a^2 - A^*), \tag{A.3.2}$$

were A^* is the area enclosed by the median surface of the ring after deformation, and q is positive inwards. From equation (A.3.1), the co-ordinates of points on the median surface after deformation are

$$\begin{aligned} x^* &= (a+w)\cos\theta - v\sin\theta, \\ y^* &= (a+w)\sin\theta + v\cos\theta. \end{aligned} \tag{A.3.3}$$

The area enclosed by the median surface is conveniently expressed in terms of a line integral around the periphery, as follows

$$\begin{aligned} A^* &= \frac{1}{2}\oint_C (-y^*dx^* + x^*dy^*), \\ A^* &= \frac{1}{2}\int_0^{2\pi}\left(-y^*\frac{dx^*}{d\theta} + x^*\frac{dy^*}{d\theta}\right)d\theta. \end{aligned} \tag{A.3.4}$$

Introducing equation (A.3.3) and rearrangement gives

$$A^* = \frac{1}{2}\int_0^{2\pi}\left(a^2 + av' + 2aw + v^2 - vw' + v'w + w^2\right)d\theta.$$

But $\int_0^{2\pi} a^2 d\theta = \pi a^2$ and due to periodicity $\int_0^{2\pi} v'd\theta = 0$, therefore,

$$A^* = \pi a^2 + \frac{1}{2}\int_0^{2\pi}\left(2aw + v^2 - vw' + v'w + w^2\right)d\theta. \tag{A.3.5}$$

Introducing (A.3.5) into equation, (A.3.2) and rearranging gives

$$\Omega = qa\int_0^{2\pi}\left[w + \frac{1}{2a}\left(v^2 - vw' + v'w + w^2\right)\right]d\theta. \tag{A.3.6}$$

Equations (A.3.1) and (A.3.6) now give, for the total potential energy, the expression

$$\begin{aligned} V &= a\int_0^{2\pi} F d\theta, \\ F &= \frac{EA}{2}\varepsilon^2 + \frac{EI}{2}\kappa^2 + q\left[w + \frac{1}{2a}\left(v^2 - vw' + v'w + w^2\right)\right], \\ \varepsilon &= \frac{v'+w}{a} + \frac{1}{2}\left(\frac{v-w'}{a}\right)^2, \text{ and } \kappa = \frac{v'-w''}{a^2}. \end{aligned} \tag{A.3.7}$$

For equilibrium, V must be stationary. Consequently, the integral in equation (A.3.7) must satisfy the Euler equations of the calculus of variations. The Euler equations for an integrand of the form of that in equation (A.3.7) are

$$\begin{aligned} \frac{\partial F}{\partial v} - \frac{d}{d\theta}\frac{\partial F}{\partial v'} &= 0, \\ \frac{\partial F}{\partial w} - \frac{d}{d\theta}\frac{\partial F}{\partial w'} + \frac{d^2}{d\theta^2}\frac{\partial F}{\partial w''} &= 0. \end{aligned} \tag{A.3.8}$$

From equation (A.3.7) the partial derivatives are

$$\begin{aligned} \frac{\partial F}{\partial v} &= \frac{1}{a}\left[EA\varepsilon\frac{v-w'}{a} + q\left(v - \frac{1}{2}w'\right)\right], \\ \frac{\partial F}{\partial v'} &= \frac{1}{a}\left(EA\varepsilon + EI\frac{\kappa}{a} + \frac{1}{2}qw\right), \end{aligned}$$

$$\frac{\partial F}{\partial w} = \frac{1}{a}\left[EA\varepsilon + q\left(a + \frac{1}{2}v' + w \right) \right],$$
$$\frac{\partial F}{\partial w'} = \frac{1}{a}\left(-EA\varepsilon \frac{v - w'}{a} - \frac{1}{2}qv \right), \qquad \text{(A.3.9)}$$
$$\frac{\partial F}{\partial w''} = \frac{1}{a}\left(-EI\frac{\kappa}{a} \right).$$

These expressions can be simplified by introducing the constitutive equations for the ring. The normal force component N and the bending moment M on a cross-section are defined by the relations

$$N = \int \bar{\sigma} dA, \text{ and } M = \int \bar{\sigma} z dA, \qquad \text{(A.3.10)}$$

where $\bar{\sigma}$ is the normal stress in the θ direction. Introduction of the expressions $\bar{\sigma} = E\bar{\varepsilon}$ and $\bar{\varepsilon} = \varepsilon + z\kappa$ and integration gives

$$N = EA\varepsilon, \text{ and } M = EI\kappa. \qquad \text{(A.3.11)}$$

Equations (A.3.11) are constitutive relations for the ring. With these relations the partial derivatives may be written as

$$\frac{\partial F}{\partial v} = \frac{1}{a}\left[N\beta + q\left(v - \frac{1}{2}w' \right) \right],$$
$$\frac{\partial F}{\partial v'} = \frac{1}{a}\left(N + \frac{1}{a}M + \frac{1}{2}qw \right),$$
$$\frac{\partial F}{\partial w} = \frac{1}{a}\left[N + q\left(a + \frac{1}{2}v' + w \right) \right], \qquad \text{(A.3.12)}$$
$$\frac{\partial F}{\partial w'} = \frac{1}{a}\left(-N\beta - \frac{1}{2}qv \right),$$
$$\frac{\partial F}{\partial w''} = \frac{1}{a}\left(-\frac{1}{a}M \right).$$

Introducing these into the Euler equations and rearranging gives the final expressions

$$aN' + M' - aN\beta - qa^2\beta = 0,$$
$$M'' - aN - a(N\beta)' - qa(v' + w) = qa^2. \qquad \text{(A.3.13)}$$

Equations (A.3.13) are equilibrium equations for the ring for the intermediate class of deformation. The equations are non-linear in the dependent variables and may be written in terms of the five dependent variables N, M, β, v, and w. They may be expressed in terms of the two variables v and w alone by introducing of the constitutive and kinematic relations. Substitution and rearrangement gives

$$\left[\frac{v' + w}{a} + \frac{1}{2}\left(\frac{v - w'}{a} \right)^2 \right]' + \frac{I}{Aa^2}\left(\frac{v - w'}{a} \right)''$$
$$- \left[\frac{v' + w}{a} + \frac{1}{2}\left(\frac{v - w'}{a} \right)^2 \right] \frac{v - w'}{a} - \frac{qa}{EA}\frac{v - w'}{a} = 0,.$$

$$\frac{I}{Aa^2}\left(\frac{v-w'}{a}\right)''' - \left[\frac{v'+w}{a}+\frac{1}{2}\left(\frac{v-w'}{a}\right)^2\right]' - a\left\{\left[\frac{v'+w}{a}+\frac{1}{2}\left(\frac{v-w'}{a}\right)^2\right]\frac{v-w'}{a}\right\}' - \frac{qa}{EA}\frac{v'+w}{a} = \frac{qa}{EA}. \tag{A.3.14}$$

Under axisymmetric loading, circular equilibrium configurations of the ring exist for all values of the applied load q. The critical load q_{CR} is the smallest load for which the ring may be maintained in equilibrium in an adjacent non-circular configuration. According to the adjacent-equilibrium criterion, two infinitesimally adjacent equilibrium configurations exist at $q=q_{CR}$, the circular one and a slightly non-circular one. Both configurations are governed by equations (A.3.14). Let v_0, w_0 represent the circular configuration and $v_0+ v_1$, $w_0+ w_1$ the non-circular one, where v_1, w_1 are infinitesimally small increments. For the circular form, v_0 and its derivatives and w_0 and its derivatives equal zero. Thus

$$\begin{aligned} v &\to v_1, \\ w &\to w_0 + w_1, \end{aligned} \tag{A.3.15}$$

are substituted in equations (A.3.14). In the resulting equation, the terms containing only q or w_0 may be omitted; the sum of such terms is equal to zero because w_0 represents an equilibrium configuration. Terms that are quadratic or cubic in v_1, w_1 may be omitted because of the smallness of the incremental displacement. The remaining terms are

$$\begin{aligned} &EAa^2(v_1'+w_1)' + EI(v_1-w_1')'' - EAaw_0(v_1-w_1') - qa^3(v_1-w_1') = 0, \\ &EI(v_1-w_1')''' - EAa^2(v_1'+w_1) - EAaw_0(v_1-w_1')' - qa^3(v_1'+w_1) = 0. \end{aligned} \tag{A.3.16}$$

A special case of these equations for axisymmetric deformation gives $w_0 = -qa^2/EA$. Replacement of w_0 by the function of q and simplification gives

$$\begin{aligned} &EAa^2(v_1'+w_1)' + EI(v_1-w_1')'' = 0, \\ &EAa^2(v_1'+w_1) - EI(v_1-w_1')''' + qa^3(w_1''+w_1) = 0. \end{aligned} \tag{A.3.17}$$

Equations (A.3.17) are the stability equations for the ring subjected to external fluid pressure. They are homogeneous and linear in v_1, w_1 and can also be derived by application of the minimum potential energy criterion. The general solution is readily found for arbitrary boundary conditions. For the complete ring, however, the boundary requirement is simply that v_1, w_1 and their derivatives be periodic in θ. A solution of the form

$$\begin{aligned} v_1 &= B\sin n\theta, \\ w_1 &= C\cos n\theta, \end{aligned} \tag{A.3.18}$$

where B and C are constants and n is a positive integer, is seen to satisfy both the differential equations and the periodicity requirement. Introducing (A.3.18) into equation (A.3.17) and simplifying gives

$$\begin{aligned} &\left[n(nB+C) + n^2\frac{I}{Aa^2}(B+nC)\right]\sin n\theta = 0, \\ &\left[(nB+C) + n^3\frac{I}{Aa^2}(B+nC) - (n^2-1)\frac{qa}{EA}C\right]\cos n\theta = 0. \end{aligned} \tag{A.3.19}$$

These equations must be satisfied for all values of θ, therefore the sine and cosine factors may be divided out. Rearrangement gives

$$\begin{aligned} n^2\left(1+\frac{I}{Aa^2}\right)B+n\left(1+n^2\frac{I}{Aa^2}\right)C=0, \\ n\left(1+n^2\frac{I}{Aa^2}\right)B+\left[\left(1+n^4\frac{I}{Aa^2}\right)-\left(n^2-1\right)\frac{qa}{EA}\right]C=0. \end{aligned} \tag{A.3.20}$$

For $n=1$ the first equation becomes $\left(1+I/Aa^2\right)(B+C)=0$. Therefore, $B=-C$ and, from (A.3.18), $v_1=-C\sin\theta$ and $w_1=C\cos\theta$. But this displacement mode is seen to represent a rigid-body translation of the ring. The ring is constrained against such translation, therefore, only modes for which $n>1$ should be considered. For a non-trivial solution, the determinant of the coefficient matrix of the amplitudes B, C in (A.3.20) must equal zero.

$$\begin{vmatrix} n^2\left(1+\frac{I}{Aa^2}\right) & n\left(1+n^2\frac{I}{Aa^2}\right) \\ n\left(1+n^2\frac{I}{Aa^2}\right) & \left(1+n^4\frac{I}{Aa^2}\right)-\left(n^2-1\right)\frac{qa}{EA} \end{vmatrix}=0. \tag{A.3.21}$$

Rearrangement gives

$$q=\frac{\left(n^2-1\right)}{1+I/Aa^2}\cdot\frac{EI}{a^3}, \quad n=2,3,4,..., \tag{A.3.22}$$

the term I/Aa^2 is much smaller than unity. For example for a rectangular cross-sectional ring of thickness h, $I/Aa^2=(h/a)^2/12$. For $h/a<0.1$, $I/Aa^2<0.0008$. Therefore, the term may be neglected to give the well-known relation for the buckling load on a ring

$$q=\left(n^2-1\right)\cdot\frac{EI}{a^3} \quad n=2,3,4,..., \tag{A.3.23}$$

the smallest eigenvalue correspond to $n=2$. For that value the equation above gives $q=3EI/a^3$. This result is considered the classical solution for a ring under external uniform fluid pressure. The next section is the application of this principle to develop a buckling model for the multi-layered pipe.

A.3.2 Circular ring on elastic foundation

The solution found in (A.3.23) can be extended to include the stabilising influence of an elastic foundation. For our purposes, a ring is considered completely filled with a soft elastic medium that is treated as an infinite set of uncoupled radial springs. For such a foundation the pressure q_f, per unity of length, between ring and foundations is given by

$$q_f=-k_f w, \tag{A.3.24}$$

where k_f, is a known constant representing the foundation elasticity modulus.

Equations (A.3.17) has been derived based on adjacent equilibrium criterion. However, they could be rederived by application of the minimum potential energy criterion. The total potential energy of the loaded ring may be written as

$$V=U_m+U_b+\Omega, \tag{A.3.25}$$

where

$$U_m = \frac{EAa}{2}\int_0^{2\pi}\left[\frac{v'+w}{a}+\frac{1}{2}\left(\frac{v-w'}{a}\right)^2\right]^2 d\theta,$$

$$U_b = \frac{EAa}{2}\int_0^{2\pi}\left(\frac{v'-w''}{a^2}\right)d\theta,$$

$$\Omega = q\int_0^{2\pi}\left[wa+\tfrac{1}{2}\left(v^2-vw'+v'w+w^2\right)\right]d\theta.$$

To determine the character of the potential energy corresponding to a deformed configuration $v = v_0$, $w = w_0$, substituting

$$\begin{aligned} v &\to v_0 + v_1, \\ w &\to w_0 + w_1, \end{aligned} \tag{A.3.26}$$

where the variation, v_1, w_1 is arbitrarily small. For the circular form, v_0 and its derivatives and w_0' and its derivatives equal zero. Furthermore, the circular form is an equilibrium configuration for all values of q, so that δV is equal to zero and only the second variation need be investigated. Introducing of equations (A.3.26) and collection of all terms that are quadratic in v_1, w_1 gives

$$\delta^2 V = \delta^2 U_m + \delta^2 U_b + \delta^2 \Omega, \tag{A.3.27}$$

where

$$\delta^2 U_m = \frac{EA}{a}\int_0^{2\pi}\left[(v_1'+w_1)^2+\frac{w_0}{a}(v_1-w_1')^2\right]d\theta,$$

$$\delta^2 U_b = \frac{EA}{a^3}\int_0^{2\pi}(v_1'-w_1'')^2\,d\theta,$$

$$\delta^2 \Omega = q\int_0^{2\pi}\left(v_1^{\,2}-v_1w_1'+v_1'w_1+w_1^{\,2}\right)d\theta.$$

But $w_0/a = -(a/EA)q$, therefore,

$$\delta^2 V = \frac{1}{a^3}\int_0^{2\pi}\left[EAa^2(v_1'+w_1)^2+EI(v_1'-w_1'')^2+qa^3\left(v_1w_1'+v_1'w_1+w_1^{\,2}-w_1'^2\right)\right]d\theta \tag{A.3.28}$$

Simplification of the integration by parts gives, for the final expression, the equation

$$\delta^2 F = \frac{1}{a^3}\int_0^{2\pi} F\,d\theta, \tag{A.3.29}$$

where, $F = EAa^2(v_1'+w_1)^2+EI(v_1'-w_1'')^2+qa^3\left(w_1^{\,2}-w_1'^2\right)$.

According to Trefftz criterion, the equations for loss of stability are obtained by introducing of F into the Euler equations of the calculus of variations. The Euler equations in this case are

$$\begin{aligned} &\frac{\partial F}{\partial v_1}-\frac{d}{d\theta}\frac{\partial F}{\partial v_1'}=0, \\ &\frac{\partial F}{\partial w_1}-\frac{d}{d\theta}\frac{\partial F}{\partial w_1'}+\frac{d^2}{d\theta^2}\frac{\partial F}{\partial w_1''}=0. \end{aligned} \tag{A.3.30}$$

Introducing of the expression for F and rearranging is found to yield the same stability equations in (A.3.17).

Bearing in mind the elastic foundation pressure acting in the ring, the strain energy of the foundation may be written as

$$U_f = -\frac{a}{2}\int_0^{2\pi} q_f w d\theta \,. \tag{A.3.31}$$

Introducing equation (A.3.24) gives

$$U_f = \frac{ak_f}{2}\int_0^{2\pi} w^2 d\theta \,, \tag{A.3.32}$$

and for second derivative of the foundation strain energy

$$\delta^2 U_f = ak_f \int_0^{2\pi} w_1^{\,2} d\theta \,. \tag{A.3.33}$$

Addition of this term to the expression for the second derivative of the total potential energy (A.3.27) and application of Trefftz criterion $\delta\left(\delta^2 V\right)=0$ gives, for the Euler equations, the expressions

$$\begin{aligned} &EAa^2\left(v_1' + w_1\right)' + EI\left(v_1 - w_1'\right)'' = 0, \\ &EAa^2\left(v_1' + w_1\right) - EI\left(v_1 - w_1'\right)''' + qa^3\left(w_1'' + w_1\right) - k_f a^4 w_1 = 0. \end{aligned} \tag{A.3.34}$$

Equation (A.3.34) differs from (A.3.17) only in the addition of the term $k_f a^4 w_1$ in the second equation. Introducing equations (A.3.18) here leads to a pair of homogeneous algebraic equations. The criterion that the determinant of the coefficients equal zero then gives the expression

$$\begin{vmatrix} n^2\left(1+\dfrac{I}{Aa^2}\right) & n\left(1+n^2\dfrac{I}{Aa^2}\right) \\ n\left(1+n^2\dfrac{I}{Aa^2}\right) & \left(1+n^4\dfrac{I}{Aa^2}+\dfrac{k_f a^2}{EA}\right)-\left(n^2-1\right)\dfrac{qa}{EA} \end{vmatrix} = 0. \tag{A.3.35}$$

Consequently,

$$q = \frac{\left(n^2-1\right)}{1+I/Aa^2}\cdot\frac{EI}{a^3} + \frac{1}{\left(n^2-1\right)}k_f a\,, \qquad n = 2,3,4,... \tag{A.3.36}$$

As previously noted, $I/Aa^2 << 1$. Therefore, approximately,

$$q = \left(n^2-1\right)\cdot\frac{EI}{a^3} + \frac{1}{\left(n^2-1\right)}k_f a\,, \qquad n = 2,3,4,... \tag{A.3.37}$$

For $k_f = 0$, equation (A.3.37) reduces to equation (A.3.23). For given values of *EI*, k_f, and *a*, the value of *n* may be determined by trial to give the smallest *q*.

Appendix 4 Buckling of multi-layered

A.4.1 Buckling for a long multi-layered cylinder under external pressure

The buckling model for long cylinder under uniform fluid pressure was originally presented by Raville, 1954 /63/. Below is presented the basis and relevant results of Raville's work.

The results below were obtained to define the stress

$$\sigma_{rc} = \frac{qa}{r}\kappa, \quad N_\theta = qa(1-\kappa), \text{ and } N'_\theta = qa\kappa, \tag{A.4.1}$$

where

$$\kappa = \frac{1}{1+\frac{b}{a}-\frac{E_f f}{E_c a}\ln\frac{b}{a}}. \tag{A.4.2}$$

where σ_{rc} is the core normal stress in radial direction, q is the uniform lateral load acting in positve radial direction (equal to -p, where p is the external pressure), a and b are respectively the inner and outer skin mean radius, N_θ and N'_θ are respectively the face tensile force per unity of length in the outer and inner skins, f is the thickness of both faces, E_f and E_c are respectively the Young's Modulus of faces and core. The core radial displacemnet is

$$u_c = \frac{qa^2}{E_f f}\left[1-\kappa+\frac{E_f f}{E_c a}\kappa\ln r/a\right]. \tag{A.4.3}$$

The radial displacement of the outer and inner faces, equals the core displacement. To comply with the compatibility equations, these displacements may be written as:

$$u = \frac{qa^2}{E_f f}(1-\kappa), \text{ and } u' = \frac{qa^2}{E_f f}\left(\frac{b}{a}\kappa\right). \tag{A.4.4}$$

Following the Raville's development four independent equations containing constants A_n, B_n, C_n, and H_n, as well as the loads q, can be obtained, see Raville, 1954 /63/ page 17.

$$-(n^2-1)\frac{q}{E_c}(1-\kappa)A_n - \left[(n^2-1)\frac{q}{E_c}(1-\kappa)-\left(\frac{n^2-1}{n^2}\right)\right]B_n - C_n = 0. \tag{A.4.5}$$

$$-(n^2-1)A_n + \left[\frac{E_c}{2G_{r\theta}}-\frac{n^2}{2}+1-\frac{E_c a(1-\nu_f^2)}{n^2 E_f f}\right]B_n - n^2 C_n + nH_n = 0. \tag{A.4.6}$$

$$\begin{aligned}(n^2-1)\frac{q\kappa}{E_c}A_n + \left[(n^2-1)\frac{q\kappa}{E_c}\frac{a}{b}+\left(\frac{n^2-1}{n^2}\right)\right]B_n \\ + \left[(n^2-1)\frac{q\kappa}{E_c}\ln b/a - \frac{b}{a}\right]C_n = 0.\end{aligned} \tag{A.4.7}$$

$$-(n^2-1)\frac{a}{b}A_n + \left[\left(\frac{E_c}{2G_{r\theta}}-\frac{n^2}{2}+1\right)\frac{a}{b}+\frac{E_c a(1-\nu_f^2)}{n^2 E_f f}\right]\frac{a}{b}B_n - \left[n^2+(n^2-1)\ln b/a\right]\frac{a}{b}C_n + nH_n = 0. \tag{A.4.8}$$

Since H_n appears only in Equations (A.4.6) and (A.4.8), it is eliminated immediately

by subtracting these equations. The result is

$$-\left(n^2-1\right)\left(\frac{a}{b}-1\right)A_n+\left[\left(\frac{E_c}{2G_{r\theta}}-\frac{n^2}{2}+1\right)\left(\frac{a^2}{b^2}-1\right)+\frac{E_c a\left(1-\nu_f^2\right)}{n^2E_f f}\left(\frac{a}{b}+1\right)\right]B_n$$
$$-\left[n^2\left(\frac{a}{b}-1\right)+\left(n^2-1\right)\frac{a}{b}\ln b/a\right]C_n=0. \qquad \text{(A.4.9)}$$

The final result comprises a system of three equations containing the three unknown constants A_n, B_n, and C_n. A buckled form of equilibrium is possible only if equations (A.4.5), (A.4.7) and (A.4.9) yields non-zero solutions for these constants; this requires that the determinant of the coefficients of A_n, B_n, and C_n be equal to zero. The equation used for the determination of the critical load is obtained from this determinant. Specifically,

$$\begin{vmatrix} \left(n^2-1\right)\frac{q}{E_c}(1-\kappa) & \left(n^2-1\right)\frac{q}{E_c}(1-\kappa)-\frac{n^2-1}{n^2} & 1 \\ \left(n^2-1\right)\frac{q}{E_c}\kappa & \left(n^2-1\right)\frac{q}{E_c}\kappa\frac{a}{b}+\frac{n^2-1}{n^2} & \left(n^2-1\right)\frac{q}{E_c}\kappa\ln\frac{b}{a}-\frac{b}{a} \\ \left(n^2-1\right)\left(\frac{a}{b}-1\right) & -\left(\frac{E_c}{2G_{r\theta}}-\frac{n^2}{2}+1\right)\left(\frac{a^2}{b^2}-1\right)-\frac{E_c a\left(1-\nu_f^2\right)}{n^2E_f f}\left(\frac{a}{b}+1\right) & n^2\left(\frac{a}{b}-1\right)+\left(n^2-1\right)\frac{a}{b}\ln\frac{b}{a} \end{vmatrix}$$

The following quadratic equation is obtained from the expansion of this determinant,

$$\left(\frac{q^2}{E_c^2}\right)\kappa(1-\kappa)\left\{n^2\frac{(1-b/a)^2}{(b/a)^2}+\left[\left(\frac{E_c}{2G_{r\theta}}+\frac{n^2}{2}\right)\left(\frac{1-(b/a)^2}{(b/a)^2}\right)\right.\right.$$
$$\left.+\frac{E_c a\left(1-\nu_f^2\right)}{n^2E_f f}\left(\frac{1+b/a}{b/a}\right)\right]\ln\frac{b}{a}\Bigg\}+\frac{q}{E_c}\left\{\frac{(1-b/a)^2}{(b/a)^2}\left[\frac{b}{a}-\kappa\left(1+\frac{b}{a}\right)\right]\right.$$
$$+\frac{n^2-1}{n^2}[1-\kappa(1-b/a)]\frac{\ln b/a}{b/a}-\frac{1}{n^2-1}[b/a+\kappa(1-b/a)]$$
$$\left.\left[\left(\frac{E_c}{2G_{r\theta}}-\frac{n^2}{2}+1\right)\left(\frac{1-(b/a)^2}{(b/a)^2}\right)+\frac{E_c a\left(1-\nu_f^2\right)}{n^2E_f f}\left(\frac{1+b/a}{b/a}\right)\right]\right\}$$
$$-\frac{1}{n^2}\frac{(1-b/a)^2}{b/a}=0. \qquad \text{(A.4.10)}$$

Finally, the critical pressure for a long sandwich cylinder can be determined based on the above expression.

A.4.2 Buckling of multi-layered cylinder with face stiffnesses

The buckling model for long multi-layered cylinder under uniform fluid pressure with faces of moderate and unequal thickness was originally presented by Raville, 1954 /64/. The development is an extension of Raville's previous work, 1954 /63/.

It has been assumed that the faces of the long cylinder were thin enough to render membrane theory applicable and that the faces were of equal thickness. This supplementary development of this work is to present a solution for the stresses and

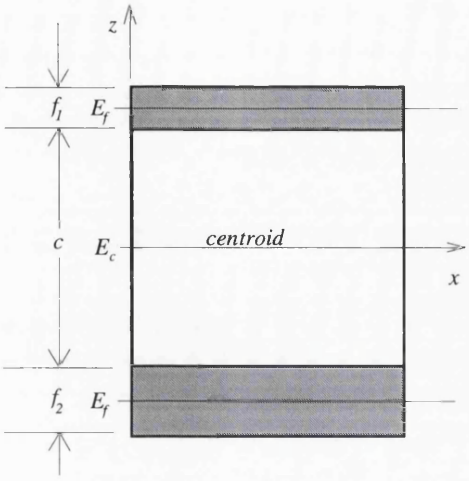

Fig. A.4.1 Dimensions of the cross-section of a sandwich with faces of unequal thickness.

critical pressure that apply to sandwich cylinders having moderately thick faces of unequal thickness. This requires that the bending moment and the transverse shear in the individual faces be considered. It is assumed, as before, that buckling takes place at stresses below the elastic limit of the sandwich materials.
The method of analysis closely follows the method used above. The same assumption, namely, that only transverse shear stresses and normal stresses on planes parallel to the faces are present. This assumption applies very well to all practical multi-layered pipe constructions because of the relatively low load-carrying capacity of the core materials in the tangential direction, as compared to that of the faces. The faces are assumed to be homogeneous and isotropic and are analysed on the basis of shell theory rather than membrane theory.

Considering the result obtained in equation (A.4.1), (A.4.2), and (A.4.3) and now taking the value of $N_\theta = E_f f_1 \varepsilon_\theta$ and $N'_\theta = E_f f_2 \varepsilon'_\theta$ according to their unequal thicknesses and different materials, these equations should be rewritten in the same fashion except for the value of κ as:

$$\sigma_{rc} = \frac{qa}{r}\kappa, \quad N_\theta = qa(1-\kappa), \quad \text{and} \quad N'_\theta = qa\kappa, \tag{A.4.11}$$

where

$$\kappa = \frac{1}{1+\dfrac{b}{a}\dfrac{f_1}{f_2}-\dfrac{E_f f_1}{E_c a}\log\dfrac{b}{a}}, \text{ and} \tag{A.4.12}$$

$$u_c = \frac{qa^2}{E_f f_1}\left[1-\kappa\left(1-\frac{E_f f_1}{E_c a}\kappa \ln\frac{r}{a}\right)\right]. \tag{A.4.13}$$

Since the values for the displacement at the faces are different, according to $u = (u_c)_{r=a}$ and $u' = (u_c)_{r=b}$, therefore, they become:

$$u = \frac{qa^2}{E_f f_1}(1-\kappa), \text{ and } u' = \frac{qab}{E_f f_2}\kappa. \tag{A.4.14}$$

Following the Raville's work, 1954 /64/ page 16, four equations containing the parameters A_n, B_n, C_n, and H_n are obtained. These are:

$$\left[(n^2-1)\gamma(1-\kappa)-(n^2-1)\right]A_n+\left[(n^2-1)\gamma(1-\kappa)+\delta_n(1+n^2\phi_1)+(1+n^4\phi_1)-\beta\right]B_n+$$
$$+\left[\beta-n^2(1+n^2\phi_1)\right]C_n+\left[n(1+n^2\phi_1)\right]H_n=0, \tag{A.4.15}$$

$$\left[n^2-1\right]A_n+\left[-\delta_n(1+\phi_1)-(1+n^2\phi_1)+\frac{\beta}{n^2}\right]B_n+\left[n^2(1+\phi_1)\right]C_n+$$
$$+\left[-n(1+\phi_1)\right]H_n=0, \tag{A.4.16}$$

$$\left[(n^2-1)\left(\gamma\kappa\frac{f_1}{f_2}-1\right)\right]A_n+\left[(n^2-1)\frac{a}{b}\gamma\kappa\frac{f_1}{f_2}+\delta_n\frac{a}{b}(1+n^2\phi_2)+\frac{a}{b}(1+n^4\phi_2)+\beta\frac{f_1}{f_2}\right]B_n+$$
$$\left[(n^2-1)\gamma\kappa\frac{f_1}{f_2}\ln\frac{b}{a}-\beta\frac{b}{a}\frac{f_1}{f_2}-(n^2-1)\ln\frac{b}{a}-n^2(1+n^2\phi_2)\right]C_n+$$
$$+\left[n\frac{b}{a}(1+n^2\phi_2)\right]H_n=0, \qquad \text{(A.4.17)}$$

$$[n^2-1]A_n+\left[-\delta_n\frac{a}{b}(1+\phi_2)-\frac{a}{b}(1+n^2\phi_2)-\frac{\beta}{n^2}\frac{f_1}{f_2}\right]B_n+$$
$$\left[(n^2-1)\ln\frac{b}{a}+n^2(1+\phi_2)\right]C_n+\left[-n\frac{b}{a}(1+\phi_2)\right]H_n=0. \qquad \text{(A.4.18)}$$

Where, in each of the above equations,

$$\gamma=q\frac{a(1-\nu_f^2)}{E_f f_1},\ \delta_n=\frac{E_c}{2G_{r\theta}}-\frac{n^2}{2},\ \phi_1=\frac{f_1^2}{12a^2},\ \phi_2=\frac{f_2^2}{12b^2},\ \beta=\frac{E_c a(1-\nu_1^2)}{E_f f_1}. \qquad \text{(A.4.19)}$$

Each of the terms in these equations contains one of the parameters A_n, B_n, C_n, and H_n that appears in the displacement equations of the cylinder. A buckled form of equilibrium is possible only if these set of equations yields solutions for these parameters which are different from zero. This requires that the determinant of the coefficients of these parameters must be equal to zero. This determinant may be written as follows:

$$\begin{vmatrix}
\gamma(1-\kappa) & \gamma(1-\kappa)+(\delta_n+n^2)\phi_1-\frac{\beta}{n^2} & \frac{\beta}{n^2-1}-n^2\phi_1 & \phi_1 \\
n^2-1 & -\delta_n(1+\phi_1)-(1+n^2\phi_1)+\frac{\beta}{n^2} & n^2(1+\phi_1) & -(1+\phi_1) \\
\gamma\kappa\frac{f_1}{f_2} & \gamma\kappa\frac{a}{b}\frac{f_1}{f_2}+(\delta_n+n^2)\phi_2\frac{a}{b}+\frac{\beta}{n^2}\frac{f_1}{f_2} & \gamma\kappa\frac{f_1}{f_2}\ln\frac{b}{a}-\frac{\beta}{n^2-1}\frac{b}{a}\frac{f_1}{f_2}-n^2\phi_2 & \phi_2\frac{b}{a} \\
n^2-1 & -\delta_n\frac{a}{b}(1+\phi_2)-\frac{a}{b}(1+n^2\phi_2)-\frac{\beta}{n^2}\frac{f_1}{f_2} & (n^2-1)\ln\frac{b}{a}+n^2(1+\phi_2) & -\frac{b}{a}(1+\phi_2)
\end{vmatrix}$$

Since terms containing, γ appear in two of the rows, the expansion of the determinant shown above results in a quadratic equation in γ. The two roots that satisfy the quadratic equation are, in general, widely separated negative values. The lower in absolute value, γ_{cr} corresponds to the critical load on the cylinder. Therefore, the critical load is

$$q_{cr}=\frac{E_f f_1}{a(1-\nu_f^2)}\gamma_{cr}. \qquad \text{(A.4.20)}$$

The results apply to long sandwich cylinders that have thin shells facings and are subjected to uniform external, lateral loading.

For the determination of critical load, the determinant should be expanded with $n=2$. The case $n=1$ represents rigid body translation of the cylinder, and values $n>2$ results in higher critical loads. The two eigenvalues of the determinant correspond to the two configurations shown in figure A.4.2. Obviously, the critical load showed in figure A.4.2(B) is considerably higher than that which corresponds to figure A.4.2(A) and is of no practical interest in the multi-layered cylinder problem.

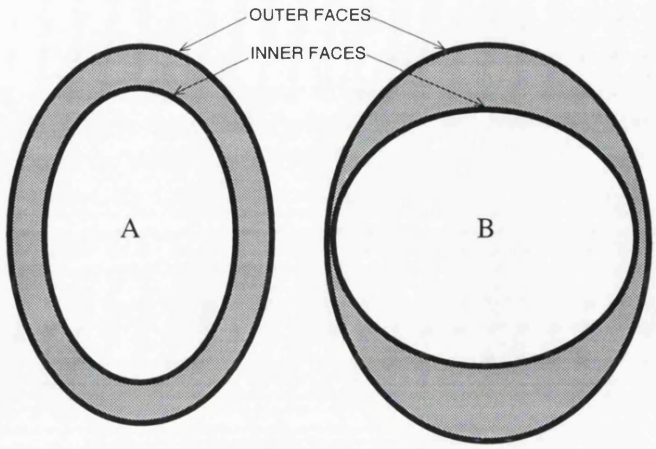

Fig. A.4.2 Configuration for two eigenvalues
of the stability determinant.

A simpler expression for this determinant is obtained if the modulus of elasticity of the core in the radial direction is assumed to be infinite. Under this assumption, the value of γ_{cr} may be written as:

$$\gamma_{cr} = \left(1-n^2\right)\frac{1+\dfrac{b f_1}{a f_2}}{1+\dfrac{b^2 f_1}{a^2 f_2}}\left\{\frac{\left(1-\dfrac{b}{a}\right)^2+\left(\phi_1\dfrac{f_1}{f_2}+\phi_2\dfrac{b}{a}\right)\left(\dfrac{f_1}{f_2}+\dfrac{b}{a}\right)+n^2\psi\left[\phi_1\left(1+\phi_2\right)\dfrac{b}{a}+\phi_2\left(1+\phi_1\right)\dfrac{f_1}{f_2}\right]}{\left(1+\phi_1\right)\dfrac{f_1}{f_2}+\left(1+\phi_2\right)\dfrac{b}{a}+n^2\psi\left(1+\phi_1\right)\left(1+\phi_2\right)}\right\},$$

where $\psi = \dfrac{E_f f_1\left(1-\dfrac{b^2}{a^2}\right)}{2G_{r\theta}b\left(1-\nu_f^2\right)}$.

This equation with $n=2$, yields values of γ_{cr} within 3% of the values obtained from the whole expansion of the determinant for usual sandwich constructions. For cylinder having very thin faces (membrane faces assumption) of equal thickness, the values of ϕ_1 and ϕ_2 are assumed to be zero, $n=2$, and the above equation reduces to

$$\gamma_{cr} = -\frac{3\left(1-b/a\right)^2}{\left(1+\dfrac{b^2}{a^2}\right)\left[1+\dfrac{2E_f f\left(1-b/a\right)}{G_{r\theta}b\left(1-\nu_f^2\right)}\right]}. \qquad \text{(A.4.21)}$$

The value of critical load is then determined from the definition (A.4.20). In Table A.4.1 there are some limit cases for the critical pressure.

E_c	$G_{r\theta}$	f_1	f_2	q_{cr}
E_c	$G_{r\theta}$	0	f_2	$-\frac{E_f f_2^3}{4(1-\nu_f^2)b^3}\frac{b}{a}$
E_c	$G_{r\theta}$	f_1	0	$-\frac{E_f f_1^3}{4(1-\nu_f^2)a^3}$
0	$G_{r\theta}$	f_1	f_2	$-\frac{E_f f_1^3}{4(1-\nu_f^2)a^3}$
∞	0	f_1	f_2	$-\frac{3E_f f_1}{a(1-\nu_f^2)}\left(\frac{1+\frac{b}{a}\frac{f_1}{f_2}}{1+\frac{b^2}{a^2}\frac{f_1}{f_2}}\right)\left(\phi_1\frac{b}{a}+\phi_2\frac{f_1}{f_2}\right)$
∞	∞	f	f	$-\frac{3E_f f}{a(1-\nu_f^2)}\left[\frac{\left(1-\frac{b}{a}\right)^2+\frac{f^2}{12ab}\left(1+\frac{b}{a}\right)^2}{1+\frac{b^2}{a^2}}\right]$

Table A.4.1 Results obtained for certain limiting cases.

A.4.3 Buckling of multi-layered cylinder of finite length

This work was originally presented by Milton Raville (1955) /65/, and Norris and Zahn (1963) /54/. The solution obtained is based on the assumption that the multi-layered cylinder elements are composed of isotropic, membrane faces and an orthotropic core. The mathematical solution of the problem , which is in the form a characteristic determinant of sixth order, is applicable to multi-layered cylinders of any length and of any core thickness. The core is considered to have such low load carrying capacity in the tangential and longitudinal directions as compared to the faces that the normal stress in the core in these directions and the shear in the core planes perpendicular to the faces and in these directions may be neglected. The action of the core and faces is related by the assumption that their displacements are equal at the interfaces between the core and faces. It means that the pipe wall is considered to buckle and behaves as an elastic continuum.

The method used to establishing the stability criterion is similar in concept to that used by Timoshenko /73/, 1936 in the analysis of the buckling of homogeneous cylinders of finite length subjected to uniform external pressure.

In this analysis the cylindrical co-ordinates r, θ, and z are used. The dimensions of the cylinder and the positive directions of the co-ordinates is indicated in figure A.4.3 The radii to the middle surfaces of the outer and inner faces are denoted by a and b, respectively, and the thickness of each face is denoted by f. The origin of the co-ordinate system is placed at the middle cross-section of the cylinder whose length is denoted by l.

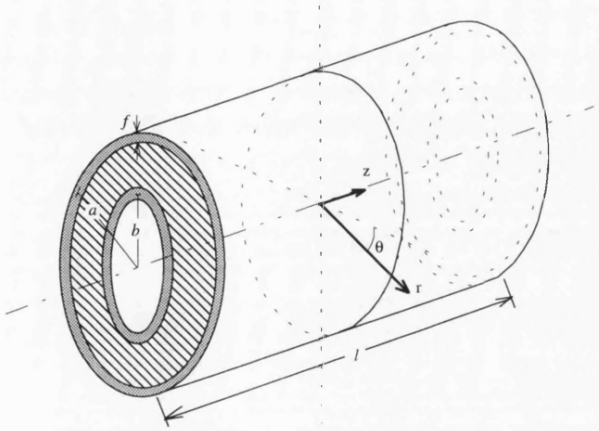

Fig. A.4.3 Multi-layered cylinder, finite length.

Since q is considered to be positive when it acts in positive r-direction, buckling occurs at a negative value of q. As previously showed, the cylinder at the instant before buckling is assumed to be in a state of uniform compression with the same stress condition existing in each cross-section. It means that the ends of the cylinder are not supported until after the cylinder has been initially compressed by a uniform load just less than the critical load. The radial stress in the core is equal to $qa\kappa/r$ and the circumferential force per unit length in the outer and inner faces is $qa(1-\kappa)$ and $qa\kappa$ respectively, where q is the intensity of uniform external loading in the positive r-direction and κ is

$$\kappa = \frac{1}{1+\frac{b}{a}-\frac{E_f f}{E_c a}\ln\frac{b}{a}}. \tag{A.4.22}$$

Following Raville's work /65/, 1955 page 18 these six equations may be written as follows:

$$\left[1-\frac{\xi}{n^2}+\delta_{n\theta}\left(1+\frac{1-\nu_f}{2}\frac{\lambda^2}{n^2}\right)\right]A_n+\left[-\left(n^2-1\right)+\nu_f\lambda^2\right]B_n+\left[-n^2-\lambda^2\right]C_n$$
$$+\left[1+\left(\frac{1+\nu_f}{4}\right)\lambda^2\right]D_n+\left[n+\frac{\lambda^2}{n}\left(\frac{1-\nu_f}{2}\right)\right]L_n+\left[\left(\frac{1+\nu_f}{2}\right)\lambda\right]R_n=0, \tag{A.4.23}$$

$$\left[1+\delta_{n\theta}-\xi+\left(n^2-1\right)\alpha(1-\kappa)\right]A_n+\left[-\left(n^2-1\right)+\nu_f\lambda^2+\left(n^2-1\right)\alpha(1-\kappa)\right]B_n$$
$$+\left[-n^2-\nu_f\lambda^2+\xi\right]C_n+\left[1+\frac{\nu_f\lambda^2}{2}+\xi+\left(n^2-1\right)\alpha(1-\kappa)\right]D_n+nL_n+\nu_f\lambda R_n=0, \tag{A.4.24}$$

$$\left[1+\frac{\xi}{n^2}\frac{b}{a}+\delta_{n\theta}\left(1+\frac{1-\nu_f}{2}\frac{\lambda^2}{n^2}\frac{b^2}{a^2}\right)+\left(\frac{1+\nu_f}{2}\right)\lambda^2\frac{b^2}{a^2}\ln\frac{b}{a}\right]A_n+\left[-\left(n^2-1\right)\frac{b}{a}+\nu_f\lambda^2\frac{b^3}{a^3}\right]B_n$$
$$+\left[-n^2\frac{b}{a}-\lambda^2\frac{b^3}{a^3}-\left(n^2-1\right)\frac{b}{a}\ln\frac{b}{a}+\nu_f\lambda^2\frac{b^3}{a^3}\ln\frac{b}{a}\right]C_n$$
$$+\left[\frac{b^2}{a^2}+\frac{1+\nu_f}{4}\lambda^2\frac{b^4}{a^4}+n^2\frac{b^2}{a^2}\ln\frac{b}{a}+\frac{1-\nu_f}{4}\lambda^2\frac{b^4}{a^4}\ln\frac{b}{a}-\frac{1+\nu_f}{2}\delta_z\frac{b^2}{a^2}\ln\frac{b}{a}\right]D_n$$
$$+\left[n\frac{b^2}{a^2}+\frac{1-\nu_f}{2}\frac{\lambda^2}{n}\frac{b^4}{a^4}\right]L_n+\left[\frac{1+\nu_f}{2}\lambda\frac{b^2}{a^2}\right]R_n=0, \tag{A.4.25}$$

$$\left[1+\delta_{n\theta}+\xi\frac{b}{a}+\nu_f\lambda^2\frac{b^2}{a^2}\ln\frac{b}{a}+\left(n^2-1\right)\alpha\kappa\right]A_n+\left[-\left(n^2-1\right)\frac{b}{a}+\nu_f\lambda^2\frac{b^3}{a^3}+\left(n^2-1\right)\alpha\kappa\frac{b}{a}\right]B_n$$
$$+\left[-n^2\frac{b}{a}-\left(n^2-1\right)\frac{b}{a}\ln\frac{b}{a}-\nu_f\lambda^2\frac{b^3}{a^3}+\nu_f\lambda^2\frac{b^3}{a^3}\ln\frac{b}{a}-\xi\frac{b^2}{a^2}+\left(n^2-1\right)\alpha\kappa\frac{b}{a}\ln\frac{b}{a}\right]C_n$$
$$+\left[\frac{b^2}{a^2}+n^2\frac{b^2}{a^2}\ln\frac{b}{a}+\frac{\nu_f}{2}\lambda^2\frac{b^4}{a^4}-\nu_f\delta_z\frac{b^2}{a^2}\ln\frac{b}{a}-\xi\frac{b^3}{a^3}+\left(n^2-1\right)\alpha\kappa\frac{b^2}{a^2}\right]D_n$$
$$+\left[n\frac{b^2}{a^2}\right]L_n+\left[\nu_f\lambda\frac{b^2}{a^2}\right]R_n=0, \qquad \text{(A.4.26)}$$

$$\left[\nu_f+\frac{1+\nu_f}{2}\delta_{n\theta}-\left(\delta_{n\theta}+1\right)\alpha(1-\kappa)\right]A_n+\left[-\nu_f\left(n^2-1\right)+\lambda^2+\left(n^2-1\right)\alpha(1-\kappa)\right]B_n$$
$$+\left[-n^2-\lambda^2+n^2\alpha(1-\kappa)\right]C_n+\left[\nu_f+\frac{1-\nu_f}{4}n^2+\frac{\lambda^2}{2}-\frac{\xi}{\lambda^2}-\alpha(1-\kappa)\right]D_n$$
$$+\left[\frac{1+\nu_f}{2}n-n\alpha(1-\kappa)\right]L_n+\left[\lambda+\frac{1-\nu_f}{2}\frac{n^2}{\lambda}\right]R_n=0, \qquad \text{(A.4.27)}$$

$$\left[\nu_f+\frac{1+\nu_f}{2}\delta_{n\theta}+\frac{1-\nu_f}{2}n^2\ln\frac{b}{a}+\lambda^2\frac{b^2}{a^2}\ln\frac{b}{a}-\left(\delta_{n\theta}+1\right)\alpha\kappa\right]A_n$$
$$+\left[-\nu_f\left(n^2-1\right)\frac{b}{a}+\lambda^2\frac{b^3}{a^3}+\left(n^2-1\right)\alpha\kappa\frac{b}{a}\right]B_n$$
$$+\left[-n^2\frac{b}{a}-\lambda^2\frac{b^3}{a^3}-\nu_f\left(n^2-1\right)\frac{b}{a}\ln\frac{b}{a}+\lambda^2\frac{b^3}{a^3}\ln\frac{b}{a}+n^2\alpha\kappa\frac{b}{a}+\left(n^2-1\right)\alpha\kappa\frac{b}{a}\ln\frac{b}{a}\right]C_n$$
$$+\left[\nu_f\frac{b^2}{a^2}+\frac{1-\nu_f}{4}n^2\frac{b^2}{a^2}+\frac{\lambda^2}{2}\frac{b^4}{a^4}+\frac{1+\nu_f}{2}n^2\frac{b^2}{a^2}\ln\frac{b}{a}-\left(\frac{b^2}{a^2}+\frac{1-\nu_f}{2}\frac{n^2}{\lambda^2}\right)\delta_z\ln\frac{b}{a}+\frac{\xi}{\lambda^2}\frac{b}{a}\right.$$
$$\left.-\left(1+n^2\ln\frac{b}{a}\right)\alpha\kappa\frac{b^2}{a^2}\right]D_n+\left[\frac{1+\nu_f}{2}n\frac{b^2}{a^2}-n\alpha\kappa\frac{b^2}{a^2}\right]L_n+\left[\lambda\frac{b^2}{a^2}+\frac{1-\nu_f}{2}\frac{n^2}{\lambda}\right]R_n=0. \qquad \text{(A.4.28)}$$

Where

$$\xi=\frac{E_c a\left(1-\nu_f^2\right)}{E_f f},\ \alpha=\frac{qa\left(1-\nu_f^2\right)}{E_f f},\ \delta_{n\theta}=\frac{E_c}{2G_{r\theta}}-\frac{n^2}{2},\ \delta_z=\frac{E_c}{G_{rz}},\ \text{and}\ \lambda=\frac{\pi a}{l}. \qquad \text{(A.4.29)}$$

These equations are satisfied if the constants A_n, B_n, C_n, D_n, L_n, and R_n are all equal to zero. This represents the uniformly compressed circular form of equilibrium of the cylinder. A buckled form of equilibrium is possible only if the set of equations yields non-zero solutions for the constants. This requires that the determinant M of the coefficients of these set of equations be equal zero:

$$M = \begin{bmatrix} A_{11} & A_{12} & A_{13} & A_{14} & A_{15} & A_{16} \\ A_{21} & A_{22} & A_{23} & A_{24} & A_{25} & A_{26} \\ A_{31} & A_{32} & A_{33} & A_{34} & A_{35} & A_{36} \\ A_{41} & A_{42} & A_{43} & A_{44} & A_{45} & A_{46} \\ A_{51} & A_{52} & A_{53} & A_{54} & A_{55} & A_{56} \\ A_{61} & A_{62} & A_{63} & A_{64} & A_{65} & A_{66} \end{bmatrix}$$

where,

$$A_{11} = -\xi\left(\frac{n^2-1}{n^2}\right) - \left(\frac{1-\nu_f}{2}\right)\frac{\lambda^2}{n^2}\delta_{n\theta} + \left(n^2-1\right)\alpha(1-\kappa);$$

$$A_{12} = \left(n^2-1\right)\alpha(1-\kappa);$$

$$A_{13} = \xi + \left(1-\nu_f\right)\lambda^2;$$

$$A_{14} = \xi - \left(\frac{1-\nu_f}{4}\right)\lambda^2 + \left(n^2-1\right)\alpha(1-\kappa);$$

$$A_{15} = -\left(\frac{1-\nu_f}{2}\right)\lambda^2;$$

$$A_{16} = -\left(\frac{1-\nu_f}{2}\right);$$

$$A_{21} = \xi\frac{b}{a}\left(\frac{n^2-1}{n^2}\right) - \left(\frac{1-\nu_f}{2}\right)\frac{\lambda^2}{n^2}\frac{b^2}{a^2}\delta_{n\theta} - \left(\frac{1-\nu_f}{2}\right)\lambda^2\frac{b^2}{a^2}\ln b/a + \left(n^2-1\right)\alpha\kappa;$$

$$A_{22} = \left(n^2-1\right)\alpha\kappa\, b/a;$$

$$A_{23} = -\xi\frac{b^2}{a^2} + \left(1-\nu_f\right)\lambda^2\frac{b^3}{a^3} + \left(n^2-1\right)\alpha\kappa\, b/a\ln b/a;$$

$$A_{24} = -\xi\frac{b^3}{a^3} - \left(\frac{1-\nu_f}{4}\right)\lambda^2\frac{b^4}{a^4} - \left(\frac{1-\nu_f}{2}\right)\lambda^2\frac{b^4}{a^4}\ln b/a + \left(\frac{1-\nu_f}{2}\right)\delta_z\frac{b^2}{a^2}\ln b/a + \left(n^2-1\right)\alpha\kappa\, b^2/a^2;$$

$$A_{25} = -\left(\frac{1-\nu_f}{2}\right)\lambda^2\frac{b^4}{a^4};$$

$$A_{26} = -\left(\frac{1-\nu_f}{2}\right)\frac{b^2}{a^2};$$

$$A_{31} = -\frac{\xi}{n^2} + (\delta_{n\theta} + 1) + \left(\frac{1-\nu_f}{2}\right)\frac{\lambda^2}{n^2}\delta_{n\theta};$$

$$A_{32} = -(n^2 - 1) + \nu_f \lambda^2;$$

$$A_{33} = -n^2 - \lambda^2;$$

$$A_{34} = 1 + \left(\frac{1+\nu_f}{4}\right)\lambda^2;$$

$$A_{35} = n^2 + \left(\frac{1-\nu_f}{2}\right)\lambda^2;$$

$$A_{36} = \left(\frac{1+\nu_f}{2}\right);$$

$$A_{41} = \frac{\xi}{n^2}\frac{a}{b} + (\delta_{n\theta} + 1)\frac{a^2}{b^2} + \left(\frac{1-\nu_f}{2}\right)\frac{\lambda^2}{n^2}\delta_{n\theta} + \left(\frac{1+\nu_f}{2}\right)\lambda^2 \ln b/a;$$

$$A_{42} = -(n^2 - 1)\frac{a}{b} + \nu_f \lambda^2 \frac{b}{a};$$

$$A_{43} = -n^2 \frac{a}{b} - \lambda^2 \frac{b}{a} - (n^2 - 1)\frac{a}{b}\ln b/a + \nu_f \lambda^2 \frac{b}{a}\ln b/a;$$

$$A_{44} = 1 + \left(\frac{1+\nu_f}{4}\right)\lambda^2 \frac{b^2}{a^2} + n^2 \ln b/a + \left(\frac{1-\nu_f}{2}\right)\lambda^2 \frac{b^2}{a^2}\ln b/a - \left(\frac{1+\nu_f}{2}\right)\delta_z \ln b/a;$$

$$A_{45} = n^2 + \left(\frac{1-\nu_f}{2}\right)\lambda^2 \frac{b^2}{a^2};$$

$$A_{46} = \left(\frac{1+\nu_f}{2}\right);$$

$$A_{51} = \lambda^2\left[\nu_f + \left(\frac{1+\nu_f}{2}\right)\delta_{n\theta} - (\delta_{n\theta} + 1)\alpha(1-\kappa)\right];$$

$$A_{52} = \lambda^2\left[-\nu_f(n^2 + 1) + \lambda^2 + (n^2 - 1)\alpha(1-\kappa)\right];$$

$$A_{53} = \lambda^2\left[-n^2 - \lambda^2 + n^2\alpha(1-\kappa)\right];$$

$$A_{54} = -\xi + \nu_f \lambda^2 + \left(\frac{1-\nu_f}{4}\right)n^2\lambda^2 + \frac{\lambda^4}{2} - \lambda^2\alpha(1-\kappa);$$

$$A_{55} = \lambda^2\left[\left(\frac{1+\nu_f}{2}\right)n^2 - n^2\alpha(1-\kappa)\right];$$

$$A_{56}=\left(\frac{1-\nu_f}{2}\right)n^2+\lambda^2;$$

$$A_{61}=\lambda^2\left[\nu_f+\left(\frac{1+\nu_f}{2}\right)\delta_{n\theta}+\left(\frac{1-\nu_f}{2}\right)n^2\ln b/a+\lambda^2\frac{b^2}{a^2}\ln b/a-(\delta_{n\theta}+1)\alpha\kappa\right];$$

$$A_{62}=\lambda^2\left[-\nu_f(n^2+1)\frac{b}{a}+\lambda^2\frac{b^3}{a^3}+(n^2-1)\alpha\kappa\frac{b}{a}\right];$$

$$A_{63}=\lambda^2\left[-n^2\frac{b}{a}-\lambda^2\frac{b^3}{a^3}-\nu_f(n^2-1)\frac{b}{a}\ln b/a+\lambda^2\frac{b^3}{a^3}\ln b/a\right.$$
$$\left.+n^2\alpha\kappa\frac{b}{a}+(n^2-1)\alpha\kappa\frac{b}{a}\ln b/a\right];$$

$$A_{64}=\xi\frac{b}{a}-\left(\frac{1-\nu_f}{2}\right)n^2\delta_z\ln b/a+\lambda^2\left[\nu_f\frac{b^2}{a^2}+\left(\frac{1-\nu_f}{4}\right)n^2\frac{b^2}{a^2}+\frac{\lambda^2}{2}\frac{b^4}{a^4}\right.$$
$$\left.+\left(\frac{1+\nu_f}{2}\right)n^2\frac{b^2}{a^2}\ln b/a-\delta_z\frac{b^2}{a^2}\ln b/a-\alpha\kappa\frac{b^2}{a^2}-n^2\frac{b^2}{a^2}\alpha\kappa\ln b/a\right];$$

$$A_{65}=\lambda^2\left[\left(\frac{1+\nu_f}{2}\right)n^2\frac{b^2}{a^2}-n^2\alpha\kappa\frac{b^2}{a^2}\right];$$

$$A_{66}=\left(\frac{1-\nu_f}{2}\right)n^2+\lambda^2\frac{b^2}{a^2}.$$

The lowest negative value of α for which this determinant equals zero is proportional to the critical load on the sandwich cylinder; this value of α will be referred to as α_{cr}. After this value is found, the value of the critical load is obtained from the definition that is:

$$q_{cr}=\frac{E_f f}{a\left(1-\nu_f^2\right)}\alpha_{cr}. \tag{A.4.30}$$

Since the determinant contains the eigenvalue, α in four of the six rows, the expansion of the determinant would result in a fourth order algebraic equation in α. Only the lowest of these roots corresponds to the actual buckling load. A literal expansion of the determinant of matrix *M* was found to be impractical. A numerical solution showed to be inaccurate due to inherent difficulties involving the subtraction of large numbers of almost equal magnitude. Therefore, the six order determinant was reduced in literal form to the fourth order determinant shown on matrix *N* below:

$$N=\begin{bmatrix} B_{11} & B_{12} & B_{13} & B_{14} \\ B_{21} & B_{22} & B_{23} & B_{24} \\ B_{31} & B_{32} & B_{33} & B_{34} \\ B_{41} & B_{42} & B_{43} & B_{44} \end{bmatrix}$$

where,

$$B_{11}=\left[(\delta_{n\theta}+1)-\frac{\xi}{n^2}\right]\left[\overline{C}-\left(\frac{1-\nu_f}{1+\nu_f}\right)n^2\overline{B}\right]+\overline{C}\left\{-\left(\frac{1+\nu_f}{1-\nu_f}\right)\left(\frac{n^2-1}{n^2}\right)\xi\right.$$
$$\left.+\left(\frac{1+\nu_f}{1-\nu_f}\right)(n^2-1)\alpha(1-\kappa)-\nu_f\frac{\lambda^2}{n^2}\delta_{n\theta}\right\}+\overline{B}\lambda^2\left\{\nu_f+\left(\frac{2\nu_f}{1+\nu_f}\right)\delta_{n\theta}\right.$$
$$\left.-\frac{2}{1+\nu_f}\left[(\delta_{n\theta}+1)-\frac{\xi}{n^2}+\left(\frac{1-\nu_f}{2}\right)\frac{\lambda^2}{n^2}\delta_{n\theta}\right]-(\delta_{n\theta}+1)\alpha(1-\kappa)\right\};$$

$$B_{12}=\left[-(n^2-1)+\nu_f\lambda^2\right]\left[\overline{C}-\left(\frac{1-\nu_f}{1+\nu_f}\right)n^2\overline{B}\right]+\overline{C}\left(\frac{1+\nu_f}{1-\nu_f}\right)(n^2-1)\alpha(1-\kappa)$$
$$+\overline{B}\lambda^2\left[(2+\nu_f)\left(\frac{1-\nu_f}{1+\nu_f}\right)(n^2-1)+\left(\frac{1-\nu_f}{1+\nu_f}\right)\lambda^2+(n^2-1)\alpha(1-\kappa)\right];$$

$$B_{13}=-n^2\left[\overline{C}-\left(\frac{1-\nu_f}{1+\nu_f}\right)n^2\overline{B}\right]+\overline{C}\left[\left(\frac{1+\nu_f}{1-\nu_f}\right)\xi+\nu_f\lambda^2\right]$$
$$+\overline{B}\lambda^2\left[\left(\frac{1-\nu_f}{1+\nu_f}\right)(2n^2+\lambda^2)+n^2\alpha(1-\kappa)\right];$$

$$B_{14}=\left[\overline{C}-\left(\frac{1-\nu_f}{1+\nu_f}\right)n^2\overline{B}\right]+\overline{C}\left[\left(\frac{1+\nu_f}{1-\nu_f}\right)\xi+\left(\frac{1+\nu_f}{1-\nu_f}\right)(n^2-1)\alpha(1-\kappa)\right]$$
$$-\overline{B}\xi+\overline{B}\lambda^2\left[-(2+\nu_f)\left(\frac{1-\nu_f}{1+\nu_f}\right)-\alpha(1-\kappa)\right];$$

$$B_{21}=(\delta_{n\theta}+1)\left(\frac{1-b^2/a^2}{b^2/a^2}\right)+\xi\left(\frac{1+b/a}{b/a}\right)+\nu_f\lambda^2\ln b/a$$
$$+(n^2-1)\alpha\kappa\left(\frac{1}{b^2/a^2}-b/a+\overline{F}\right);$$

$$B_{22}=-(n^2-1)\left(\frac{1-b/a}{b/a}\right)-\nu_f\lambda^2(1-b/a)+(n^2-1)\alpha\kappa\left(\frac{1}{b/a}-b/a+\overline{F}\right);$$

$$B_{23}=-2\xi-n^2\left(\frac{1-b/a}{b/a}\right)+\nu_f\lambda^2(1-b/a)-\left[(n^2-1)\right.$$
$$\left.-\nu_f\lambda^2 b^2/a^2-(n^2-1)\alpha\kappa\right]\frac{1}{b/a}\ln b/a;$$

$$B_{24}=-\xi(1+b/a)-\frac{\nu_f\lambda^2}{2}(1-b^2/a^2)+(n^2-\nu_f\delta_z)\ln b/a$$
$$+(n^2-1)\alpha\kappa(1-b/a-\overline{F});$$

$$B_{31}=\overline{A}\left\{(\delta_{n\theta}+1)\left(\frac{1-b^2/a^2}{b^2/a^2}\right)+\frac{\xi}{n^2}\left(\frac{1+b/a}{b/a}\right)+\left(\frac{1+\nu_f}{2}\right)\lambda^2\ln b/a\right\}$$
$$+\lambda^2\left\{\left(\frac{2}{1+\nu_f}\right)(1-b^2/a^2)\left[(\delta_{n\theta}+1)-\frac{\xi}{n^2}+\left(\frac{1-\nu_f}{2}\right)\frac{\lambda^2}{n^2}\delta_{n\theta}\right]\right.$$
$$\left.+\left[\left(\frac{1-\nu_f}{2}\right)n^2+\lambda^2 b^2/a^2\right]\ln b/a-(\delta_{n\theta}+1)\alpha\kappa(1-b/a+\overline{F})\right\};$$

$$B_{32}=\overline{A}\left[-(n^2-1)\left(\frac{1-b/a}{b/a}\right)-\nu_f\lambda^2(1-b/a)\right]+\lambda^2\left\{\left(\frac{2}{1+\nu_f}\right)\right.$$
$$(1-b^2/a^2)\left[-(n^2-1)+\nu_f\lambda^2\right]+(1-b/a)\left[\nu_f(n^2-1)\right]$$
$$\left.-\lambda^2\left(1-\frac{b^3}{a^3}\right)+(n^2-1)\alpha\kappa\overline{F}\right\};$$

$$B_{33}=\overline{A}\left\{-n^2\left(\frac{1-b/a}{b/a}\right)+\lambda^2(1-b/a)-\left[\frac{n^2-1}{b/a}-\nu_f\lambda^2 b/a\right]\ln b/a\right\}$$
$$+\lambda^2\left\{\left(\frac{2}{1+\nu_f}\right)(1-b^2/a^2)(-n^2-\lambda^2)+n^2(1-b/a)\right.$$
$$+\lambda^2(1-b^3/a^3)-\left[\nu_f(n^2-1)-\lambda^2 b^2/a^2\right]b/a\ln b/a+n^2\alpha\kappa\overline{F}$$
$$\left.+(n^2-1)\alpha\kappa\frac{b}{a}\ln b/a\right\};$$

$$B_{34}=\xi(1+b/a)-\left(\frac{1-\nu_f}{2}\right)n^2\delta_z\ln b/a+\overline{A}\left\{-\left(\frac{1+\nu_f}{4}\right)\lambda^2(1-b^2/a^2)\right.$$
$$\left.+\left[n^2+\left(\frac{1-\nu_f}{2}\right)\lambda^2 b^2/a^2-\left(\frac{1+\nu_f}{2}\right)\delta_z\right]\ln b/a\right\}$$

$$+\lambda^2\left\{\left(\frac{2}{1+\nu_f}\right)\left(1-b^2/a^2\right)\left[1+\left(\frac{1+\nu_f}{4}\right)\lambda^2\right]-\left(1-b^2/a^2\right)\left[\nu_f\right.\right.$$
$$\left.+\left(\frac{1-\nu_f}{4}\right)n^2+\frac{\lambda^2}{2}\left(1+b^2/a^2\right)\right]+\left[\left(\frac{1+\nu_f}{2}\right)n^2-\delta_z\right]b^2/a^2\ln b/a$$
$$\left.-\alpha\kappa\left[-b/a\left(1-b/a\right)+\overline{F}\right]-n^2\alpha\kappa\frac{b^2}{a^2}\ln b/a\right\};$$

$$B_{41}=\overline{B}\left\{\left(\delta_{n\theta}+1\right)\left(\frac{1-b^2/a^2}{b^2/a^2}\right)+\frac{\xi}{n^2}\left(\frac{1+b/a}{b/a}\right)+\left(\frac{1+\nu_f}{2}\right)\lambda^2\ln b/a\right\}+\overline{D}\left\{-\frac{\xi}{n^2}\left[1\right.\right.$$
$$\left.\left.+\left(\frac{1+\nu_f}{1-\nu_f}\right)\left(n^2-1\right)\right]-\nu_f\frac{\lambda^2}{n^2}\delta_{n\theta}+\left(\delta_{n\theta}+1\right)+\left(\frac{1+\nu_f}{1-\nu_f}\right)\left(n^2-1\right)\alpha\left(1-\kappa\right)\right\};$$

$$B_{42}=\overline{B}\left\{-\left(n^2-1\right)\left(\frac{1-b/a}{b/a}\right)-\nu_f\lambda^2\left(1-b/a\right)\right\}+\overline{D}\left\{-\left(n^2-1\right)+\nu_f\lambda^2\right.$$
$$\left.+\left(\frac{1+\nu_f}{1-\nu_f}\right)\left(n^2-1\right)\alpha\left(1-\kappa\right)\right\};$$

$$B_{43}=\overline{B}\left\{-n^2\left(\frac{1-b/a}{b/a}\right)+\lambda^2\left(1-b/a\right)-\left[\frac{n^2-1}{b/a}-\nu_f\lambda^2 b/a\right]\ln b/a\right\}$$
$$+\overline{D}\left\{\left(\frac{1+\nu_f}{1-\nu_f}\right)\xi-n^2+\nu_f\lambda^2\right\};$$

$$B_{44}=\overline{B}\left\{-\left(\frac{1+\nu_f}{4}\right)\lambda^2\left(1-b^2/a^2\right)+\left[n^2+\left(\frac{1-\nu_f}{2}\right)\lambda^2 b^2/a^2-\left(\frac{1+\nu_f}{2}\right)\delta_z\right]\ln b/a\right\}$$
$$+\overline{D}\left\{\left(\frac{1+\nu_f}{1-\nu_f}\right)\xi+1+\left(\frac{1+\nu_f}{1-\nu_f}\right)\left(n^2-1\right)\alpha\left(1-\kappa\right)\right\}.$$

Where

$$\overline{A}=\left(\frac{3+\nu_f}{1+\nu_f}\right)n^2+\left(\frac{2}{1+\nu_f}\right)\lambda^2-\left(\frac{2}{1-\nu_f}\right)\left(\frac{n^2\alpha\kappa}{1-b^2/a^2}\right)\left[-b/a\left(1-b/a\right)+\overline{F}\right],$$

$$\overline{B}=1-\frac{\nu_f\lambda^2}{n^2},$$

$$\overline{C}=\left(\frac{1-\nu_f}{1+\nu_f}\right)n^2+2\left(\frac{1-\nu_f}{1+\nu_f}\right)\lambda^2+\left(\frac{1-\nu_f}{1+\nu_f}\right)\frac{\lambda^2}{n^2}+\alpha\left(1-\kappa\right)\lambda^2,$$

$$\overline{D}=\left(\frac{1-\nu_f}{2}\right)\frac{\lambda^2}{n^2}\left(1-b^2/a^2\right),\text{ and}$$

$$\overline{F} = \frac{1-\nu_f^{\,2}}{\xi} \ln b/a .$$

A procedure was devised from which the desired eigenvalue can be determined from this determinant by trial and error. For a given set of parameters containing the dimensions and physical constants of the cylinder, the assumed value of the eigenvalue is varied until the value of the determinant becomes equal zero. The numerical results obtained are shown in figures A.4.4 (a), (b) and (c), based on physical constant for honeycomb cores and two different ratios of the mean radius of inner to the outer face; that is $\alpha = 0.95$, and $\alpha = 0.98$. The ratios E_c/G_θ, and E_c/G_z, were chosen to represent the average values of these quantities for honeycomb cores. The value of $\xi = 1$, represents a cylinder that has a weak core; that is, a core having relatively low values of E_c, G_θ, and G_z. For this case, values of α_{CR} as a function of the length to radius ratio is showed in figures A.4.4(a) for $E_c/G_\theta = 4$, and $E_c/G_z = 10$, and figure A.4.4(b) for $E_c/G_\theta = 10$, and $E_c/G_z = 4$. The value of $\xi = 1000$, represents a cylinder having a stiff core. This case was presented by figure A.4.4(c) for $E_c/G_\theta = 4$, and $E_c/G_\theta = 10$. Since the value of ξ depends not only upon the ratio, $m = E_f/E_c$, but also the radius to face thickness ratio, a/f, the range of values is quite wide. However, most of the constructions have dimensions and physical properties such that they lie between in the range between 1 and 1000.

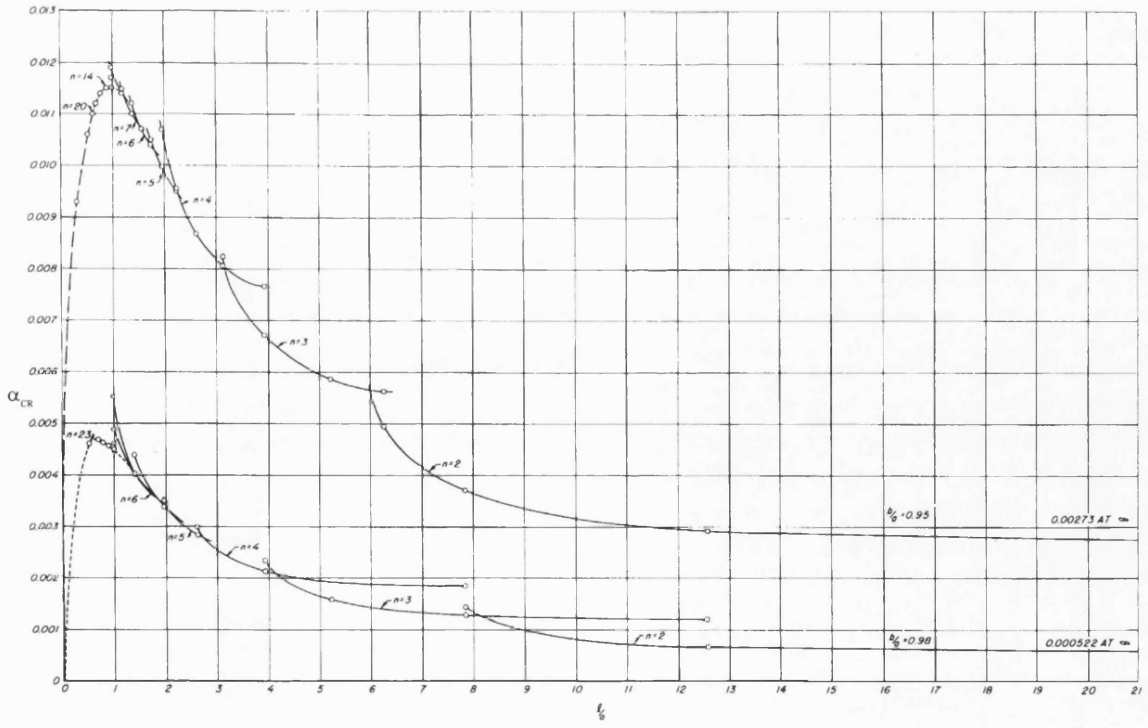

Fig. A.4.4(a) Critical pressure in terms of α_{CR} versus the length to radius ratio, $\xi = 1$.

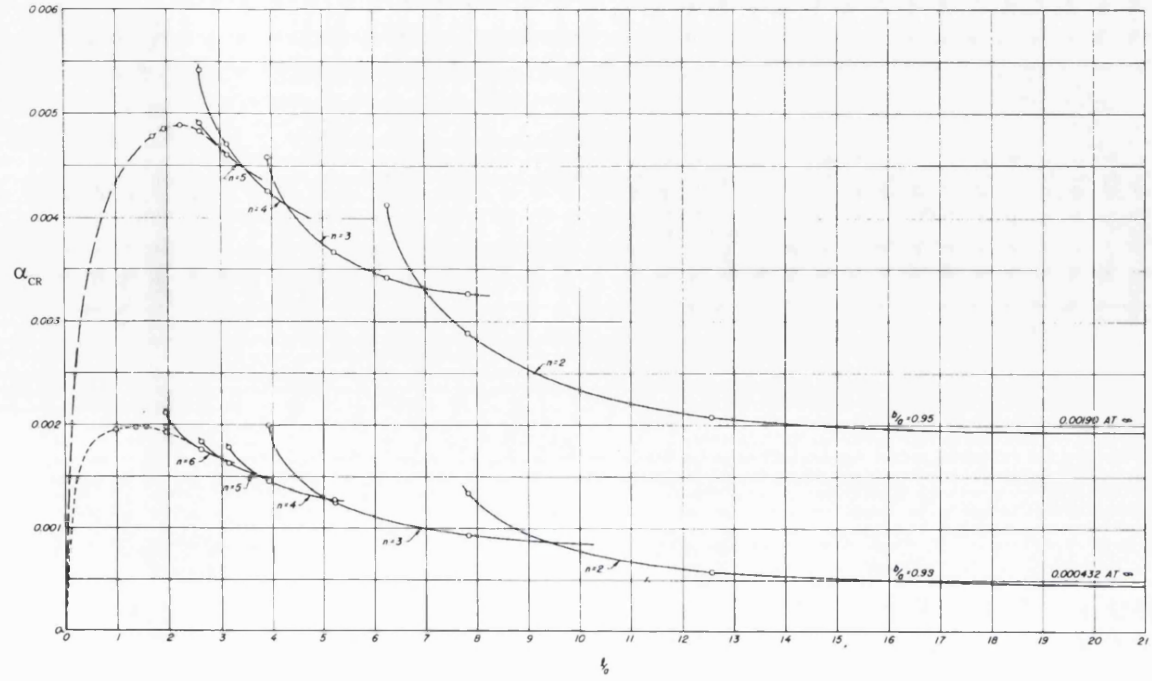

Fig. A.4.4(b) Critical pressure in terms of α_{CR} versus the length to radius ratio, $\xi = 1$.

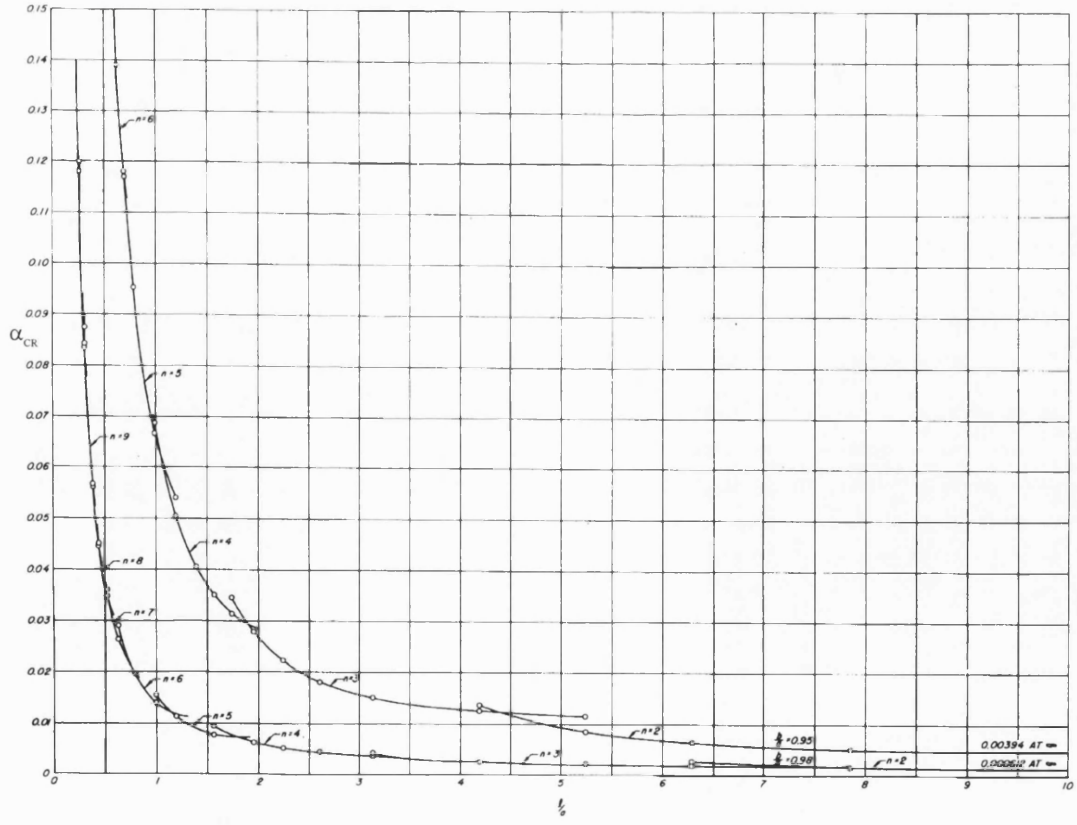

Fig. A.4.4(c) Critical pressure in terms of α_{CR} versus the length to radius ratio, $\xi = 1000$.